

AD-A152 198

3230

①  
LTH

Contract DAAK-40-76-C-1329

**Final Technical Report  
for  
MANUFACTURING METHODS  
FOR  
HIGH SPEED MACHINING  
OF ALUMINUM**

**1 FEBRUARY 1978**

In response to Technical Requirement Number 6088.

Submitted to:  
Manufacturing Methods and Technology Branch (DRDMI-EAT)  
U.S. Army Missile Research and Development Command  
Redstone Arsenal, Alabama 35898

Submitted by:



**VOUGHT CORPORATION**  
michigan plant

38111 Van Dyke Avenue • Sterling Heights, Michigan 48077

an LTV company

This document has been approved  
for public release and its  
distribution is unlimited.

DTIC  
ELECT  
APR 3 1985

85

03

12

127

A

DTIC FILE COPY

**Final Technical Report  
for  
MANUFACTURING METHODS  
FOR  
HIGH SPEED MACHINING  
OF ALUMINUM**

**1 FEBRUARY 1978**

In response to Technical Requirement Number 6088.

Submitted to:  
Manufacturing Methods and Technology Branch (DROMI-EAT)  
U.S. Army Missile Research and Development Command  
Redstone Arsenal, Alabama 35898

Submitted by:



**VOUGHT CORPORATION**  
michigan plant

38111 Van Dyke Avenue • Sterling Heights, Michigan 48077

an LTV company



Accession For

NTIS GTRC

DTIC TAB

Unannounced

Justification

By

DTIC

DTIC

DTIC

DTIC

DTIC

DTIC

DTIC

DTIC

DTIC

DTIC

DTIC

## PREFACE

This Final Technical Report covers the work performed under Contract Number DAAK-40-76-C-1329 from 16 November 1976 to 9 December 1977. The manuscript was released by the authors in February 1978 for publication.

This contract with the Vought Corporation, a division of LTV, Incorporated, was initiated under Technical Requirement Number 6089, "Manufacturing Methods for High Speed Machining of Aluminum". It was accomplished under the technical direction of Mr. John Malonas of the Manufacturing Methods and Technology Branch (DRDME-EAT) U.S. Army Missile Research and Development Command, Redstone Arsenal, Alabama 35809.

The contract was conducted under Mr. D.M. Halberda, Manufacturing Services Manager. The principal investigator was Mr. Jack McGee, Manufacturing Technology Engineer Specialist. Others who actively participated in the development and preparation of this report were: C.R. Casto, Design Engineer; D.O. Edge, P.B. Richardson and R.L. Thompson, Equipment Engineers; and D.A. Kutcher and T.E. Wojcik, N/C Programmers.

This project was accomplished as a part of the U.S. Army Missile Manufacturing Methods Program, the primary objective of which is to develop, on a timely basis, manufacturing processes, techniques and equipment for use in the economical production of USAMC materials and components.

Your comments are solicited on the potential utilization of the information contained herein as applied to your present and/or future production programs. Suggestions concerning additional manufacturing methods development required on this or other subjects will be appreciated.

# TABLE OF CONTENTS

<u>Section</u>	<u>Title</u>	<u>Page</u>
	PREFACE . . . . .	ii
1.0	INTRODUCTION . . . . .	1
2.0	MATERIALS . . . . .	4
	2.1 Workpiece . . . . .	4
	2.2 Cutting Tool . . . . .	5
3.0	CUTTING TEMPERATURE TESTS . . . . .	7
	3.1 Introduction . . . . .	7
	3.2 Experimental Setup . . . . .	9
	3.3 Thermocouple Calibration Procedure . . . . .	19
	3.4 Experimental Procedure . . . . .	30
	3.5 Effect of Speed and Geometry on Cutting Temperature . . . . .	33
	3.6 Effect of Feed Rate on Cutting Temperature . . . . .	38
	3.7 Effect of Cutting Fluids on Cutting Temperatures . . . . .	41
	3.8 Conclusions . . . . .	41
4.0	CUTTING FLUID OPTIMIZATION TESTS . . . . .	49
	4.1 Introduction . . . . .	49
	4.2 Application Method . . . . .	50
	4.2.1 Flood Application Method . . . . .	50
	4.2.2 Mist Application Method . . . . .	51
	4.2.3 Manual Application Method . . . . .	51
	4.2.4 Electrostatic Cooling Method . . . . .	52
	4.3 Selection of Candidate Cutting Fluids . . . . .	52
	4.4 Cutting Fluid Evaluation . . . . .	52
	4.4.1 Cutting Temperature Tests . . . . .	52
	4.4.2 Surface Finish Tests . . . . .	53
	4.4.3 Intergranular Corrosion Tests . . . . .	53
	4.4.4 Cost Analysis . . . . .	60
	4.5 Conclusions . . . . .	60
5.0	MODIFICATION OF EQUIPMENT . . . . .	61
	5.1 Introduction . . . . .	61
	5.2 Omimil OM-3 Machining Center . . . . .	61
	5.2.1 Safety Chip Guard . . . . .	61
	5.2.2 Bryant High-Speed Spindle System . . . . .	63
	5.2.3 Installation of Bryant High-Speed Spindle . . . . .	68
	5.2.4 Table Feed System . . . . .	72
	5.3 Bullard VTL Machine . . . . .	73
	5.3.1 ECCO High-Speed Spindle System . . . . .	73
	5.3.2 Installation of ECCO High-Speed Spindle . . . . .	75
	5.3.3 Safety Chip Guard . . . . .	77

TABLE OF CONTENTS  
(Continued)

<u>Section</u>	<u>Title</u>	<u>Page</u>
6.0	MACHINING TEST EQUIPMENT AND GENERAL PROCEDURES . . .	79
6.1	Peripheral End Milling . . . . .	79
6.2	Drilling . . . . .	83
6.3	Turning . . . . .	85
6.4	General . . . . .	87
7.0	TEST RESULTS - CUTTER GEOMETRY . . . . .	89
7.1	Statistical Model for Tests . . . . .	89
7.2	Fast Speed Tests . . . . .	91
7.3	High Speed Tests . . . . .	92
8.0	TEST RESULTS - MACHINING PARAMETERS . . . . .	97
8.1	Introduction . . . . .	97
8.2	Peripheral End Milling . . . . .	97
8.2.1	Feed Rate Optimization . . . . .	97
8.2.2	Depths of Cut . . . . .	99
8.2.3	Cutting Speeds . . . . .	105
8.3	Drilling . . . . .	116
8.4	Turning . . . . .	118
8.4.1	Feed Rate Optimization . . . . .	120
8.4.2	Depths of Cut . . . . .	128
8.4.3	Cutting Speed Optimization . . . . .	128
8.5	General Observations . . . . .	128
9.0	TEST RESULTS - CUTTING FORCE, HORSEPOWER, CUTTER DEFLECTION AND PULL-OUT . . . . .	131
9.1	Cutting Forces . . . . .	131
9.1.1	Test Procedure . . . . .	131
9.1.2	Force Measurements . . . . .	133
9.1.3	General Observations on Cutter Forces . . . . .	134
9.2	Horsepower . . . . .	139
9.2.1	Test Procedure . . . . .	140
9.2.2	Horsepower Measurements . . . . .	140
9.2.3	General Observations on Horsepower Measurements . . . . .	148
9.3	Cutter Deflection . . . . .	149
9.3.1	Test Procedure . . . . .	149
9.3.2	Cutter Deflection Measurements . . . . .	150
9.3.3	General Observations on Cutter Deflections . . . . .	150
9.4	Cutter Pullout . . . . .	155
9.4.1	Test Procedure . . . . .	155
9.4.2	Cutter Pullout Measurements . . . . .	156

TABLE OF CONTENTS  
(Continued)

<u>Section</u>	<u>Title</u>	<u>Page</u>
10.0	TEST RESULTS - SURFACE FINISH AND RESIDUAL STRESS. .	158
	10.1 Introduction . . . . .	158
	10.2 Surface Finish . . . . .	158
	10.2.1 Test Procedure . . . . .	158
	10.2.2 Surface Finish Measurements . . . . .	160
	10.2.3 General Observations on Surface Finish Measurements . . . . .	164
	10.3 Residual Stress . . . . .	164
	10.3.1 Test Procedure . . . . .	165
	10.3.2 Residual Stress Measurements . . . . .	166
	10.3.3 General Observations on Residual Stress Measurements . . . . .	171
11.0	COST AND PRODUCTION TIME ANALYSIS . . . . .	172
	11.1 Introduction . . . . .	172
	11.2 Cost and Production Time Calculations . . . . .	172
	11.3 Application . . . . .	172
	11.4 Potential Realization . . . . .	179
	11.5 Conclusion . . . . .	181
12.0	CONCLUSIONS AND RECOMMENDATIONS . . . . .	182
Appendix	BIBLIOGRAPHY . . . . .	186

# LIST OF ILLUSTRATIONS

<u>Figure</u>	<u>Title</u>	<u>Page</u>
1	Illustration of Dr. Salomon's Theory for The Effect of Cutting Speed on Cutting Temperature . . .	2
2	Locations of Thermal Energy Sources in Metal Cutting: (1) Along Shear Plane and (2) Tool-Chip Interface .	7
3	Idealized View of Heat Source At the Tool-Chip Interface . . . . .	8
4	Idealized Cutting Speed - Cutting Temperature Plot .	8
5	Experimental Setup Used to Determine Cutting Temperatures . . . . .	9
6	Lathe Used to Measure Cutting Temperatures . . . . .	10
7	Thermoelectric Circuit at Cutting Tool . . . . .	11
8	Mercury Contact Brush and Cutting Fluid Pump . . . . .	12
9	Cutting Temperature Recording Instruments . . . . .	13
10	Cutting Fluid Test Setup . . . . .	15
11	Cutting Fluid Transmission Line and Nozzle . . . . .	16
12	Crimped Cutting Fluid Nozzle Tip . . . . .	17
13	Thermocouple Clamped by Chipbreaker . . . . .	18
14	Schematic Diagram Showing the Manner by Which Tool-Chip Interface Temperatures Are Measured by the Thermoelectric Technique. (A) Hot Junction, (B) Cold Junction . . . . .	19
15	Arrangement for Calibration of Tool-Work Thermocouple	20
16	Temperature Calibration Curves for Low Carbon Steel Against (a) 18-14-1 HSS, and (b) K2S Cemented Carbide . . . . .	21
17	Compensating Circuit . . . . .	21
18	Compensating Circuit Calibration Setup . . . . .	22
19	Carbide - Work Calibration Setup . . . . .	22

LIST OF ILLUSTRATIONS  
(Continued)

<u>Figure</u>	<u>Title</u>	<u>Page</u>
20	Carbide-Aluminum Thermocouple Setup Calibration . .	24
21	Instrumentation for Carbide-Aluminum Thermocouple Calibration Setup . . . . .	25
22	VC-2 Carbide Insert/2014-T652 Aluminum Thermocouple Calibration Setup . . . . .	27
23	Thermocouple Calibration Curves for VC-2 Carbide Inserts and 2014-T652 Aluminum . . . . .	29
24	Oscillograph Calibration Showing Millivolt Output Per Centimeter . . . . .	31
25	Typical Recording of Tool-Work Thermocouple Output .	32
26	Effect of Cutting Speed and Cutter Geometry on Cutting Temperature When Turning 2014-T652 Aluminum	34
27	Effect of Cutter Geometry on Cutting Temperature When Turning 2014-T652 Aluminum . . . . .	37
28	Effect of Feed Rate on Cutting Temperature When Turning 2014-T652 Aluminum . . . . .	39
29	Effect of Cutting Speed and Feed Rate on Cutting Temperature When Turning 2014-T652 Aluminum . . . .	40
30	Effect of Cutting Speed and Water on Cutting Tem- perature When Turning 2014-T652 Aluminum . . . . .	42
31	Effect of Cutting Speed and Codol 0741 on Cutting Temperature When Turning 2014-T652 Aluminum . . . .	43
32	Effect of Cutting Speed and Coolant B on Cutting Temperature When Turning 2014-T652 Aluminum . . . .	44
33	Effect of Cutting Speed and Coolant C on Cutting Temperature When Turning 2014-T652 Aluminum . . . .	45
34	Effect of Cutting Speed on Cutting Temperature When Turning 2014-T652 Aluminum - Dry . . . . .	46
35	Summary of Effect of Cutting Speed and Coolants on Cutting Temperature When Turning 2014-T652 Aluminum	47

LIST OF ILLUSTRATIONS  
(Continued)

<u>Figure</u>	<u>Title</u>	<u>Page</u>
36	Cutting Fluid Pumps on Omnimil . . . . .	51
37	Stress Corrosion Test Fixture with Specimen Installed	54
38	Condition of Two A356 and One 7075 Aluminum Stress Corrosion Specimens After 30 Days Exposure to Coolant C . . . . .	55
39	Condition of Two Al-356 and One Al-7075 Stress Corrosion Specimens After 30 Days Exposure to Coolant B . . . . .	56
40	Condition of Two Al-356 and One Al-7075 Stress Corrosion Specimens After 30 Days Exposure to Coolant B . . . . .	56
41	Conditions of Candidate Coolants After 30 Days . . . . .	57
42	Condition of Two Al-6061 and One Al-7075 Stress Corrosion Specimens After 36 Days Exposure to Coolant C . . . . .	58
43	Condition of Two Al-6061 and One Al-7075 Stress Corrosion Specimens After 36 Days Exposure to Coolant B . . . . .	58
44	Condition of Two Al-6061 and One Al-7075 Stress Corrosion Specimens After 36 Days Exposure to Coolant B . . . . .	59
45	Condition of Candidate Coolants After 66 Days . . . . .	59
46	Omnimil Before Modification . . . . .	62
47	Omnimil After Modification . . . . .	62
48	Work Area of Modified Omnimil . . . . .	63
49	High-Speed Spindle and Clamp Ring . . . . .	64
50	Solid State, Variable Frequency, PTI TR 6300, 25 KW Power Supply . . . . .	65
51	37.5 KVA Isolation Transformer . . . . .	65
52	Panel for Omnimil High-Speed Spindle . . . . .	66

LIST OF ILLUSTRATIONS  
(Continued)

<u>Figure</u>	<u>Title</u>	<u>Page</u>
53	Spindle Motor Coolant Supply System . . . . .	67
54	Lubrication Panel Assembly for Spindle Reservoir Oil	67
55	Fast and Slow Speed Spindle on Sundstrand OM-3 Omnimil	68
56	Fast Spindle on Sundstrand OM-3 Omnimil Extended on H-Axis . . . . .	69
57	Original Fast Spindle and Housing for OM-3 Omnimil .	69
58	High-Speed Spindle Adaptor for Sundstrand OM-3 Omnimil . . . . .	70
59	Installed Bryant Spindle Housing . . . . .	70
60	Installing Bryant Spindle in Omnimil Adaptor . . . .	71
61	Installing Clamp Ring for Bryant Spindle . . . . .	71
62	Installed High-Speed Spindle . . . . .	72
63	Typical Unbalanced Cylindrical Part (G&C Shell) . .	73
64	Bullard Vertical Turret Lathe With Installed High- Speed Spindle . . . . .	74
65	Ekstrom, Carlson Company (ECCO) Spindle Mounted on Bullard VTL Side Tool Post . . . . .	74
66	Motor-Generator Frequency Converter for ECCO Router .	76
67	ECCO Spindle Motor Cooling System . . . . .	76
68	Adapter Plate for ECCO Spindle . . . . .	77
69	Safety Chip Guard for Bullard VTL . . . . .	78
70	Safety Chip Guard Installed on ECCO Router . . . . .	78
71	Spindle Horsepower Nomograph . . . . .	80
72	Three-Axes Milling Table Dynamometer and Test Setup .	81
73	Instrumentation for Measuring Cutting Forces . . . .	81

LIST OF ILLUSTRATIONS  
(Continued)

<u>Figure</u>	<u>Title</u>	<u>Page</u>
74	X-Y Plottars Used to Record Cutting Force Traces . .	82
75	General Peripheral End Milling Test Setup . . . . .	83
76	Tool Life Test Specimen for Peripheral Milling Tests	84
77	Drilling Test Setup . . . . .	84
78	Drilling Test Specimen . . . . .	85
79	Comparison of Conventional and End Mill Turning on VTL	86
80	Dynamically Balanced End Mills . . . . .	88
81	Effect of Inclination Angles and Effective Rake Angles on Tool Life When Face Milling 4340 Steel (RC 54) . .	90
82	End Mills for Optimum Cutter Geometry Test . . . . .	90
83	Effect of Cutter Geometry on Machining Load . . . . .	91
84	Cutter Wear Curve for Conventional Cutting Speed . .	92
85	Effect of Cutting Speed on Carbide Cutter Wear . . .	93
86	Wearlands Developed After Cutting 1.17 Miles of Al-7075-T651 . . . . .	94
87	End View of 25-Degree Helix, 5-Degree RR Brased Carbide End Mill . . . . .	95
88	Effect of Cutter Geometry on Cutter Wear . . . . .	95
89	Effect of Feed Rate on Cutter Wear . . . . .	98
90	Effect of Radial Depths of Cut on Machine Loads for Al-7075-T651 . . . . .	100
91	Effect of Cut Depths on Spindle Loading for 7075- T651 Aluminum . . . . .	102
92	Effect of Cut Depths on Spindle Loading for 6061- T651 Aluminum . . . . .	103
93	Effect of Cut Depths on Spindle Loads for A356-T6 Aluminum . . . . .	104

LIST OF ILLUSTRATIONS  
(Continued)

<u>Figure</u>	<u>Title</u>	<u>Page</u>
94	Effect of Cut Depth on Cutter Wear . . . . .	106
95	Theoretical Effect of Cutting Speed on Carbide Cutter Life . . . . .	109
96	Theoretical Effect of Cutting Speed on HSS Cutter Life	110
97	Typical Effect of Cutting Speed on Chip Surface for Al-7075-T651 . . . . .	111
98	Approximate Effect of Cutting Speed on Cutter Wear .	114
99	Typical Test Drill After Producing 5,547 Holes . . . .	117
100	Typical Chips Produced When Drilling Al-7075-T651 At 100 Inches/Minute Feed Rate . . . . .	119
101	Typical Al-7075-T651 High-Speed Drilling Test Specimen	119
102	Typical Workpieces for Turning Tests . . . . .	120
103	Recommended Cutter-Workpiece Orientation for End Mill Turning . . . . .	121
104	Typical Wearlands Produced on End Mills by Aluminum Alloys . . . . .	121
105	Effect of Feed Rate on Tool Life for Al-6061-T6 . . .	122
106	Effect of Feed Rate on Tool Life for Al-A356-T6 . . .	123
107	Effect of Feed Rate on Tool Life for Al-7075-T6 . . .	124
108	Continuous Chip Produced by End Mill Turning at 14,400 RPM . . . . .	125
109	Effect of Feed Rate on Chip Welding . . . . .	127
110	Router Bit Made From 2-Flute End Mill . . . . .	127
111	Theoretical Effect of Cutting Speed on Cutter Life for Al-A356-T6 . . . . .	129
112	Matrix for Cutting Force Tests - Cutting Force and Power Data . . . . .	132

LIST OF ILLUSTRATIONS  
(Continued)

<u>Figure</u>	<u>Title</u>	<u>Page</u>
113	Cutting Force Diagram for Climb Milling . . . . .	134
114	Effect of Feed Rate on Cutting Force for Al-6061-T651 Aluminum . . . . .	135
115	Effect of Cutting Speed on Cutting Force for Al-6061-T651 Aluminum . . . . .	135
116	Effect of Radial Depth of Cut on Cutting Force for Al-6061-T651 Aluminum . . . . .	136
117	Effect of Feed Rate on Feed and Thrust Force for 6061-T651 Aluminum . . . . .	137
118	Effect of Cutting Speed on Feed and Thrust Force for 6061-T651 Aluminum . . . . .	137
119	Effect of Radial Depth of Cut on Feed and Thrust Force for 6061-T651 Aluminum . . . . .	138
120	Effect of Feed Rate on Spindle and Cutter Horsepower for Al-6061-T651 Aluminum . . . . .	141
121	Effect of Cutting Speed on Spindle and Cutter Horsepower for Al-6061-T651 Aluminum . . . . .	141
122	Effect of Depths of Cut on Spindle and Cutter Horsepower for Al-6061-T651 Aluminum . . . . .	142
123	Effect of Feed Rate on Spindle Horsepower for Al-7075-T651 Aluminum . . . . .	143
124	Effect of Cutting Speed on Spindle Horsepower for Al-7075-T651 Aluminum . . . . .	143
125	Effect of Depths of Cut on Spindle Horsepower for Al-7075-T651 Aluminum . . . . .	144
126	Effect of Depths of Cut on Spindle Horsepower for Al-A356-T6 Aluminum . . . . .	145
127	Effect of Aluminum Alloy on Spindle Horsepower . . . . .	146
128	Effect of Depths of Cut and Carbide Cutters on Spindle Horsepower for 7075-T651 Aluminum . . . . .	147

LIST OF ILLUSTRATIONS  
(Continued)

<u>Figure</u>	<u>Title</u>	<u>Page</u>
129	Effect of Feed Rate on Cutter Deflection for 6061-T651 Aluminum . . . . .	151
130	Effect of Cutting Speed on Cutter Deflection for 6061-T651 Aluminum . . . . .	151
131	Effect of Depths of Cut on Cutter Deflection for 6061-T651 Aluminum . . . . .	152
132	Effect of Depths of Cut on Cutter Deflection for Al-7075-T651 Aluminum . . . . .	153
133	Effect of Depths of Cut on Cutter Deflection for Al-A356-T6 Aluminum . . . . .	154
134	Typical Examples Showing the Effect of Cut Geometry on Cutter or Spindle Pull-out and Resulting Axial Depth of Cut Errors . . . . .	157
135	Surface Finish Test Blocks . . . . .	159
136	Surface Finish Nomenclature . . . . .	160
137	Effect of Cutting Velocity on Surface Finish for 7075-T651 Aluminum . . . . .	161
138	Effect of Cutting Velocity on Surface Finish for 6061-T651 Aluminum . . . . .	162
139	Effect of Cutting Velocity on Surface Finish for A356-T6 Aluminum . . . . .	163
140	Residual Surface Stress Profiles in Al-7075-T651 Produced by End Milling . . . . .	168
141	Residual Surface Stress Profiles in Al-6061-T651 Produced by End Milling . . . . .	169
142	Residual Surface Stress Profiles in Al-A356-T6 Produced by End Milling . . . . .	170
143	High-Speed Machined G&C Shells . . . . .	180

# LIST OF TABLES

<u>Table</u>	<u>Title</u>	<u>Page</u>
I	Typical Calibration Data Obtained with Insert SPG-#1 for VC-2 Carbide/2014-T652 Aluminum Thermocouple . .	23
II	Effect of Cutter Insert and Temperature on EMF Output of VC-2 Carbide/2014-T652 Thermocouple for High Impedance System . . . . .	26
III	Mathematical Description of Calibration Curves for Inserts When MV >2.0 . . . . .	28
IV	Tool Life Test Results . . . . .	108
V	Theoretical Most Economical Cutting Speeds for Selected Cutters as Developed from Figures 95 and 96	115
VI	Summary of Horsepower and Metal Removal Rate Data Developed from End Milling Tests on 6061-T651 Aluminum . . . . .	148
VII	Residual Stress Measurements . . . . .	167
VIII	Cost and Production Time Equations . . . . .	173
IX	Production Times and Costs for Machining One Part by Conventional Operation 50 . . . . .	175
X	Production Times and Costs for Machining One Part by High Speed Milling Operation 50 . . . . .	176
XI	Production Times and Costs for Machining One Part by Conventional Operation 60 . . . . .	177

## 1.0 INTRODUCTION

↓  
The objective of this program was to develop manufacturing methods and technology for machining aluminum at significantly higher speeds than is currently practiced. Additionally, the methodology developed was to be satisfactorily demonstrated as being both practical and cost-effective when compared with current machining practices.

To accomplish these objectives, a three-phase program was conducted. In Phase I, cutting tools and machining parameters were tested for the purpose of making machining recommendations for selected aluminum alloys. Expanded machining data; e.g., tolerances, finishes, deflection, cutting forces, horsepower, residual stresses and cutting temperature were also developed to ascertain the effects of high speed machining on product integrity.

In Phase II, Guidance and Control Shells (~~Part No. 10150247~~) for the Lance missile were machined, in part, with the new methods to establish cost data for comparison with present methods. Also, performance data for the methods were analyzed, and interrelationships were developed among pertinent machining properties and variables.

In Phase III, new high-speed machining methodologies developed in the program were demonstrated to representatives of the Government and the aluminum fabricating industry. ←

A survey conducted at the beginning of the program uncovered only a limited amount of useful information for high-speed machining. Based on that survey, it appears that the late C. Salomon of Germany<sup>1\*</sup> was the first to publish experimental results for high-speed machining. In 1931, Salomon reported that thermocouple measurements made in high-speed milling tests indicate that tool-chip interface temperatures drop at higher cutting speeds (see Figure 1), so that it is possible to machine faster and still have the tool last longer, providing machine tools can be made to cut fast enough. Sielmann<sup>2</sup> conducted tests in 1958 on 1045 steel with a 150-horsepower lathe at cutting speeds up to 18,000 feet/minute. Evidently, these tests were not successful from the standpoint of increasing tool life with cutting speed, as the ceramic cutters used, apparently, failed, more or less, instantly when operated at cutting speeds in excess of 9,000 feet/minute. About the same time, Vaughn<sup>1,3</sup> conducted more extensive and elaborate studies for high speed machining. While the results of Vaughn's studies showed that the optimum cutting speed for most materials is greater than 100,000 feet/minute, these were probably shelved due to a lack of appropriate machine tools. More recently, however, machine tool technology had progressed to the point where interest in high speed machining was once again aroused. This technology included advancements in numerical control systems, bearing design, spindle design, frequency converter power supplies, pallet changing, automatic tool changing and cutter materials. As a consequence,

\* Superscript numbers in text refer to references in bibliography.

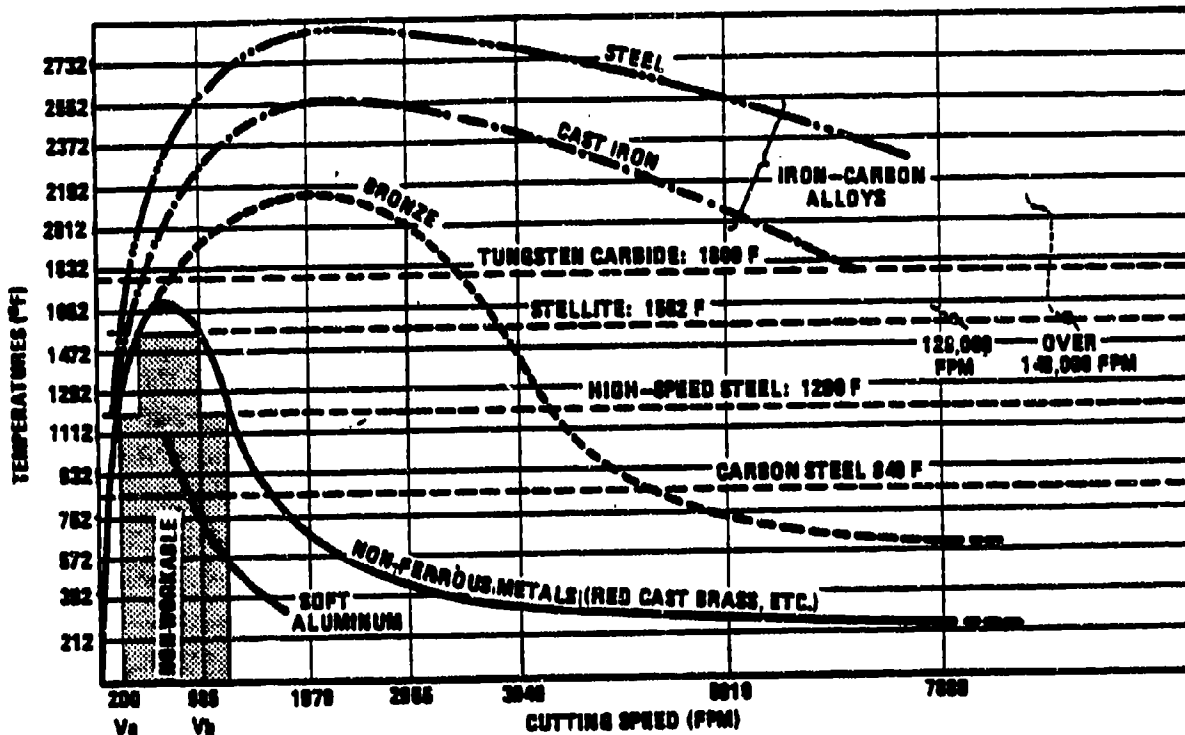


Figure 1. Illustration of Dr. Salomon's Theory for The Effect of Cutting Speed on Cutting Temperature

King and McDonald<sup>4</sup> set out to prove and advance Vaughn's research. In doing so, these researchers worked with the Bryant Grinder Corporation and others to equip an existing Sundstrand, five-axes, Model CM-3, Cimimil with a 20,000 rpm, 20 horsepower spindle. Based on results obtained with that modified machine, King and McDonald reported such a good potential for the high-speed machining of aluminum that the Vought Corporation modified one of its Sundstrand Cimimils in a duplicative manner for use on its research and developmental programs. Vought also purchased some special, solid carbide end mills for evaluation that were designed or developed by those researchers; but other than these inputs, this Vought conducted program was, essentially, an independent developmental effort.

This Technical Report presents the results that were generated under this program. As a synopsis, it can be generally stated that the high speed machining of aluminum is an intriguing, relatively safe process and that anyone would probably be reluctant to go back to conventional feeds and speeds after being exposed to it for a week or two. Specifically, Section 2.0 discusses the selection of workpiece test materials and cutting tools. In Section 3.0, cutting temperature tests are described

in detail, and cutting fluid selection is discussed in Section 4.0. Machine modifications made to a Sundstrand Omnimil and Bullard Vertical Turret Lathe to obtain a high-speed machining capability are described in Section 5.0, and testing procedures used to establish high-speed machining methods are discussed in Section 6.0. Cutter geometry and optimization tests are described in Section 7.0. In Section 8.0, test results are presented for machining parameter optimization. Test results for cutting force, deflection and horsepower are given in Section 9.0, and the effects of high-speed machining on surface finish and residual stress generation are discussed in Section 10.0. The residual stress tests and analyses were accomplished at the Metcut Research Associates, Incorporated laboratories. An economic analysis for high-speed machining was also conducted by Metcut, and the results are given in Section 11.0. In Section 12.0, conclusions and recommendations, based on information derived from this program, are presented.

## 2.0 MATERIALS

### 2.1 Workpiece

Work materials for this program were limited to aluminum and its alloys and were selected from that category on the basis of being representative of missile fabrication. Additionally, the most-difficult and least-difficult-to-machine alloys and tempers in this classification were sought to define parameter limits. For example, A356-T6 cast aluminum is one of the more difficult-to-machine aluminum alloys. It has a machinability index (I) of 140<sup>5</sup>, which signifies that it can be machined approximately 40% faster than S1112 steel. Consequently, and because A356-T6 aluminum is the same material from which the demonstration part (Lance Shell Guidance Set, part number 10162178) was to be machined, it was one of the alloys selected. Other alloys considered were:

<u>ALLOY</u>	<u>MACHINABILITY INDEX (I)<sup>5</sup></u>
7075-T6	120
2014-T6	140
2024-T4	150
6061-T6	190
2011-T3	200
218-T	240

After costing out these materials in the quantities required for testing, work material requirements were reduced to and ordered in the following alloys, sizes, and quantities:

<u>ALLOY</u>	<u>SIZE</u>	<u>QUANTITY</u>
A356-T6	2 by 12 by 36 inches	20
A356-T6	24 OD by 18 ID by 18 inches	6
A356-T6	Lance Shell Casting	5
7075-T651	2 by 48 by 144 inches	2
7075-T6	24 OD by 18 ID by 18 inches	6
6061-T651	2 by 48 by 144 inches	2
6061-T6	24 OD by 18 ID by 18 inches	6

This group of alloys encompasses a wide range of machinability, and all are familiar missile and aerospace materials. The A356-T6 aluminum could present some unpredictable problems; since it is a cast material, and its principal additive is silicon (about 7%). Both the insoluble free silicon particles in this alloy and any sand from casting molds would be abrasive and increase tool-wear.

## 2.2 Cutting Tool

At the beginning of this program, solid carbide end mills were generally considered to be optimum for the high-speed milling of aluminum. That type of cutter not only provided good wear and cutting temperature resistance, but King<sup>+</sup> stated at a seminar in Dallas, Texas on September 15, 1976, that solid carbide cutters would probably not be hurled through space if broken while turning at high speeds. Instead, such cutters would likely fracture and fall harmlessly to the machining table, thus providing a margin of safety.

For solid carbide end mills, there is a practical limit to the size that should be purchased. For example, there was difficulty in obtaining solid carbide end mills in a 1.25-inch diameter size. These had to be special made at considerable cost and long lead time. For these reasons, brazed carbide end mills were purchased initially for all sizes larger than 1.25-inch diameter. When these cutters proved to be safe and satisfactory, brazed carbide end mills were subsequently purchased in smaller sizes.

High speed steel (HSS) cutters containing 4-percent cobalt were also purchased initially to activate tests, provide a backup, and to provide a reference datum against which to compare cutter development gains. This type of end mill performed creditably throughout the program and was used extensively.

A list of cutters procured for this program would include (see page 6):

Cutter Type	Size and Shape				Qty
	Inch/Inches Diameter	Flute	Inch Flute Length	Inches Overall	
End Mill, Brazed Carbide	1.5	2	1.5	4	9
	1.0	2	1.5	4	8
	2.0	3	2.0	4.5	2
	1.75	3	2.0	4.5	1
End Mill, Brazed Carbide	1.5	3	2.0	4.5	2
End Mill, Solid Carbide	0.5	2	3/4	6	12
	0.75	2	7/8	6	6
	1.0	2	3/4	6	6
	1.25	2	1-3/8	6	9
End Mill, Solid Carbide	1.0	2	2-1/4	4.5	2
End Mill, CoHSS	0.5	4	1-1/4	3-1/4	4
	1.0	4	2	4.5	6
	1.25	4	2-1/2	5	6
	1.5	4	4.0	6-1/2	3
	2.0	4	2.5	5	2
	1.0	2	1-1/2	4	8
	1.25	2	2	4.5	4
End Mill, CoHSS	2.0	2	3	5.5	6
Drill, Solid Carbide	0.25	2	2	3-1/4	30
Drill, HSS	0.25	NAS 907, Type "C"		2.5	12
Insert Holder, Lathe	1 x 1-1/4 x 6, A-SVER-85C				1
Insert Holder, Lathe	1 x 1-1/4 x 6, SVER-85				1
Carbide Inserts	3/16 x 3/4 x 3/4, SPG 633				12
Carbide Inserts	3/16 x 3/4 x 3/4, SNG 633				12
Carbide Inserts	1/8 x 3/4 x 3/4, SEG 623J				25

### 3.0 CUTTING TEMPERATURE TESTS

#### 3.1 Introduction

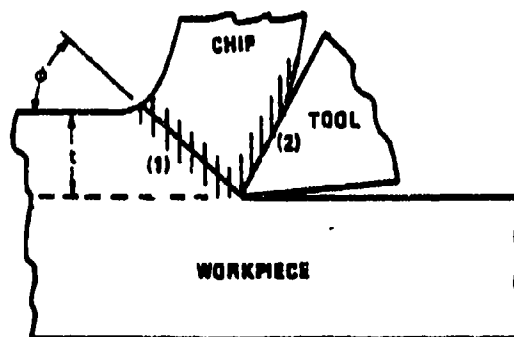
It is generally accepted that tool life decreases as cutting speeds are increased and that their relationship over a practical range can be expressed mathematically<sup>6</sup> as follows:

$$VT^n = C$$

where

V = Cutting Speed  
T = Tool Life  
n = Material Constant  
C = Material Constant

The principal reason for the tool life decrease can be attributed to the temperature rise which accompanies increased cutting speeds. To explain, these are two important heat sources involved in the metal cutting process. One involves plastic deformation energies along shear planes; and the other involves frictional energies along tool-chip contact areas as illustrated in Figure 2. It has been shown<sup>7</sup> that the quantities of heat developed at these sources are directly proportional to shear velocities and chip velocities, respectively, and that both, in turn, are directly proportional to cutting speed  $u$ . Thus, as cutting speeds are increased, the output from these heat sources increase; and, all things being equal, chips and tools get hotter.



SA 4981-1

Figure 2. Locations of Thermal Energy Sources in Metal Cutting:  
(1) Along Shear Plane and (2) Tool-Chip Interface

The action of increased tool temperature is to soften or weaken the tool material so that it abrades and wears more readily<sup>8</sup>. Cutting tools have even been known to fail by welding to workpiece material. Thus, there would seem to be definite thermal restraints to high speed machining; and it was the purpose of this investigation to determine whether or not such restraints would prohibit the high speed machining of aluminum alloys. This was accomplished by measuring the temperature of tool-chip contact areas, as illustrated in Figure 3, for various machining speeds, feeds, and cutter geometries on 2014-T652 aluminum.

SA 4881-2

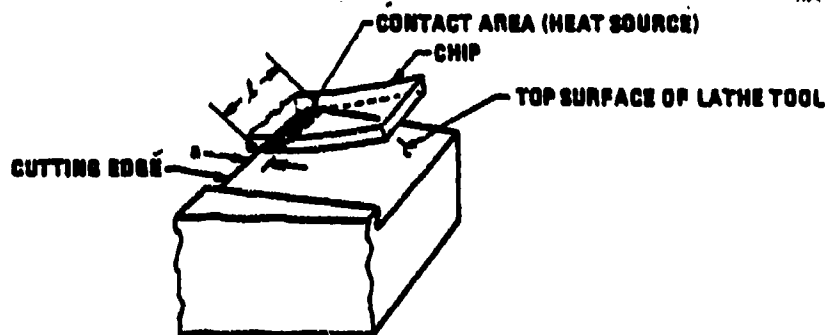


Figure 3. Idealized View of Heat Source At The Tool-Chip Interface

A secondary purpose of this investigation was to determine, if convenient, whether or not the cutting temperature for a given material peaked at some unique cutting speed. It had been verified<sup>7</sup> that, essentially, all the work of cutting is transformed into thermal energy, and most of that energy is carried off in the chips. A small amount of the energy goes into the workpiece, and an even smaller amount goes into the tool (cf. Figure 2). At high cutting speeds, as much as 80% of the energy may be carried off by the chips. It is this circumstance which makes high speed machining possible. Additionally, other investigators<sup>1,3</sup> have presented evidence which indicates that the cutting temperature for a given material will increase with cutting speeds to a point; after which, the cutting temperature decreases with further cutting speed increases. Such an occurrence, illustrated in Figure 4, would provide

SA 4881-3

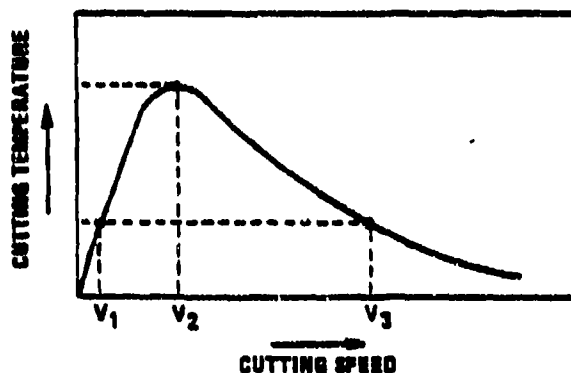


Figure 4. Idealized Cutting Speed - Cutting Temperature Plot

two cutting speeds, one normal ( $V_1$ ) and one very fast ( $V_3$ ), which should produce the same cutting temperature and, therefore, cutter life. Any speed falling between these two would be expected to yield a shorter cutter life, reaching a minimum at the  $V_2$  cutting speed. If this proved to be the case, it would open up a number of possibilities. Primarily, it would establish high speed machining as a meaningful process, provided equipment having the speed ranges required could be made available. For these reasons, this concept, was investigated within the limits of the contractors time frame and readily available equipment and facilities.

### 3.2 Experimental Setup

The test setup used in this investigation is illustrated in Figure 5. Machining was accomplished on a 48-inch swing, infinitely variable cutting speed, No. 2502 Monarch lathe. Pictorial views of the setup are presented in Figures 6, 7, 8, and 9. The thermoelectric circuit is patterned after one described by Shaw except that it embraces an additional compensating circuit developed by Trigger, Campbell, and Chao<sup>9</sup> which enables throwaway insert cutting tools to be used. This compensating device uses the IR drop resulting from thermoelectric flow in a closed circuit to nullify the parasitic emf introduced by dissimilar lead materials attached to cutting inserts.

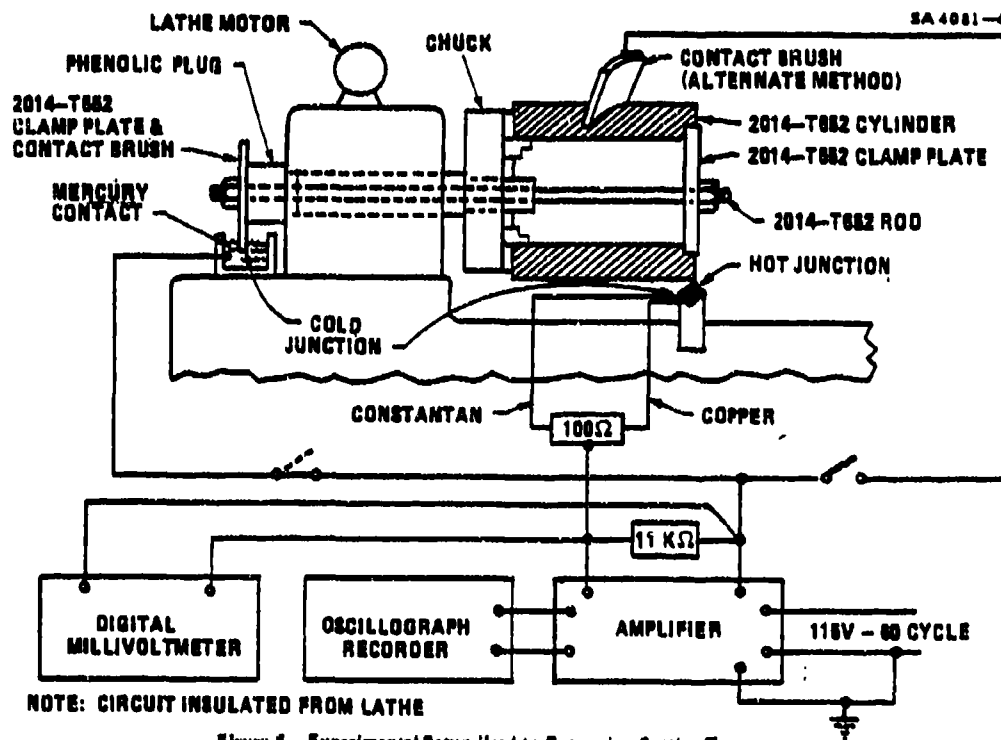
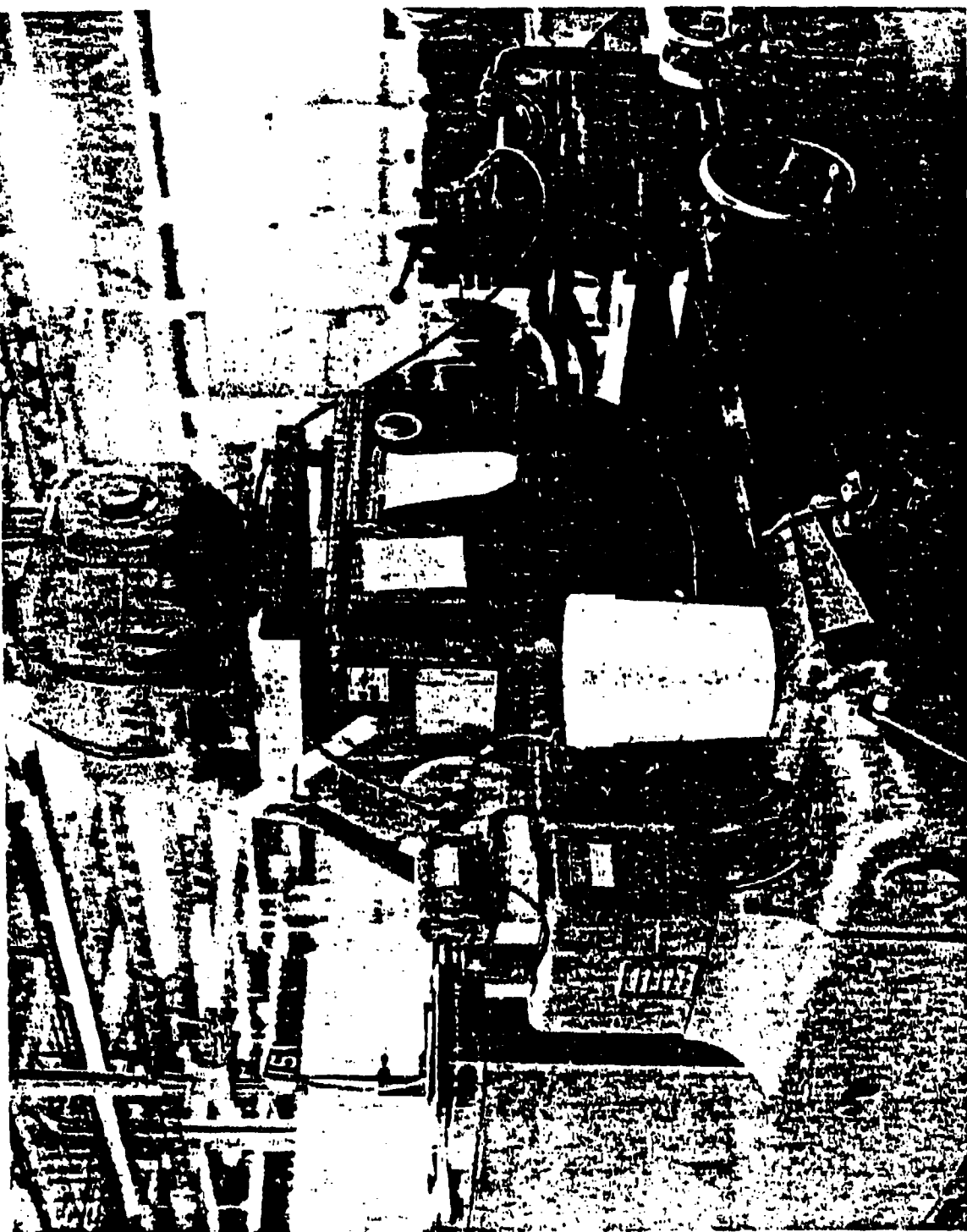


Figure 5. Experimental Setup Used to Determine Cutting Temperatures

Figure 6. Leds Used to Measure Cutting Temperature



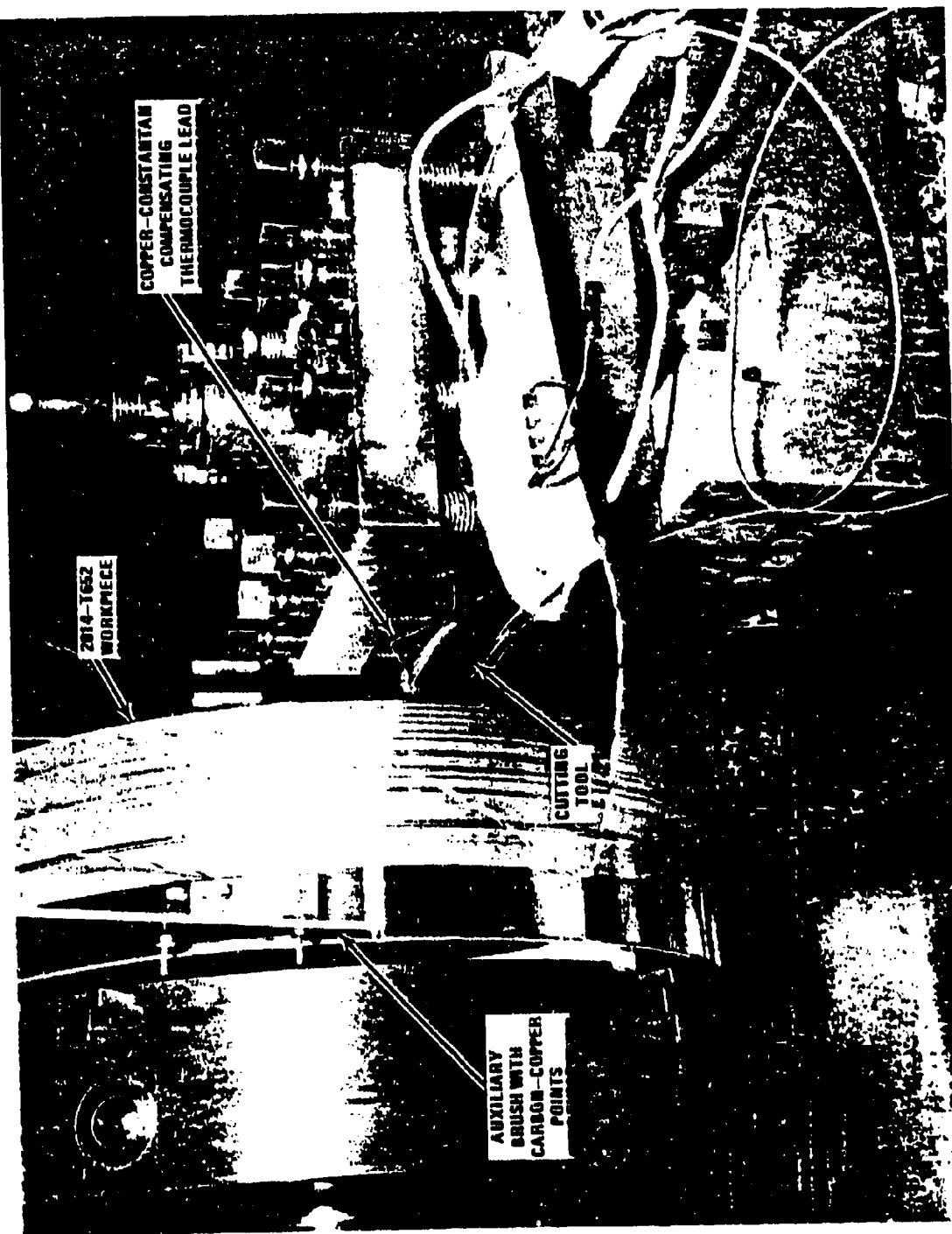


Figure 7. Thermoelectric Circuit at Cutting Tool

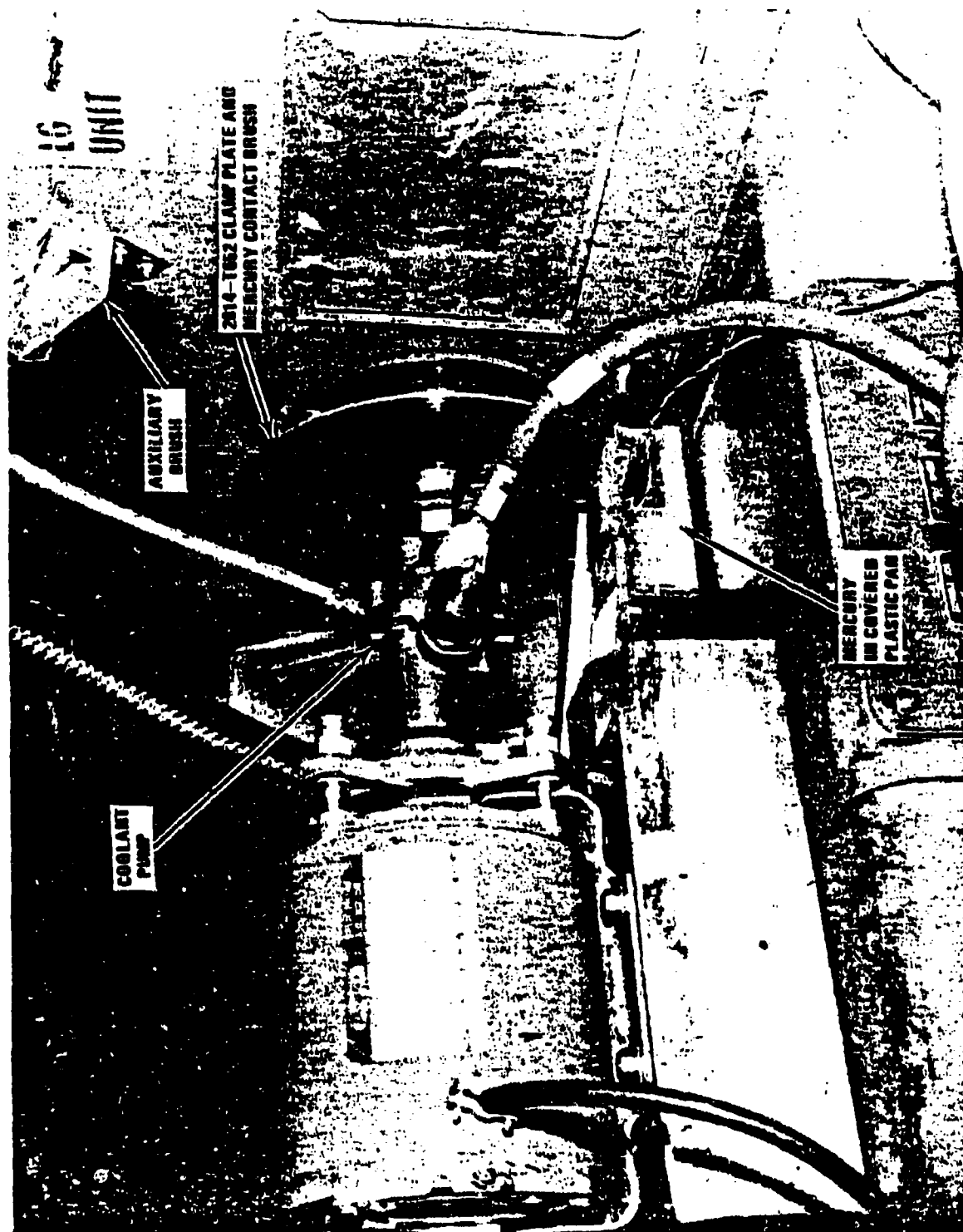


Figure 8. Mercury Contact Brush and Cooling Field Pump

6-15594

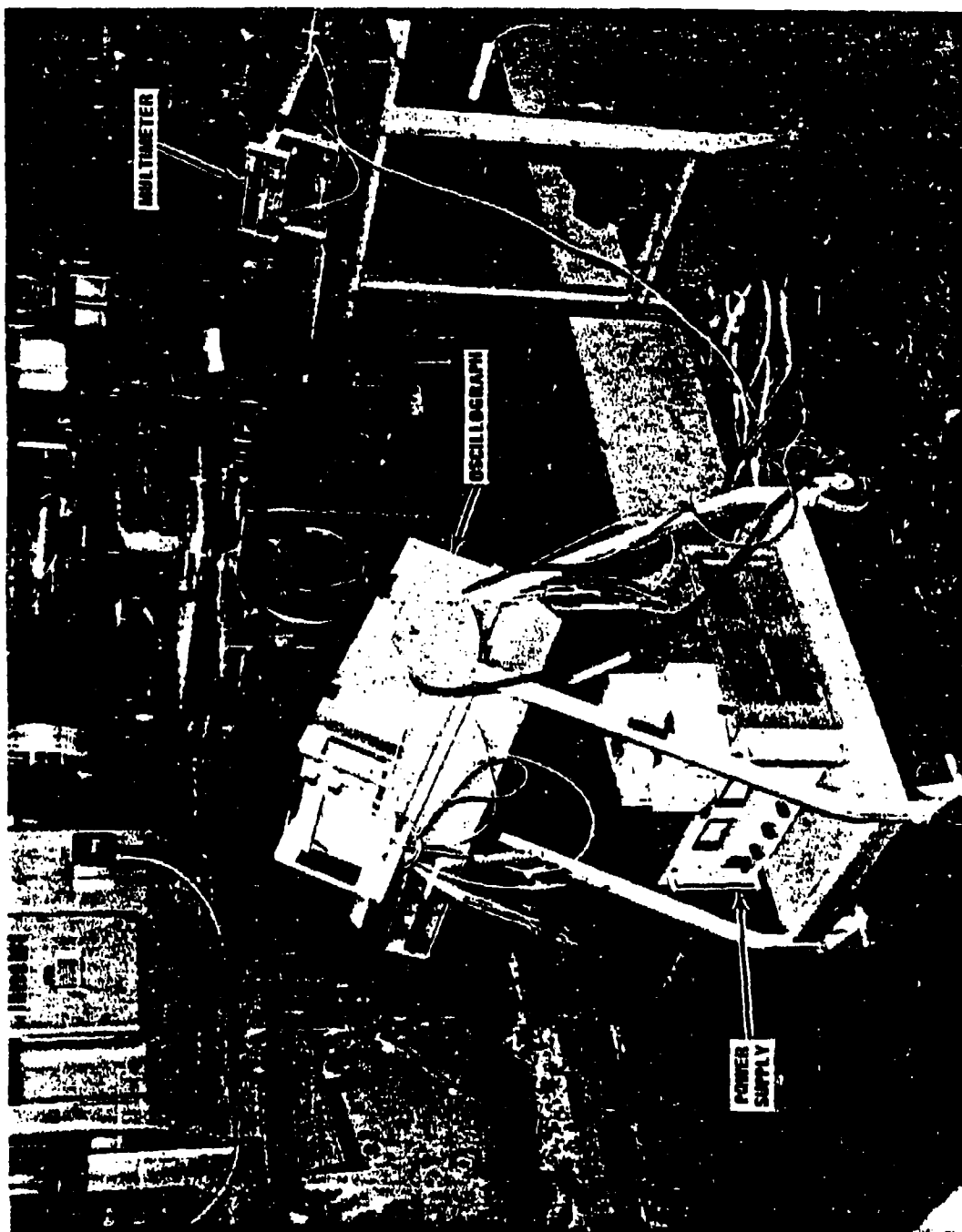


Figure 8. Cutting Temperature Recording Instruments

The workpiece was a forged 2014-T652 aluminum cylinder approximately 22 inches in diameter by 12 inches long by 7/8-inch wall thickness. The internal diameter was step-machined 1/4-inch larger by 1/4-inch deep to locate and retain a 20.313 diameter by 5/16-inch thick clamping plate made of 2014-T652 aluminum. The cylinder was clamped firmly in an insulated four-jaw chuck which acted outwardly against the cylinder's internal wall. As a safety feature, the cylinder was also clamped axially with a drawbar-like device which also served as a part of the thermoelectric circuit. This device was composed of the aforementioned clamping plate, a 3/4-inch diameter 2014-T652 aluminum rod which was approximately 61 inches long and threaded on both ends, a 2-inch thick by 4.125 inch diameter by 6-inch diameter stepped phenolic plug, a 1/4-inch thick by 10-inch diameter tapered 2014-T652 aluminum clamp/mercury-contact plate, and assorted washers and nuts. These details were assembled as illustrated in Figure 3.

Three different workpiece brushes were tried during this investigation. The first brush was made from a strip of 2014-T652 aluminum sheet stock which was contoured on one end to fit the workpiece perimeter as indicated in Figures 5 (alternate method) and 7. The use of this method was discontinued when it was verified that aluminum rubbing against aluminum produced galling, seizing, and poor thermoelectric signals. The second method tried was a variation of the first in that a pair of copper-carbon points were attached to the brush as shown in Figure 7. While this method was not totally satisfactory, especially at high cutting speeds, its use was not discontinued until it was found that cutting fluids getting on the contact points caused questionable thermoelectric signals to be transmitted. The setup finally adopted for use in this investigation was the more expensive, but more reliable, mercury-contact brush illustrated in Figure 5 and portrayed in Figure 8.

A part of the instrumentation used to measure tool-workpiece thermocouple outputs is shown in Figure 9. The x-y millivolt recorder shown on top of the cart at the left, with its 24 volt power supply beneath, is a Honeywell, Model 2206, Visicorder, light beam oscillograph. The light beam signal was transmitted by a Honeywell M100-120 galvanometer in the recorder. Not shown on top of the power supply is a Sanborn, Model 8875, instrumentation amplifier which was made necessary when an 11,000 ohm resistor (cf. Figure 5) was added to the thermoelectric circuit to reduce the effects of brush contact, resistance variations. The digital multimeter, shown on top of the table in Figure 9, is Non-Linear Systems' Model MX-1. This instrument was used to calibrate tool-workpiece thermocouples and the recorder as well as provide a direct readout for cutting temperature emfs.

Initially, cutting tests were conducted dry. As a follow-on, different coolants and concentrations were evaluated to determine their effect on cutting temperature. The test setup used to evaluate coolants is shown in Figures 10, 11, and 12. In Figure 10, three carefully mixed commercial coolants are shown awaiting their turn to be tested. Each coolant was pumped from its container to the cutting zone by the adjustable flow rate, portable pump more clearly shown in Figure 6. After each coolant was tested, the pump and lines were washed out with water taken from the container shown. Additionally, water was also used as a coolant.

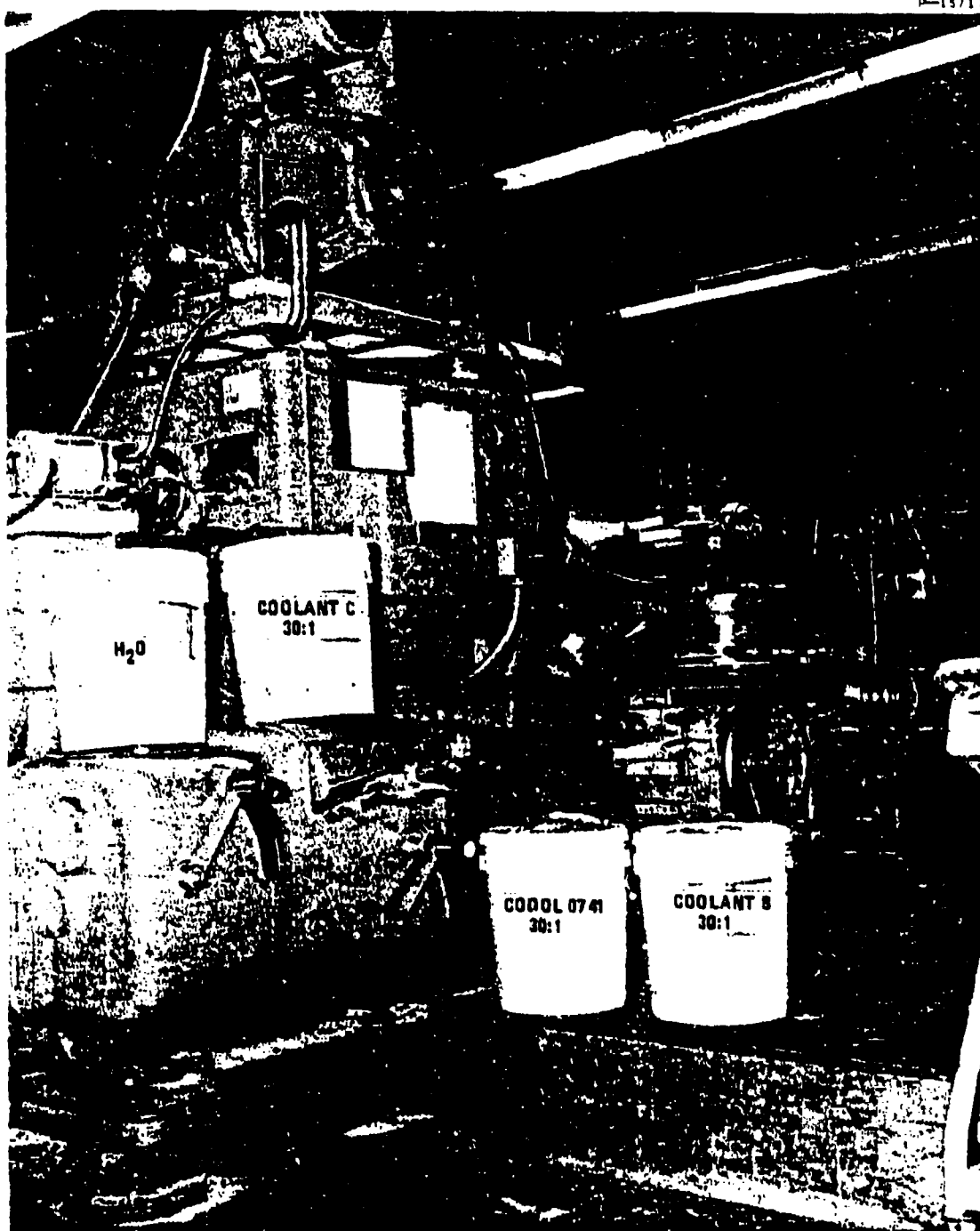


Figure 10. Cutting Fluid Test Setup

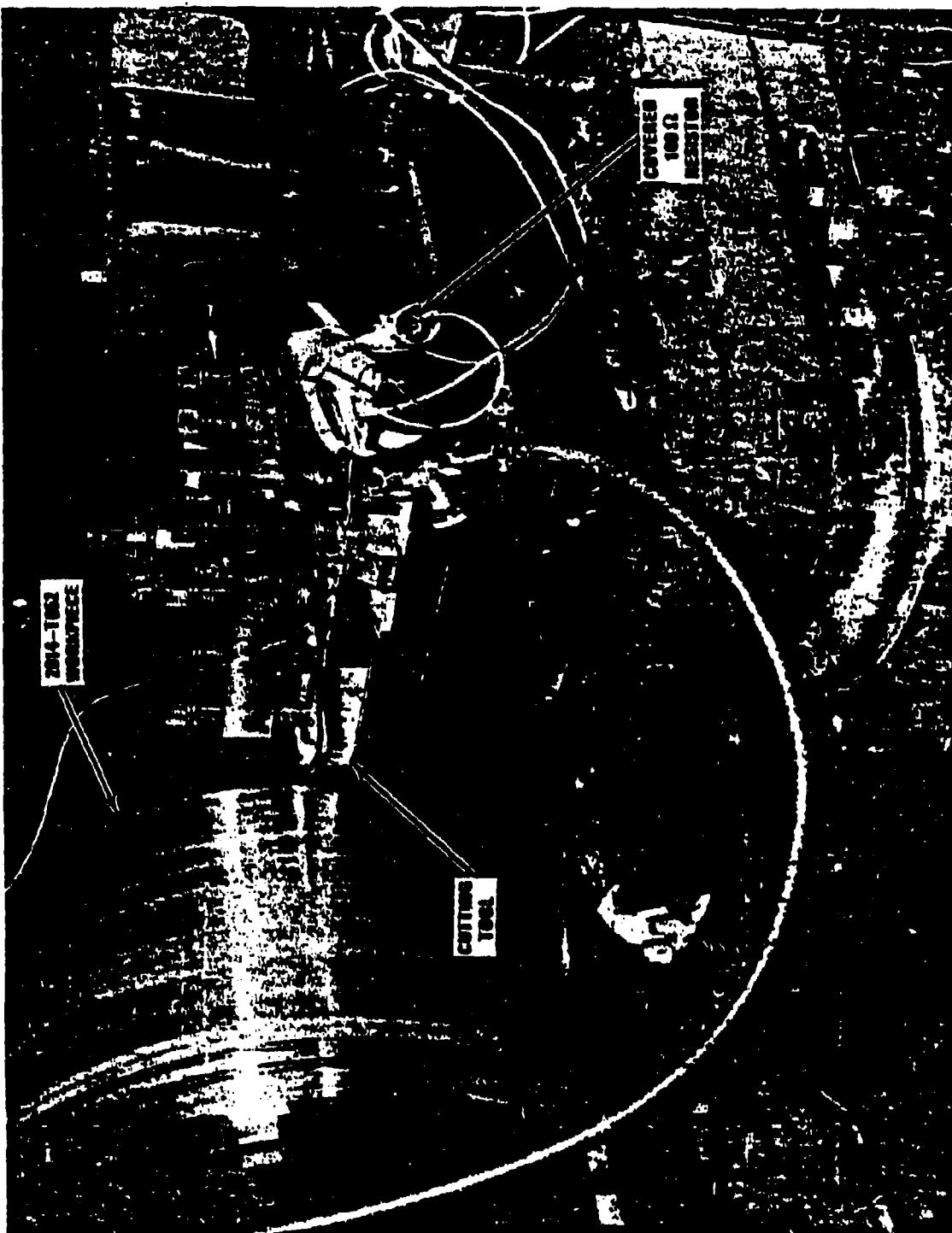


Figure 11. Cutting Field Transmission Line and Burial

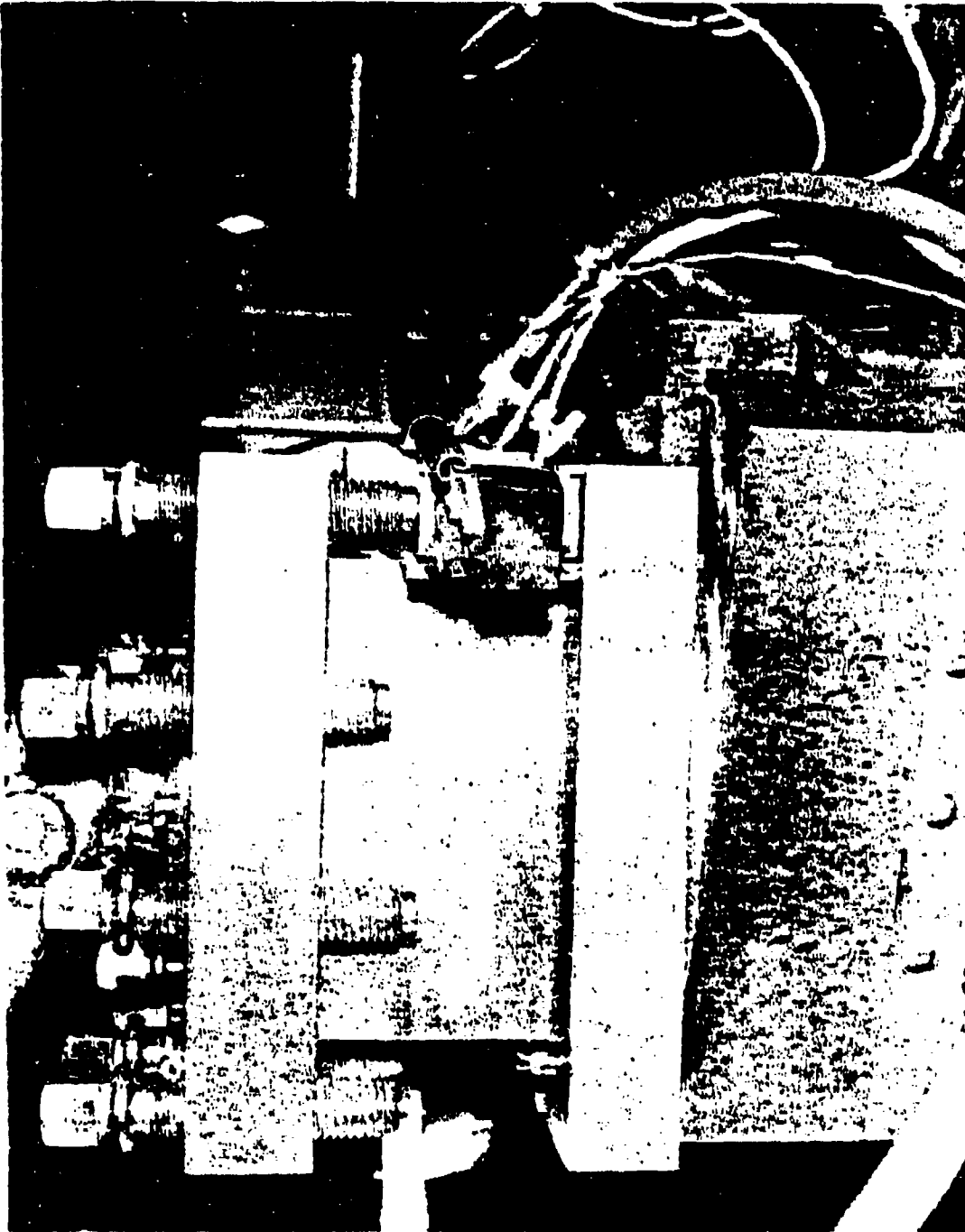


Figure 12. Crimped Cutting Field Nozzle Tip

1-16024-1-1

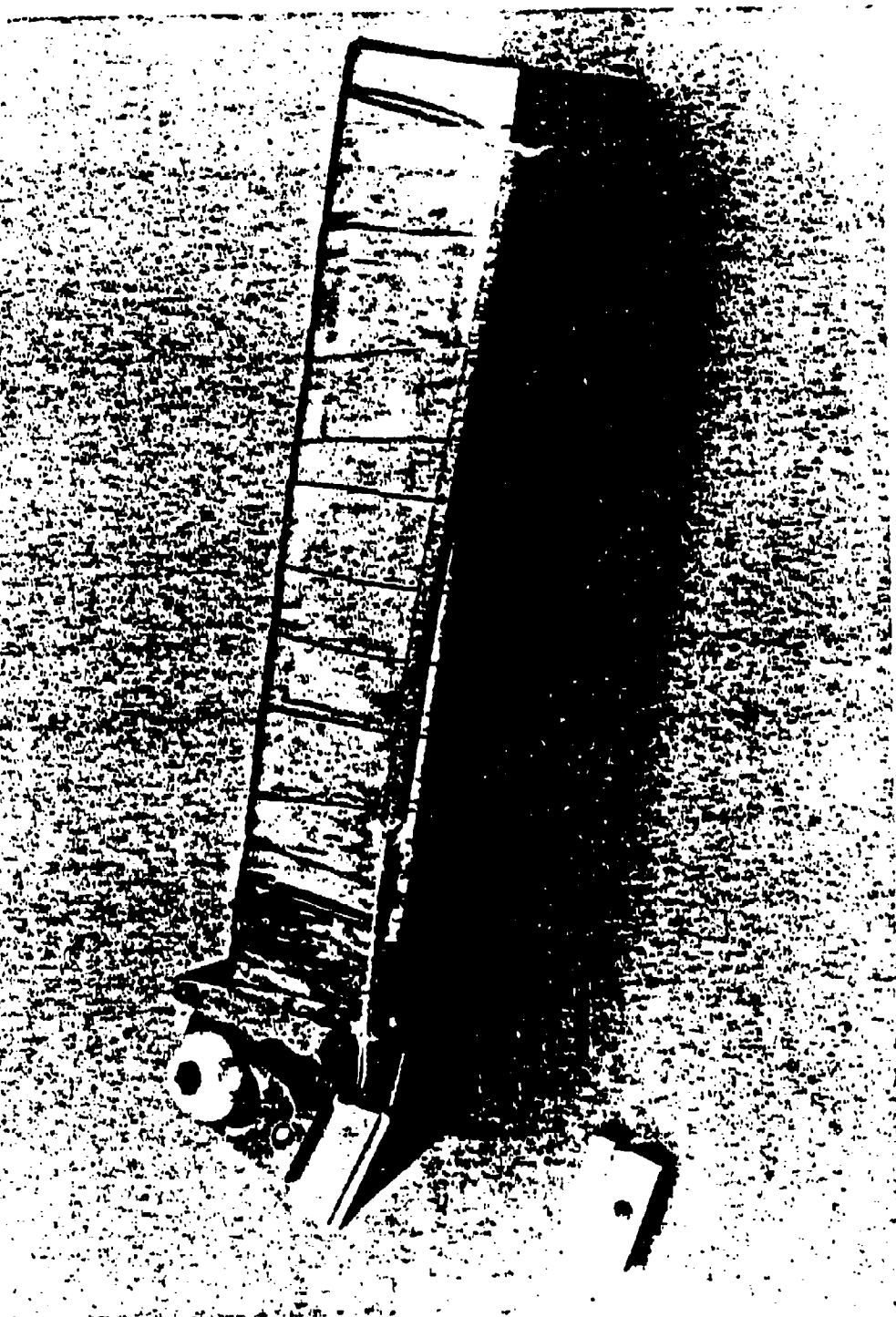


Figure 12. Transverse Clamped by Clasp



In this method, the cutting tool serves as one leg of a thermocouple, and the workpiece serves as the other. The tool-work contact area serves as the hot junction in the thermoelectric circuit. The emf generated thereby the thermocouple is proportional to the cutting temperature, provided the cold junctions are not heated appreciably above room temperature.

The laws of thermoelectric circuits that are applicable here are summarized as follows<sup>7</sup>:

1. The emf in a thermoelectric circuit depends only on the difference in temperature between the hot and cold junctions, and is independent of the gradients in the parts making up the system.
2. The emf generated is independent of the size and resistance of the conductors.
3. If the junction of two metals is at uniform temperature, the emf generated is not affected if a third metal, which is at the same temperature, is used to make the junction between the first two.

The simplest and possibly the most accurate method for calibrating the tool-work thermocouple is illustrated in Figure 15<sup>7</sup>. As shown, the most convenient form of workpiece is as a long chip. This will allow the cold end of the chip to remain near room temperature. It is advisable to grind the end of the tool to a small diameter to insure uniform temperature and to limit the quantity of heat transferred to the cold end of the tool. To further assure that the cold end of the tool remains

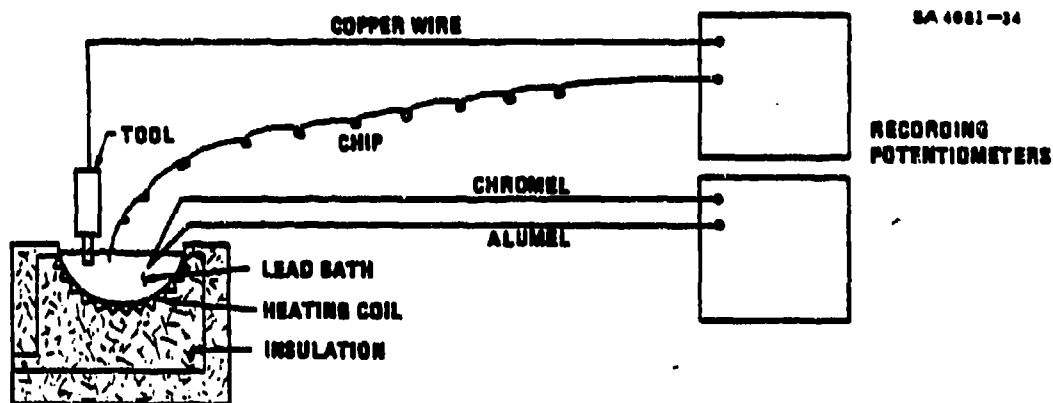


Figure 15. Arrangement for Calibration of Tool-Work Thermocouple

near room temperature, a long tool should be used; or possibly, two similar tools should be clamped together. According to the third law above, the lead bath will have no extraneous effect on the emf measured so long as it remains at uniform temperature. The temperature of the lead bath is measured with a chromel-alumel thermocouple. Temperature-emf calibrations for this pair are well known. Thus, the emf generated

at different temperatures for the unknown tool-chip pair are compared with the emf generated by the known chromel-alumel pair; and calibration curves for the tool-chip thermocouple are plotted, accordingly. Two typical calibration curves<sup>7</sup> are shown in Figure 16.

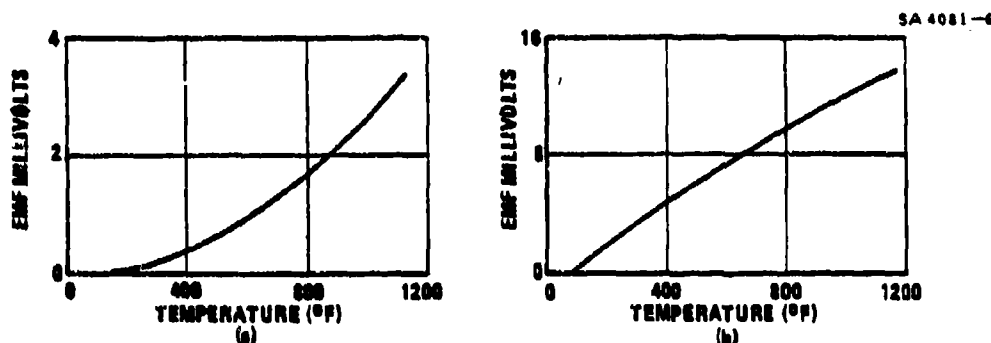


Figure 16. Temperature Calibration Curves for Low Carbon Steel Against (a) 18-14-1 HSS, and (b) K28 Cemented Carbide.

The foregoing method would not be suitable for use with carbide inserts because the inserts cold junction would not remain at room temperature once cutting had commenced. Neither could the aft end of the toolholder be made the cold junction as this would introduce an extraneous material. For either case, parasitic emfs or erroneous readings would be generated. To circumvent this situation, a method described by Sickmann<sup>9</sup>, which combines techniques developed by the University of Illinois and Massachusetts Institute of Technology, was adapted for use in this investigation. The circuit for the method, shown schematically<sup>10</sup> in Figure 17, utilizes a copper-constantan thermocouple lead attached to the inserts so-called cold junction. Over the temperature range which the cold junction would vary, the thermoelectric output of copper and constantan with respect to carbide are nearly equal and of opposite polarity. When these two leads are connected to a variable resistor and the outputs are balanced, the effect of any temperature variation with room temperature at the cold junction will be compensated for or nulled. This method was used to measure cutting temperatures in this study.

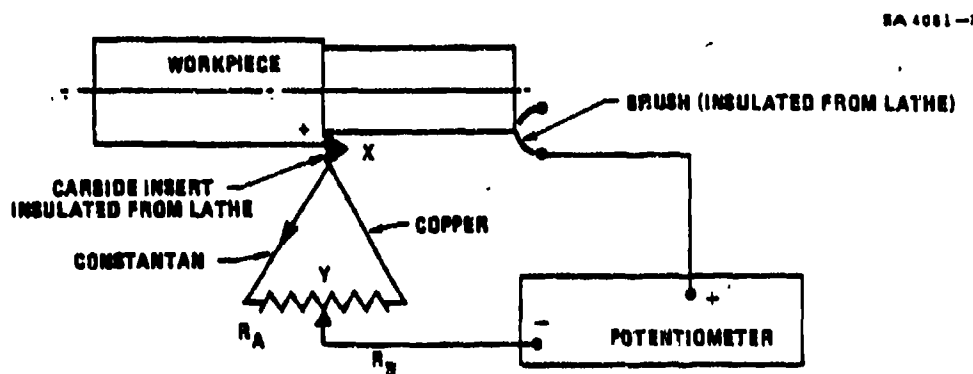


Figure 17. Compensating Circuit

To calibrate thermocouples made up of a carbide insert and a workpiece material for the above method, a technique similar to one described by Siekmann<sup>9</sup> and shown in Figures 18 and 19 was employed. As a first step, the compensating circuit to eliminate intermediate hot junction potentials at the cold junction of inserts was established. In Figure 18, a direct contact to the simulated cutting tip was made with the ideally suited copper-constantan thermocouple. Next, a 100-ohm variable resistor was placed in series with the thermocouple leads and adjusted so that the emf generated by the carbide-copper-constantan thermocouple junction not being at room temperature was balanced out to approximately zero at all temperatures up to 900°F. Next, the carbide-work thermocouple was calibrated as shown in Figure 19. There, the compensating lead, consisting of the copper-constantan thermocouple and the adjusted 100-ohm resistor, was clamped to the carbide rod and connected to the millivoltmeter with a copper wire. The other lead, consisting of a long 2014-T652 aluminum chip taken from the specimen to be machined, was also connected to the millivoltmeter with a copper wire. Both leads were immersed in molten "Cerroband", as illustrated. By varying the temperature of the bath and using a chromel-alumel thermocouple for a reference, calibration curves were determined.

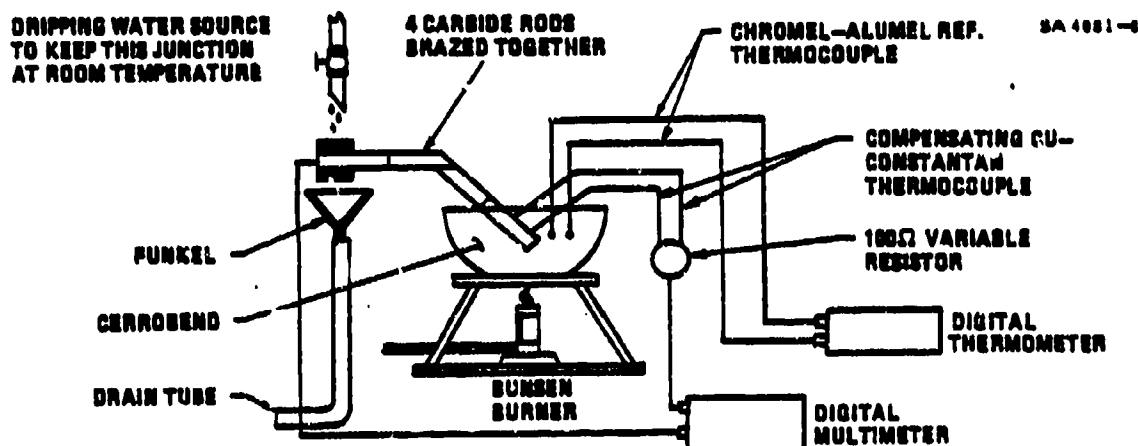


Figure 18. Compensating Circuit Calibration Setup

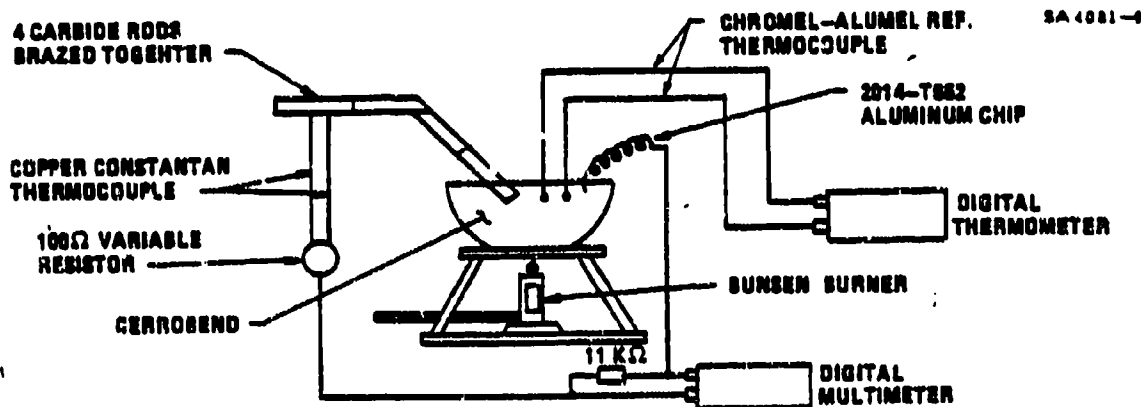


Figure 19. Carbide - Work Calibration Setup

The carbide side of the calibration circuit was made up of four short VC-2 carbide bars which were brazed together as shown in Figure 20 (cf. Figure 19). Brazing presented no thermoelectric problems, as the temperature drop across the brazes was found to be insignificant. The carbide-work-reference junction temperature was not significantly effected by any thermal gradients in the "Cerroband" bath as these were all clamped within very close proximity of each other and carefully lowered into the bath by means of double clamps mounted on the iron stand shown in Figure 20. The temperature of the bath was varied between 150°F and 950°F, because "Cerroband" solidifies near the lower value, and aluminum melts near the higher value. Calibration readings were taken at 50°F intervals during both the heating and cooling cycle as indicated in Table I. Millivolt values at each temperature were averaged to minimize any errors attributable to instrumentation response or thermal gradients. A Honeywell, Model 2206, Visicorder light beam oscillograph, see Figure 21, was used initially to record millivolt outputs for the tool-work thermocouple. However, its use was terminated when it was found that the Fluke, Model 2100A, digital thermometer and the Non-Linear Systems, Model MX-1, digital multimeter could be used to establish values for reference and tool-work thermocouples, respectively, more readily and, perhaps, more accurately. The aluminum chip shown in Figures 20 and 21, which was shorter and tightly curled originally, was annealed to give it ductility. Also shown in Figure 21 are the dripping water source and the drain funnel and tube used to keep the cold junction of the carbide rod in Figure 10 at room temperature. Finally, the entire calibration circuit was electrically insulated from supporting fixtures and the surrounding work area.

TABLE I - TYPICAL CALIBRATION DATA OBTAINED WITH INSERT  
SPG-#1 FOR VC-2 CARBIDE/2014-T652 ALUMINUM  
THERMOCOUPLE

Temperature (°F)	Millivolts		
	Heating Up	Cooling Down	Average
150	—	0.36	0.36
200	0.65	0.65	0.65
250	0.89	0.93	0.91
300	1.19	1.23	1.21
350	1.49	1.55	1.52
400	1.84	1.87	1.85
450	2.17	2.19	2.18
500	2.50	2.52	2.51
550	2.88	2.86	2.87
600	3.18	3.19	3.18
650	3.54	3.55	3.54
700	3.87	3.91	3.89
750	4.25	4.26	4.26
800	4.61	4.62	4.61
850	4.97	4.96	4.97
900	5.31	5.31	5.31
950	5.68	5.63	5.66

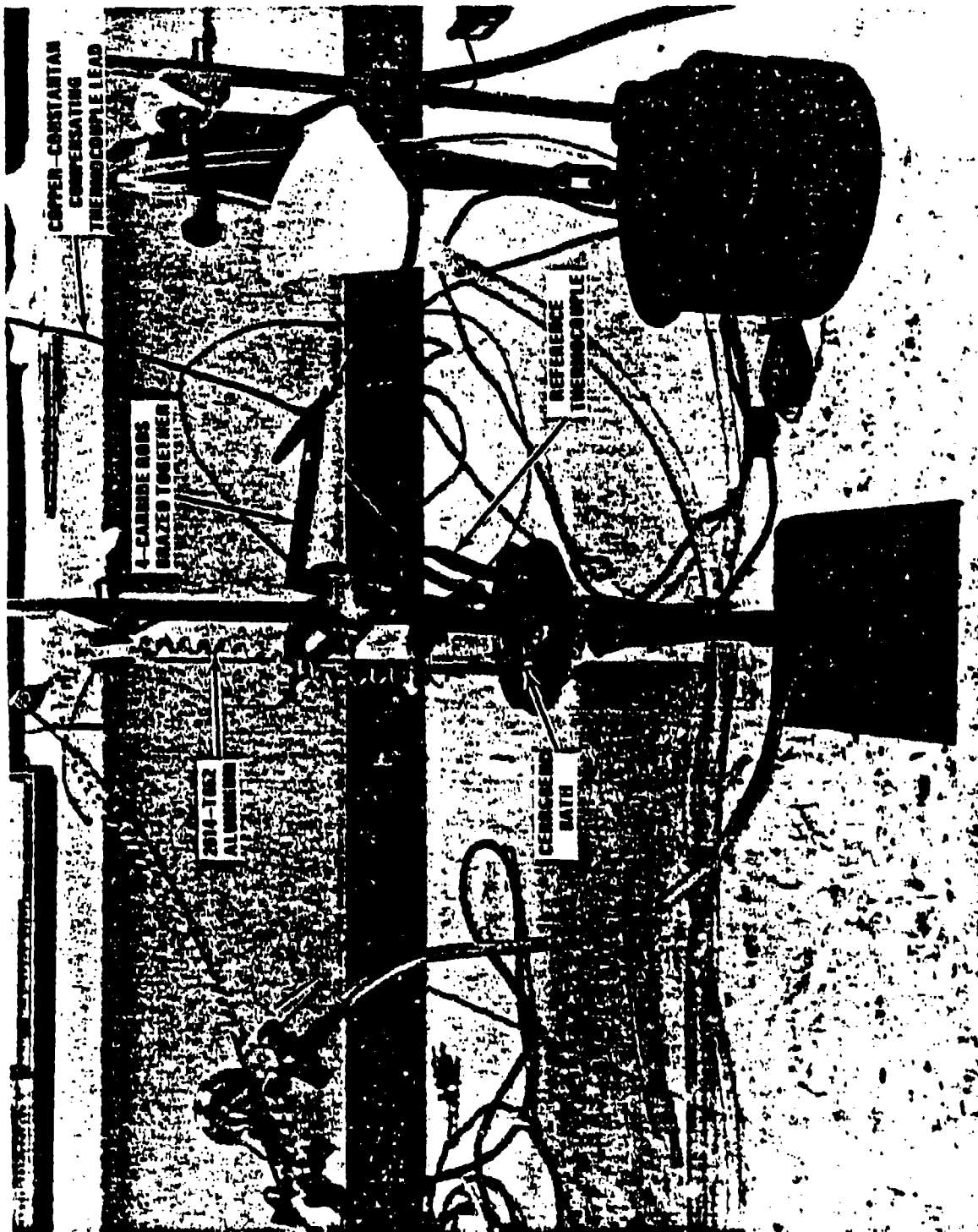


Figure 23. Coddle-Aluminum Thermocouple Setup Calibration

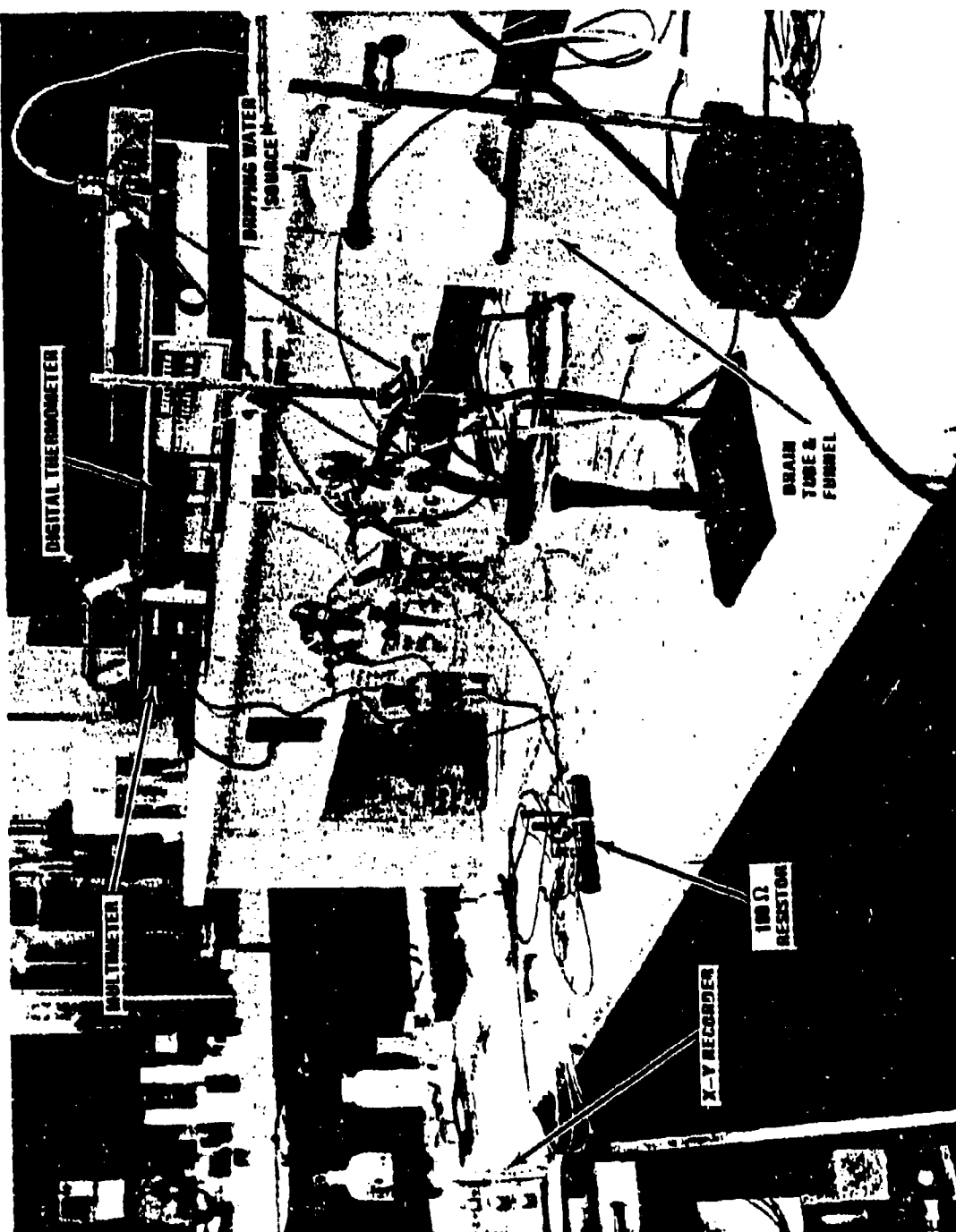


Figure 21. Instrumentation for Carbide - Aluminum Thermocouple Calibration Setup

To be most accurate, the cutter and alloy that will be used in a machining test should also be used to calibrate the cutter-alloy thermocouple. This general rule results from the well known fact that slight differences in the chemical composition of carbide tips or workpieces can significantly effect the emf output of a tool-work thermocouple.<sup>9</sup> For this reason, the carbide rod that was designed to reduce heat buildup at the cold junction (see Figure 20) was replaced with a carbide tip or insert as shown in Figure 22. There, it can be seen that the compensating copper-constantan thermocouple lead has been clamped to the 'cold' junction of the insert. It was found that the wires in this lead would oxidize and emit false signals if heated too many times. As a consequence, the exposed tips of the wires were sanded or clipped after each calibration. With the chip being from the test workpiece, calibrations were performed with this setup for four SEG-623J, two SNG-633, and two SPG-633 inserts. The results, which have been increased 25% to correct for 11,000 ohms resistance subsequently placed in the circuit to minimize possible variations in brush resistance, are given in Table II.

TABLE II - EFFECT OF CUTTER INSERT AND TEMPERATURE  
ON EMF OUTPUT OF VC-2 CARBIDE/2014-T652  
THERMOCOUPLE FOR HIGH IMPEDANCE SYSTEM

Temperature (°F)	Millivolts/Insert Number							
	SEG-1	SEG-2	SEG-3	SEG-4	SPG-1	SPG-2	SNG-1	SNG-2
150	0.36	0.40	0.48	0.46	0.45	0.46	0.46	0.46
200	0.74	0.79	0.84	0.83	0.81	0.81	0.84	0.83
250	1.09	1.15	1.20	1.20	1.14	1.20	1.23	1.19
300	1.46	1.54	1.64	1.51	1.51	1.56	1.64	1.54
350	1.86	1.94	2.04	1.91	1.90	1.99	2.04	1.95
400	2.25	2.31	2.40	2.28	2.32	2.41	2.44	2.35
450	2.64	2.73	2.78	2.70	2.73	2.85	2.88	2.74
500	3.05	3.15	3.20	3.08	3.14	3.29	3.30	3.16
550	3.49	3.58	3.64	3.50	3.59	3.73	3.74	3.59
600	3.86	4.00	4.09	3.91	3.98	4.16	4.20	4.01
650	4.30	4.45	4.51	4.29	4.43	4.64	4.66	4.45
700	4.71	4.88	4.95	4.70	4.86	5.11	5.11	4.91
750	5.18	5.33	5.36	5.08	5.32	5.56	5.58	5.36
800	5.59	5.79	5.80	5.51	5.77	6.05	6.03	5.79
850	6.00	6.23	6.23	5.89	6.21	6.50	6.45	6.25
900	6.45	6.70	6.68	6.39	6.64	6.94	6.94	6.73
950	6.83	7.14	7.11	6.81	7.07	7.36	7.39	7.13

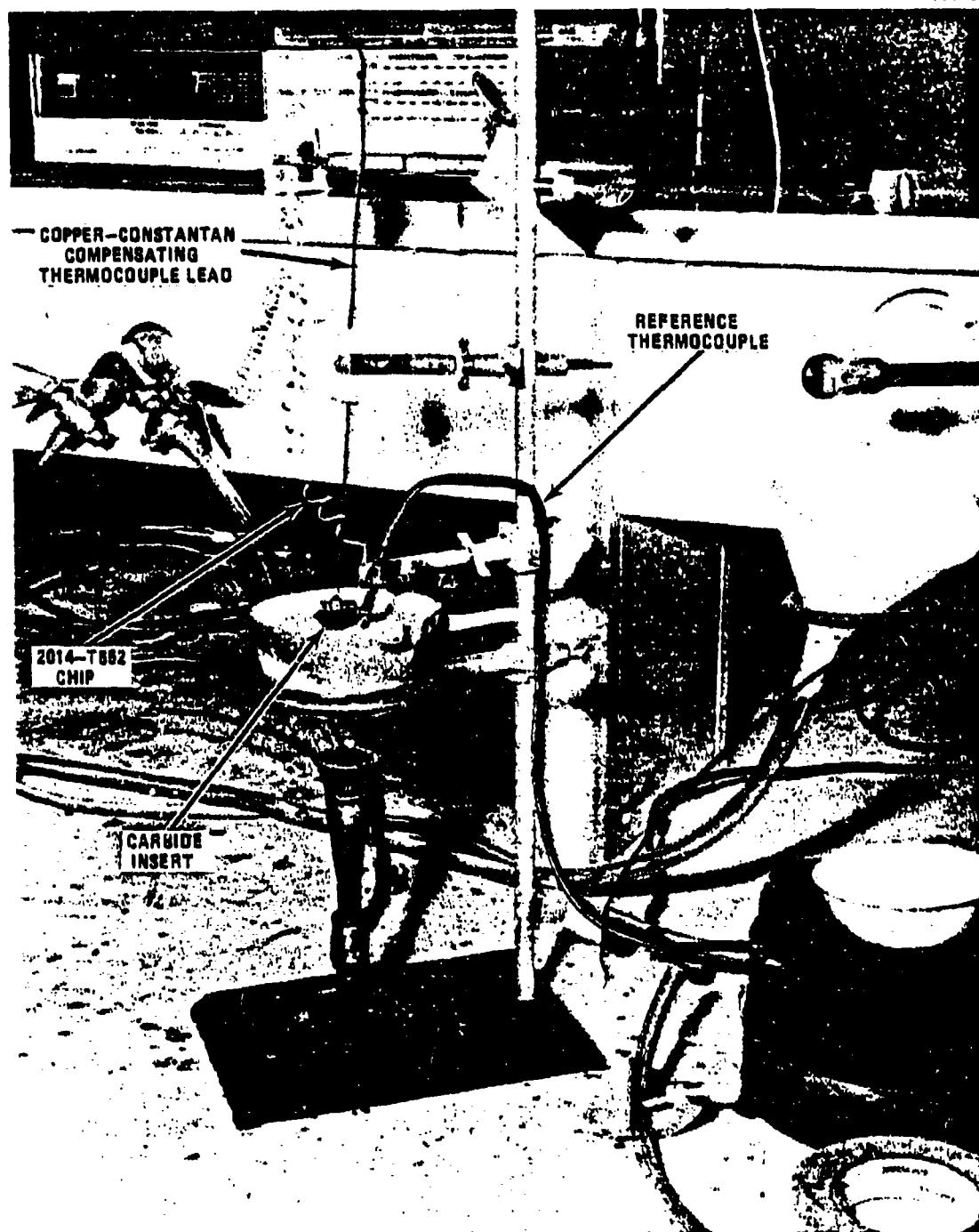


Figure 22. VC-2 Carbide Insert/2014-T662 Aluminum Thermocouple Calibration Setup

As events were to prove, only three of the inserts were used to measure cutting edge temperatures. Calibration curves for these three inserts are presented in Figure 23. There, it can be seen that the curves are linear from about 350° to 950°F. As the curves rise above 950°F and get into the melting range of aluminum, they can be expected to change and to deteriorate. For computational purposes, however, it was assumed that the curves remained linear to 1200°F. Using linear regression, equations for these three calibration curves, when  $MV > 2.0 < 8.1$ , were found to be:

(1) For SEG-4 Insert

$$\theta = 123 (MV) + 120$$

(2) For SPG-1 Insert

$$\theta = 115.5 (MV) + 135$$

(3) For SNG-1 Insert

$$\theta = 111.4 (MV) + 129$$

where:

$\theta$  = Temperature, degrees Fahrenheit  
 $MV$  = Millivolts.

Slopes and intercepts for the unplotted curves are included in Table III. A comparison of these values and data in Table II indicates that the SEG-2, SPG-1, and SNG-2 inserts have the same exact chemical composition. The chemical composition of the SEG-3 insert may be identical to these, but the chemical composition of the chemically-alike SPG-2 and SNG-1 inserts is not. Based on these and similar observations, it can be concluded that all the carbide inserts in a standard package do not necessarily have the same chemical composition and, therefore, calibration curves. Calibration variations, as shown in Figure 23, can produce temperature errors up to 80°F. For these reasons, it is important in close tolerance work that the correct calibration for a given insert be known and not assumed.

TABLE III - MATHEMATICAL DESCRIPTION OF CALIBRATION CURVES  
 FOR INSERTS WHEN  $MV > 2.0$

Property	INSERT							
	SEG-1	SEG-2	SEG-3	SEG-4	SPG-1	SPG-2	SNG-1	SNG-2
Slope (m)	119.5	114.5	117.0	123.0	115.5	110.5	111.4	114.6
Intercept (b)	133	137	121	120	135	135	129	135

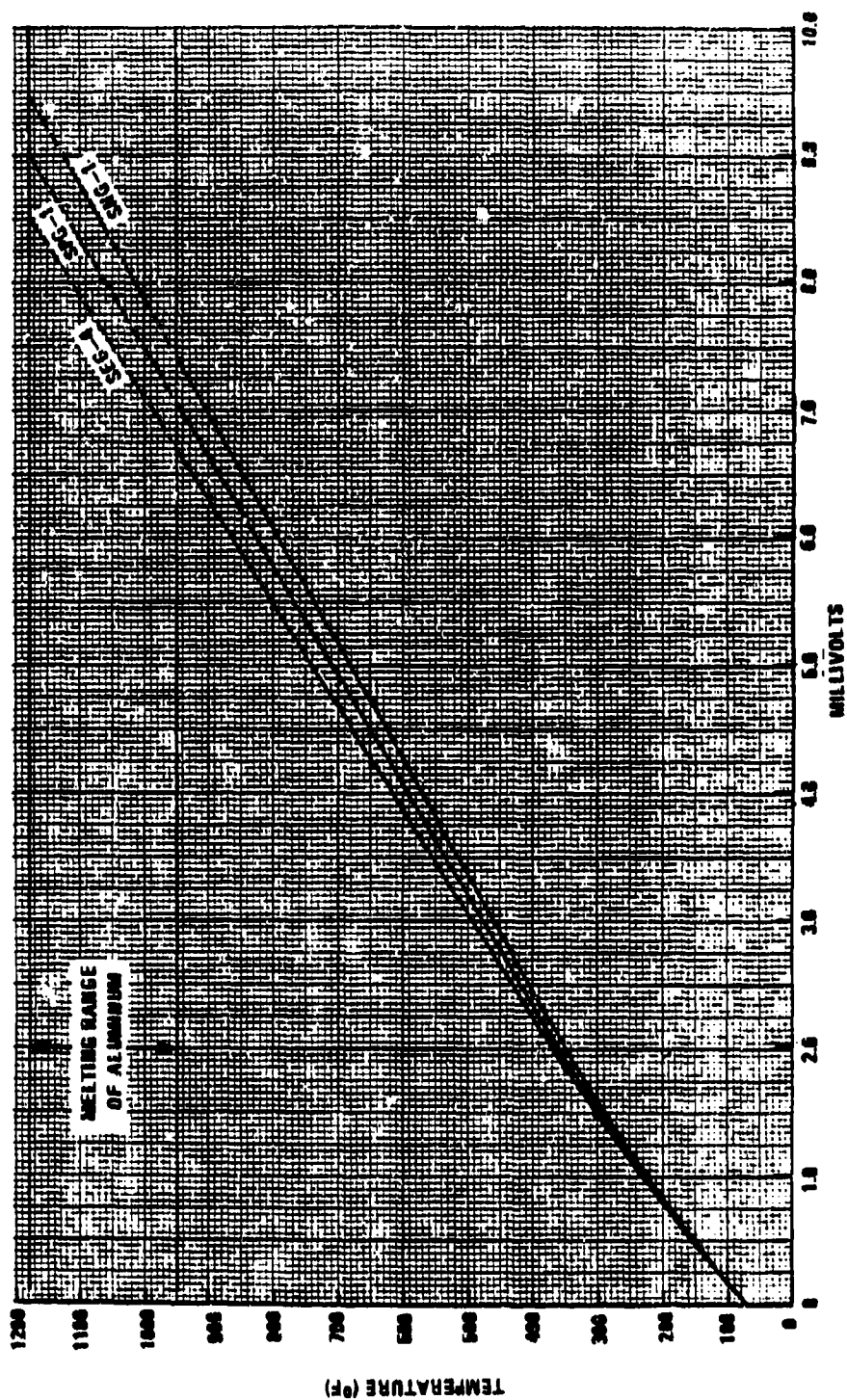


Figure 23. Thermocouple Calibration Curves for VC-2 Carbide Inserts and 2014-T652 Aluminum

### 3.4 Experimental Procedure

After clamping the aluminum cylinder securely in the lathe with an insulated chuck and combination brush-draw bar device, it was lightly turned to provide a concentric surface. The tool to be experimented with was then clamped in an insulated toolholder so that side or radial cuts could be made. A turret, box toolholder was used in this case to support the cutting tools so that carbide inserts and thermocouple wires could be examined and replaced without having to remove the tool from its holder. The copper-constantan thermocouple lead was then clamped to the carbide insert, and connections at the other cold junction of the toolwork thermocouple; i.e., the mercury vessel, were completed.

Prior to connecting the thermocouple leads to the x-y oscillograph recorder, the recorder was calibrated. This was accomplished with the help of a variable resistance, battery powered, millivolt source and a digital multimeter. With this equipment, discrete millivoltages were passed through the recorder, and their traces were recorded as shown in Figure 24. When distances between the millivolt traces were measured, it was found that their variation was, essentially, linear with millivolt input. As a consequence, an equation was developed to convert trace displacement measurements to millivolts. In all, this calibration procedure was repeated on four separate occasions for different conditions. The calibration equation developed for use with the mercury brush system and the principal one was:

$$MV = 0.598 \lambda$$

where:

$$MV = \text{Millivolts}$$

$$\lambda = \text{Distance between investigated and zero millivolt traces (centimeters).}$$

The thermocouple leads were connected to the recorder and the whole system was checked with a multimeter, a process that was to be repeated several times, to assure that it was insulated from other systems.

To commence measuring cutting temperatures, the proper feed and depth of cut were first set on the lathe. Afterwards, the lathe was started, and the cutting speed was adjusted to a desired value with a rheostat control. Just prior to engaging the lathe feed mechanism, the recorder and cutting fluid, if one were used, were activated. The tool was then started and allowed to cut for ten to twenty seconds; during which time, the emf (millivolts) was recorded with the oscillograph as exemplified in Figure 25. The average displacement from zero of such an emf trace was then measured and converted to temperature with the aid of Figures 23 and 24 or their corresponding equations. Between each run, it was often necessary to remove a built-up-edge (BUE) formed between the cutting edge and chipbreaker. Failure to do so could have resulted in an

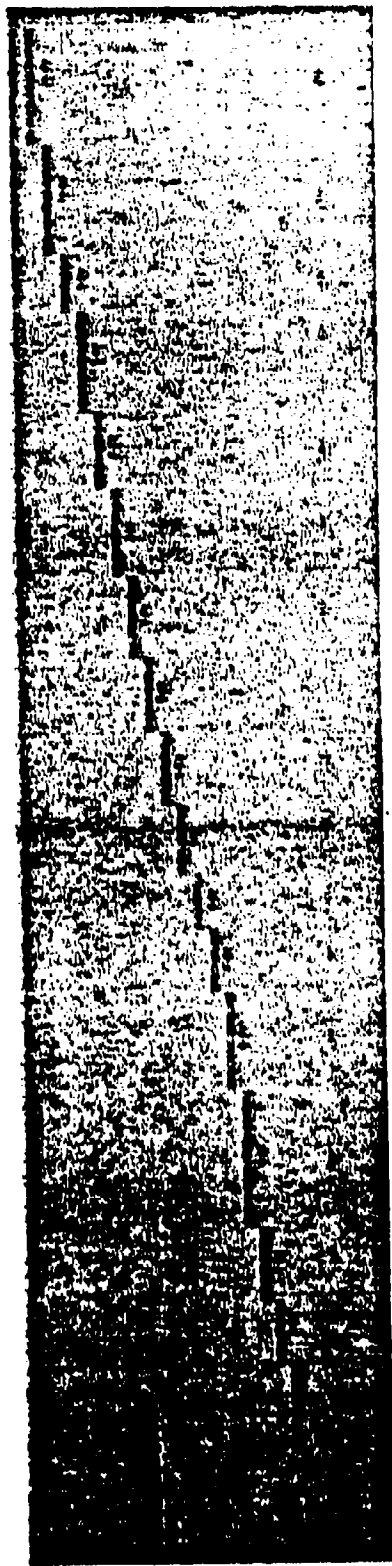


Figure 24. Scanning Calibration Showing Minimum Budget Per Coordinate

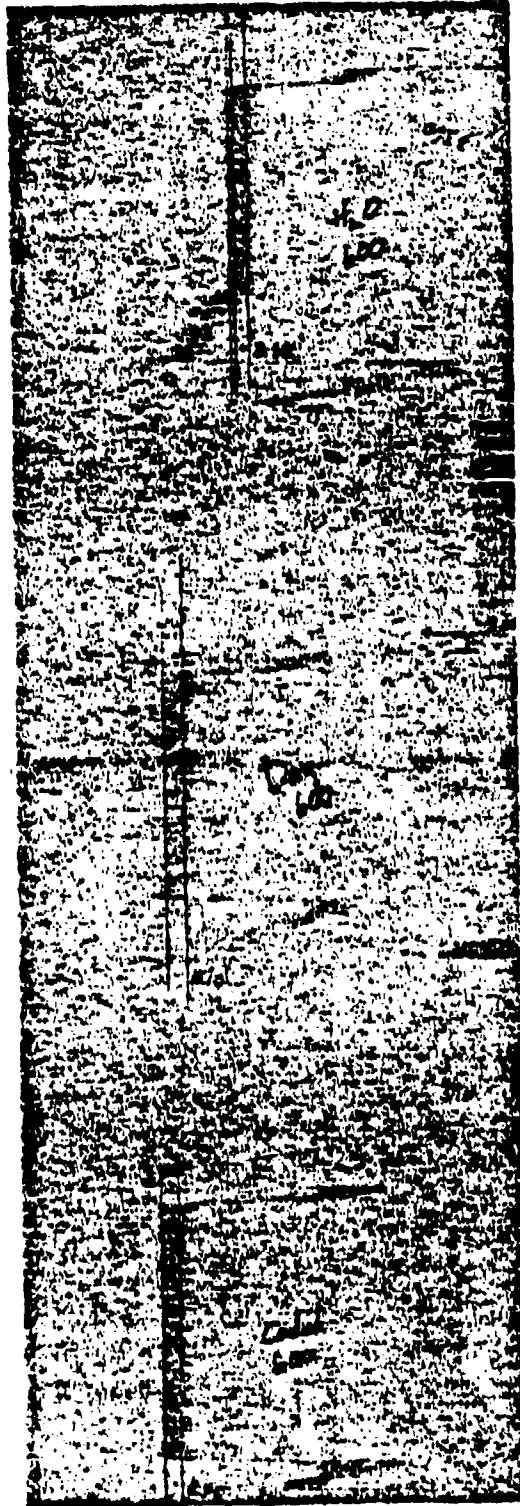


Figure 25. Typical Recording of Tool-Work Thermocouple Output

altered cutter geometry or material and, therefore, an incorrect temperature measurement.

Repeating this procedure for all investigations, the temperature output from the tool-chip thermocouple was determined for C-2 carbide cutting tools having side rakes of  $-5^\circ$ ,  $5^\circ$ , and  $13^\circ$  and back rakes of  $-5^\circ$ ,  $0^\circ$ , and  $5^\circ$ , respectively, operated at cutting speeds ranging from 100 to 4,700 feet/minute and a feed rate of 0.0075 inch/revolution. Similar cutting temperature determinations were established for a 0.015 inch/revolution feed rate and for four cutting fluids, one of which was water. Depth of cut was maintained constant at 0.100 inch on the diameter to conserve material.

Several reruns were required to cover the different brush systems and electrical systems used and to substantiate paradoxical data obtained from the cutting fluid studies. Additionally, aluminum, being a material that tends to gall, seize, and weld, proved troublesome from the standpoint of reproducing cutting temperature data. To provide enough material to complete the study, two forged 2014-T652 aluminum cylinders, approximately 20 inches inner diameter by 22 inches outer diameter by 12 inches long, were procured. Both cylinders were fabricated from the same mill run to insure uniform chemical and physical properties. Data reproducibility among the various systems was found to be good after obvious discrepancies were eliminated. In the final analysis, only data developed with the mercury brush system was used. Reproducibility with this system was found to be within approximately plus or minus 0.3 millivolt ( $\pm 30^\circ\text{F}$ ).

### 3.5 Effect of Speed and Geometry on Cutting Temperature

The change in cutting edge temperature with cutting speed is shown in Figure 26 for three different lathe cutter geometries. The curves in that figure have been normalized to the extent that each was plotted on log-log paper, and the mathematical expression for each was determined by linear regression. The equations thus derived were used to help construct the curves shown in Figure 26 and are superimposed thereon for reference. Also superimposed on that figure is the melting range or spectrum for aluminum and its alloys. From that expanded plot, it is seen that each cutting temperature curve tends to peak near the melting point of aluminum. This is partly understandable, because it would not be expected that the cutting temperature of a material would exceed its melting temperature. The fact that one of the curves appears to pass through the melting range can probably be explained by one of two reasons. First, the melting temperature of the particular alloy used in this investigation may have been approximately  $1,200^\circ\text{F}$ . Secondly, data points for that portion of the curve lying above  $950^\circ\text{F}$  were calculated by extrapolating calibration curve data (cf. Figure 23), a dubious procedure at best; therefore, the slope of that portion of the curve lying in and above the melting range may need to be corrected downward. In any event, these curves and melting spectrum tend to indicate that the cutting temperature for aluminum alloys will probably never exceed  $1,200^\circ\text{F}$ .

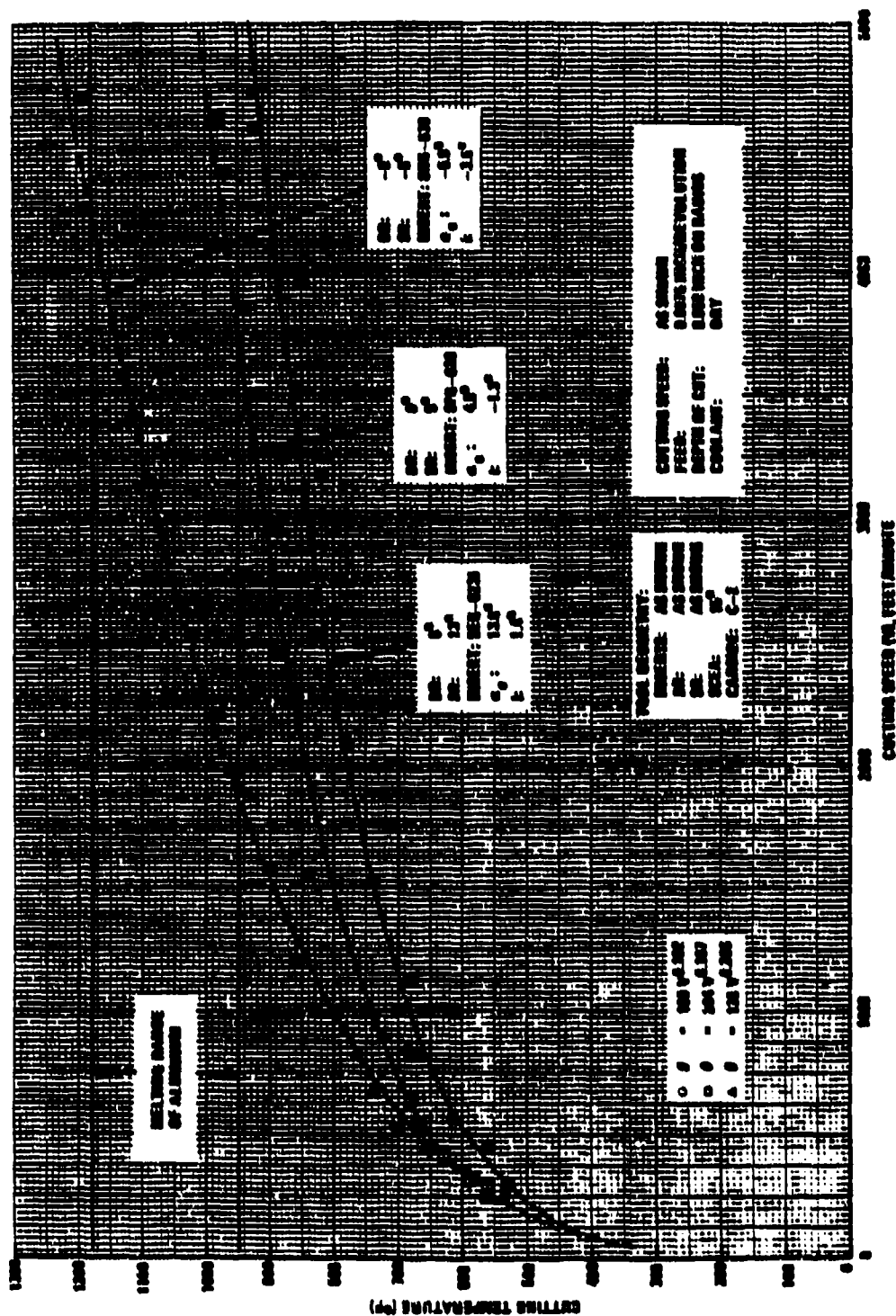


Figure 2A. Effect of Cutting Speed and Cutter Geometry on Cutting Temperature When Turning 2014-T62 Aluminum

Previously, Datsko<sup>11</sup> had found for a wide range of materials that the cutting velocity producing a 60-minute tool life ( $V_{60}$ ) with high speed steel (HSS) cutters would generate a corresponding cutting edge temperature of  $975^\circ \pm 25^\circ\text{F}$ . Similarly, for a cutting velocity yielding a 20-minute tool life ( $V_{20}$ ), the corresponding cutting edge temperature would be  $1,025^\circ \pm 25^\circ\text{F}$ . At a cutting edge temperature of  $1,200^\circ\text{F}$ , tool life would, by extrapolation, be approximately 0.5-minute. Based on these and the above observations, it was concluded that: (1) since aluminum is normally turned with cutters having the geometries shown in the lower two curves, carbide cutters, if not HSS cutters, can withstand the cutting edge temperatures developed when machining aluminum alloys at very high velocities, and (2) a slight change in cutting edge temperature; e.g.,  $50^\circ\text{F}$ , can have a significant effect on cutter life.

Each of the curves in Figure 26 follow another similar pattern. That is, the cutting temperatures associated with each rise sharply between cutting speeds of zero and 250 feet/minute, moderately between cutting speeds of 250 and 1,000 feet/minute, and slowly between cutting speeds of 1,000 and 5,000 feet/minute. Additionally, the two lower curves appear to be trying to plateau or level off at cutting speeds beyond 1,500 feet/minute. At that cutting speed, the corresponding cutting edge temperature for each reaches 80% of the value it attains at 5,000 feet/minute and 70% of the value it would probably attain at 10,000 feet/minute. Thus, it was concluded that most of a cutting edge temperature rise occurs at low rather than high cutting speeds and that this is one feature or characteristic which does much toward opening the door to high speed machining.

The plateauing effect observed for the curves in Figure 26 suggested that cutting edge temperatures may cease to rise once corresponding cutting speeds have reached some unique, high velocity. This concept was explored with the lower curve in Figure 26. There, it was assumed that the cutting edge temperature would continue to rise slowly toward the melting temperature ( $1,200^\circ\text{F}$ , maximum) of the aluminum alloy. Using the equation for this curve and extrapolating, the theoretical cutting speed that would generate a cutting edge temperature of  $1,200^\circ\text{F}$  was found to be 19,600 feet/minute. Beyond that cutting speed, it would not be reasonable to expect a further cutting edge temperature rise; because such a resultant cutting edge temperature would have to exceed the melting temperature of the aluminum workpiece, an unlikely occurrence. Since it is unlikely that cutting edge temperature will increase beyond  $1,200^\circ\text{F}$  in this case and this temperature is reached at a cutting speed of approximately 19,600 feet/minute, it was postulated that there is a unique cutting speed at which cutting edge temperatures cease to rise. If this be the case, several interesting possibilities arise. For one, it would be theoretically possible in this example to continue turning at infinitely higher speeds than 19,600 feet/minute, because there should be no further rise in cutting edge temperature and, therefore, no further reduction in cutter life. Another interesting possibility involves cutter geometry. The cutter geometries represented by

the top two curves in Figure 26 should, based on the curve equations, generate a cutting edge temperature of 1,200°F at cutting speeds of approximately 4,500 and 13,000 feet/minute. At cutting speeds below 19,600 feet/minute, both these cutter geometries should yield shorter tool lives than the cutter geometry represented in the lower curve; because both would generate higher cutting edge temperatures. Conversely, for all cutting speeds in excess of 19,600 feet/minute, all three cutter geometries should generate the same upper limit, cutting edge temperature of approximately 1,200°F and, theoretically, the same tool life. However, there are other factors which effect tool life besides cutting temperature. One of these would be cutter strength, and it would not be surprising to find that the superior strength offered by the cutter geometry for the top curve would lead to a superior tool life when all are operated at cutting speeds above 19,600 feet/minute. Similarly, the cutter geometry for the middle curve might yield the next best tool life. Thus, in effect, it may be found that the influence of cutter geometry on tool life tends to reverse at cutting speeds near that at which cutting edge temperatures cease to rise and that there may be tradeoffs at lesser speeds. While no reversing trend (cf. Figure 4) for cutting edge temperatures was observed in this limited velocity study, the plateauing effect that was evidenced suggests that such is possible and that infinitely high cutting speeds are feasible for aluminum alloys.

The influence of cutter geometry on providing cutting edge temperature relief is clearly demonstrated in Figure 26. As shown in that figure for a cutting speed of 3,000 feet/minute, cutting edge temperature was decreased from 1,230°F to 1,003°F to 920°F by switching from a double negative rake (-5° back rake (BR), -5° side rake (SR)) cutter to a positive rake (0° BR, 5° SR) cutter to a double positive rake (5° BR, 13° SR) cutter, respectively. Based on the Datsko findings reported above, these cutting temperature improvements would be expected to increase tool life for HSS cutters from nil to well over 60-minutes. When cutter geometry data in Figure 26 were converted to effective (true) rake angles and replotted as shown in Figure 27, the effect of cutter geometry on cutting temperature became more meaningful. In the latter figure, it is seen that cutting edge temperatures decrease as effective rake angles are increased. However, increasing effective rake angles has the adverse effect of weakening cutters. Thus, to the extent that adequate cutter strength is maintained, it is evident from Figure 27 that cutter geometry can be progressively manipulated to increase tool life by reducing cutting edge temperatures.

Since end mills generally have effective rake angles ranging from 10° to 34°, it can be concluded from Figure 27 that this type of cutter will produce minimal cutting edge temperatures. Additionally, milling cutter teeth can operate at significantly higher peak temperatures than can a lathe tool<sup>7</sup>. This happens because the rest period that obtains between cuts in an intermittent operation such as milling allows the temperature to drop very rapidly when cutting ceases. Based on these and Datsko's observations, it was concluded that aluminum alloys can be satisfactorily

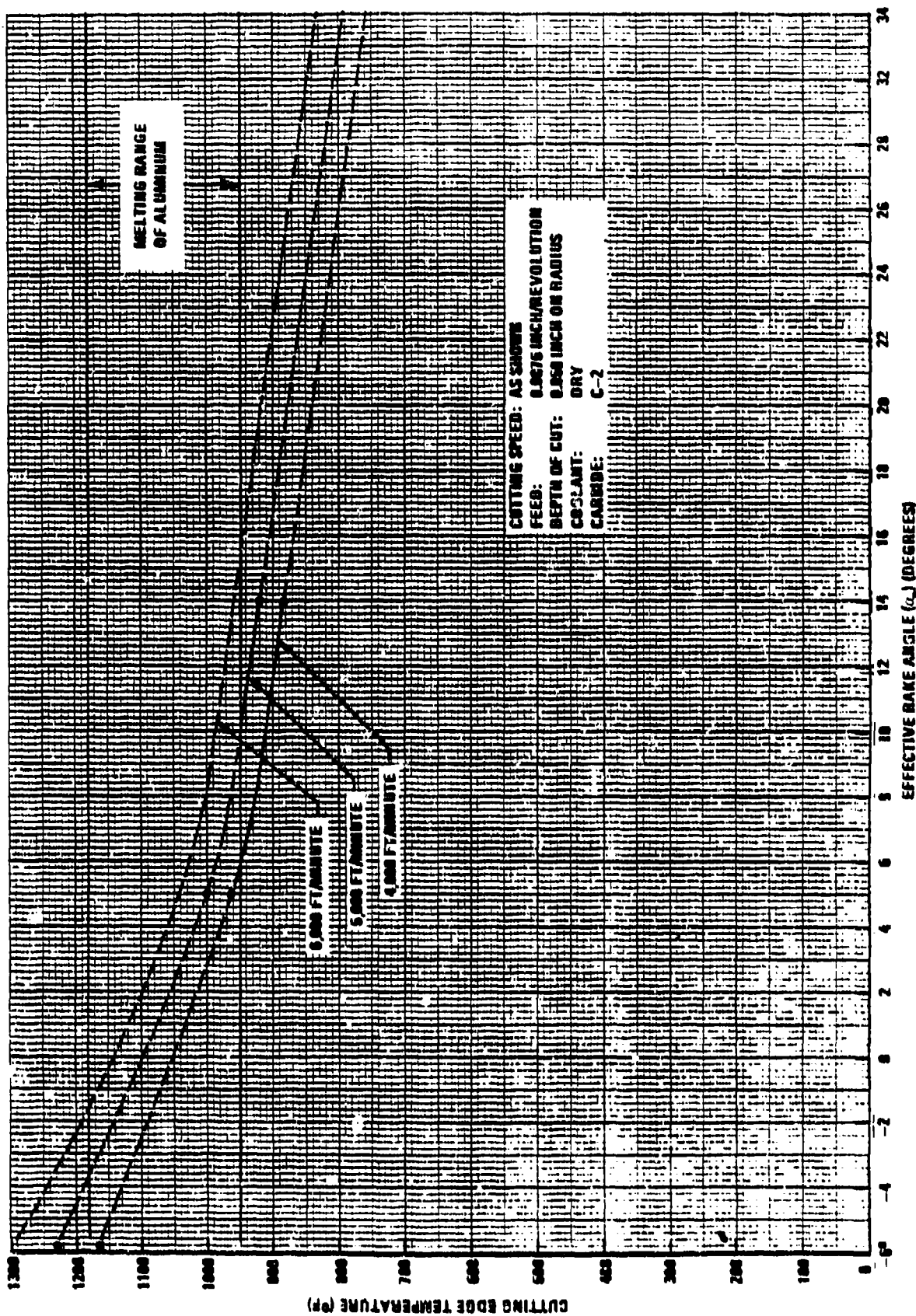


Figure 27. Effect of Cutter Geometry on Cutting Temperature When Turning 2014-T652 Aluminum

milled at cutting speeds to at least 5,000 feet/minute with high speed steel end mills and no cutting fluid. While this conclusion subsequently proved to be substantially correct, it was found that cutting fluids which help maintain cutter clearance, by minimizing aluminum buildup on cutter clearance angles or flanks, improve the life of end mills appreciably.

### 3.6 Effect of Feed Rate on Cutting Temperature

The variation in cutting temperature with feed rate is shown in Figures 28 and 29. As before, the curves in both plots were normalized to the extent that log-log or linear plots were made for each, and mathematical expressions were determined for all by linear regression. In turn, the derived equations were used to help construct the curves and were superimposed on the plots along with the melting range for aluminum alloys.

It is seen in Figure 28 that feed rate does not have a large effect on cutting temperatures for aluminum alloys. For instance, lowering the feed rate 0.001 inch/revolution will only reduce cutting temperatures about 12°F, or cutting the feed rate in half will only reduce cutting temperatures about 100°F. While this does not appear to be much of a reduction, it should be remembered from Datako's work that a 50°F drop in cutting temperature can triple cutter life, a worthwhile gain. No exact reason can be given for the data scatter shown for feed rates between 0.006 and 0.0075 inch/revolution. These points were established first, and it may be that the recording system had not become stabilized yet. In any event, it is believed that the scattered data points are invalid and that the linear data points are correct. The results of this study demonstrate that some cutting temperature relief for aluminum alloys can be obtained by reducing feed rates at normal cutting speeds.

The plateauing effect observed for the curves in Figure 26 is seen again in Figure 29, where changes in cutting temperature with cutting speed are shown for feed rates of 0.0075 and 0.015 inch/revolution. Again, both curves tend to peak near the melting point of aluminum and to plateau at cutting speeds beyond 1,500 feet/minute. The heavier (0.015 inch) feed rate curve plateaus faster than the lighter (0.0075 inch) feed rate curve, and the two will converge near the melting point of the aluminum alloy. Based on the curve equations and Figure 26 results, the two curves will converge near a cutting temperature of 1,200°F and a cutting speed of 19,000 feet/minute, the theoretical points in this instance at which cutting temperatures cease to rise. If this be the case, doubling the feed rate at cutting speeds beyond 19,000 feet/minute may not have any further effect on cutting temperatures for aluminum alloys; and this would raise another interesting possibility. That is, to the extent that a cutter material which can withstand a 1,200°F temperature and adequate cutter strength, machine rigidity, horsepower, jig and fixture strength, and et cetera are provided, it would be theoretically possible at cutting speeds beyond 19,000 feet/minute to continue turning aluminum at infinitely higher feed rates than 0.0075 inch/revolution. Such a capability would greatly improve metal removal rates and would be made possible because there would be no further rise in cutting temperature and, therefore, no further reductions in cutter life at such speeds and feeds.

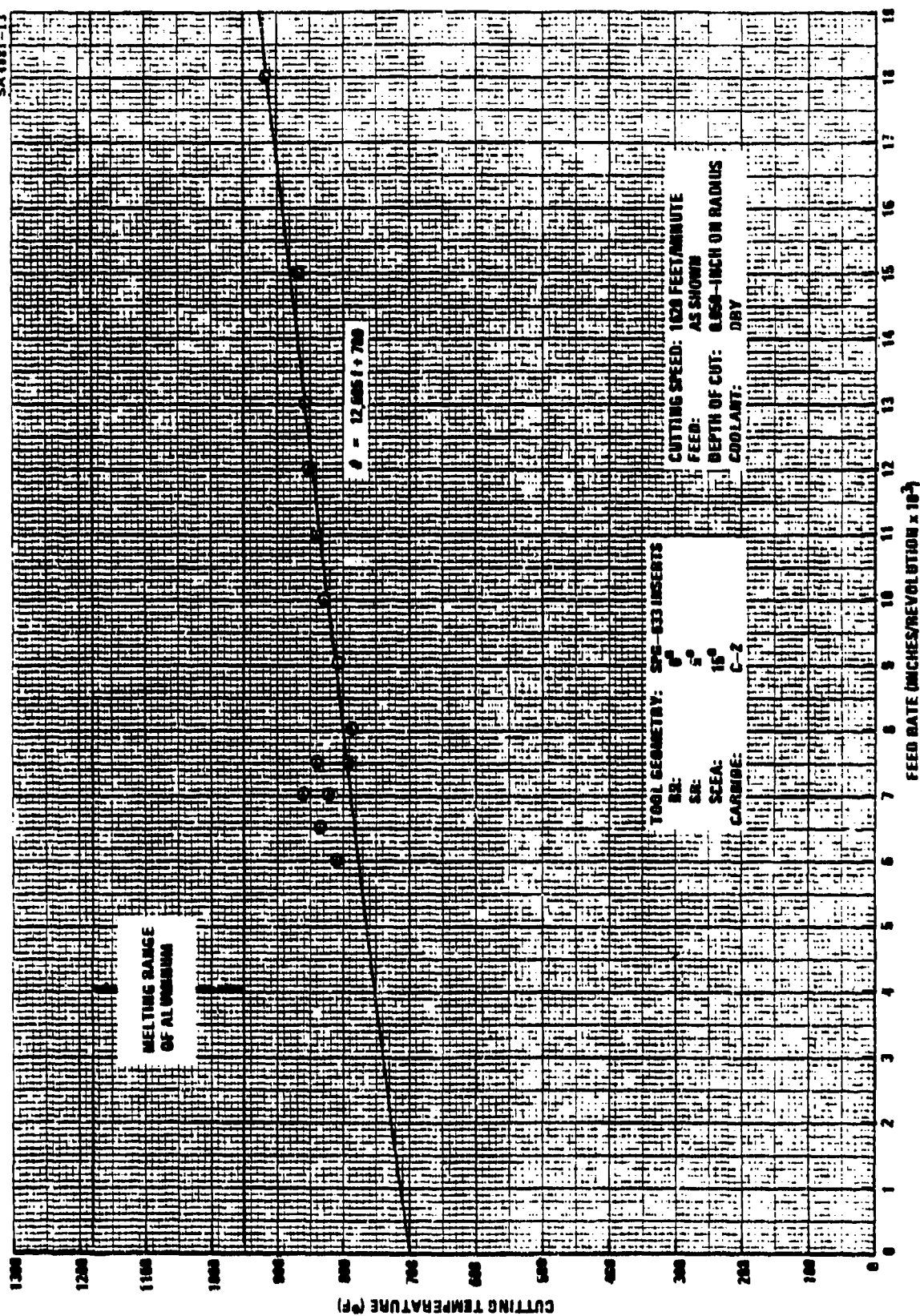


Figure 20. Effect of Feed Rate on Cutting Temperature When Turning 2014-T652 Aluminum

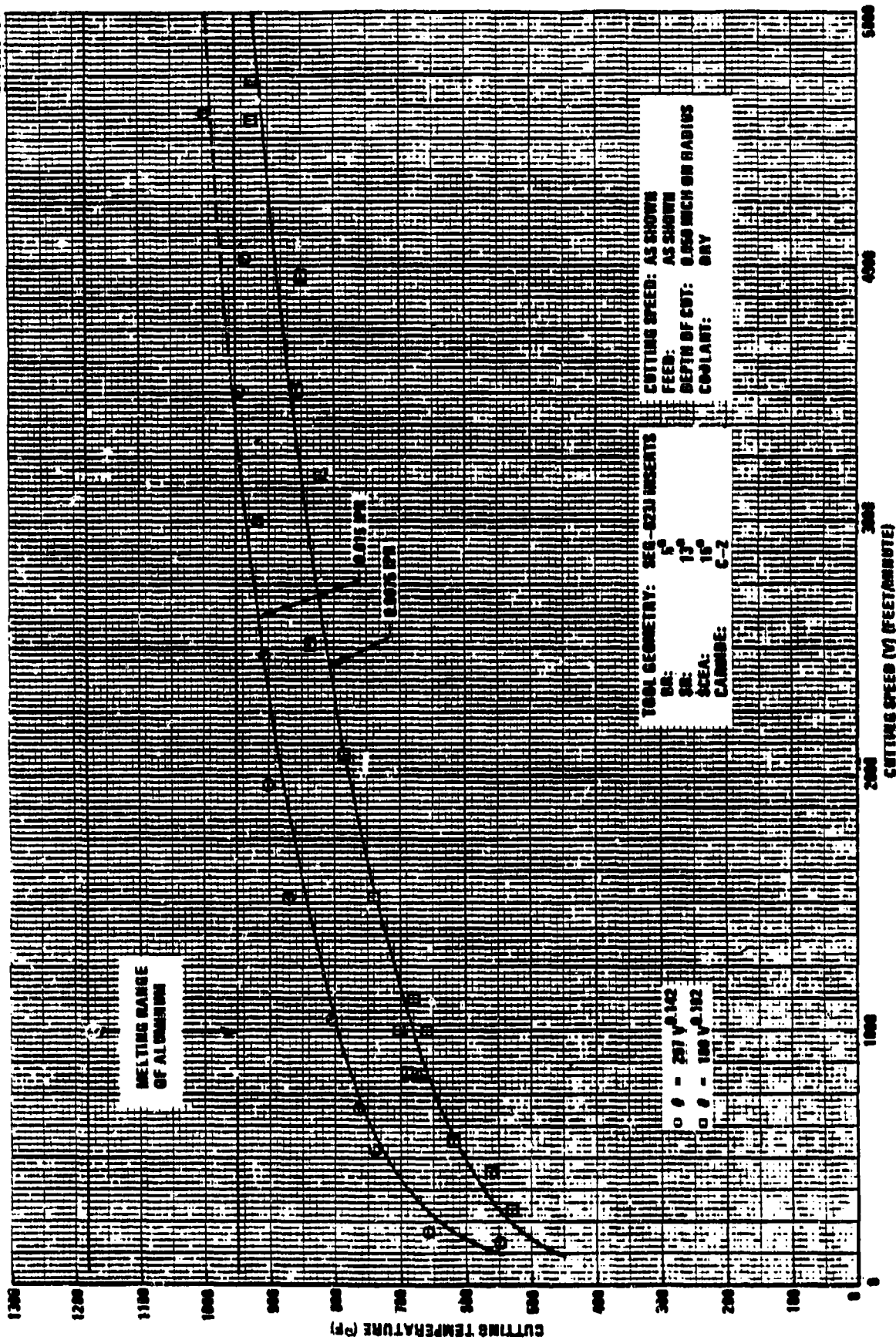


Figure 29. Effect of Cutting Speed and Feed Rate on Cutting Temperature When Turning 2014-T662 Aluminum

### 3.7 Effect of Cutting Fluids on Cutting Temperatures

All of the cutting edge temperature studies above were conducted without cutting fluids. While no prohibitive thermal restraints to the high speed milling of aluminum alloys surfaced as a result of dry cutting, it was decided to ascertain what cutting edge temperature relief cutting fluids might provide. In line with that investigation, it was also decided to evaluate cutting fluids in the hope that one cutting fluid might provide superior cooling to the others. The cutting fluids selected were Codol 0741 (Stuart Oil Company), Coolant B, and Coolant C (names available upon request). Of these, Codol 0741 was the cutting fluid then used at Vought Corporation. Each of these cutting fluids was mixed with water at a ratio of 1:30, as recommended by the respective manufacturers, and applied as a flood coolant (cf. Figure 10). Tap water was selected as a reference cutting fluid and was tested along with the other three cutting fluids.

Variations in cutting edge temperature with cutting speed and the different coolants are given in Figures 30 through 33. For comparative purposes, variations obtained when no cutting fluid was used are presented in Figure 34 (cf. Figure 26). Again, linear regression was used to obtain a mathematical expression for each curve. Unlike the plots obtained from dry cutting data, the plots for the cutting fluid data were linear up to a cutting speed of approximately 1,500 feet/minute; at which point, the curves changed directions and were again linear. For this reason, mathematical expressions were developed for both legs of these curves, as well as the whole curve. The results obtained from all of these analyses are summarized in Figure 35.

It is seen in Figure 35 that the commercial cutting fluids did not prove to be effective in this study for reducing cutting edge temperatures. While such a result is still difficult to accept, none of the efforts made to reverse it, including installing a mercury brush system in the thermoelectric circuit, were successful. Water was the only beneficial coolant found among the three commercial coolants as can be deduced from the table superimposed on Figure 35. Values shown in that table were derived with the statistically developed cutting temperature equations which were also superimposed on the figure for convenience. These equations should compensate for some of the inherent inaccuracies (about  $\pm 30^\circ\text{F}$ ) of the thermoelectric measuring system. Of the commercial cutting fluids, Codol 0741 appeared to be the best coolant, and it was closely followed, in turn, by Coolant B and Coolant C.

### 3.8 Conclusions

Since aluminum alloys melt at a temperature between  $950^\circ\text{F}$  and  $1,180^\circ\text{F}$  and the cutting edge temperature curves developed in this study tend to peak in that range at high speeds, it is predicted that  $1,200^\circ\text{F}$  will be the approximate upper limit for cutting edge temperatures when machining aluminum alloys. Several cutter materials exist which can withstand that

**TOOL GEOMETRY**

DR: 5°  
 SR: 13°  
 SCEA: 19°  
 INSERT: SEG-023J  
 CARBIDE: C-2

CUTTING SPEED: AS SHOWN  
 FEED: 0.0075 INCH/REVOLUTION  
 DEPTH OF CUT: 0.060 INCH (RADIUS)  
 CUTTING FLUID: WATER, FLOOD

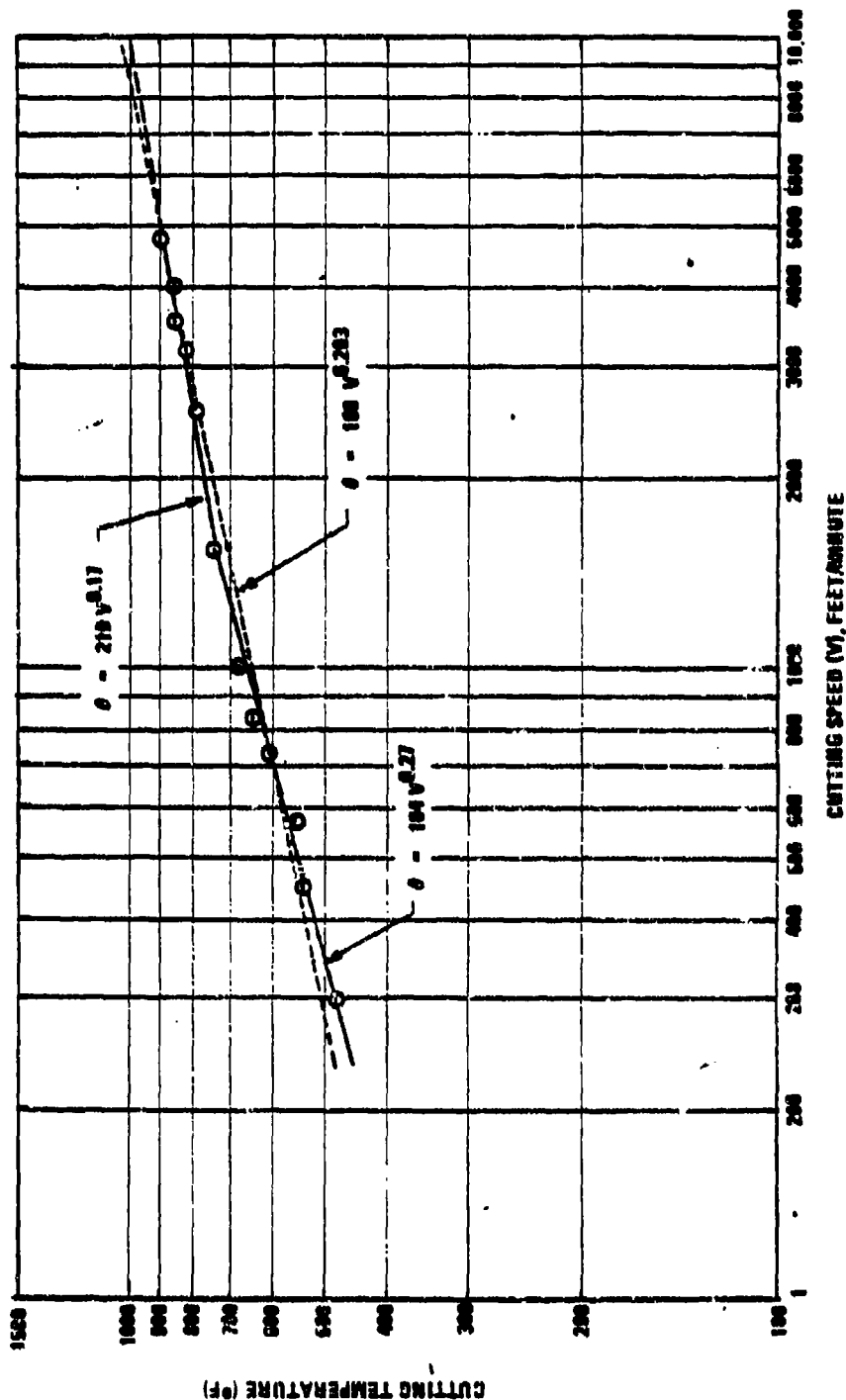


Figure 30. Effect of Cutting Speed and Water on Cutting Temperature When Turning 7052 Aluminum

## TOOL GEOMETRY

BR: 6°

SR: 13°

SCA: 16°

INSERT: SEG-623J

CARBIDE: C-2

CUTTING SPEED: AS SHOWN  
 FEED: 0.0075 INCH/REVOLUTION  
 DEPTH OF CUT: 0.060 INCH OR RADIUS  
 CUTTING FLUID: CODOI 8741 (1:30), FLOOD

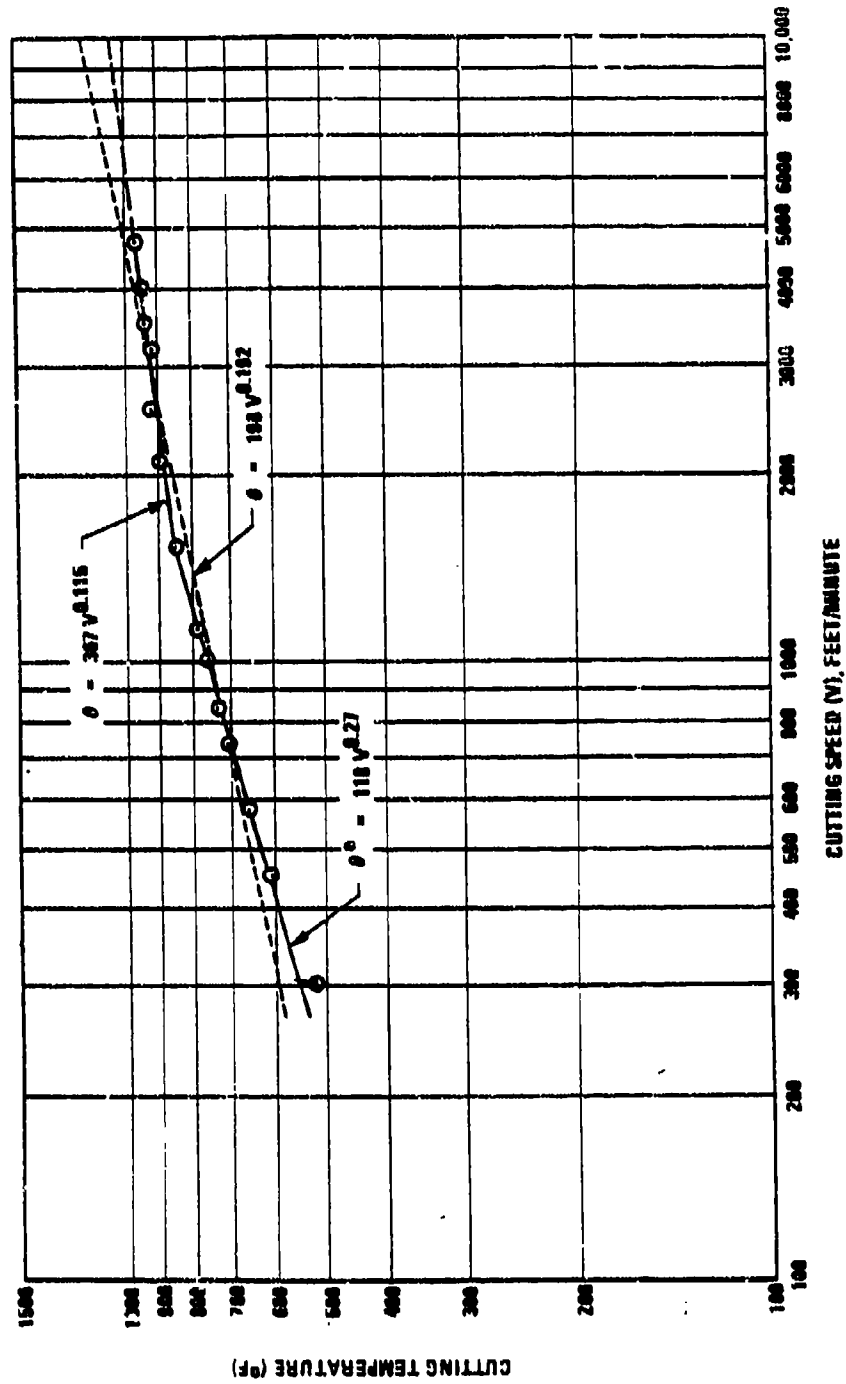


Figure 31. Effect of Cutting Speed and Coda 8741 on Cutting Temperature When Turning 2014-T652 Aluminum

## TOOL GEOMETRY

DR: 5°

SR: 15°

SCRA: 15°

INSERT: SEB-023J

CARBIDE: C-2

CUTTING SPEED: AS SHOWN

FEED: 0.0075 INCH/REVOLUTION

DEPTH OF CUT: 0.100 INCH ON RADIIUS

CUTTING FLUID: COOLANT B (1:30), FLOOD

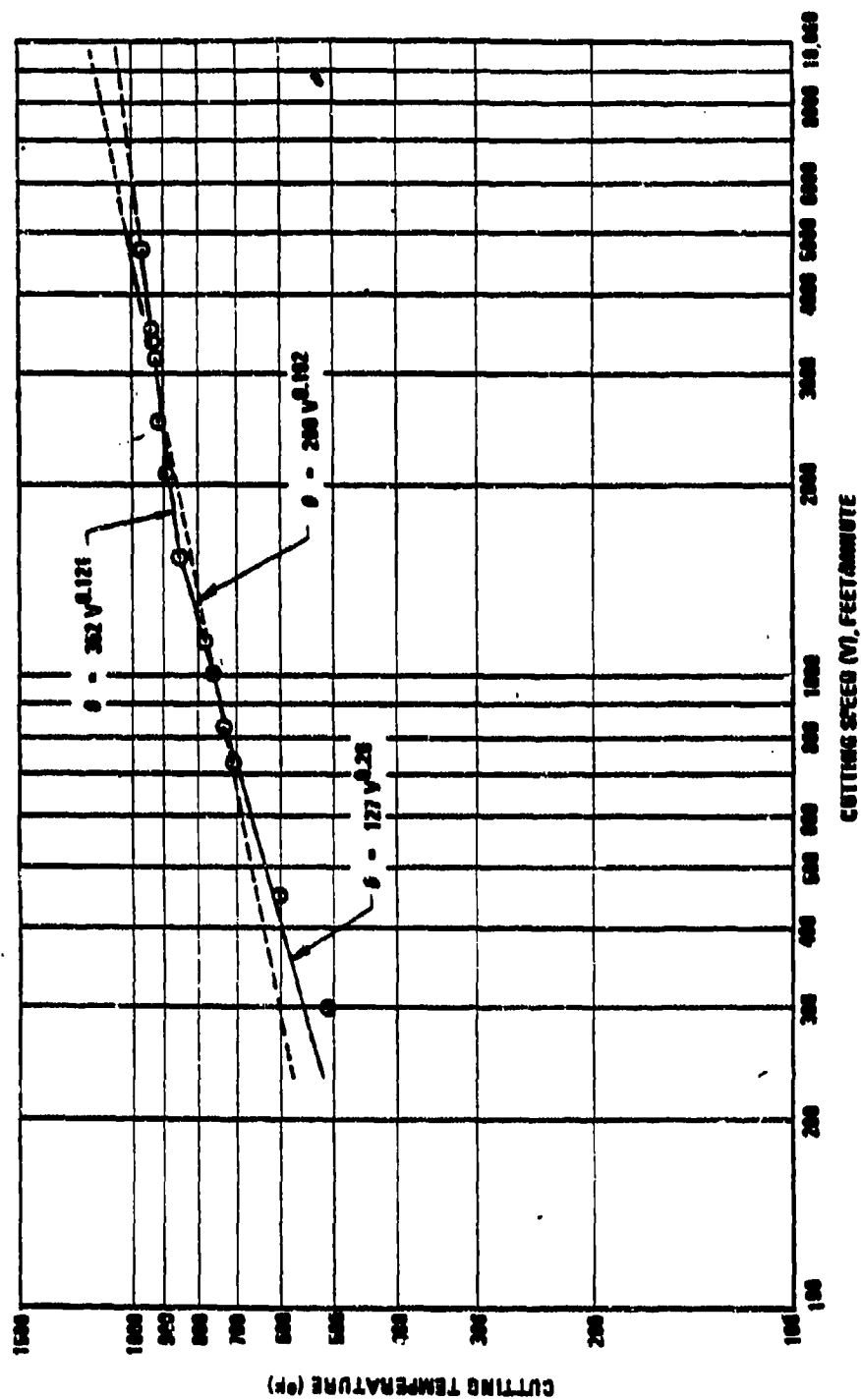


Figure 32. Effect of Cutting Speed and Coolant B on Cutting Temperature When Turning 2014-T652 Aluminum

## TOOL GEOMETRY

RA: 6°  
 SR: 13°  
 SCA: 16°  
 INSERT: SEG-623J  
 CARBIDE: C-2

CUTTING SPEED: AS SHOWN  
 FEED: 0.0075 INCH/REVOLUTION  
 DEPTH OF CUT: 0.068 INCH ON RADIUS  
 CUTTING FLUID: COOLANT C (1:30), FLOOD

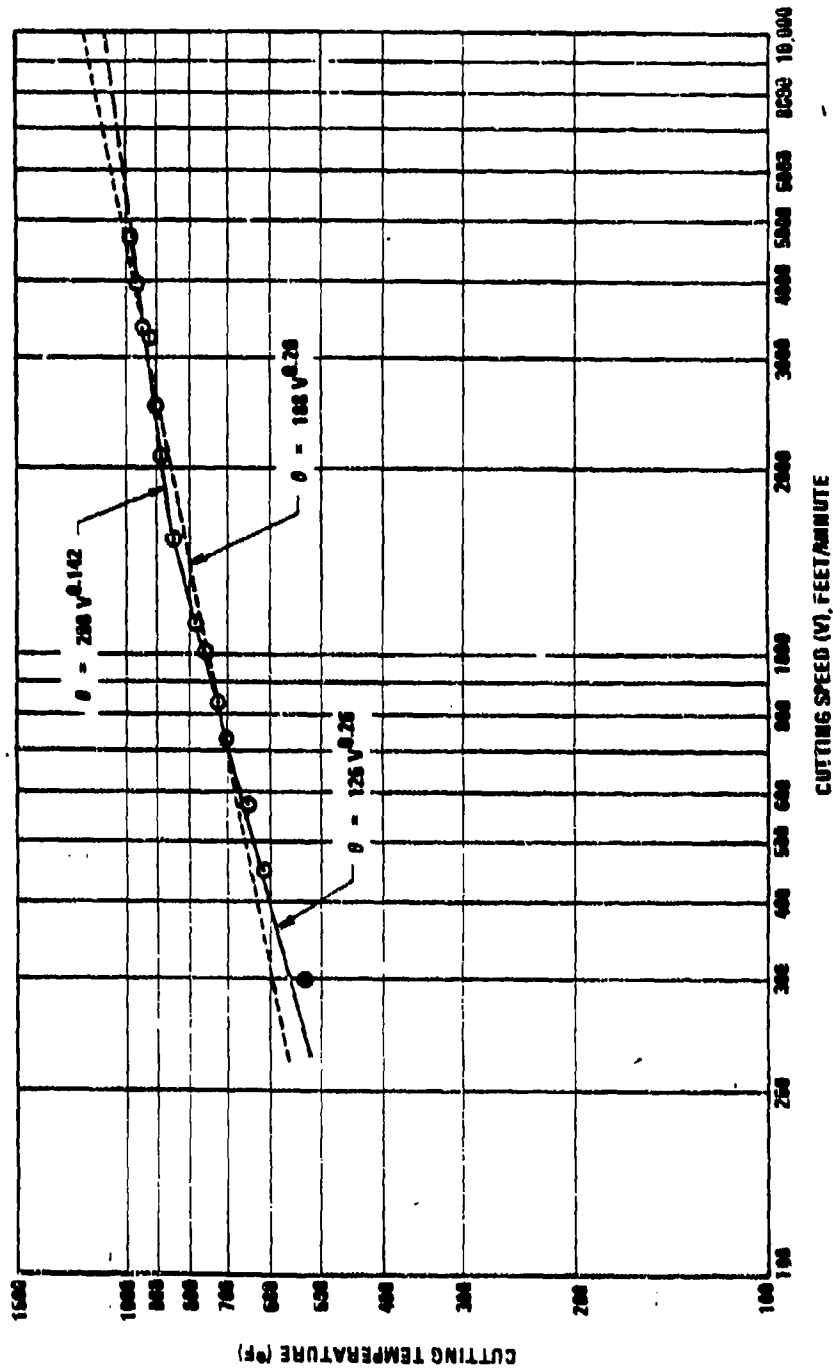


Figure 33. Effect of Cutting Speed and Coolant C on Cutting Temperature When Turning 2014-T652 Aluminum

## TOOL GEOMETRY

OR: 5°

SR: 12°

SCA: 16°

INSERT: SG-8234

CARBIDE: C-2

CUTTING SPEED: AS SHOWN

FEED: 0.0075 INCH/REV (GLUEH)

DEPTH OF CUT: 0.060 INCH (RADHOC)

CUTTING FLUID: DRY

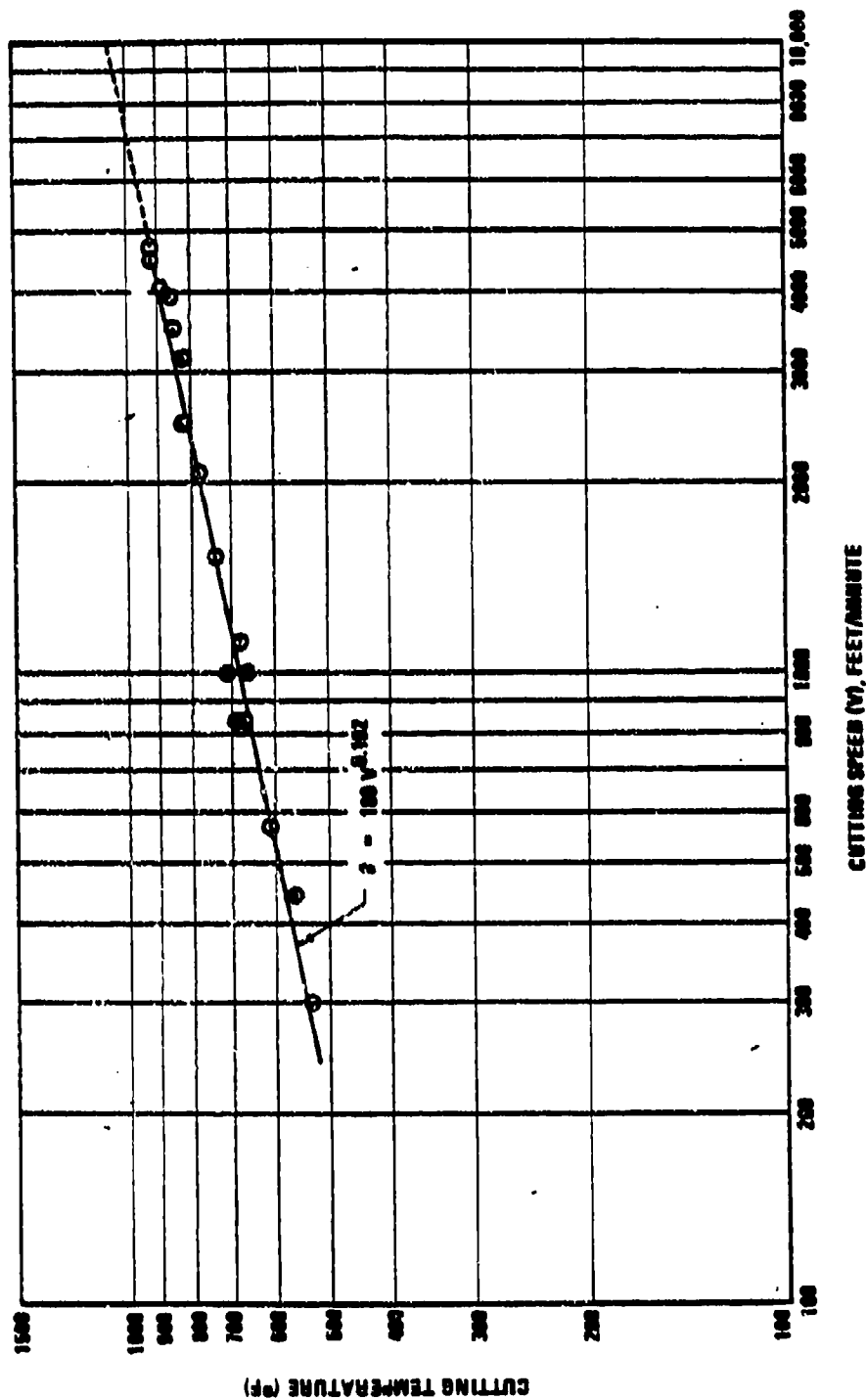


Figure 34. Effect of Cutting Speed on Cutting Temperature When Turning 2014-T652 Aluminum - Dry

COOLANT	CUTTING EDGE TEMPERATURE (°F)			
	500 FT/MIN.	1000 FT/MIN.	5000 FT/MIN.	10,000 FT/MIN.
DRY	504	678	924	1065
WATER	505	658	902	1038
COOLANT B	638	765	977	1073
COOLANT 0743	632	762	977	1064
COOLANT C	634	768	1002	1106

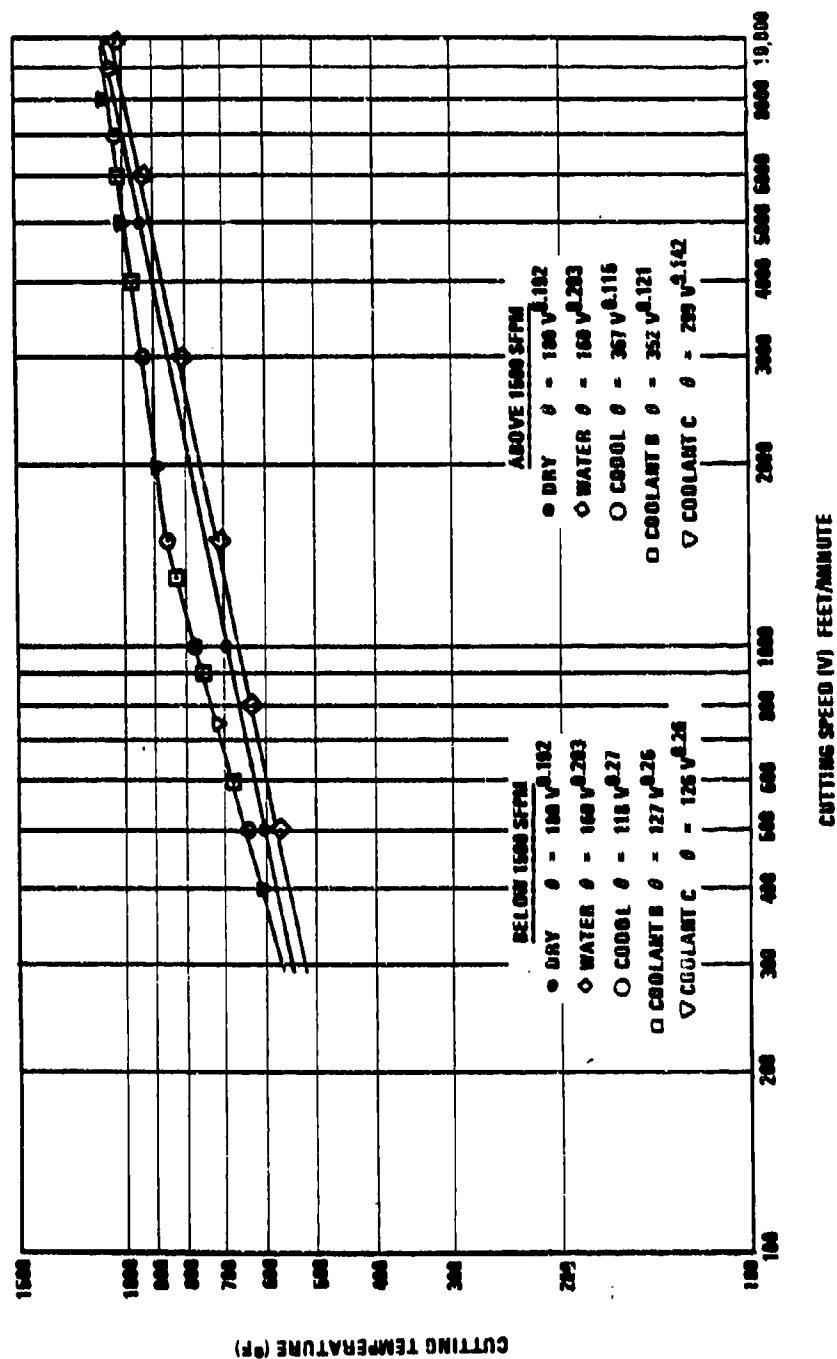


Figure 25. Summary of Effect of Cutting Speed and Coolants on Cutting Temperature When Turning T652 Aluminum

kind of temperature; and cutter geometry and feed rates can be manipulated to provide some cutting temperature relief, if needed. Additionally, intermittent cutting and, perhaps, cutting fluids can be used to provide further cutting temperature relief. Based on these observations, it was concluded there are no uncorrectable thermal restraints which prohibit the high speed machining of aluminum alloys.

Theoretically, aluminum has a critical cutting speed; beyond which, there is no further increase in cutting temperature. If this cutting speed can be reached and surpassed in a practical sense, it will open the way to vastly improved metal removal rates for it follows that: (1) cutting speeds can be infinitely increased, (2) feed rates, being directly and indirectly linked to cutting speeds, can be infinitely increased on both accounts, and (3) optimum cutter geometry configurations will reverse from a high shear to a high strength mode with attendant economies.

#### 4.0 CUTTING FLUID OPTIMIZATION TESTS

##### 4.1 Introduction

Cutting fluids are not always required for the machining of aluminum and its alloys, but their use is nearly always beneficial and recommended. At low cutting speeds, the lubricating action of cutting fluids improves surface finish by reducing friction, built-up edges, and tearing of machined surfaces. At high cutting speeds, the cooling action of cutting fluids improves tool life by reducing cutting temperature. Furthermore, at excessive cutting speeds, both the cooling and lubricating actions of cutting fluids improve surface finish and tool life by alleviating incipient welding between hot chips and cutters and curbing high cutting temperatures. While the heat generated by aluminum machining is relatively low, the use of cutting fluids is, none the less, recommended, because these will improve the already good machinability of aluminum through reduction of friction and cooling.

There are other advantages to using cutting fluids in high speed machining operations. One of the more important advantages is thought to be the improved chip control provided by cutting fluids. Aluminum chips, newly formed at high cutting speeds, are very hot and wildly tossed about the machining area. Such chips, which can burn machine operators and cause other discomfort, can be cooled and suppressed with multi-nozzle high pressure, cutting fluid systems. This and lesser systems can also be used advantageously to flush or wash chips free from cutting areas. Finally, a list of advantages for using cutting fluids would include:

- a. Protect finished part surfaces from corrosion
- b. Lubricate machine-tool slideways
- c. Lower cutting force requirements
- d. Lower part temperature
- e. Improve dimensional stability
- f. Closer tolerances

Cutting fluids for aluminum generally fall into one of the following classifications:

- a. Mineral Oil
- b. Emulsions
- c. Chemical solutions

There are a number of good cutting fluids available from any one of these categories with which to machine aluminum. Each has its advantages and disadvantages, and a problem arises when the time arrives to select one. Many times, a trade-off has to be made; e.g., selecting a cutting fluid with less cooling capability to avoid using one that stains, contaminates, inhibits welding, is expensive, is toxic, lowers machinability, induces stress-corrosion, yields unacceptable surface finishes or dimensions, or produces some other unacceptable disadvantage. When a cutting fluid has been selected for a process, it must undergo considerable testing to prove

that it is both economical and safe to use. Even then, it is not uncommon for some production problem to be traced back, months later, to the cutting fluid being used. For this reason, it is considered to be both risky and expensive to switch to a new cutting fluid; and, therefore Vought will continue to use its current cutting fluid as a base while testing others. The purpose of this investigation was to identify and substantiate at least one acceptable coolant method for the high-speed machining of aluminum alloys.

#### 4.2 Application Method

To be effective, cutting fluids must reach the cutting edge of tools. This means that a cutting fluid must be correctly placed, rather than randomly directed, to ever reach the tool-chip interface. At high cutting speeds, this requirement becomes more difficult to achieve. Like the case for grinding wheels, cutters or workpieces turning at high speeds tend to fan, blow or hurl the cutting fluid away from the cutting edge; and it is questionable if any cutting fluid ever gets to the tool-chip interface. There are several basic methods for applying cutting fluid to the cutting zone, and each of these can be further divided into sub-methods as illustrated by the crimped nozzle applicator in Figure 12 for the flood application method. Each method has its advantages, disadvantages and economics; and those discussed below were investigated for the purpose of selecting the one best suited for general high-speed machining operations.

##### 4.2.1 Flood Application Method

Since flooding is the most common method for applying cutting fluids, it was the first to be investigated. Most production machine tools, including the Sundstrand Omnimil and the Bullard Vertical Turret Lathe used in this program, are equipped with a flood coolant system. This system normally consists of a low pressure pump and a network of pipes, valves and nozzles through which a cutting fluid is delivered from a sump to the cutting zone. Generally, the cutting fluid floods the tool, chip and work and then drains into the chip pan; from whence, it returns to the sump pump and is recycled. The low pressure pump on the Omnimil is shown in Figure 36 along with a high pressure pump that was installed as a backup should such be needed to force cutting fluid into tool-chip interfaces. The high pressure pump which could put out 75 psi pressure and a flow rate of 20 gallons/minute through a 3/4-inch pipe was not needed however, as the low pressure pump proved to be adequate for delivering properly placed cutting fluid to tool-chip interfaces. At times, the flood method appeared to be too adequate; because on such occasions, a choking mist was generated about the Omnimil by a combination of a fast turning cutting and a copious flow of cutting fluid. For that reason, the flood application method is not generally recommended for high-speed machining with end mills over 1.0 inch in diameter.

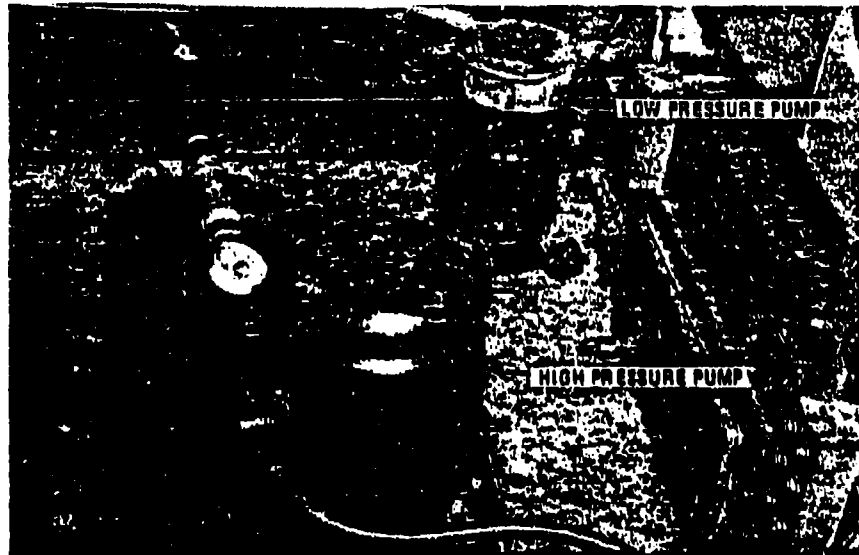


Figure 38. Cutting Fluid Pumps on Omnimil

#### 4.2.2 Mist Application Method

The problem of introducing an offensive vapor mist into the atmosphere is also a limitation for this application method. However, the pressure-fed type mist generator on the Sundstrand Omnimil was found to produce a less offensive vapor mist than the combination of large, fast turning cutters and flood applications. Additionally, the pressure-fed generator delivered enough lubrication to cutting edges to minimize chip build-up on cutter flanks. For these reasons, and because the mist application method provided superior cooling, it is the method Yought generally recommends for high-speed and milling operations when one is required.

#### 4.2.3 Manual Application Method

Some dramatic results were obtained when films of cutting fluid or tapping compound were brushed on parts to be high-speed machined. Machine loads were observed to drop as much as 19% on such occasions. However, this method of application was found to be too expensive and unsafe for general usage.

#### 4.2.4 Electrostatic Cooling Method

This method of cooling may yet find applications in high-speed machining for such materials as titanium steel, and super alloys. It is a low cost method which, according to the survey made, reduces the temperature of a heated object immediately when an electrostatic field is applied to the object. This method was proposed but not investigated, because the high-speed machining of aluminum did not present any difficult cooling problems.

#### 4.3 Selection of Candidate Cutting Fluids

As mentioned in paragraph 4.1, selecting an optimum cutting fluid is difficult; because there are such a large number and variety of commercially available cutting fluids from which to choose. Each of these would have its advantages and disadvantages, and it is doubtful if all could ever be evaluated within the scope of a given program. For that reason, cutting fluid testing is generally limited to a few selected products which have a good potential. In this instance, the application methods established in paragraph 4.2 reduced the number of candidate cutting fluids by tending to limit selections to emulsions or water soluble oils. For these reasons, the cutting fluids selected for evaluation in this program were limited to:

<u>NAME</u>	<u>MANUFACTURER</u>
Codol 0741	Stuart Oil Company
Coolant B	Anonymous*
Coolant C	Anonymous*

Specifically, Codol 0741 was selected because it was the cutting fluid then being used at Vought for aluminum machining applications. Coolant B was selected because it was used at Vought on occasions and was known to have good compatibility with aluminum. Coolant C was selected because it was a relatively inexpensive, premium cutting fluid.

#### 4.4 Cutting Fluid Evaluation

##### 4.4.1 Cutting Temperature Tests

The results of this investigation are reported in detail in paragraph 3.7 and are summarized in Figure 35. Essentially, none of the selected cutting fluids appeared to lower cutting temperatures, while water did. Abbreviated tests made with leaner concentrations of the cutting fluids and spray mists did not alter those results significantly. As a consequence, the selected cutting fluids were considered to be overactive and better lubricants than coolants. Since water did not lower cutting temperature appreciably at high speeds, it was felt that no other economical cutting fluid would either and testing was discontinued.

\*Names supplied upon request.

Of the cutting fluids tested, Codol 0741 appeared to be the best coolant, and it was very closely followed, in turn, by Coolant B and Coolant C, respectively.

#### 4.4.2 Surface Finish Tests

Surface finish tests were conducted on a lathe with a setup like that shown in Figure 11. Using a cutting speed of 2,410 feet/minute (447 rpm), a feed of 0.0075 inch/revolution, a radial depth of cut of 0.035-inch, and SEG-623J carbide inserts, a cut approximately 3 inches long by 20.6 inches diameter was made with no cutting fluid. The feed mechanism was then disengaged and the tap water cutting fluid (cf. Figure 10) activated. The feed mechanism was then re-engaged, and another cut approximately 3 inches long was made using water as a cutting fluid. Similarly, 3 inch long by 20.6 inches diameter cuts were made using the selected commercial solutions, mixed 1:30, as cutting fluids. (Note: The hose and nozzle through which the cutting fluids were pumped were rinsed with water at the conclusion of each test to prevent one cutting fluid from mixing with another). After concluding this series of tests, the Al 2014-T652 workpiece was removed from the lathe, and the generated surfaces were measured with a Taylor-Hobson Surtronic 2 profilometer. The as-measured surface finishes obtained were:

<u>CUTTING FLUID</u>	<u>SURFACE FINISH (RMS)</u>
Dry	40-44
Water	40-44
Coolant B	39-41
Codol 0741	38-40
Coolant C	40-42

Again, little difference was noted in the results produced by the three commercial cutting fluids.

#### 4.4.3 Intergranular Corrosion Tests

The purpose of this test was to determine if any of the candidate cutting fluids (Codol 0741, Coolant B, Coolant C) had any detrimental chemical effects on aluminum alloys A356, 6061 and 7075 by performing ambient temperature stress corrosion tests for the nine combinations.

The hardware used in conducting the stress corrosion tests was the following:

- a. Test Specimens: All test specimen dimensions were 0.25-inch thick by 0.75-inch wide by 10.0 inches long. The A356 specimens were prepared from a Lance missile G&C Shell, and the 6061 and 7075 specimens were prepared from plate material. All materials were in the T6 temper.
- b. Stress Corrosion Fixtures: The nine test fixtures were made of aluminum and conformed to Figure 37 dimensions. These fixtures were previously fabricated by Vought's Engineering Test Laboratory in accordance with TR 66-52210-061.

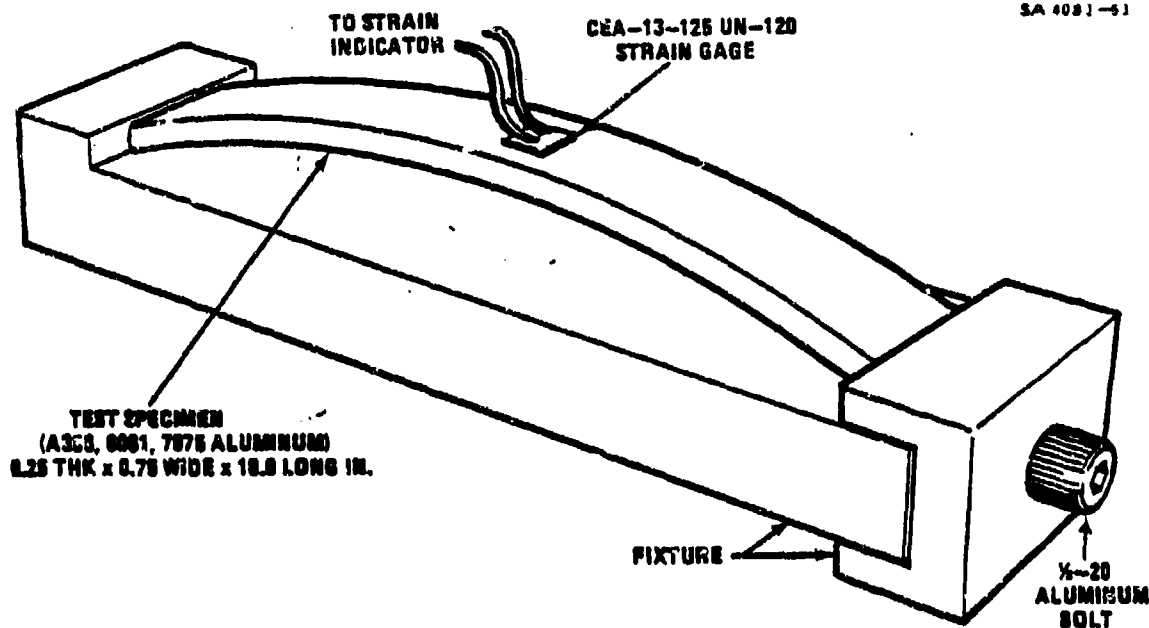


Figure 37. Stress Corrosion Test Fixture With Specimen Installed

c. Candidate Test Coolants:

Adequate quantities of the three candidate cutting fluid materials were mixed 1:30 by volume with tap water. The fluids exhibited no unpleasant odors after mixing.

Each test specimen was strain gaged, using CEA-125-UN-120 strain gages. These strain gages were applied at the center location of test specimens, as indicated in Figure 37, and connected to a strain indicator. After taking a no-load reading, a specimen was placed in one of the stress corrosion fixtures and then stressed, using the 1/2"-20 bolt (cf. Figure 37) and the strain gage indicator. Stress was applied until the specimen was at 70% of the yield strength literature value. The strain data used as a guideline in applying 70% stress levels to test specimens are given as follows:

Test Specimen Material	Yield Strength (PSI)	70% Yield Strength (PSI)	Modulus Of Elasticity (E) (PSI)	Strain @ 70% $S_{tu}$ Strain = $\frac{.7 S_{tu}}{E}$
A356-T6	28000	19600	$10.4 \times 10^6$	1885 $\mu$ in/in
6061-T6	38000	26600	$9.9 \times 10^6$	2687
7075-T6	62000	43400	$10.3 \times 10^6$	4213

The strain gage was then removed, and the specimen and fixture were submerged approximately 1/4-inch in one of the three fiberglass tanks which contained the test coolants. This same procedure was used in preparing all eighteen (18) specimens for testing.

In the first half of the tests, nine (9) of the eighteen (18) specimens, consisting of six (6) A356 and three (3) 7075 specimens, were submerged in the three tanks of cutting fluid. Of these, two (2) A356 and one (1) 7075 specimens were placed in each tank of cutting fluid. The specimens were allowed to remain exposed in the coolants (with the top of the fiberglass tanks covered) for 30 days. After the exposure was completed, the specimens and fixtures were removed from the fluids, water rinsed, and the specimens were metallurgically examined. The metallurgical examinations revealed that no stress cracking or corrosion had occurred to any of the A356 or 7075 aluminum specimens. The only effect noted was that some darkening of the specimens had occurred and was more predominant on the A356 than the 7075 specimens. Figures 38 through 40 portray the post-test condition of the test specimens. Examination of the coolants showed that the Coolant C experienced some breakdown and exhibited lumpiness and an unpleasant odor. The Coolant B and Codol 0741 fluids did not exhibit any breakdown and did not have any lumpiness or unpleasant odors. Figure 41 shows the condition of the fluids after 30 days.

NI6012

SA 4081-42

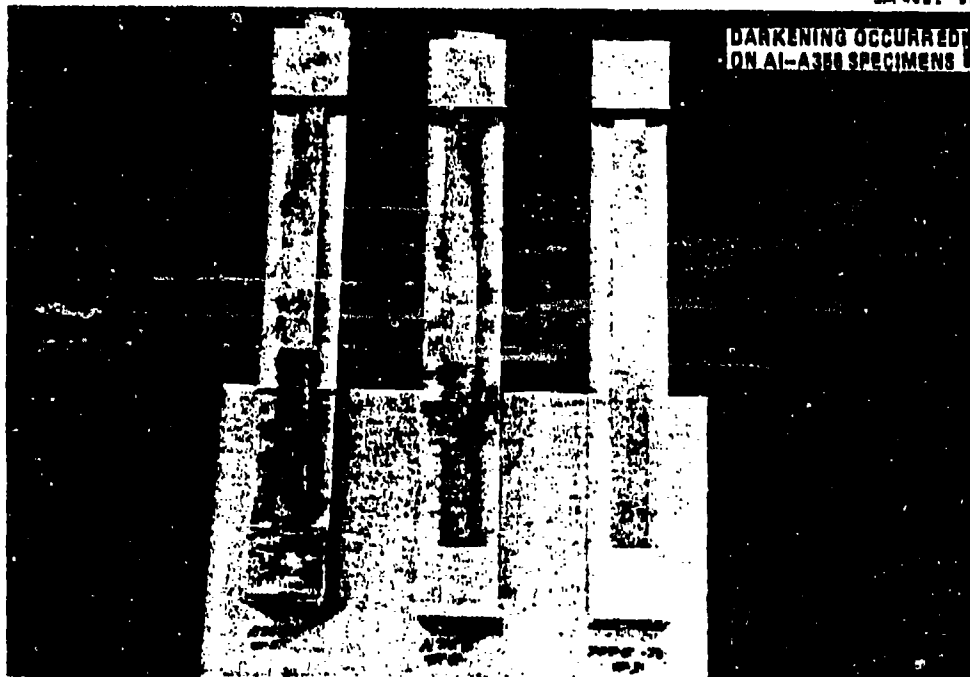


Figure 38. Condition of Two A356 and One 7075 Aluminum Stress Corrosion Specimens After 30 Days Exposure to Coolant C



Figure 38. Condition of Two Al-356 and One Al-7075 Stress Corrosion Specimens After 30 Days Exposure to Cadmium (Cd)

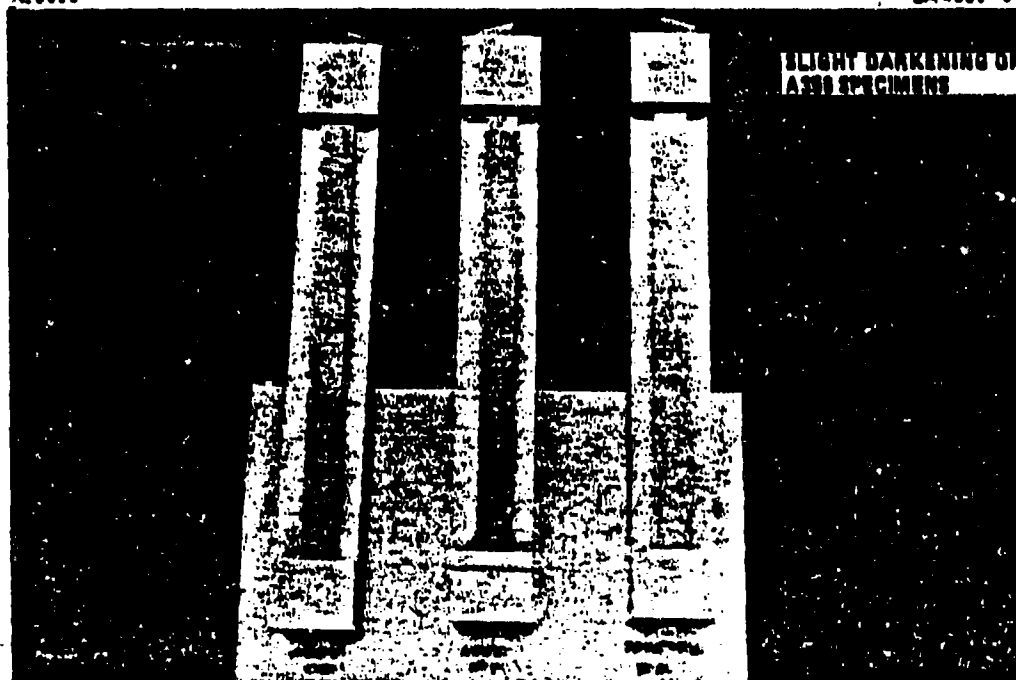


Figure 40. Condition of Two Al-356 and One Al-7075 Stress Corrosion Specimens After 30 Days Exposure to Coolant B

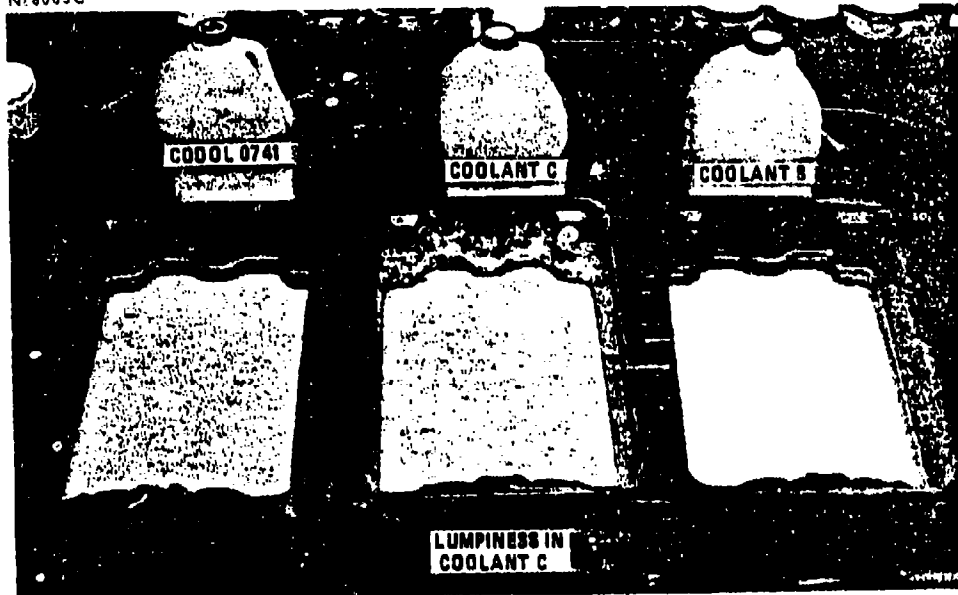


Figure 41. Conditions of Candidate Coolants After 30 Days

The above procedure was then repeated for the nine (9) remaining specimens which consisted of six (6) 6061-T651 and three (3) 7075-T651 specimens. All of these specimens were stressed to 70% of yield strength, placed into the three (3) 30-day old test fluids, and allowed to remain for thirty-six (36) days. After the exposure was completed, the samples were removed, rinsed with water, and metallurgically examined. The metallurgical examinations revealed that no stress cracking or corrosion had occurred to any of the 6061 or 7075 aluminum specimens. Figures 42 through 44 portray the post-test condition of the specimens. Examination of the coolants after sixty-six (30 + 36) days showed that Coolant C had excessive breakdown (uniform lumpiness and very unpleasant odor). Some lumpiness and odor were noted in the Codol 0741 and, to a lesser extent, Coolant B fluids. Figure 45 shows the condition of the fluids after sixty-six (66) days.

The results of these tests revealed that all three fluids were compatible with aluminum and safe to use when machining that material. The results also indicated that Coolant B, followed closely by Codol 0741, had the greatest resistance to bacteria growth of any of the three fluids. Additionally, the results showed that Coolant B would be less likely to stain any of the tested aluminum alloys.

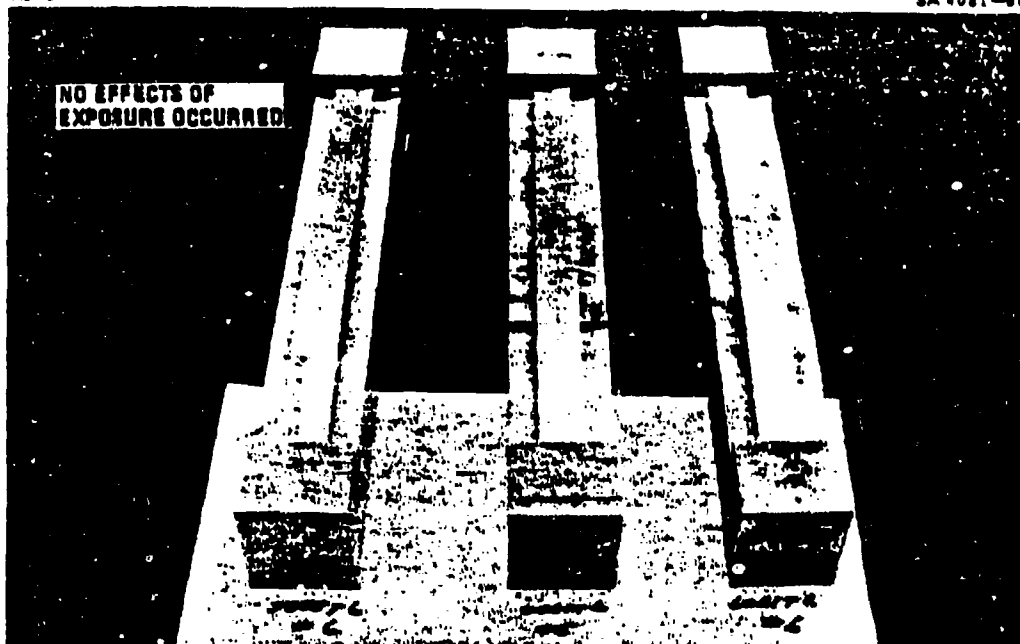


Figure 42. Condition of Two Al-6061 and One Al-7075 Stress Corrosion Specimens After 30 Days Exposure to Content C



Figure 43. Condition of Two Al-6061 and One Al-7075 Stress Corrosion Specimens After 30 Days Exposure to Content 6741

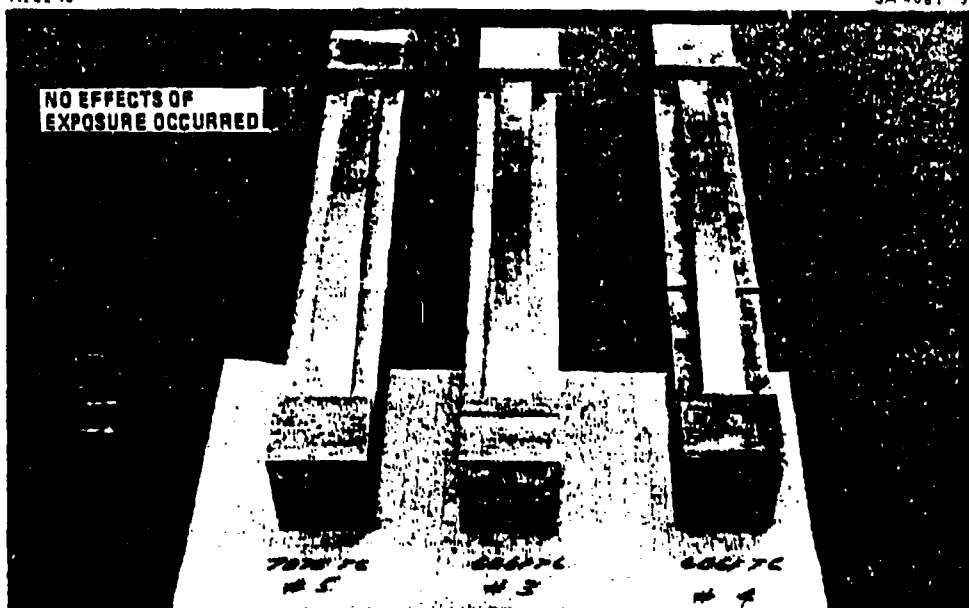


Figure 44. Condition of Two Al-6061 and One Al-7075 Stress Corrosion Specimens After 36 Days Exposure to Coolant B



Figure 45. Condition of Candidate Coolants After 66 Days

#### 4.4.4 Cost Analysis

Pricing requests were submitted to local distributors of the three candidate cutting fluids by Vought purchasing agents. Prices obtained for the three fluids in varying quantities were as follows:

<u>Cutting Fluid</u>	<u>5-9 Drums</u>	<u>10-19 Drums</u>	<u>20-39 Drums</u>	<u>Over 40 Drums</u>
Coolant B	\$4.79/gal.	\$4.74/gal.	\$4.69/gal.	\$4.64/gal.
Codol 0741	4.01/gal.	3.95/gal.	3.89/gal.	3.83/gal.
Coolant C	-----	3.63/gal.	-----	-----

To be fair, a cost analysis would have to include indirect costs as well as direct costs. This would include such entries as cost per gallon, replenishment cost, cutting fluid life, cost of additives, filtration costs, maintenance costs, product improvement, production rate improvement, tool life improvement, and others. An analysis of that magnitude was beyond the scope and, perhaps, time frame of this program; therefore, none was made. However, based upon the above prices and Figure 45, it is conceivable that Codol 0741 would be the least expensive cutting fluid.

#### 4.5 Conclusions

Other tests, e.g., machinability, dermatitis, and toxicity could have been performed, but it was felt that the results so obtained would not significantly alter any rankings established by the foregoing tests. Based on the results of those foregoing tests, none of the candidate cutting fluids were found to be overall superior to Codol 0741. Therefore, Codol 0741 was considered to be an acceptable cutting fluid for high speed machining applications; and it was selected for use in the remainder of this program.

## 5.0 MODIFICATION OF EQUIPMENT

### 5.1 Introduction

The state-of-the-art existing at the time of this program limited high speed machining to only a few of the several machining processes. Those that employed a revolving spindle rather than a revolving workpiece offered the most potential for high speed machining applications. For instance, it could be hazardous to attempt to turn an unbalanced part on a lathe at 4,000 rpm; whereas it would present virtually no problem to turn a milling cutter at that speed. Additionally, there were no known reciprocating machine tools capable of producing high cutting speeds except those utilizing ultrasonic vibration; and ultrasonic vibrations were too weak to drive even a modest-size tool or workpiece. For these reasons, high speed machining process selections were limited to rotating spindle type machine tools.

To provide a high speed spindle capability, a Sundstrand OM-3 Omnimil, 5-axis, N/C machining center and a Bullard VTL, 3-axis, N/C machine were retrofitted with high speed spindles. Additionally, safety features and other provisions had to be incorporated into these new high speed systems. These modifications, which provided high speed end milling, drilling, and turning facilities, are described in more detail below.

### 5.2 Omnimil OM-3 Machining Center

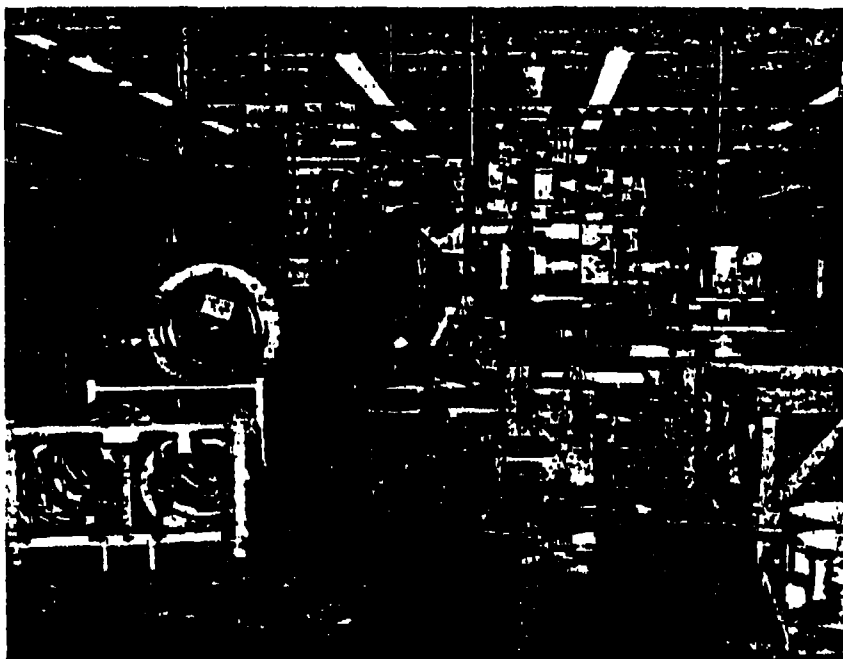
Views of the Omnimil before and after modifications are presented in Figures 46 and 47, respectively. The work area for the modified Omnimil is shown in Figure 48. In making these changes, it became necessary to give up the automatic tool changing and pallet (part) changing systems shown in Figure 46. As a result, the productivity of the machine was greatly reduced. The principal modifications made for the Omnimil are discussed in the following subsections.

#### 5.2.1 Safety Chip Guard

The housing shown built around the worktable in Figures 47 and 48 was installed primarily to prevent high velocity objects; e.g., broken cutters, from striking and injuring someone. This protective enclosure was effective the only time it was tested and also caught many of the chips produced when machining.

The housing was of laminated construction, being formed from four-layers of 0.062-inch thick 7075-T6 aluminum that was subsequently riveted together. In front, it had a sliding section which provided access for loading and unloading parts and tools. The top of the enclosure was made of plexiglas to maintain better illumination in the work area. Four pull-pins were provided for attaching the structure

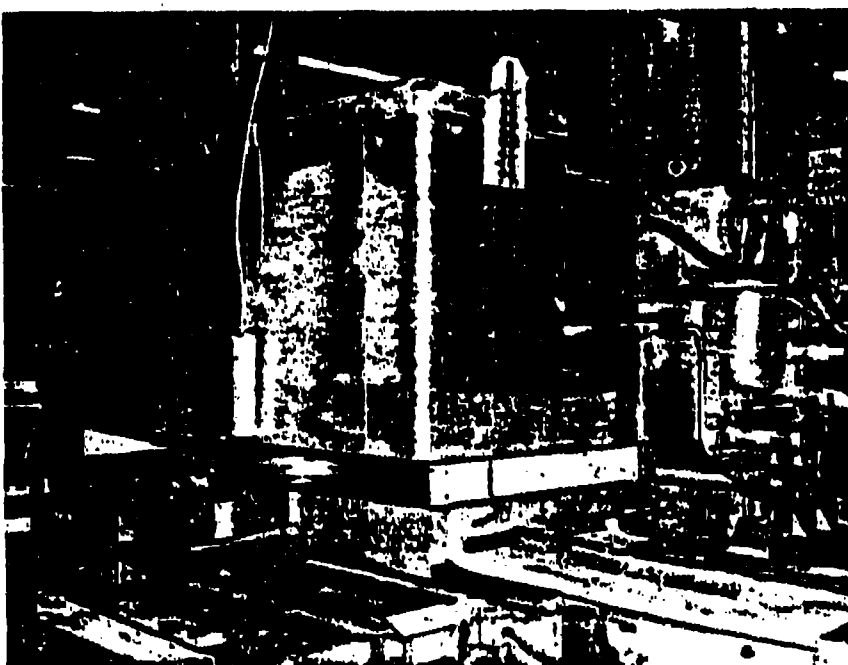
N-18991



SA 4881-40

Figure 46. Diesel Before Modification

N-45781



SA 4881-41

Figure 47. Diesel After Modification



Figure 48. Work Area of Modified Omnimil

to brackets mounted on the worktable. When desired, this non-permanent housing was easily removed from the machine by an overhead hoist. Overall, the housing was approximately four feet high, four feet wide, and eight feet long.

#### 5.2.2 Bryant High-Speed Spindle System

The high speed spindle shown in Figure 49 was designed and manufactured by the Bryant Grinder Corporation. It was designated as Special Bryant Model H-914-VC, motorized spindle and had the following characteristics:

- a. Speed range of 10,800 rpm to 20,000 rpm, infinitely variable.
- b. Horsepower rate of 20 horsepower at 20,000 rpm, 10 horsepower at 10,800 rpm, peak for intermittent service.
- c. Milling tool holder, Number 30 Standard M.M. taper, manual tool changing.
- d. Spindle bearings, ABEC Grade 9, precision ball with oil-air mist lubrication.
- e. Spindle motor cooling, water with air-to-water cooler.
- f. Spindle housing dimensions of 6.63 inches diameter maximum by 13.75 inches in length.

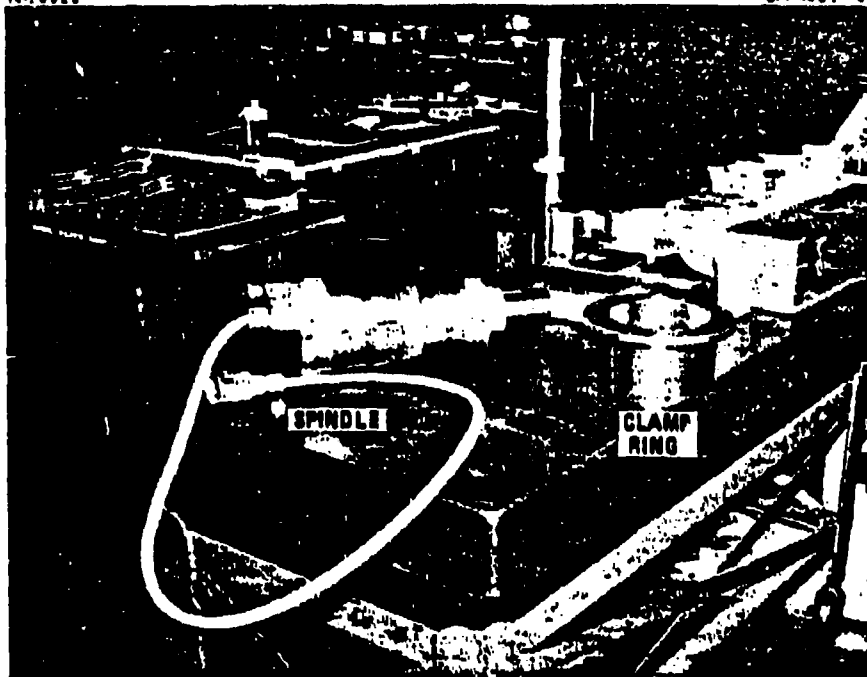


Figure 48. High-Speed Spindle and Clamp Ring

To power this spindle motor, a solid state, variable frequency PTI TR6300, 30 KVA, 100 ampere power supply was installed as shown in Figure 50. An isolation transformer (see Figure 51) was installed between the power supply and inlet power lines to provide the correct voltage (230 V, 3 phase, 60 Hz) and to furnish line isolation. A control panel (Figure 52), installed between the power supply and spindle, provided:

- a. Digital tachometer and speed control rheostat
- b. Spindle load meter
- c. Elapsed time meter
- d. Spindle motor temperature gage
- e. Over-current protection
- f. Feed hold output
- g. Oil reservoir warning indicator
- h. Coolant system indicators for normal and malfunction conditions and malfunction interlocks.

N-16108

SA 4081-44

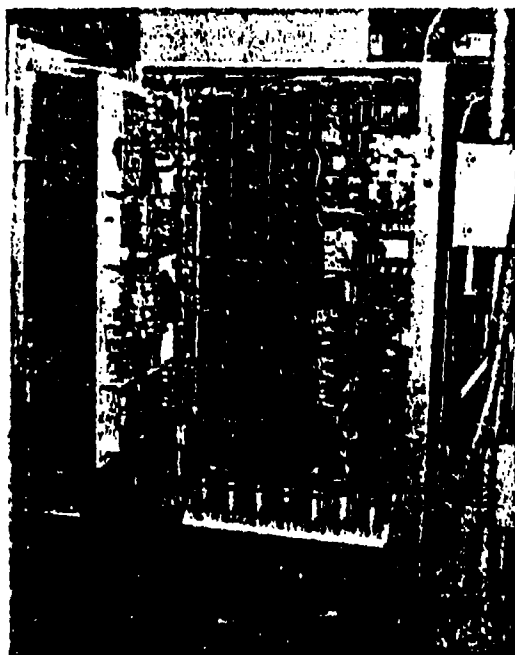


Figure 80. Solid State, Variable Frequency, PTI TR 8300,  
25 KW Power Supply

N-16106

SA 4081-45

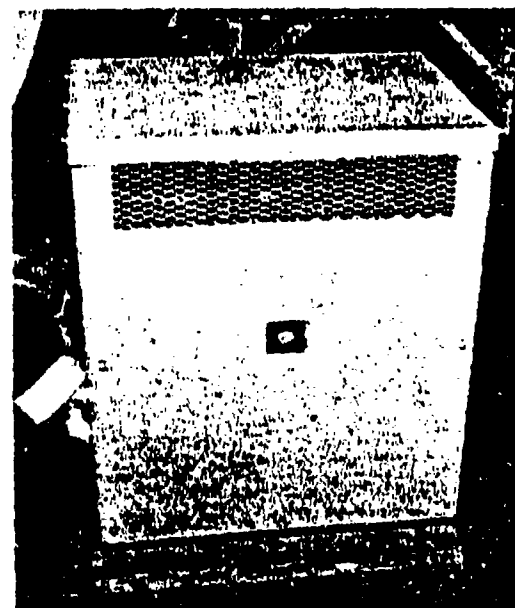


Figure 81. 37.5 KVA Isolation Transformer

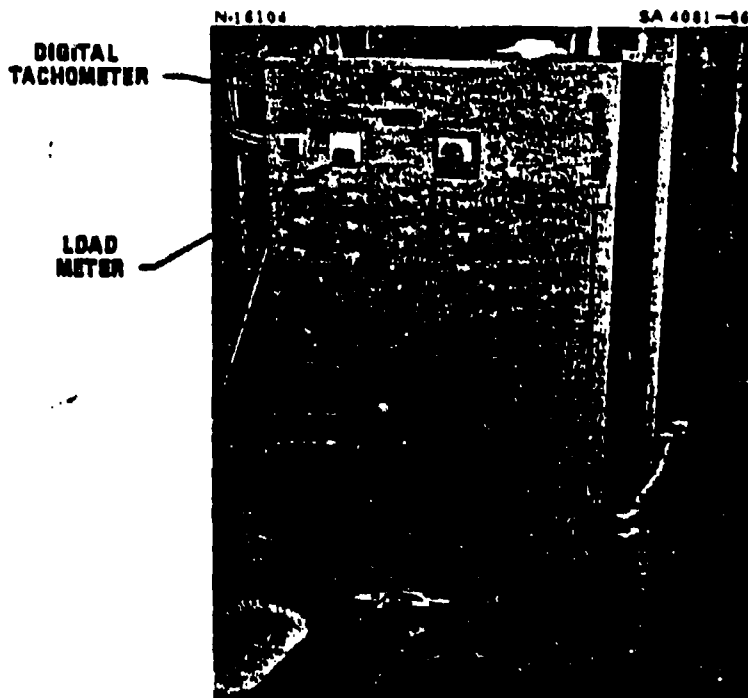


Figure 52. Panel for Omnimil High-Speed Spindle

- i. Spindle over-temperature indicator and malfunction interlocks.
- j. Bi-level over current indicator and automatic system shutdown.
- k. Switches for all power control functions.

To supply coolant to the spindle motor, a 30-gallon tank assembly (Figure 53) consisting of a pump; a 480-volt, 3-phase, 60 Hz motor; a pressure regulator; pressure gages; and a flow switch were installed.

A spindle lubrication system consisting of a lubrication panel assembly and an oil-air mist blender were installed to provide cooling to the bearings and internal pressurization of the spindle housing. The lubrication panel assembly (Figure 54) embodies 25- and 5-micron automatic drain type air filters, a manual air line shutoff valve, a solenoid valve operable from the main control station, an air pressure regulator, an oil mist pressure switch, a large capacity reservoir, and an oil-mist generator with float switch which will provide approximately 600 hours lubrication reserve. The air-oil mist blender which mixes clean air with oil-mist from the mist generator to provide internal pressurization of the spindle housing mounts to the top of the Omnimil.

N-16108

SA 4081-67



Figure 53. Spindle Motor Coolant Supply System

N-16109

SA 4081-68

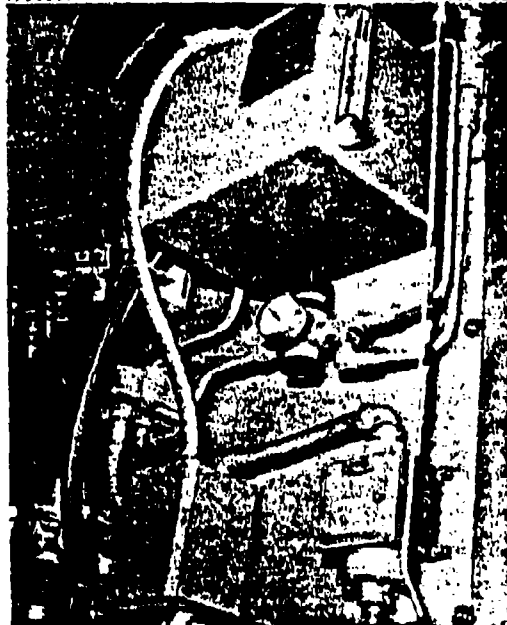


Figure 54. Lubrication Panel Assembly for Spindle Reservoir Oil

### 5.2.3 Installation of Bryant High-Speed Spindle

The regular slow (10 to 990 rpm) and fast (40 to 4,000 rpm) speed spindles on a Sundstrand OM-3 Omnimil are shown in Figure 55. When the fast speed spindle was fed out along its H-axis, it protruded from the swiveled machining head as shown in Figure 56. From that position the fast spindle and its housing (Figure 57) were removed from the machining head after disconnecting about 3 lines and removing some 16 fasteners. The adaptor or high speed spindle housing shown in Figure 58 was designed and fabricated at Vought to replace the one shown in Figure 57. A spindle casting, less spindle and bearings, could have been purchased from Sundstrand and machined to accept the Bryant spindle; but the quoted lead time was not acceptable. The Vought designed adaptor is shown installed in Figure 59. For good rigidity, this new spindle housing was mounted on a solid bearing block, replacing the roller bearings. The 7.5-inch travel on the H-axis was lost as a result of these changes. Additionally, capabilities for the automatic tool changer were lost for the Bryant spindle because of its manual draw bar operation. Continuing, the Bryant spindle (cf. Figure 49) was positioned in its special housing as indicated in Figure 60 and clamped in place by the Vought designed and fabricated clamp ring shown being installed in Figure 61. Installation of the spindle was completed when the clamp ring was bolted to the new housing and all electrical, cooling, and lubricating lines were connected as shown in Figure 62.

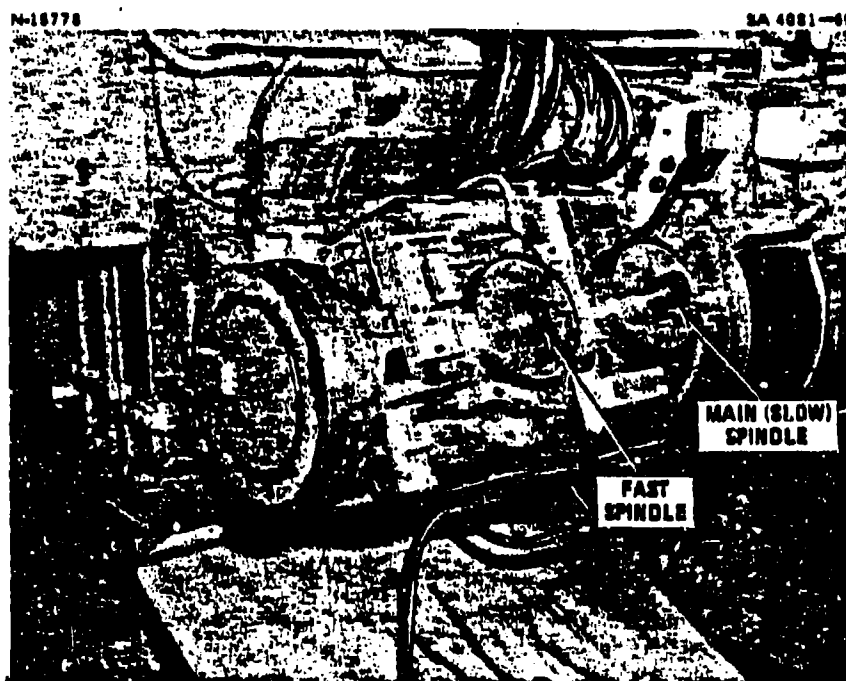


Figure 55. Fast and Slow Speed Spindle on Sundstrand OM-3 Omnimil

N-5779

SA 4081-70

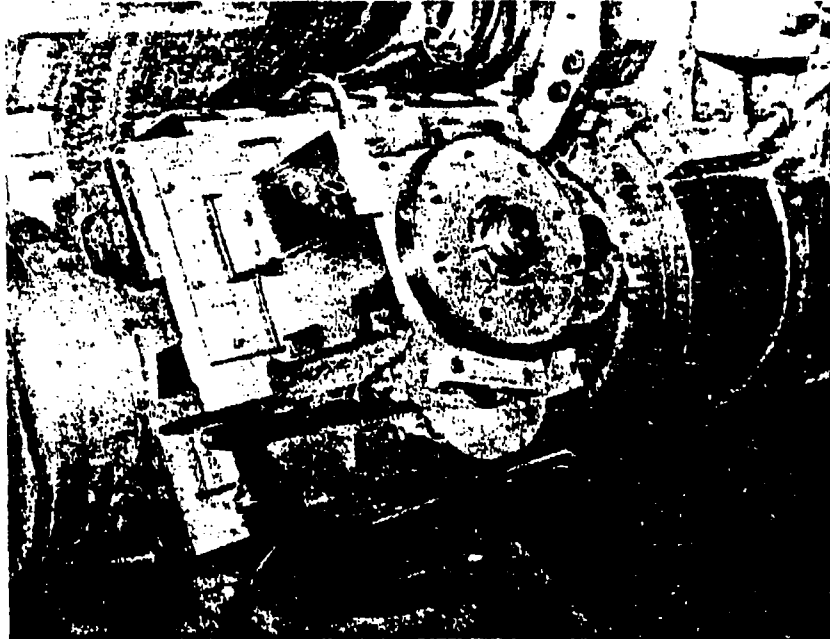


Figure 56. Fast Spindle on Sundstrand OM-3 Omnimil Extended on H-Axis

N-16016

SA 4081-71

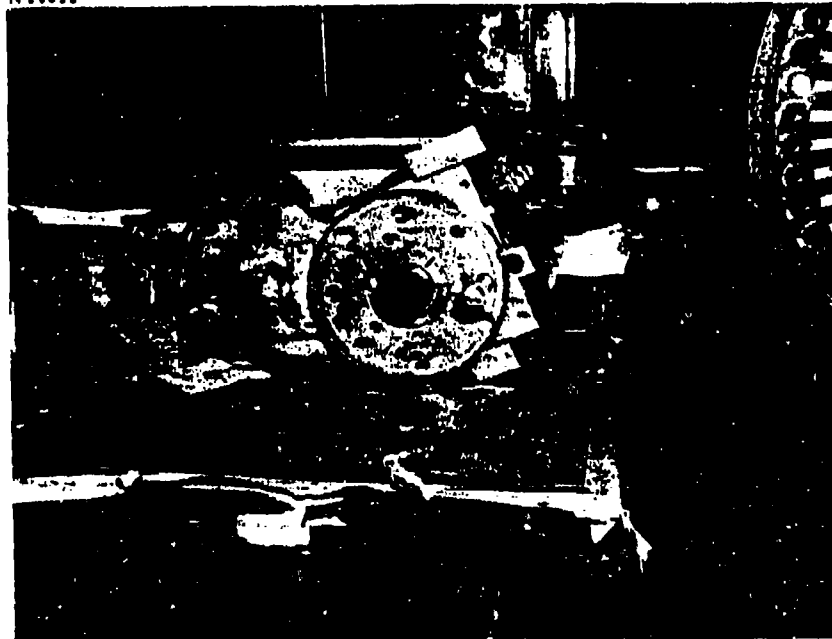


Figure 57. Original Fast Spindle and Housing for OM-3 Omnimil

N-18782

SA 4081-72

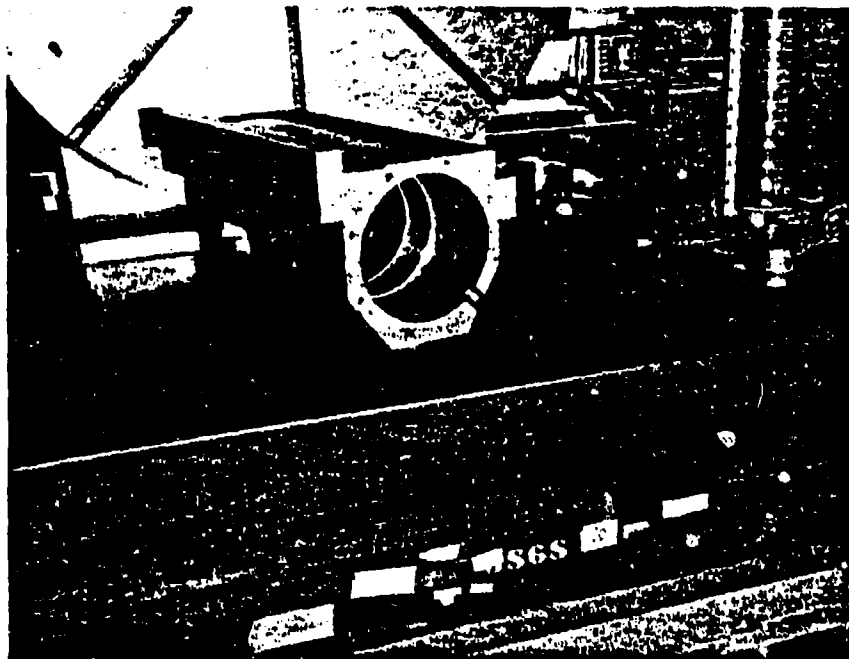


Figure 58. High-Speed Spindle Adapter for Sandstrand OM-3 Omnimat

N-16017

SA 4081-73

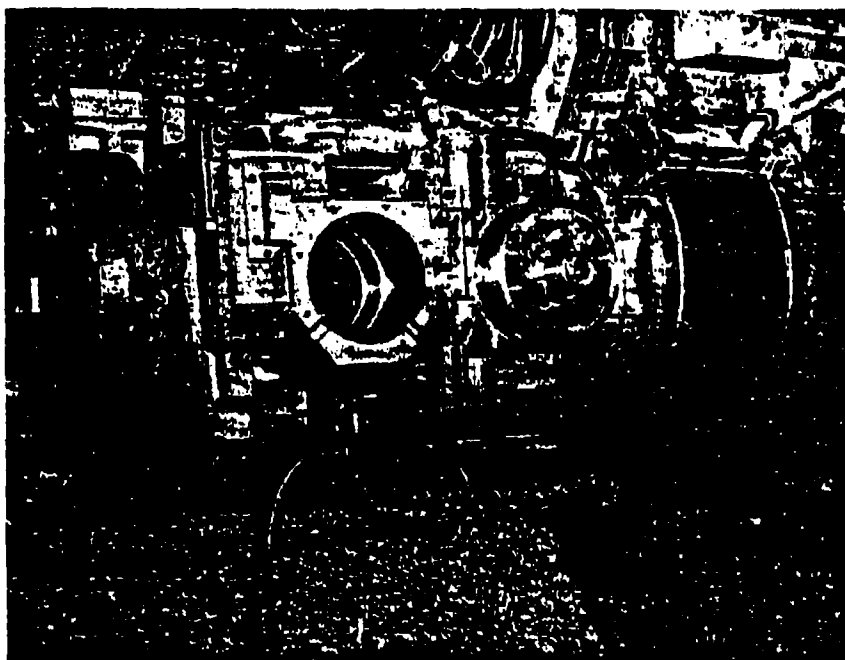


Figure 59. Installed Bryant Spindle Housing

N-16026

SA 4081-74

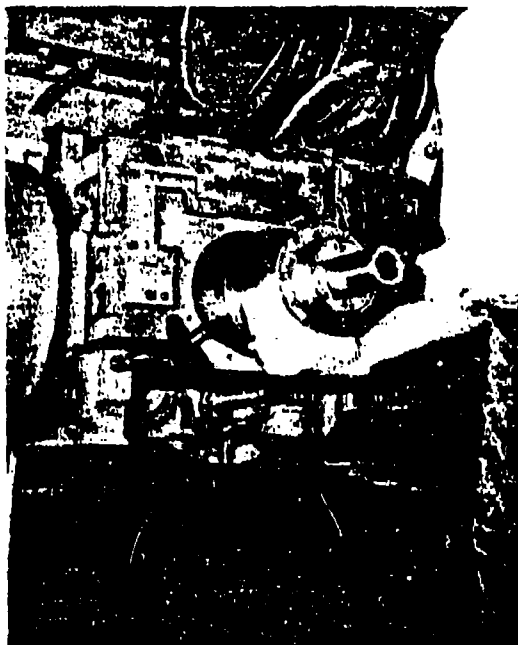


Figure 60. Installing Bryant Spindle in Omnimil Adapter

N-16027

SA 4081-75



Figure 61. Installing Clamp Ring for Bryant Spindle

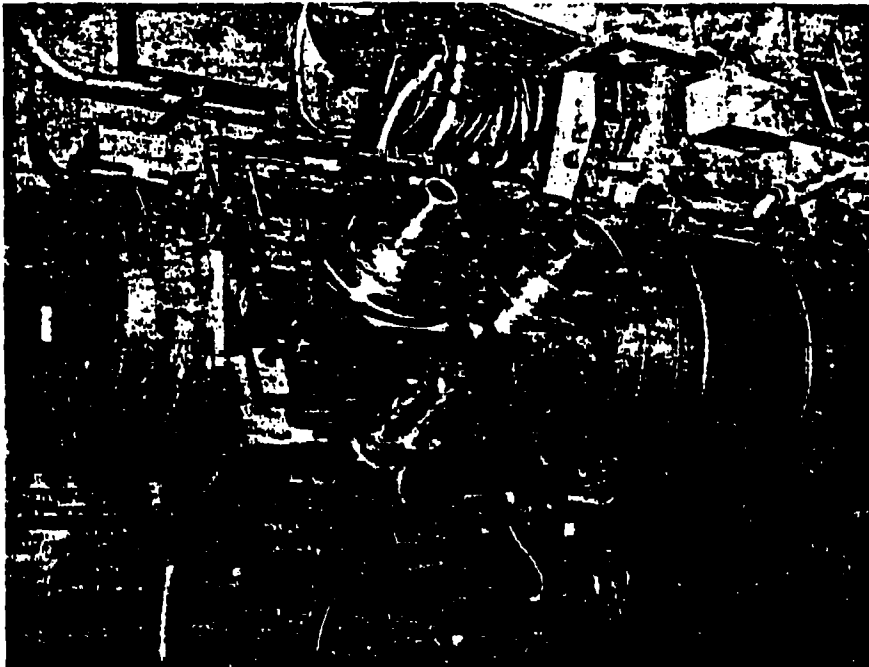


Figure 62. Installed High-Speed Spindle

The Sundstrand fast speed spindle and the Bryant high speed spindle, as described above, are interchangeable. As a consequence, operations can be converted from high speed milling to conventional milling, or conversely, in approximately 2 hours, excluding alignment time.

#### 5.2.4 Table Feed System

Previously, the OM-3 Omnimil had been equipped with a Sundstrand, S1 SWINC, CNC, master control unit, having a 11/05SC minicomputer. This control provided a maximum feed rate of 200 inches/minute. As events were to prove, that feed rate was not close to being fast enough. For a 20,000 rpm spindle, feed rates to 400 inches/minute can now be recommended and feed rates to 1,000 inches/minute may not be unrealistic. It is said that the above control unit can be modified to provide feed rates up to 400 inches/minute by making one hardware and two software modifications; however, such a modification remains to be evaluated. In any event, future users of this type of equipment should specify higher feed rates for their machines than was used in this program.

#### 5.3 Bullard VTL Machine

Unbalanced parts such as the guidance and control (G&C) shells shown in Figure 63 have to be turned at relatively low speeds to minimize machine vibrations. To provide a more competitive turning process for such parts in particular and a better turning capability for machining

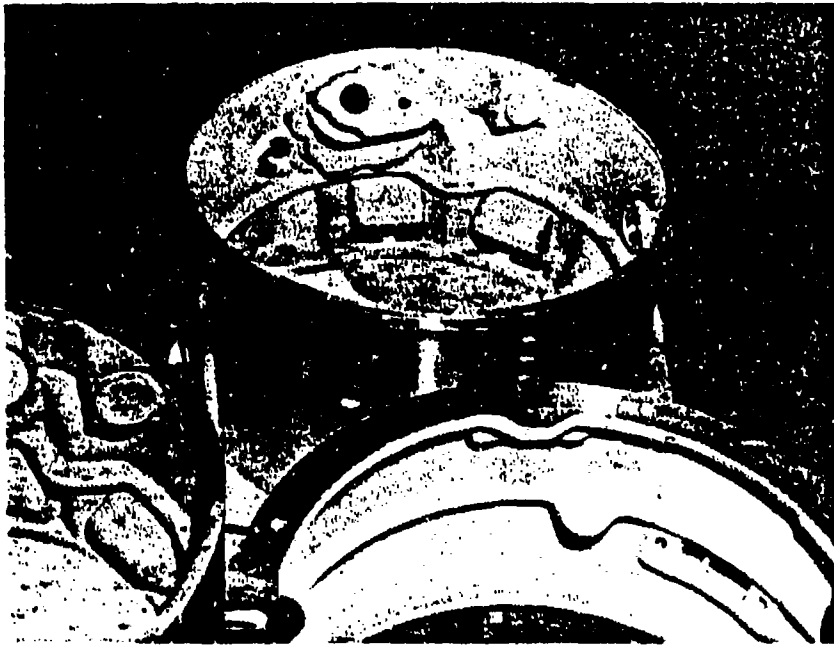


Figure 63. Typical Unbalanced Cylindrical Part (G&C Shell)

centers in general, a Bullard Vertical Turret Lathe (VTL), 3-axis, N/C machine was fitted with a high speed spindle for developmental studies as shown in Figure 64. Details for this relatively simple modification are described below.

#### 5.3.1 ECCO High-Speed Spindle System

A standard router spindle made by Ekstrom, Carlson and Company (ECCO) was procured for installation on the Bullard vertical turret lathe. That spindle, which is shown mounted to the side tool post of the Bullard in Figure 65 and is similar in size to that in Ekstrom, Carlson drawing P-548, had the following specifications:

Horsepower	20 at 14,400 rpm, 10 at 7,200 rpm, and 5 at 3,600 rpm
Spindle speeds	3
Cycles	240, 120, 60
Drive motor	Drive AC
Drive motor cooling	4 to 6 gpm - water
Cooling system	225-gallon recirculating tank (optional)
Spindle nose	40 machine tool taper
Drawbar	Manual
Spindle lubrication	Oil mist
Spindle brake	Dynamic
Horsepower meter	Yes

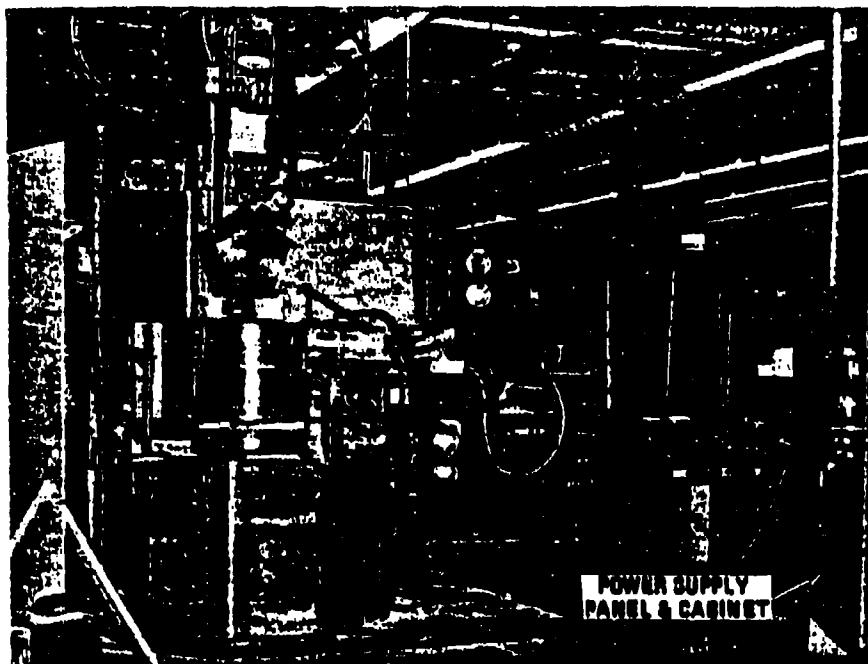


Figure 64. Ballard Vertical Turret Lathe With Installed High-Speed Spindle

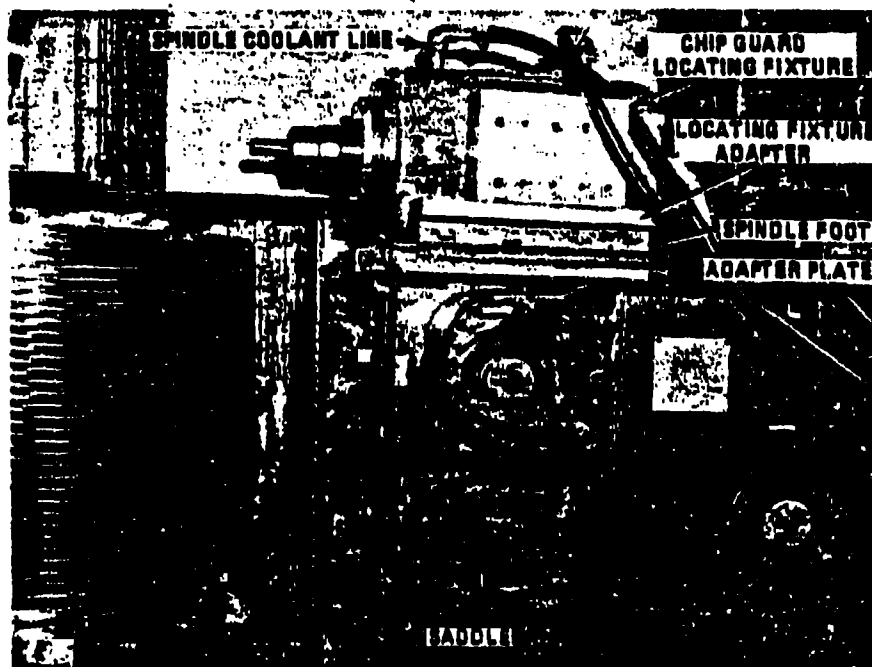


Figure 65. Ekstrom, Carlson Company (ECCO) Spindle Mounted on Ballard VTL Side Tool Post

Frequency converter	Furnished
Bearings	Class 7
High spindle temperature	Automatic shutdown
Low lubrication level	Automatic shutdown
Reversible	No
Overall dimensions	See drawing P-548

To power this spindle motor, the Louis Allis (Litton) motor-generator frequency converter shown in Figure 66 was used to supply 20 KW/10 KW/2 KVA at 240/120/60 Hertz through the ECCO tri-variable frequency power supply shown in Figure 64. DC plugging was used for braking. A control panel installed in the power supply cabinet (cf. Figure 64) between the power supply and spindle provided:

- a. Spindle load meter
- b. Switches for all power control functions
- c. Motor overload light and automatic shutdown system
- d. Spindle over temperature light and malfunction interlocks
- e. Lube level light and malfunction interlocks
- f. Air pressure low light and malfunction interlocks
- g. Speed selector switch.

A change in plans led to using two (2) coupled 55-gallon barrels for a spindle motor coolant supply reservoir as shown in Figure 67. A spare Browne and Sharpe pump, operating off 115 volts and a 1/4-horsepower motor, was used to deliver coolant to the spindle motor at pressures to 30 psi.

An Alemite, serial number V-4, lubricating system was supplied by ECCO to deliver oil mist to front and rear bearings in the spindle motor.

### 5.3.2 Installation of ECCO High-Speed Spindle

Through four (4) holes in its base, the ECCO high speed router was bolted to an adapter plate which, in turn, was bolted to a tool-post adapter and clamped in the side tool post as shown in Figure 65. A composite view of the adapter plate assembly is shown in Figure 68. Alignment for this simple installation was enhanced by a keyway slot provided in the router base and duplicated in the adapter plate for two different positions.

This setup was not very versatile. For instance, if the spindle or cutter were retracted an inch or two, the Bullard side saddle (see Figure 65) would hit a limit switch. Conversely, if the spindle were advanced an inch or two, the side saddle would hit the main rotary table. To provide needed flexibility, different length tool holders were used and an additional locating (keyway) position was machined in the adapter plate. No provisions were made for machining off-center, which was later found to be advantageous in producing good surface finishes. Additionally, feed rates could only be set by trial and error

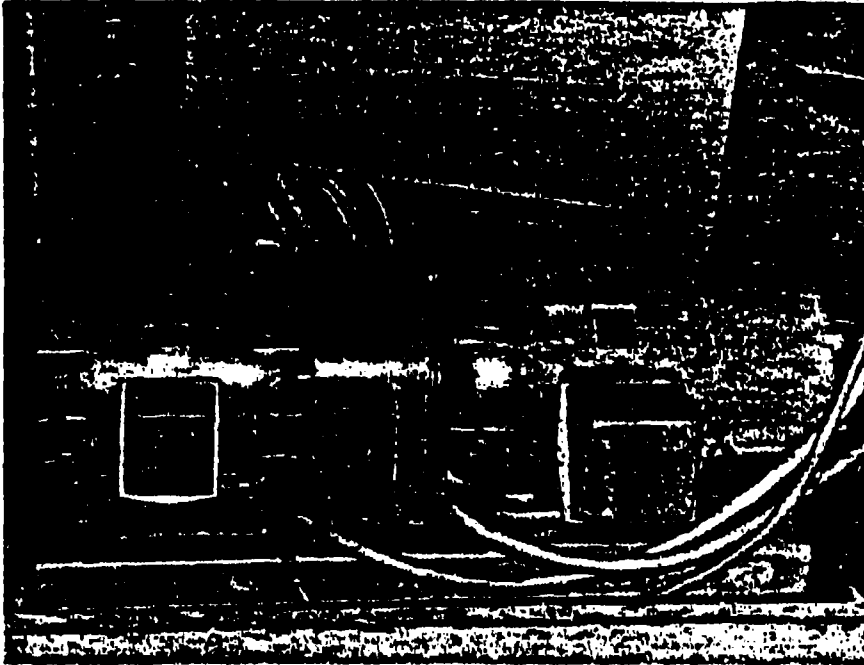


Figure 66. Motor-Sensor Frequency Converter for ECCO Reactor

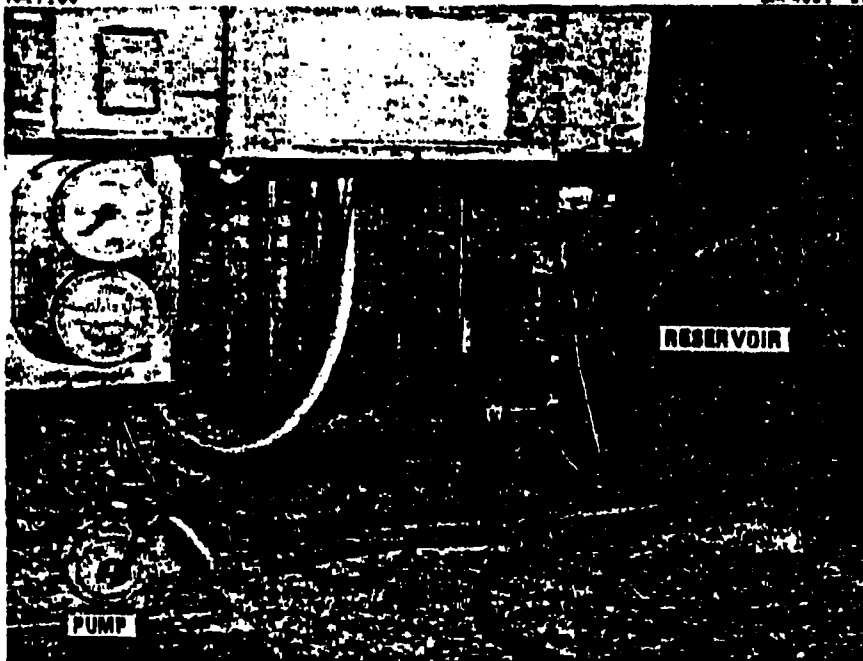


Figure 67. ECCO Spindle Motor Cooling System

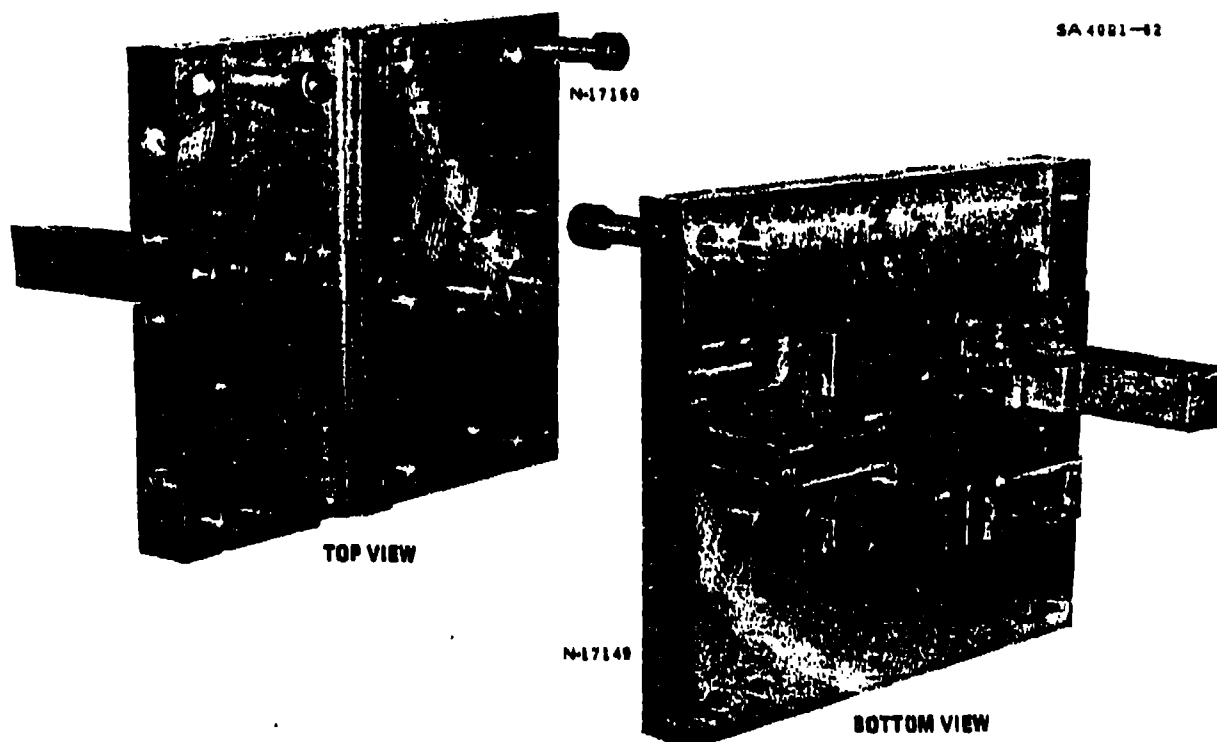


Figure 68. Adapter Plate for ECCO Spindle

procedures, because table speeds (revolutions per minute) could not be programmed or overridden at the low end of the speed range that had to be used. In summation, this setup proved to be useful but awkward for test purposes.

### 5.3.3 Safety Chip Guard

The shield shown in Figure 69 was designed and built to protect personnel from broken cutters and chips. As shown in Figures 64 and 70, that guard which had a 10-inch inside diameter was open on one side to provide chip relief and surrounded the cutter elsewhere to provide safety. It also fit over the router housing and was mitered against the workpiece to minimize exposed areas. The guard was positioned by sliding it in and out of a locating fixture with the aid of two round guide bars as shown in Figure 70. The locating fixture was bolted to a cap plate which, in turn, was bolted to the router base and its adapter plate. While seldom tested, this guard proved to be effective in restraining partially broken cutters on at least two occasions.

N-17101

SA 4081-63

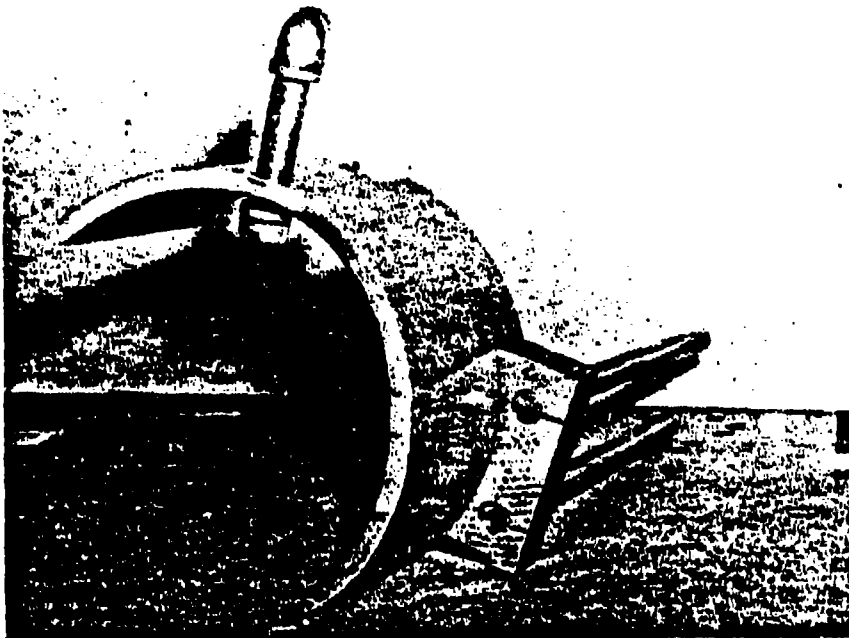


Figure 66. Safety Chip Guard for Bullard VTL

N-16717

SA 4081-64

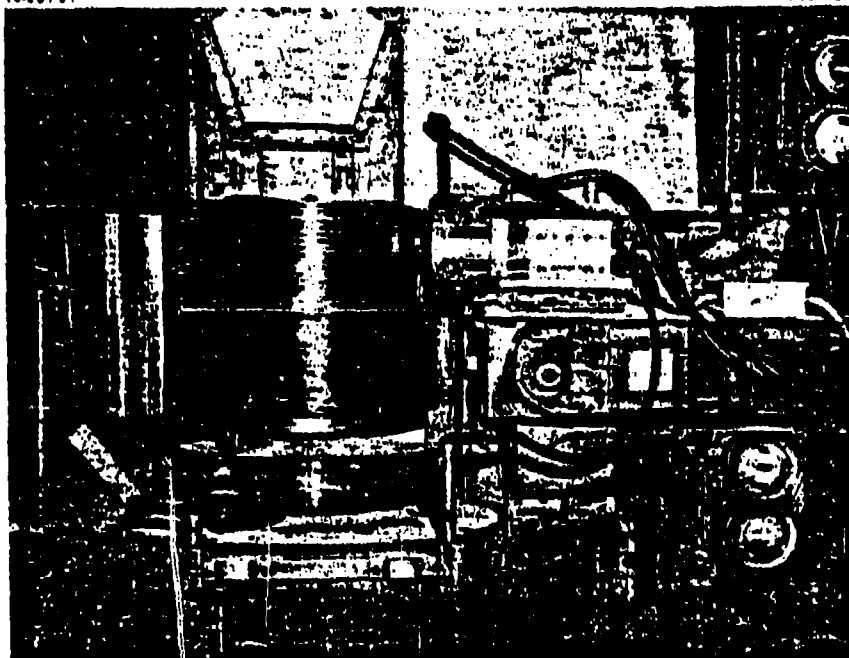


Figure 70. Safety Chip Guard Installed on ECCO Router

## 6.0 MACHINING TEST EQUIPMENT AND GENERAL PROCEDURES

### 6.1 Peripheral End Milling

The modified Sundstrand, Model CM-3, 5-axes, numerical control (N/C) Omnimil described in Section 5 (cf. Figures 47 and 62) was used to conduct a wide variety of peripheral end milling tests on the aluminum alloys selected in Section 2. This machine was ideally suited for developmental studies because its speed and feed were infinitely variable between 10,800 to 20,000 revolutions/minute and 0 to 200 inches/minute, respectively. Additionally, it was equipped with a digital tachometer and could be operated in either an automatic or manual mode.

The load meter on this machine was recalibrated so that it could be used indirectly to measure spindle horsepower. The meter itself was recalibrated so that a reading of 100% was equal to 80 amperes and other percentile readings were proportional; i.e., 25% equals 20 amperes or:

$$\text{Amperes (I)} = 80 (\% \text{ reading}/100)$$

Voltage was found to vary linearly with spindle speed as shown below:

<u>Speed (rpm)</u>	<u>DC (volts)</u>
10,800	132
14,400	177
18,000	223
20,200	251

Analytically, these data were found to be related as follows:

$$\text{Volts (E)} = (\text{rpm} - 379)/79$$

Thus, by reading the load meter and digital tachometer, spindle horsepower could be read directly from the nomograph presented in Figure 71, or computed from the above expressions for direct current values and the following relationship:

$$\text{Spindle horsepower (HP}_s\text{)} = EI/746$$

While the power going into a spindle is called the spindle horsepower, the power coming out of the spindle to drive a cutter is called the cutter horsepower. The ratio of these two values is a measure of the efficiency of a given spindle. In this program, cutter horsepower was calculated from the expression:

$$\text{Cutter horsepower (HP}_c\text{)} = 3.03 \times 10^{-5} F_c V$$

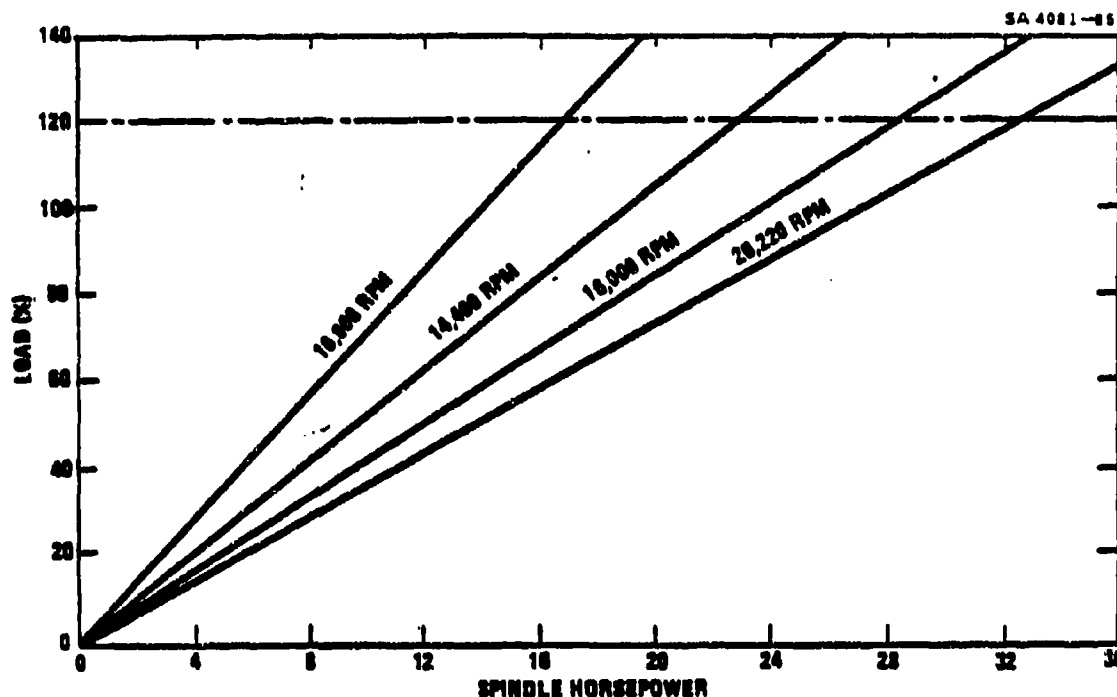


Figure 71. Spindle Horsepower Nomograph

where:

- $F_c$  = Cutting force (pounds)  
 $V$  = Cutting velocity (feet/minute).

Cutting forces ( $F_c$ ) were measured with a 3-axes milling table dynamometer mounted in a vertical position on an angle block as shown in Figure 72. Feed forces ( $F_f$ ) and thrust forces ( $F_t$ ) were also measured with this dynamometer which was purchased from Cook, Smith and Associates of Concord, Massachusetts. The output of the dynamometer was picked up, balanced and amplified with a Midwestern, Model 210, oscillograph (see Figure 73) and recorded with two X-Y plotters as shown in Figure 74.

The test setup shown in Figure 73 was used with and without the dynamometer to conduct peripheral and milling tests for:

- Optimum radial and axial depths-of-cut
- Cutter deflection
- Cutter pullout
- Cutting force measurements
- Horsepower computations.

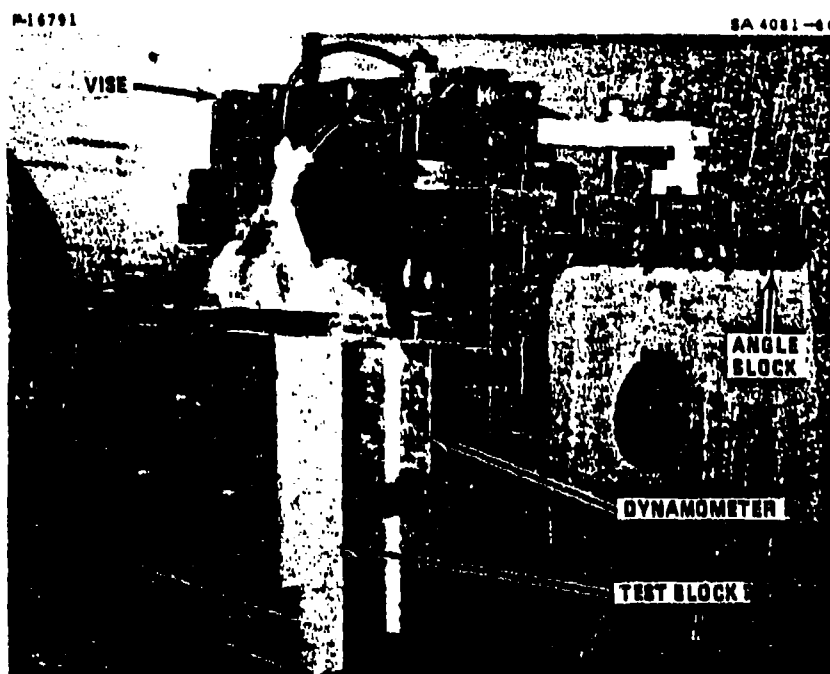


Figure 72. Three-Axis Milling Table Dynamometer and Test Setup

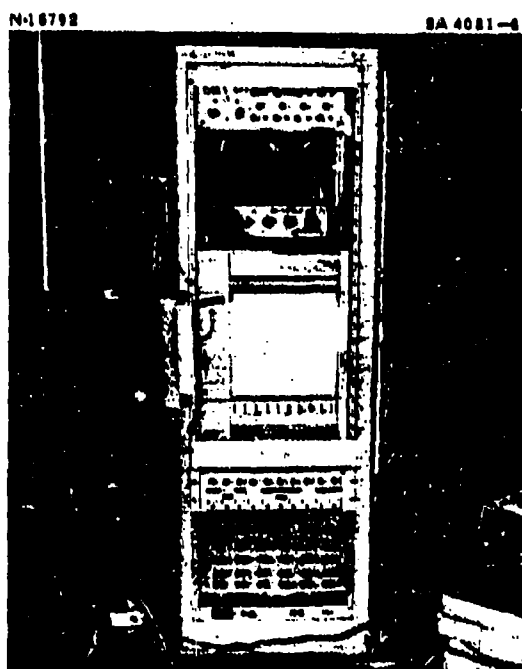


Figure 73. Instrumentation for Measuring Cutting Forces

P-16791

SA 4081-86

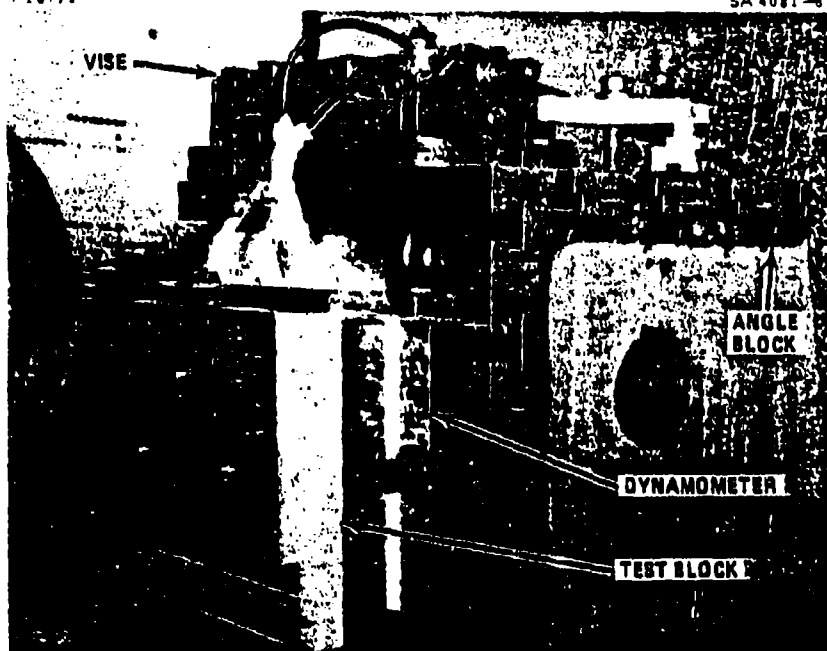


Figure 72. Three-Axes Milling Table Dynamometer and Test Setup

N-16792

SA 4081-47

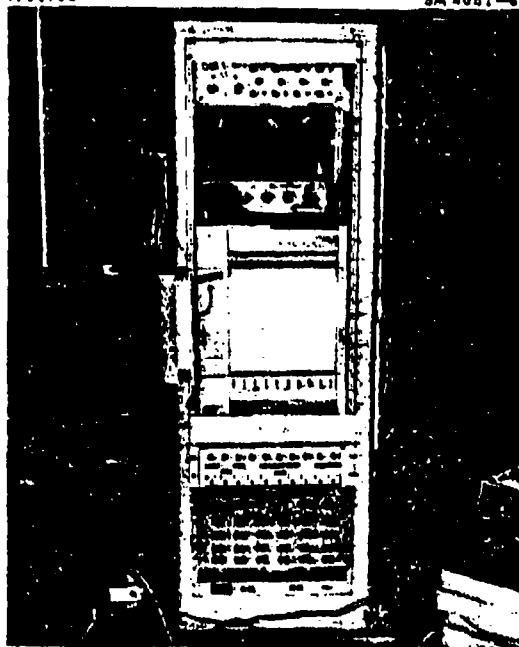


Figure 73. Instrumentation for Measuring Cutting Forces

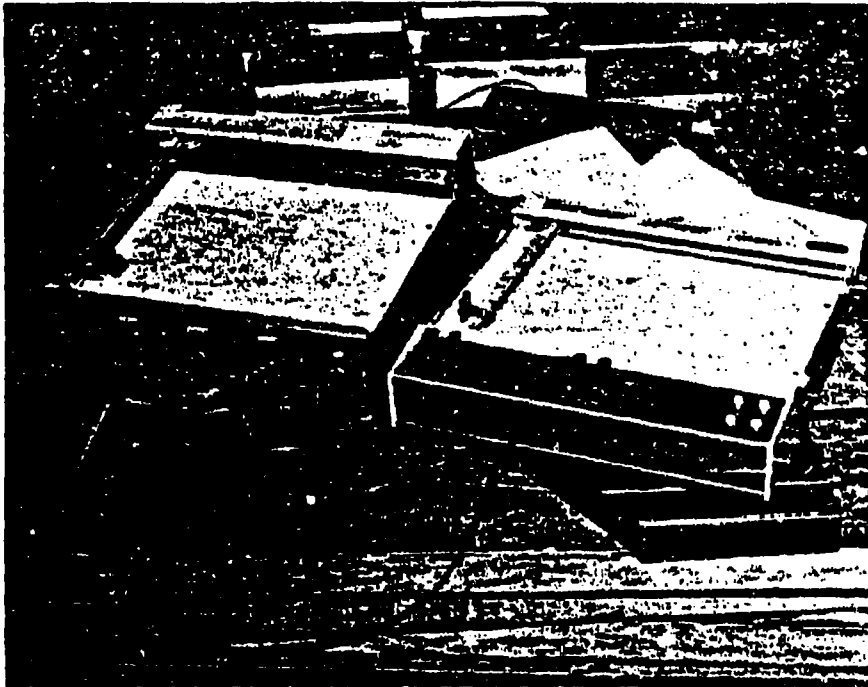


Figure 74. X-Y Plotters Used to Record Cutting Force Traces

For this setup, workpieces for all the aluminum alloys were approximately 2.25 inches thick by 12 inches square. These were drilled, counterbored and bolted directly to the dynamometer as indicated in Figure 72. The Omnimal was operated in the manual mode for all of the above tests.

By mentally removing the dynamometer in Figure 72 and replacing it with the vise shown on top of the angle block in that picture one can, after further mentally rotating the angle block 90 degrees, visualize the peripheral and milling setup used to machine specimens for:

- a. Surface finish tests
- b. Residual stress tests.

Specimens for these tests were approximately one-inch thick and two inches square prior to machining. Machining was accomplished manually by jogging the Z-axis to machine the vertically mounted specimens.

The test setup shown in Figure 75 was used to conduct peripheral and milling tests for:

- a. Cutter geometry
- b. Cutting speed
- c. Feed rates
- d. Tool life.



Figure 75. General Peripheral End Milling Test Setup

Another view of this setup is shown in Figure 76. There, it can be observed that the machining test pieces which measured approximately 2 inches thick by 12 inches wide by 36 inches long were securely bolted to two angle blocks which, in turn, were bolted to the rotary work table. In conjunction with this setup and these tests, N/C tapes were prepared. Generally, these tapes directed a cutter to cut back and forth (climb and conventional milling) a length of 31 inches plus its diameter at the maximum feed rate of 200 inches/minute. When necessary, that feed rate was overridden downward toward zero, as required, in 5% increments without reprogramming. At the completion of each pass, cutters were directed by the N/C tapes to pause about 0.1 second, feed downward 0.25 inch and resume cutting in the opposite direction or, when signaled, to pull out of the cut for inspection. In this manner, these tests were performed in an automatic mode.

## 6.2 Drilling

Much the same equipment and setup that were used for peripheral and milling tests (cf. Figure 75) were used for drilling tests. As before, the high speed spindle in the Omnimil (cf. Figure 62) was used to power cutters (drills), and workpieces were bolted to the same two angle blocks as shown in Figure 77. Even the workpieces were the same. In this case, used workpiece specimens from the peripheral end milling

N-16107

SA 4081-90

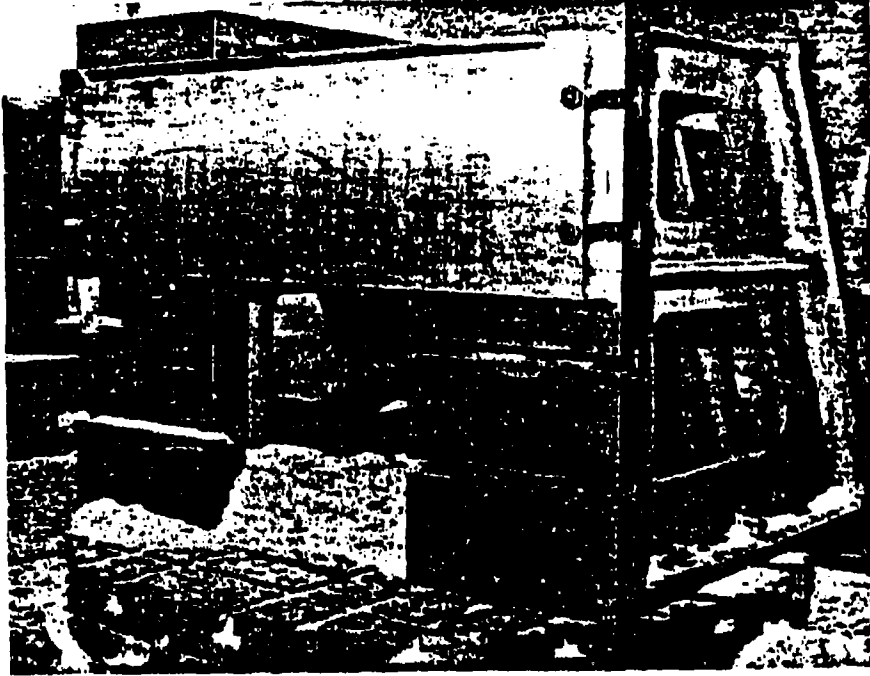


Figure 76. Tool Life Test Specimen for Peripheral Milling Tests

N-16211

SA 4081-91

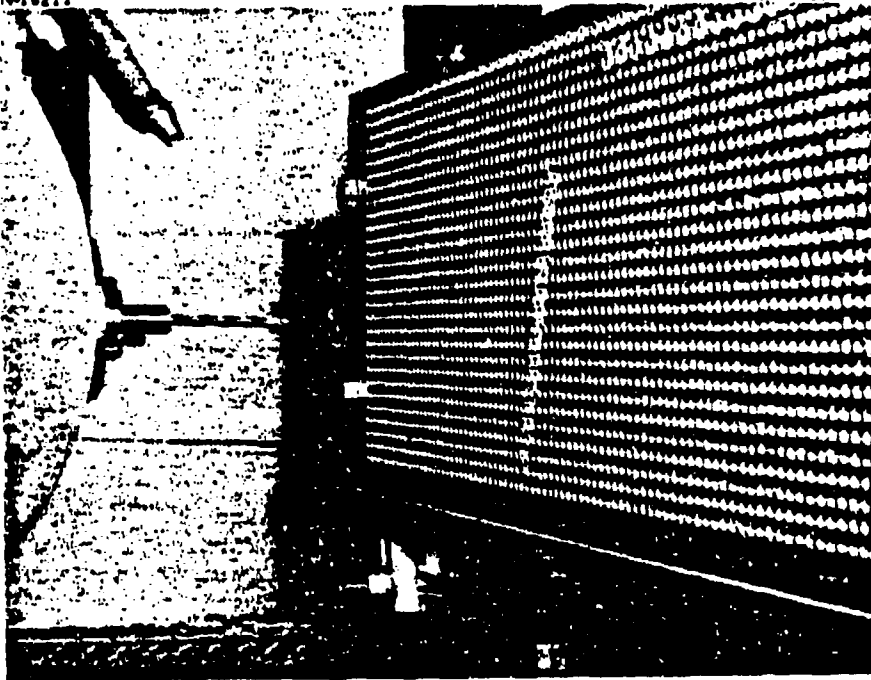
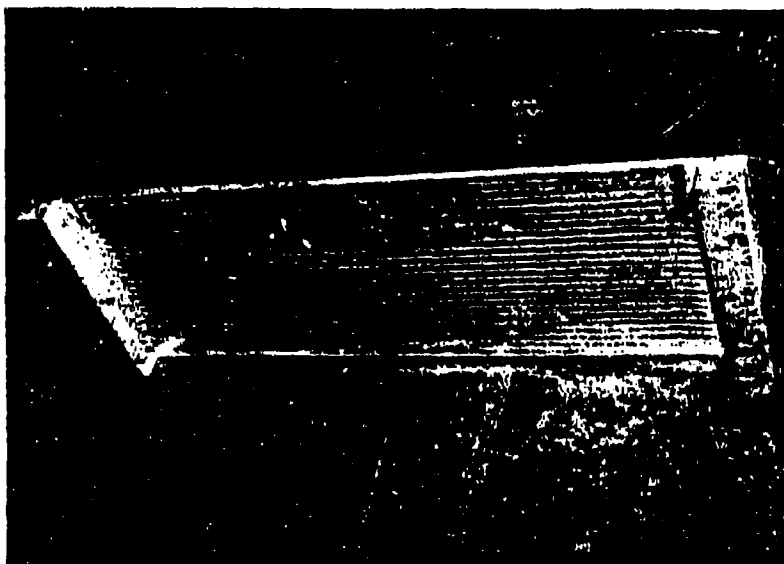


Figure 77. Drilling Test Setup

tests (see Figure 78) were turned over and bolted to the angle blocks. The uncut sections left at each of the milled sides provided clearance for drill penetration, and the 1/2-inch thick web that was left provided material for drill tests. An N/C tape was also prepared for these tests. This tape directed that holes be positioned on 3/4-inch centers at 200 inches/minute and drilled at a feed rate of 200 inches/minute. Further, this tape directed that fourteen rows of holes be drilled on 3/4-inch centers and that 43 holes be drilled per row. By incrementing 3/8-inch down once and to the right twice, the total number of holes was increased by a factor of four, or a total of 2,408 holes were drilled per plate. A drill could also be signaled to pull out of the work area for inspection after completing any row of holes. In this manner, drilling tests were also performed in an automatic mode.

N-17181

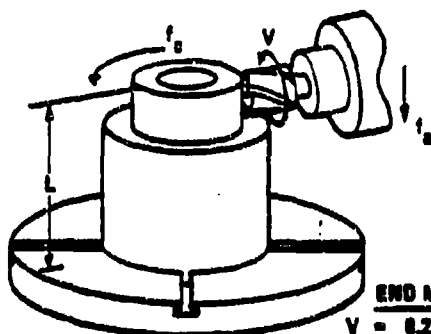


SA 4081-42

Figure 78. Drilling Test Specimen

### 6.3 Turning

Turning tests were performed on a Bullard vertical turret lathe, equipped with a high speed spindle, as shown in Figure 70, using end mills as cutting tools. The mechanics of this method are presented in Figure 79 along with those for conventional turning with a vertical lathe. The merits of using the end mill method for turning unbalanced parts like the G&C shell (cf. Figure 63) can be deduced with the aid of the analytical relationships presented in Figure 79. For example, the 22-inch diameter by 11 inches long G&C shells are conventionally turned at a cutting speed of only 179 rpm and a feed rate of 0.010



#### END MILL

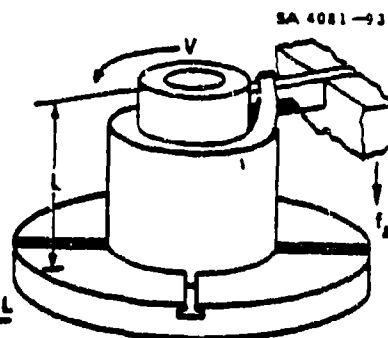
$$V = 0.262 d N$$

$$f_s = f_t M = \pi d N$$

$$N = f_s / C = f_t / \pi d$$

$$f_s = f_t N = f_t M$$

$$T = L / f_s$$



#### CONVENTIONAL

$$V = 0.262 D N$$

$$N = 3.82 V / D$$

$$f_s = f_t N$$

$$T = L / f_s$$

where:

C = CIRCUMFERENCE OF PART  
D = DIAMETER OF PART  
L = LENGTH OF PART  
M = REVOLUTIONS/MINUTE FOR CUTTER  
N = REVOLUTIONS/MINUTE FOR PART  
T = MACHINING TIME/PASS  
V = CUTTING VELOCITY

d = CUTTER DIAMETER  
d<sub>R</sub> = RADIAL DEPTH OF CUT  
f<sub>s</sub> = AXIAL FEED (INCH/MINUTE)  
f<sub>s</sub> = CIRCUMFERENTIAL FEED (INCH/MINUTE)  
f<sub>t</sub> = FEED (INCH/REVOLUTION)  
f<sub>t</sub> = FEED (INCH/TOOTH)  
t = NUMBER OF CUTTING EDGES

Figure 78. Comparison of Conventional and End Mill Turning on VT1.

inch/revolution. The same task was accomplished with a 2-inch diameter, 3-flute, end mill operated at a feed rate of 0.010 inch/tooth, a radial depth of cut of 0.5 inch and a cutting speed of 14,400 revolutions/minute. When these data were substituted into the Figure 79 equations, it was found that the machining time per pass (T) for the conventional method was 6.2 minutes while that for the end mill method was 3.6 minutes. From these results, it was concluded that the end mill method of turning could be economically competitive in special cases.

Another economic consideration is setup time cost. For instance, if a lathe setup could be eliminated by doing both turning and milling on a machining center, as could be the case for the G&C shell, the end mill method might still save enough time to be cost effective even though it was not faster. Thus, while it is not ordinarily possible to beat conventional lathe turning for machining cost effectiveness, there are special situations; e.g., unbalanced parts and eliminated setups, which will enable end mill turning to be the more cost effective.

The rotary table on the Bullard VTL had a speed range that was infinitely variable from 0 to 468 revolutions/minute. According to the Figure 79 equations, the feed rate produced on a G&C shell at the top Bullard speed would be:

$$f_c = \pi DN = \pi (22) (468) = 32,346 \text{ inches/minute}$$

and the chip load would be:

$$f_t = 32,346/3 (14,400) = 0.75 \text{ inch/tooth}$$

Both of these values would stress an end mill beyond its endurance, so it was concluded that realistic feed rates could be increased without limit on the Bullard. In contrast, the feed rate range obtainable from the Omnimil was found to be too limited. For this reason, feed rate studies for this program were performed on the Bullard VTL.

To feed the 2-inch diameter cutter at a rate of 0.010 inch/tooth while it was turning at 14,400 revolutions/minute in the example above, the Bullard would have to rotate the G&C shell at the following calculated speed (cf. Figure 79):

$$N = f_c/C = f_t t M/\pi D$$

$$N = 0.010 (3) (14,400)/\pi (22) = 6.25 \text{ rpm}$$

The rotary table on the Omnimil had a top speed of 2 revolutions/minute, so it could not be used for this application. For the Bullard VTL which did have enough table speed, it was found that the table could not be N/C programmed to turn accurately at such a slow speed due to a loss of resolution and override control on the low side of the Bullard's speed range. It was found, however, that table speeds as low as 1.7 revolutions/minute could be set with reasonable accuracy by manually adjusting relay contacts in the circuitry on a trial-and-error basis. In contrast, downfeeds ( $f_d$ ) on the Bullard could be and were satisfactorily programmed. Thus, tests for this operation were performed partially in a manual mode and partially in an automatic mode.

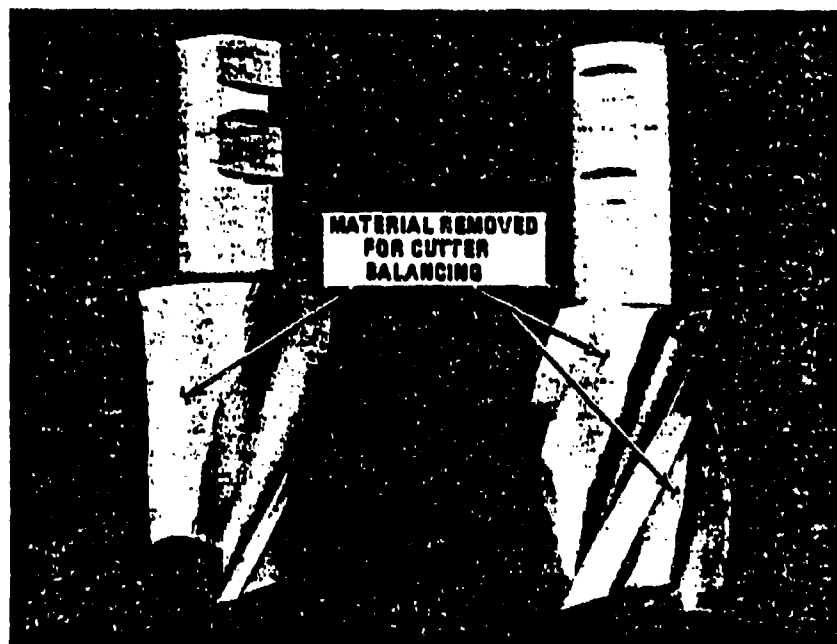
#### 6.4 General

Axial depths of cut were not programmed for any of the operations because of variations in cutter lengths. This parameter was generally set by manually touching-off a workpiece and then incrementing in a desired depth for each cut or succeeding cut.

At the higher spindle speeds, it was found that cutter balance could seriously hinder machining operations. The magnitude of the hinderance also appeared to be a function of cutter size. That is, a cutter under one inch in diameter could generally be run up to 20,000 revolutions/minute without emitting a loud noise or exhibiting much vibration. However, such cutters, if significantly unbalanced, would generally produce a hammering action and yield a shorter tool life. On the other hand, the largest cutters tested (2-inch diameter) would, if out-of-balance, generally commence producing a siren-like noise and vibrating the machine frame at spindle speeds around 15,000 revolutions/

minute. If spindle speeds were further increased, both the noise and vibration would increase until, at 20,000 revolutions/minute, both would probably be intolerable. The same result was also noted for cutters having diameters between one and two inches but to a proportionately lesser degree. Thus as a normal maintenance policy, newly procured cutters were spun up to 20,000 revolutions/minute; and if found necessary, the cutters were shipped to a vendor for dynamic balancing. There, balancing was accomplished by grinding metal off the backside of cutters as portrayed in Figure 80. Similarly, toolholders were dynamically balanced by drilling or grinding metal from appropriate points along the surface of toolholder bodies. It was also found advantageous to grind opposing set-screw slots in the shank of end mills. This procedure not only helped balance a cutter, but it was frequently noted that rotating a cutter in the toolholder improved cutter runout and balance. In summation, it was established that the success or failure of high speed machining depends largely upon cutter balance. Therefore, extra care and expense were expended to provide good spindle, toolholder and cutter balance in this program.

N-16614



SA 4881-94

Figure 80. Dynamically Balanced End Mills

## 7.0 TEST RESULTS - CUTTER GEOMETRY

### 7.1 Statistical Model for Tests

It has been shown<sup>7</sup> that the functional angles on a cutting tool are related as follows:

$$\sin \alpha_e = \sin^2 i + \cos^2 i \sin \alpha_n$$

where:

$\alpha_e$  = effective rake angle

$\alpha_n$  = normal rake angle

$i$  = inclination angle.

If optimum values for two of these angles could be established, then the third angle would be fixed mathematically and the optimum cutter geometry would be completely defined.

An experimental technique was developed<sup>12</sup> which solves the above equation experimentally as illustrated in Figure 81. There, it can be seen that a cutter having an inclination angle of  $-7\frac{1}{2}^\circ$  and an effective rake angle of  $-5^\circ$  will yield the longest tool life between regrinds and is, therefore, the optimum for face milling 4340 steel, R<sub>h</sub> 54. Similar tests were performed on other materials; and the results were correlated with respective material properties, using a multiple linear regression technique and a digital computer. From that study, the following empirical equation was developed for predicting optimum face mill geometries:

$$\alpha_e \text{ opt} = 19.79^\circ - (0.167 S_y)^\circ + (0.08 RA)^\circ + (0.077 S_{U_1})^\circ + (10.1 S_y/S_{U_1})^\circ$$

Using this equation, handbook data, and test results reported by Oxford<sup>13</sup>, which stated that a helix angle of  $45^\circ$  would produce the best finish on aluminum, as guides, cutter geometries which would bracket the optimum value were estimated. A total of nine geometries were estimated in all. These were divided into groups of three, having inclination (helix) angles of  $25^\circ$ ,  $35^\circ$ , and  $45^\circ$ , respectively. In turn, each inclination angle group of three had corresponding radial rake angle values of  $5^\circ$ ,  $10^\circ$ , and  $15^\circ$ . Brazed carbide cutters having these nine cutter geometries were procured for optimum cutter geometry testing (cf. Figure 81), and these 1.5-inch diameter cutters are shown in figure 82.

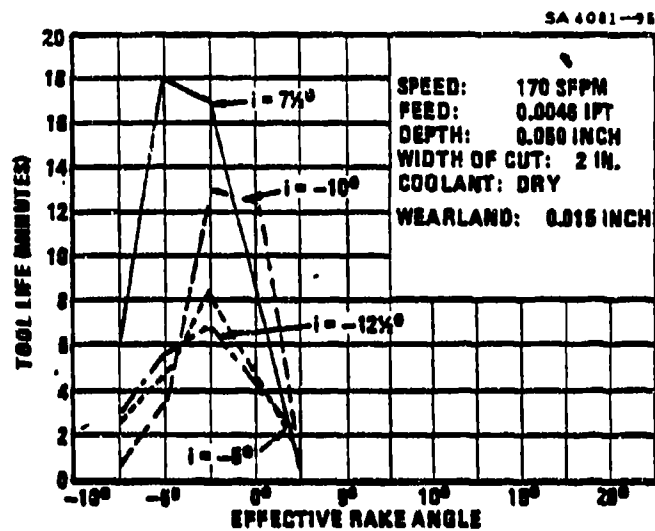


Figure 81. Effect of Inclination Angles and Effective Rake Angles on Tool Life When Face Milling 4340 Steel (RC 54)

N-18763 SA 4081-96

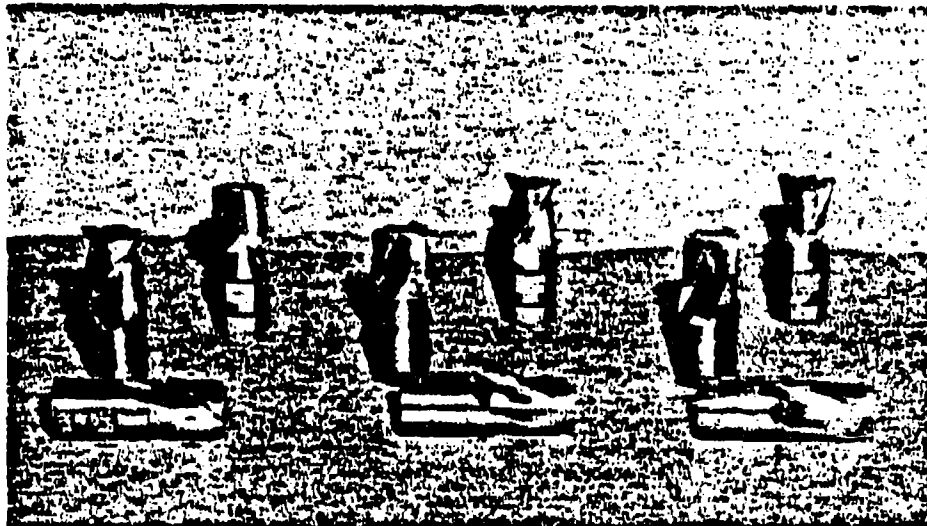


Figure 82. End Mills for Optimum Cutter Geometry Test

Fast Speed Tests

While waiting for the Bryant high speed spindle to be installed in the Omnimil, it was decided to try and get a head start on the optimum cutter geometry tests by using the fast spindle that was already in the Omnimil. This decision was encouraged by the fact that the fast spindle in that machine would turn up to 4,000 revolutions/minute.

To establish a starting point for this test, all nine cutters were tested (cf. Figure 75) for cutting efficiency with the aid of the load meter on the Omnimil. The results obtained are presented in Figure 83, where it can be deduced that a cutter having a helix angle of 25° and a radial rake angle of 5° probably has as good strength and cutting efficiency as any of the other geometries tested. It should also be noted that carbide inserts on the 15° radial rake angle cutters, having helix angles of 35° and 45°, broke while cutting. These inserts were too acute and appeared to grab and then snap in the 7075-T651 aluminum workpiece. The cutter having a helix angle of 35° and a radial rake angle of 10° also exhibited a good cutting efficiency, but it was not felt to be as strong as the 25° helix angle, 5° radial rake angle cutter; so the latter was selected for initial testing.

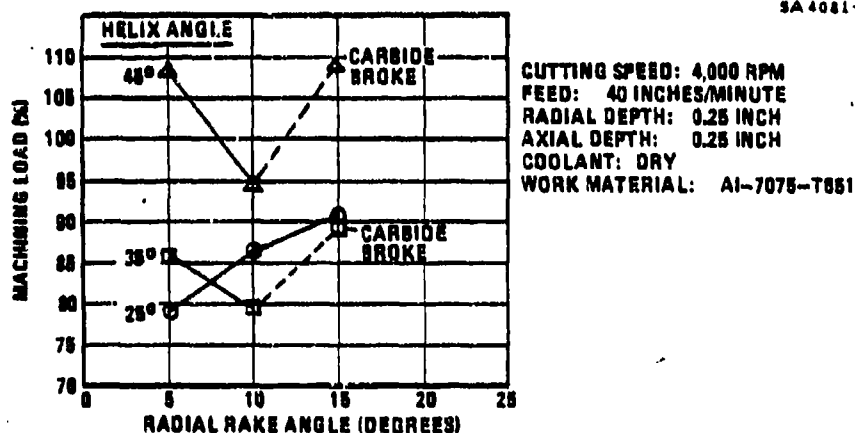


Figure 83. Effect of Cutter Geometry on Machining Load

When conducting a similar test for steel, Oxford<sup>13</sup> found that his test curves were linear and had negative slopes. The 35° and 45° helix angle curves in Figure 83 started out that way; but at a radial rake angle of 10°, these curves reversed and the slopes became positive. In further contrast, the slope of the 25° helix angle curve was positive throughout, and the curve was nearly linear. No good explanation can be offered for this behavior now; but it appears evident that 15° radial rake angle cutters are less than optimum.

Using the end mill having a 25° helix angle and a 5° radial rake angle, tool life tests were initiated on 7075-T651 aluminum workpieces (cf. Figure 75). The results obtained are given in Figure 84. As shown, that end mill cut for 544 minutes (9.07 hours) without exhibiting any appreciable wear. During that time, the end mill traveled 1,816 feet through the work material. Testing was stopped at these points because it was believed that too much material would be required to complete the tests.

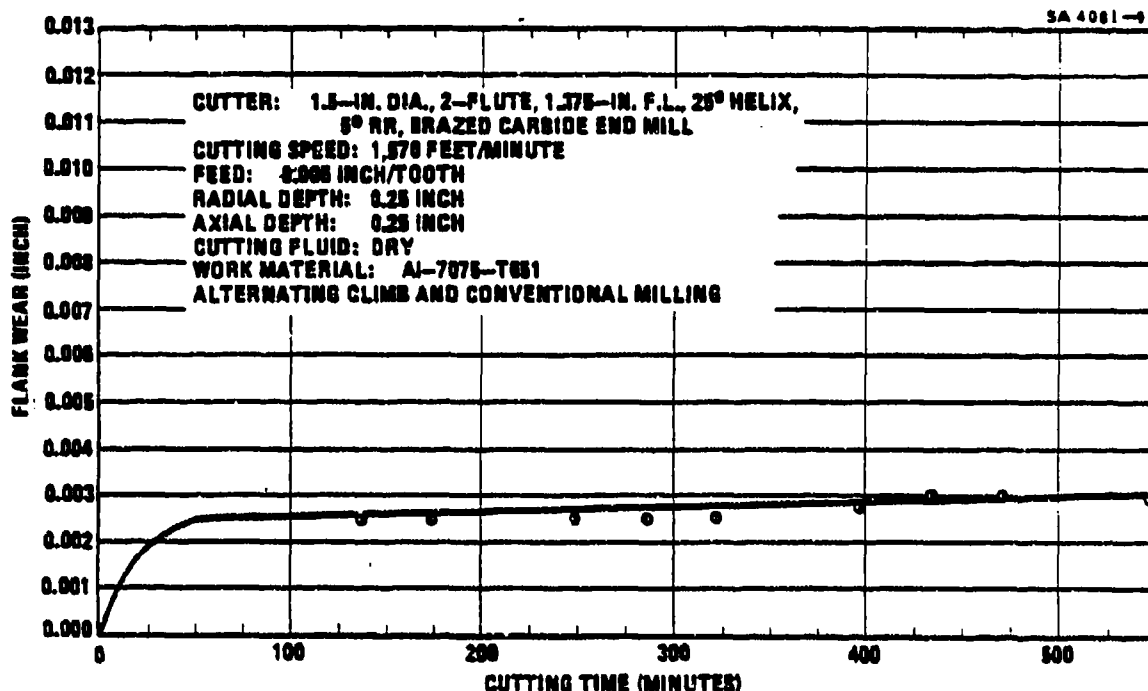


Figure 84. Cutter Wear Curve for Conventional Cutting Speed

### 7.3

#### High Speed Tests

Following installation of the Bryant high speed spindle, optimum cutter geometry tests were resumed with the cutters shown in Figure 82. As before, these tests were initiated on 7075-T651 aluminum with the end mill having a 5° radial rake angle and 25° helix angle. In an attempt to hasten cutter wear, a normal procedure for optimum cutter geometry determinations, the modified Conimil was operated at a top spindle speed and feed rate of 20,000 revolutions/minute and 200 inches/minute, respectively. The results obtained with this combination are presented in Figure 85. There, it can be seen that the selected end mill, which had a runout of 0.001 inch T.I.R., cut 372 minutes (6.2 hours) before the test was stopped. During that time, the cutter traveled 6,200 feet or 1.17 miles through the work material. By extrapolation, it was estimated that this cutter would

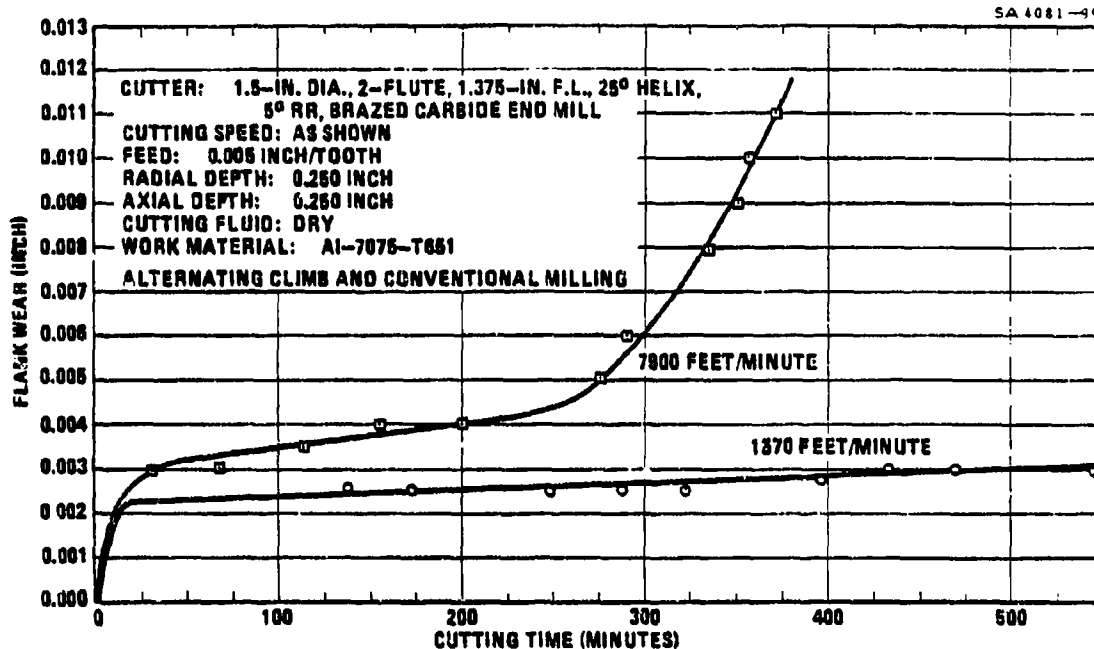
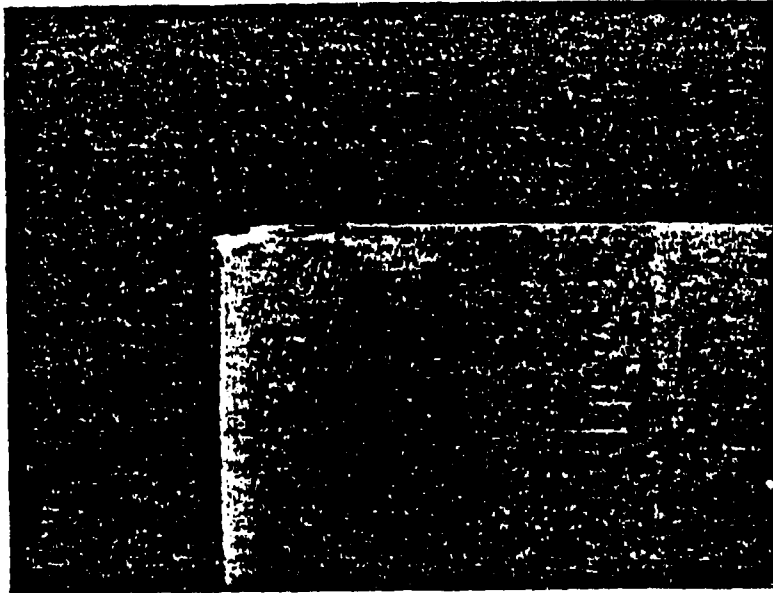


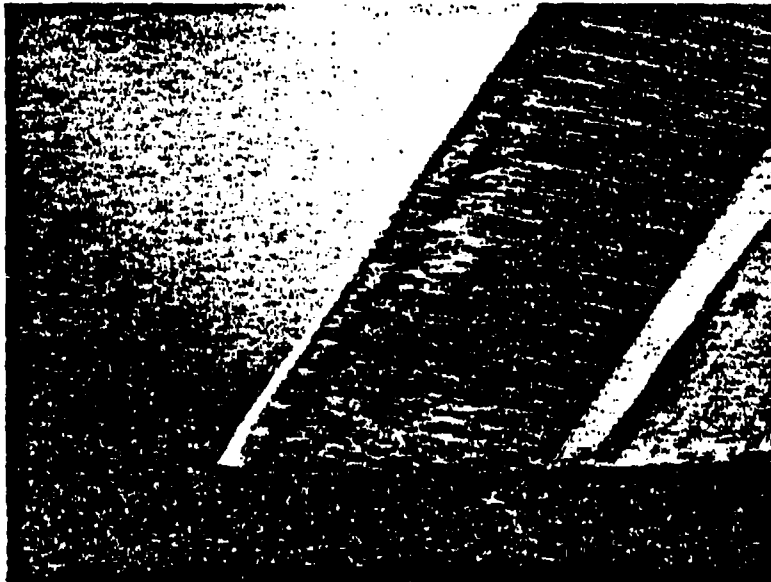
Figure 85. Effect of Cutting Speed on Carbide Cutter Wear

have cut for 7 hours before developing a 0.015-inch wearland, a normal tool life end point. The wearland which developed on the flank and top rake of this cutter is shown in Figure 86, and an end view of the cutter is shown in Figure 87. For comparative purposes, the results obtained from the fast speed tests (cf. Figure 84) were superimposed on Figure 85. In summation, it can be deduced from this figure that cutting speed has a definite effect on cutter wear but that cutter wear is generally not going to be much of a high speed machining problem when cutting aluminum alloys.

Work material depletion began to surface as a problem at this point; therefore, cutting efficiency tests were rerun to develop some quick indices, using the higher cutting speed and feed of 20,000 revolutions/minute and 200 inches/minute, respectively. The results obtained virtually mirrored those shown in Figure 83, including the breakage of carbide inserts on two cutters having 15° radial rake angle and 35° and 45° helix angles. Based on these results, it appeared that the cutter having a 15° radial rake angle and 25° helix angle might be one of the quickest to eliminate; therefore testing was resumed with it. Actually, the reverse may have been true; for as shown in Figure 88, that end mill cut for 229 minutes or 3.8 hours before testing was stopped. Testing was stopped at that point because the end mill was developing built-up-edges on its flanks and, as a consequence,



**TOP RAKE WEARLAND**



**PLANK WEARLAND**

**Figure 88. Wearlands Developed After Cutting 1.17 Miles of AJ-7078-T881**

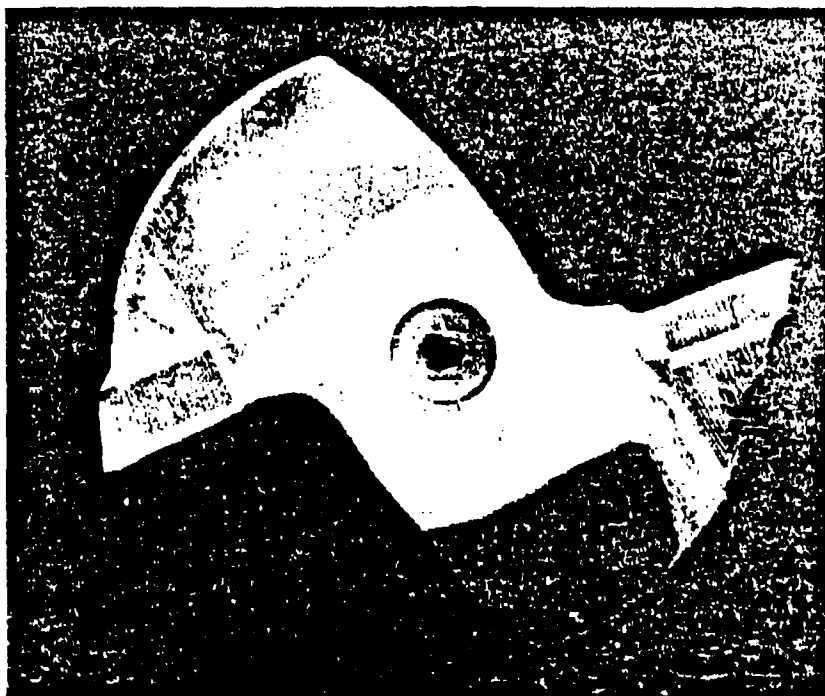


Figure 87. End View of 25-Degree Helix, 5-Degree RR Brazed Carbide End Mill

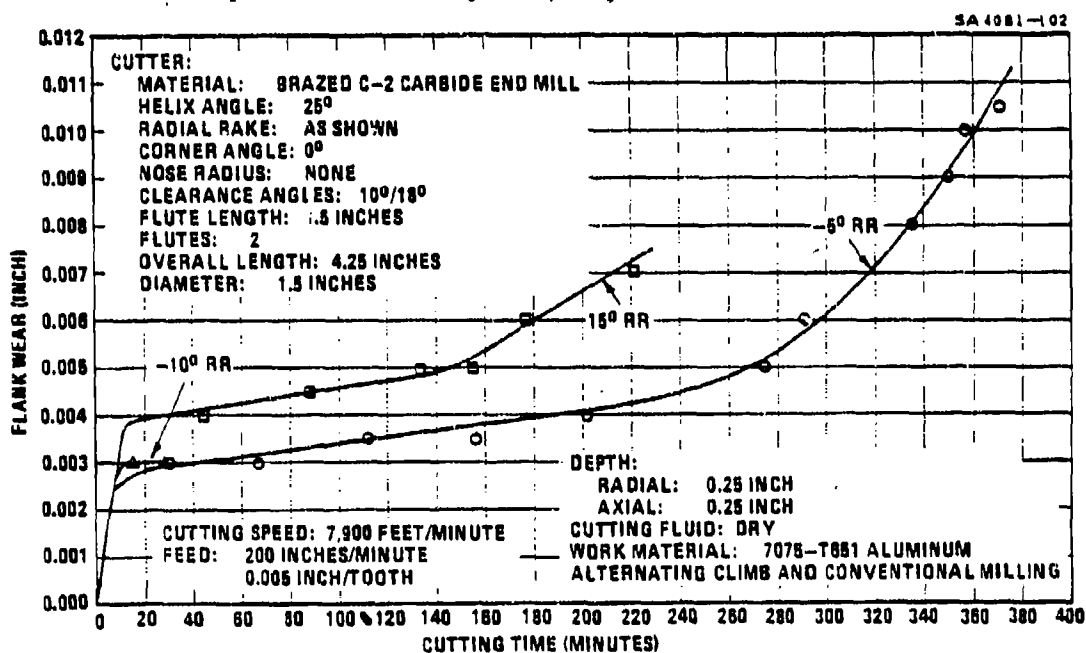


Figure 88. Effect of Cutter Geometry on Cutter Wear

was cutting so hard that it was pegging the load meter needle and tripping the overload interlock switch which shut down the Omnimil. Had the built-up-flanks not occurred, that end mill might have cut for 5 hours before developing a terminal tool life value of 0.015-inch wearland. Nevertheless, that end mill would not have lasted as long as the one having a 3° radial rake angle and 25° helix angle as can be deduced from Figure 88, where results for the latter were superimposed for comparative purposes. Only meager data were recorded for the end mill having a 25° helix angle and 10° radial rake angle and that too was superimposed on Figure 88 for comparative purposes. While only a guess can be made for the 10° radial rake angle cutter, it would be expected to wear more slowly than the 15° radial rake angle cutter and to wear nearly on par with the 5° radial rake angle cutter. While the end mill having a 35° helix angle and 10° radial rake angle showed some potential (see Figure 83), it developed two nicks in 7 minutes which promised to abbreviate its tool life. At this point, tests were terminated because it did not appear that any of the cutters would outperform the one having a 25° helix angle and a 5° radial rake angle. Additionally, the optimum cutter geometry tests were terminated because cutter wear and geometry had degenerated into a minor problem for this program, and work material was being too rapidly depleted.

It had been planned to use the statistical method illustrated in Figure 81 to establish optimum cutter geometries in this study. However, that method could not be advantageously applied, because cutting speeds could not be increased to the point where cutter flanks would develop 0.015 inch wearlands in minutes instead of hours. The next best method to use for this investigative purpose was probably that shown in Figure 88; but to produce defensible data, even that method required that some cutter lives be measured in hours. In short, there does not appear to be a simple, direct method for establishing an optimum cutter geometry for the high speed milling of aluminum. Until such a method is established or a better cutter geometry is found, a 25° helix angle, 5° radial rake angle, carbide end mill will prove to be more than adequate and is recommended for the high speed machining of aluminum alloys.

## 8.0 TEST RESULTS - MACHINING PARAMETERS

### 8.1 Introduction

The objective of this event was to develop optimized machining procedure and parameters for the selected combinations of aluminum alloys and machining processes so that future missile components could be fabricated at maximum economical speeds. Synonymous with maximum economical speeds is maximum metal removal rates. Consequently, to the extent possible, rough machining cuts were used in developing economic machining conditions. Rough machining is used in removing the bulk of material from missile forgings, castings or raw material and is, thus, better suited to high-speed machining operations than finish machining. The determination of economic machining parameters requires a knowledge of the machining conditions that will yield high metal removal rates or extended cutter lives. The plan which was outlined to develop that knowledge here consisted principally of optimizing cutter geometries and materials, coolants, feed rates, depths of cut and cutting speeds, in much that order.

Cutter geometry, cutter material and coolant optimization were discussed in previous sections. In this section, feed rate, depth of cut and cutting speed optimization data and results obtained from end milling, drilling and turning tests on 7075-T651, 6061-T651 and A356-T6 aluminum are presented. This type of information should be especially useful to spindle designers and N/C programmers.

The extraordinarily long tool lives produced by carbide cutters (cf. Figure 85) were hindering the development of high speed machining technology in these tests and appeared to be squandering both time and material. To rectify that situation by reducing cutter life to a more acceptable level, testing was continued with high speed steel (HSS) cutters when feasible. The HSS end mills used were off-the-shelf items and generally had 30° helix angles, 10° radial rake angles, and 12° primary clearance angles. These cutters contained 4% cobalt and may have been more heat resistant than normal. In any event, these standard priced cutters, which lowered tool life some 56% under that for carbide cutters, proved to be more than adequate for a 20,000 revolutions/minute spindle in most cases. Thus, the substitution of high speed steel cutters for carbide cutters in these studies was found to be not only expedient but, generally, proper.

### 8.2 Peripheral End Milling

#### 8.2.1 Feed Rate Optimization

The maximum Oximil feed rate was limited to 200 inches/minute. For two- and four-flute cutters, that feed produced a maximum chip load of 0.005 and 0.0025 inch/tooth, respectively, at a cutting speed of 20,000 revolutions/minute. Since aluminum can be readily cut at chip loads up to 0.010 inch/tooth, it became evident that it was futile to

attempt an evaluation of feed rates on the Omnimil. Instead, this parameter study was shifted to the Bullard V.T.L. machine which had no practical upper chip load limitation. The results obtained will be discussed in paragraph 8.4.1.

Feed rate tests were performed on the Omnimil for 6061-T651 aluminum at chip loads of 0.0025 and 0.005 inch/tooth. The results of these tests are given in Figure 89, where it can be observed that the heavier chip load produced a slower rate of cutter wear and, therefore, a longer tool life. It was expected that this trend would continue up to feed rates of approximately 0.010 inch/tooth, after which, the trend would reverse.

SA 4881-103

**CUTTER:**

MATERIAL: COBALT HSS END MILL  
DIAMETER: 1.5 INCHES  
OVERALL LENGTH: 4.5 INCHES  
FLUTE LENGTH: 2 INCHES  
FLUTES: 2  
HELIX: 30°  
RADIAL RAKE: 10°  
CORNER ANGLE: 6°  
NOSE RADIUS: 0.020  
CLEARANCE: 12°/22°

CUTTING SPEED: AS SHOWN  
FEED: AS SHOWN  
DEPTH:

RADIAL: 0.25 INCH  
AXIAL: 0.50 INCH

CUTTING FLUID: WATER SOLUBLE OIL MIST (1:30)  
WORK MATERIAL: 6061-T651 ALUMINUM  
ALTERNATING CLIMB AND CONVENTIONAL MILLING

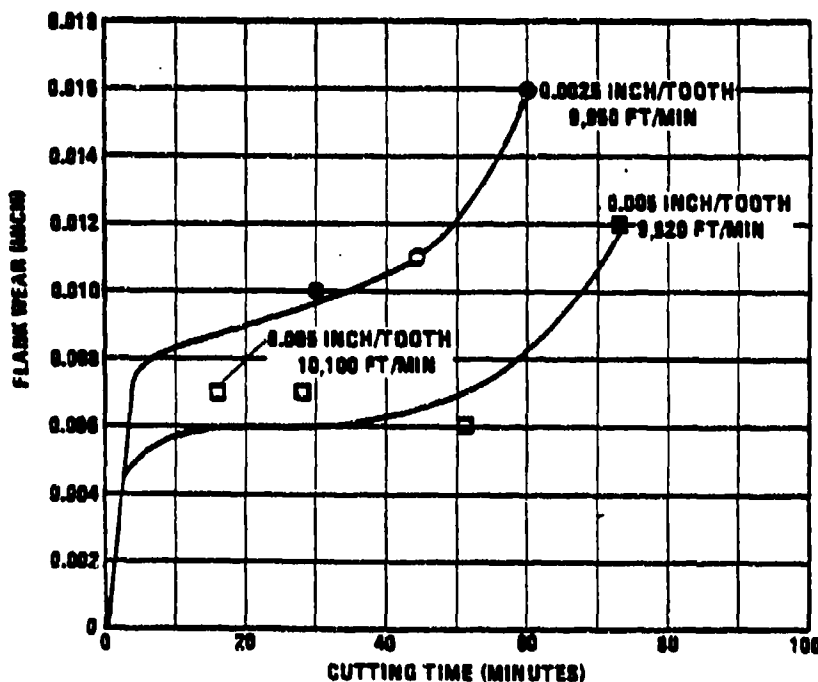


Figure 89. Effect of Feed Rate on Cutter Wear

### 8.2.2 Depths of Cut

One of the first characteristics noted about the high speed machining process was that normal depths of cut could not be made with it. For instance, the relatively light depth of cut taken in the tests referenced by Figure 83 either raised the load meter needle to a high value or pegged it. When cut depths were further increased, it was found that protective, overload interlocks in the spindle system would shutdown the spindle's and Conimil's operations. An investigation revealed that the interlocks were activating at an input load of 40 amperes or approximately 13.5 horsepower when the spindle was operated at 20,000 revolutions/minute. For a "rule of thumb" efficiency of 65%, this meant that the spindle could only put out a maximum of 8.8 horsepower. This lack of power helps explain why the spindle was not capable of making deeper cuts.

After discussing this power deficiency problem with the spindle's manufacturer, the Bryant Grinding Corporation, the overload, interlock, trip point was reset to 90 amperes input or approximately 30 horsepower at a spindle speed of 20,000 revolutions/minute. Based on a 65% efficiency, the output capability of the spindle was raised to approximately 20 horsepower by this action. At the same time, the interlock was being reset, the load meter was recalibrated (see subsection 6.1) so that ampere measurements could be extracted directly from it. Additionally, it was noted that a 5% machine load or about 4 amperes or 1.4 horsepower were required to turn the spindle, unloaded, at 20,000 revolutions/minute. Overall, these procedures decreased the spindle's protection but enabled it to make deeper depths of cut.

Using the more powerful spindle, depth of cut studies were performed for the three aluminum alloys. All tests were conducted with a spindle speed of 20,000 revolutions/minute and a feed rate of 200 inches/minute. High speed steel (HSS) and mills were used to machine the 7075-T651 and 6061-T651 aluminum alloys. For the most part, these HSS and mills had a 1.25-inch diameter, 4-flutes and a 2.5-inch flute length. For the few cases where the radial depth of cut exceeded approximately 1.25-inch, a 2.0-inch diameter, 4-flute, 2.5-inch flute length cutter was used. To machine the surprisingly abrasive A356-T6 aluminum alloy, carbide cutters had to be used. For this case, brazed-carbide end mills, having 3-flutes, 2-inch flute lengths and 1.75-inch diameters, were pressed into service. The variation in tooth density here was not thought to be significant, because preliminary tests had not indicated any appreciable difference in the machining loads generated by 2- and 4-flute end mills under the test conditions used. The test setup used is shown in Figure 72. With this setup, radial depths of cut were varied over a range that produced a practical spectrum of machine loads. The machine load produced by each variation was noted, and the data obtained were plotted in the manner shown in Figure 90. There, it can be observed that the plot is linear.

CUTTER: 1.25-IN. DIA., 4-FLUTE, 2.5-IN. F.L., HSS END MILL  
 CUTTING SPEED: 6,000 FEET/MINUTE  
 FEED: 0.0025 INCH/TOOTH  
 AXIAL DEPTH: 1.5 INCH  
 CUTTING FLUID: WATER SOLUBLE OIL MIST (1:30)  
 CLIMB CUTTING

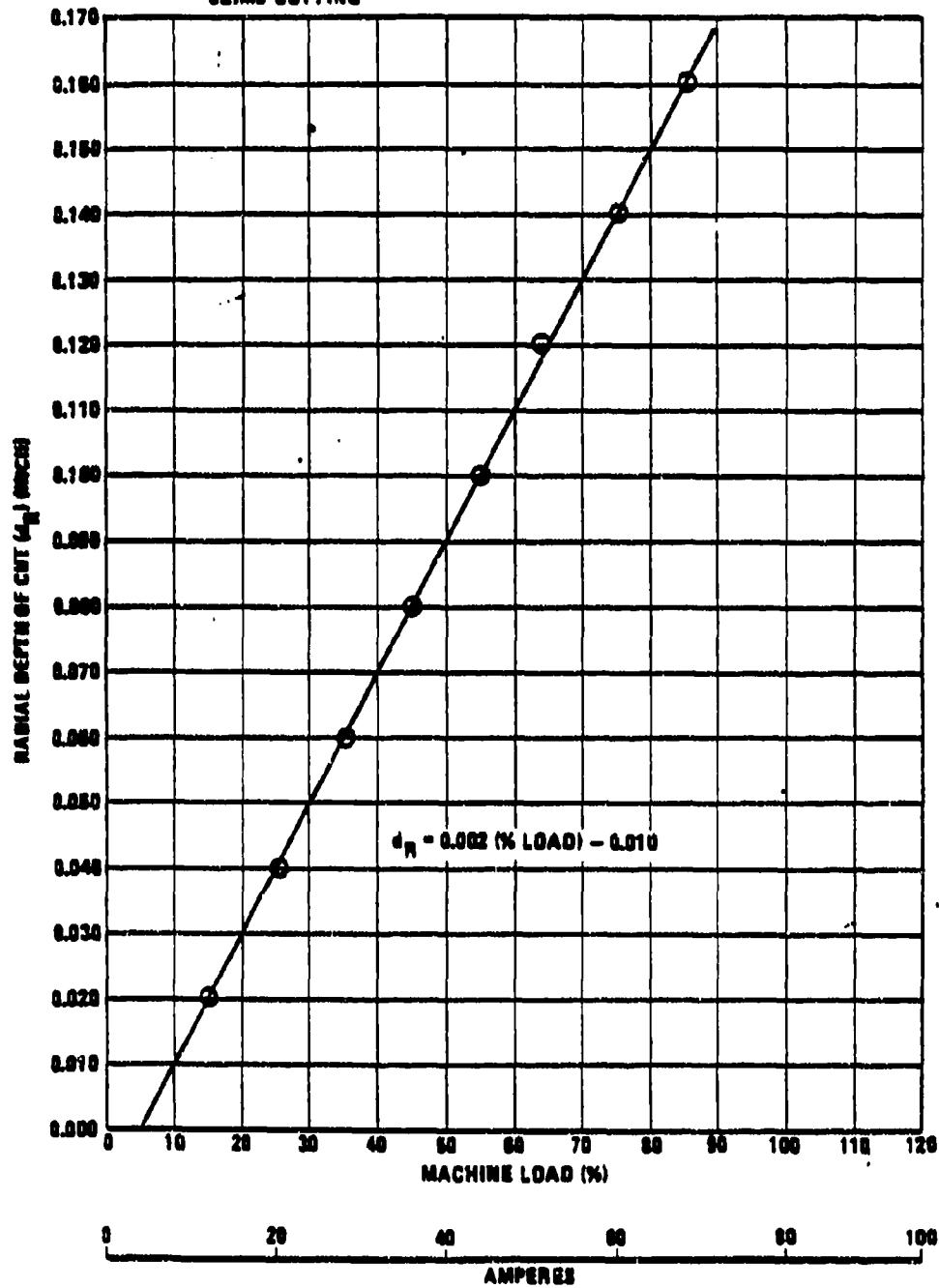


Figure 90. Effect of Radial Depths of Cut on Machine Loads for Al-7075-T851

The analytical expression for that curve which has been superimposed on the plot was developed with the aid of multiple regression. This procedure was repeated for each aluminum alloy at axial depths of cut of 2.0, 1.5, 1.0, 0.75, 0.50, 0.25, and 0.125 inches, respectively. The curves for each alloy were gathered and replotted by material as shown in Figures 91 through 93. These curves are not conservative because each was developed with a relatively sharp (0.000 to 0.003 inch wearland) cutter. It follows that duller cutters will generate higher spindle loads and that some allowances will have to be made. However, these curves provide a good starting point for the programmer having to prepare an N/C tape for high speed machining. To further guide the programmer and provide some spindle protection, recommended operating bands or ranges were superimposed on these curve plots. For instance, if the spindle is to be run continuously, it should not be operated at a machine load over 50% (40 amperes). For short or intermittent runs which provide an opportunity for the spindle to cool down, spindle loads to 75% would be in order. Spindle loads over 75% have been red-lined, because breakdowns occur with greater frequency and magnitude in that zone. While spindle loads over 100% have been recorded for some cuts; e.g., plunging the full cutter diameter into the corner radius of a pocket, these have been very brief in duration. Any attempt to machine at a 100% load for very long would probably result in a bent spindle shaft or some other catastrophe. While these recommended operating ranges were not comprehensively developed and are subject to change, these were based on the contractor's experiences which included the bending of two spindle shafts; however, no bearing failures were experienced. To further aid in the selection of cut depths, equations developed for each curve (cf. Figure 90) are presented as follows:

<u>Al-7075-T651</u>	
<u>Axial Depth</u> <u>(inch)</u>	<u>Radial Depth</u> <u>(inch)</u>
2.0	$d_R = 0.0014 (\% \text{ load})$
1.5	$d_R = 0.002 (\% \text{ load}) - 0.010$
1.0	$d_R = 0.0034 (\% \text{ load}) - 0.016$
0.75	$d_R = 0.0048 (\% \text{ load}) - 0.033$
0.50	$d_R = 0.0073 (\% \text{ load}) - 0.042$
0.25	$d_R = 0.0145 (\% \text{ load}) - 0.048$
0.125	$d_R = 0.0223 (\% \text{ load}) + 0.107$

<u>Al-6061-T651</u>	
<u>Axial Depth</u> <u>(inch)</u>	<u>Radial Depth</u> <u>(inch)</u>
2.0	$d_R = 0.0016 (\% \text{ load})$
1.5	$d_R = 0.0022 (\% \text{ load}) - 0.012$
1.0	$d_R = 0.0035 (\% \text{ load}) - 0.016$
0.75	$d_R = 0.0050 (\% \text{ load}) - 0.034$
0.50	$d_R = 0.0083 (\% \text{ load}) - 0.070$
0.25	$d_R = 0.0171 (\% \text{ load}) - 0.079$
0.125	$d_R = 0.0304 (\% \text{ load}) - 0.115$

**CUTTER:**

○ 1.250-IN. DIA., 4-FLUTE, 2.5-IN. F.L., COBALT HSS END MILL

□ 2.000-IN. DIA., 4-FLUTE, 2.5-IN. F.L., COBALT HSS END MILL

CUTTING VELOCITY: 20,200 RPM

FEED: 200 INCHES/MINUTE

CUTTING FLUID: WATER SOLUBLE OIL MIST (1:30)

CLIMB CUTTING

SA 4081-105

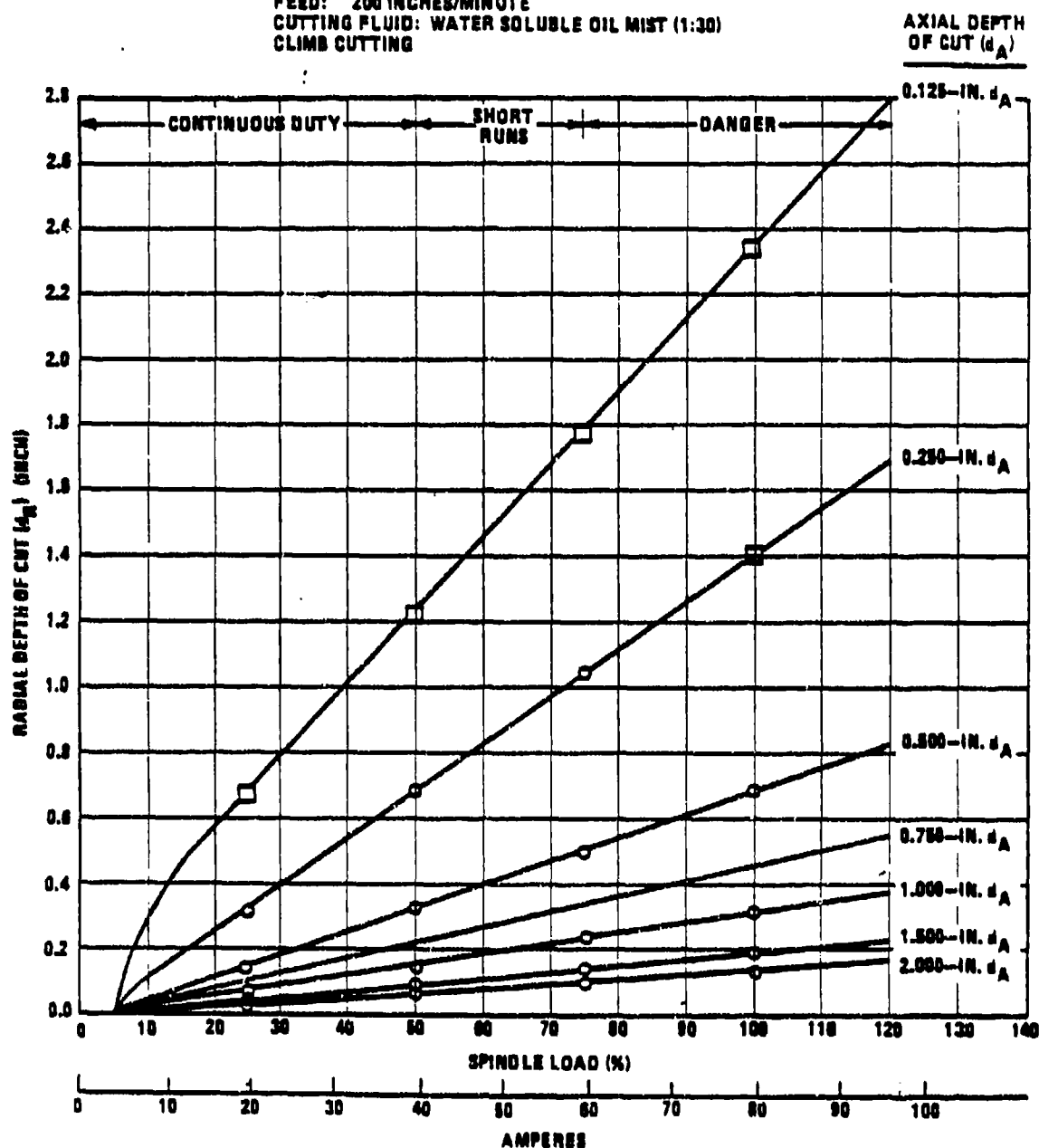


Figure 91. Effect of Cut Depths on Spindle Loading for 7075-T851 Aluminum

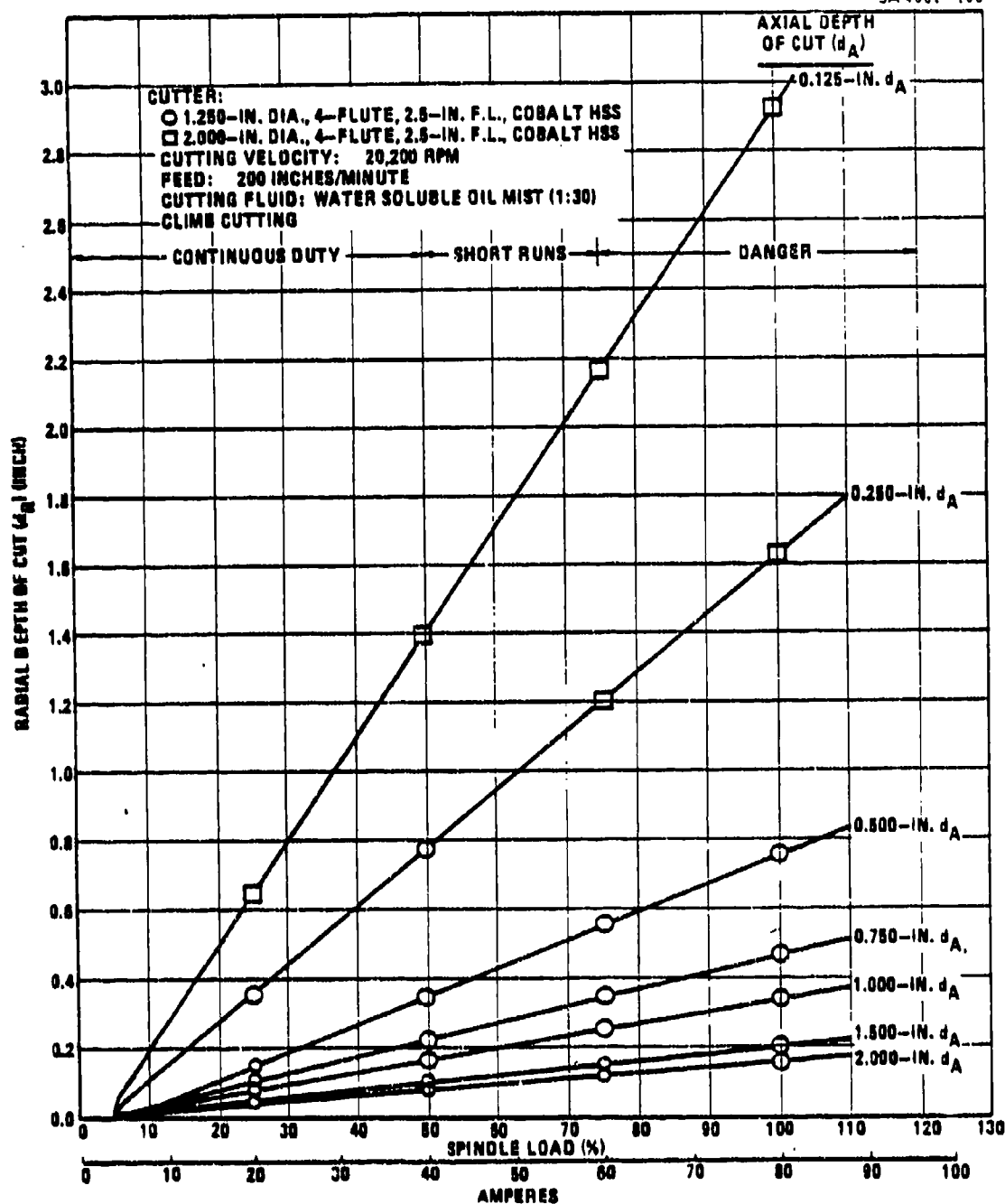


Figure 92. Effect of Cut Depths on Spindle Loading for 6061-T651 Aluminum

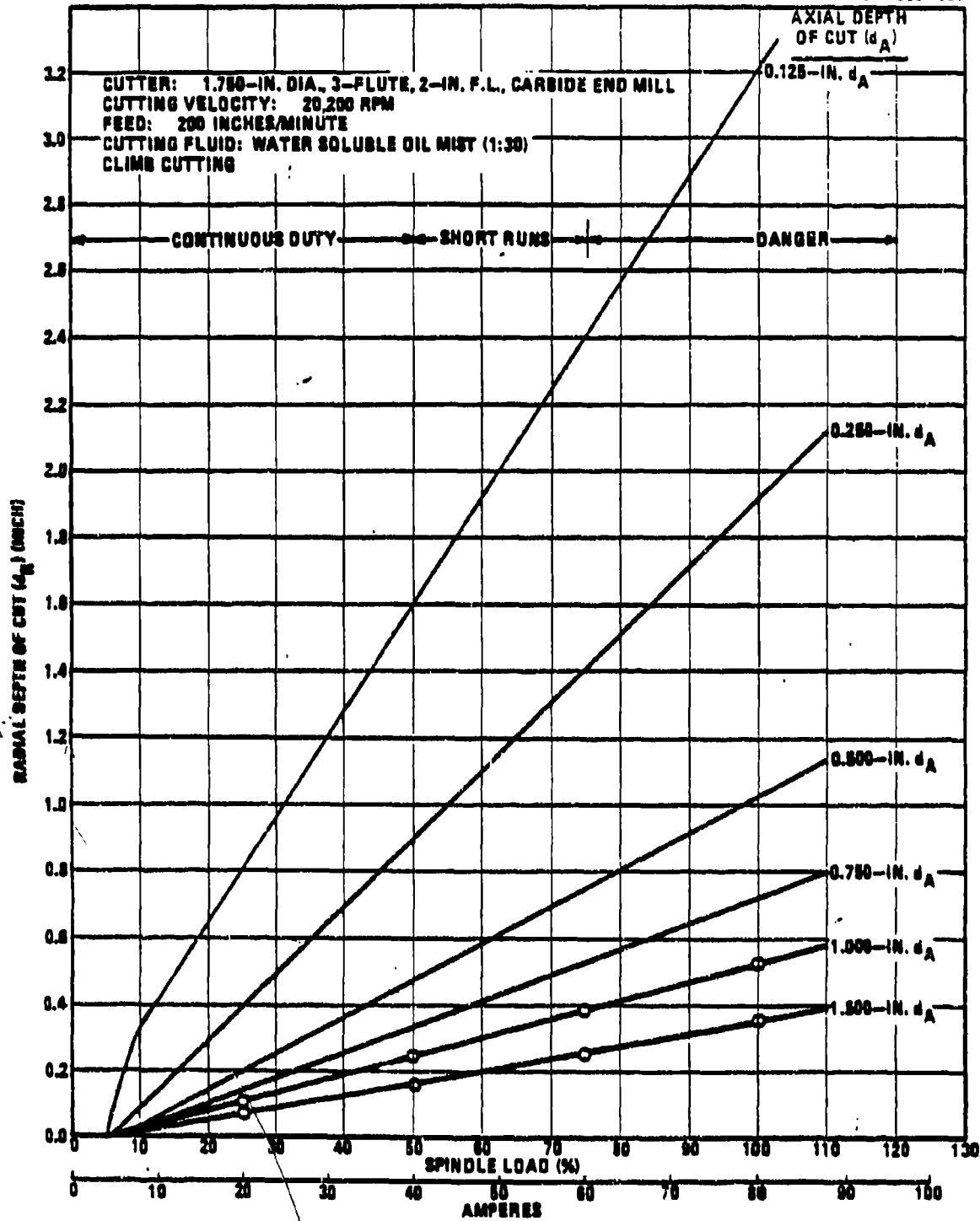


Figure 93. Effect of Cut Depths on Spindle Loads for A356-T8 Aluminum

Al-A356-T6

<u>Axial Depth</u> <u>(inch)</u>	<u>Radial Depth</u> <u>(inch)</u>
1.5	$d_R = 0.0038$ (% load) - 0.031
1.0	$d_R = 0.0056$ (% load) - 0.041
0.75	$d_R = 0.0079$ (% load) - 0.070
0.50	$d_R = 0.0112$ (% load) - 0.092
0.25	$d_R = 0.0209$ (% load) - 0.166
0.125	$d_R = 0.0320$ (% load) - 0.008

When selecting a cut depth, it should be borne in mind that increased cut depths not only burden the spindle but decrease cutter life as well. From the typical example shown in Figure 94, it can be seen that the faster wearing cutter is the one making the deepest depth of cut. Along with the depth-of-cut tests, cutting force, cutter deflection and cutter pullout tests were conducted, simultaneously. At the end of each pass across a 12-inch workpiece (cf. Figure 72), during which spindle loads for systematically varying axial and radial depths-of-cut were noted, the end mill was allowed to dwell in the cut until it had returned to its undeflected position. The end mill was then worked back and forth a fraction of an inch to produce a small, undeflected flat on the machined surface. Cutter deflection was then determined by measuring the height of the resulting step with a depth gage micrometer. The distance that a cutter pulls out of the spindle during a cut was measured in much the same way. For that test, another depth gage micrometer was used to measure the axial depth-of-cut after each pass. The difference between that measurement and the original setting was the measure of cutter pullout. Force readings were obtained by activating the Midwestern Model 210 oscillograph and X-Y recorders shown in Figures 73 and 74 and converting the recordings from millimeters to pounds of force. These tests will be discussed in subsequent sections.

8.2.3 Cutting Speeds

The objective of this investigation was to develop Taylor tool life curves so that most economical and productive cutting speeds could be established directly and analytically. Normally, this is an easy task to accomplish; but due to the ease with which aluminum can be machined, tool lives and material consumption were found to be too excessive. These results stretched out test schedules, necessitated tooling and cutter material changes with attendant retesting cycles, and fostered additional procurement delays. When these delays were coupled with the spindle breakdown delays, it was found that there was not enough time left to fully complete this task.

While it may be generalized that tool life and cutting speed do not appear to limit the high speed machining of aluminum, the investigators for this program were anxious to develop some technology in these

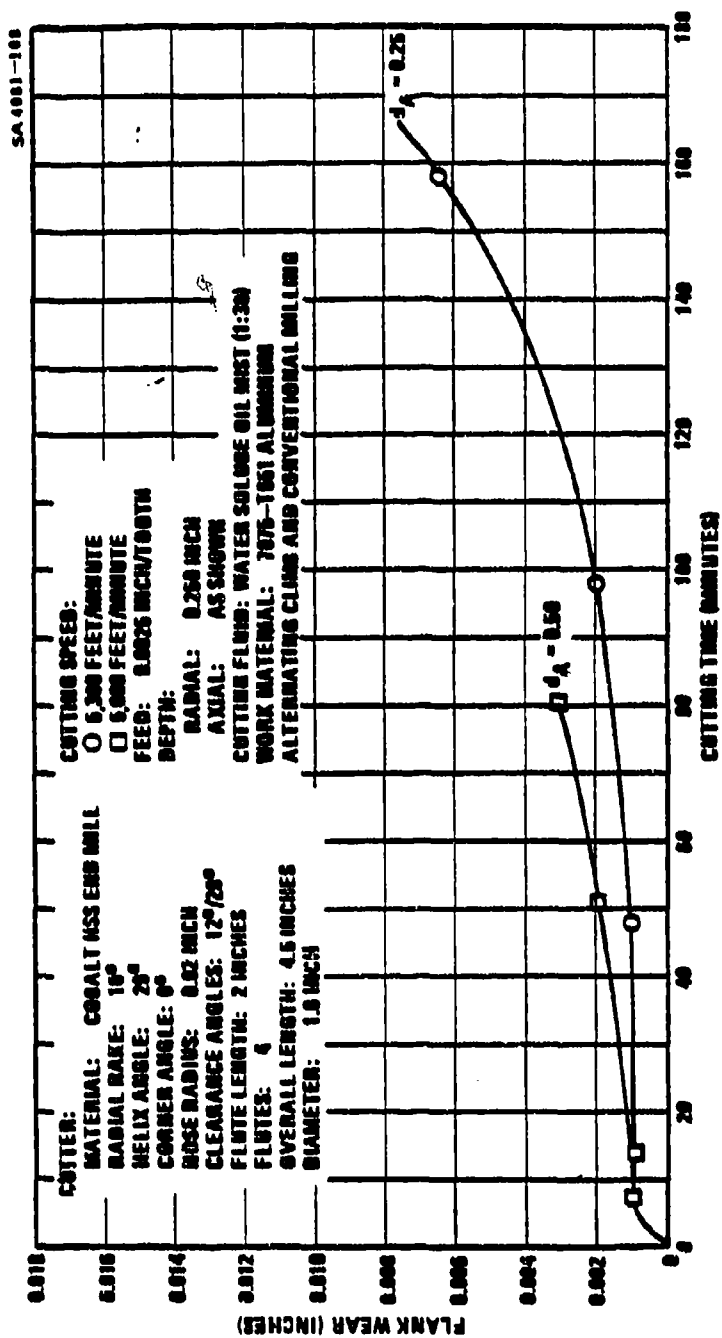


Figure 94. Effect of Cut Depth on Cutter Wear

areas. Consequently, the fragmentary data developed and presented in Table IV was pieced together as shown in Figures 95 and 96. The estimated slope of 0.3 for these curves was based on results developed by Datsko<sup>11</sup>. Using that value, extrapolated curves were drawn through firm data points as shown. Although these curves are useful for discussion purposes, these have not been substantiated; and the reader is cautioned not to attach too much credibility to them.

To verify the two extrapolated points on Figure 95, it was estimated that at least two plates of material, measuring 2 inches by 48 inches by 144 inches, and 25 hours of cutting time would be required for the tests. If there were any premature failures or scatter in the test results, even more time and material would have been required. For these reasons, such tests were not pursued.

The theoretical curve in Figure 95 indicates that a cutting speed of 46,643 feet/minute will give a one-minute tool life for the referenced carbide cutter. On the other hand, if the cutting temperature ceases to rise beyond a cutting speed of 19,600 feet/minute as suggested in subsection 3.5, a cutter life of at least 15 minutes might be obtainable at any cutting speed with the referenced cutter.

The cutter in Figure 84 gave no sign of ever wearing out. An estimate of its tool life can be made with the aid of the Taylor tool life equation superimposed on Figure 95. That equation was developed from the curve and predicts that the end mill will cut for 81,120 minutes before resharpening is required when operated at a cutting speed of 1,570 feet/minute. While it would be difficult to imagine an end mill cutting that long in practice, this analysis does indicate that, barring premature failure, the referenced end mill will yield an extraordinary tool life when operated under the favorable conditions shown.

Micrographs made of chips produced by the two firm cutting speeds are presented in Figure 97. There, it can be deduced that aluminum appears to tear at lower cutting speeds. It may be that the higher cutting temperature generated at the higher cutting speed has some bearing on this result. For both cases, however, the cutting tool remained relatively cool to the touch.

A general idea of what the most economical tool life and cutting speed would be for end milling aluminum can be obtained from Figure 95 and the following equation<sup>14</sup>:

TABLE IV - TOOL LIFE TEST RESULTS

Work Material	Tool Material	Cutting			Speed (ft/min.)	Feed (in./tooth)	Depth		Tool Life	Criterion (Wear/tear)	Helm./Radial Rate
		Dia.	Flutes	Flute Length			Axial	Radial			
Al-7075-T651	C-2	1.494	2	1-3/8	Dry	0.006	0.25	0.25	372 min. 6300 R	0.011/0.004	25°/5°
	C-2	1.5	2	1-3/8	Dry	0.006	0.25	0.25	220 + min. 3000 + R	0.006/0.007 Tool dragging BUE on flank	25°/15°
	C-2	1.5	2	1-3/8	Dry	0.006	0.25	0.25	7 + min. 110 + R	Chipped edge (2 places)	35°/10°
	C-2	1.5	2	1-3/8	Dry	0.006	0.25	0.25	0 min.	Broken upon contacting work	45°/15°
	C-2	1.5	2	1-3/8	Dry	0.006	0.25	0.25	1.34 min.	Breaks starting 6th pass	35°/15°
	C-2	1.5	2	1-3/8	Dry	0.006	0.25	0.25	27 + min. 444 + R	0.002/0.003	25°/10°
	C-2	1.5	2	1-3/8	Dry	0.006	0.25	0.25	1.34 + min.	Overloading spindle motor	45°/5°
	C-2	1.5	2	1-3/8	Dry	0.005	0.25	0.25	0 + min. 123 + R	Overloading spindle motor	45°/10°
	C-2	1.5	2	1-3/8	Dry	0.006	0.25	0.25	5 + min. 83 + R	0.003 Uniform	35°/5°
	Cobalt HSS	1.050	2		Dry	0.006	0.25	0.25	70 min. 723 R	Cutter loaded with aluminum	35°/10°
Al-7075-T651	Cobalt HSS	1.0	4	2	Water soluble oil mist	0.0015	0.25	0.25	70 + min. 800 + R	0.0015 Accidentally chipped teeth	25°/10°
	Cobalt HSS	1.0	4	2		0.0025	0.25	0.25	166 min. 2,769 R	0.004/0.007 Heavy burr	25°/10°
	Cobalt HSS	1.0	4	2		0.0025	0.50	0.25	50 + min. 3330 + R	0.003 Uniform	25°/10°
	Cobalt HSS	1.012	2	2		0.006	0.50	0.25	16 min. 271 R	0.004/0.005 Rounded edges Dropped servo	35°/10°
Al-4041-T651	Cobalt HSS	1.00	2	2		0.0025	0.50	0.25	69 min. 496 R	0.007/0.016	30°/10°
	Cobalt HSS	1.07	2	1-3/4	Water soluble oil mist	0.006	0.50	0.25	75 min. 1250 R	0.003/0.012 U 0.018/0.020 L	30°/10°
Al-A356-T6	C-2	1.0	2	1-1/2	Water soluble oil flood	0.006	0.25	0.50	20 min. 295 R	0.015/0.018	25°/12°

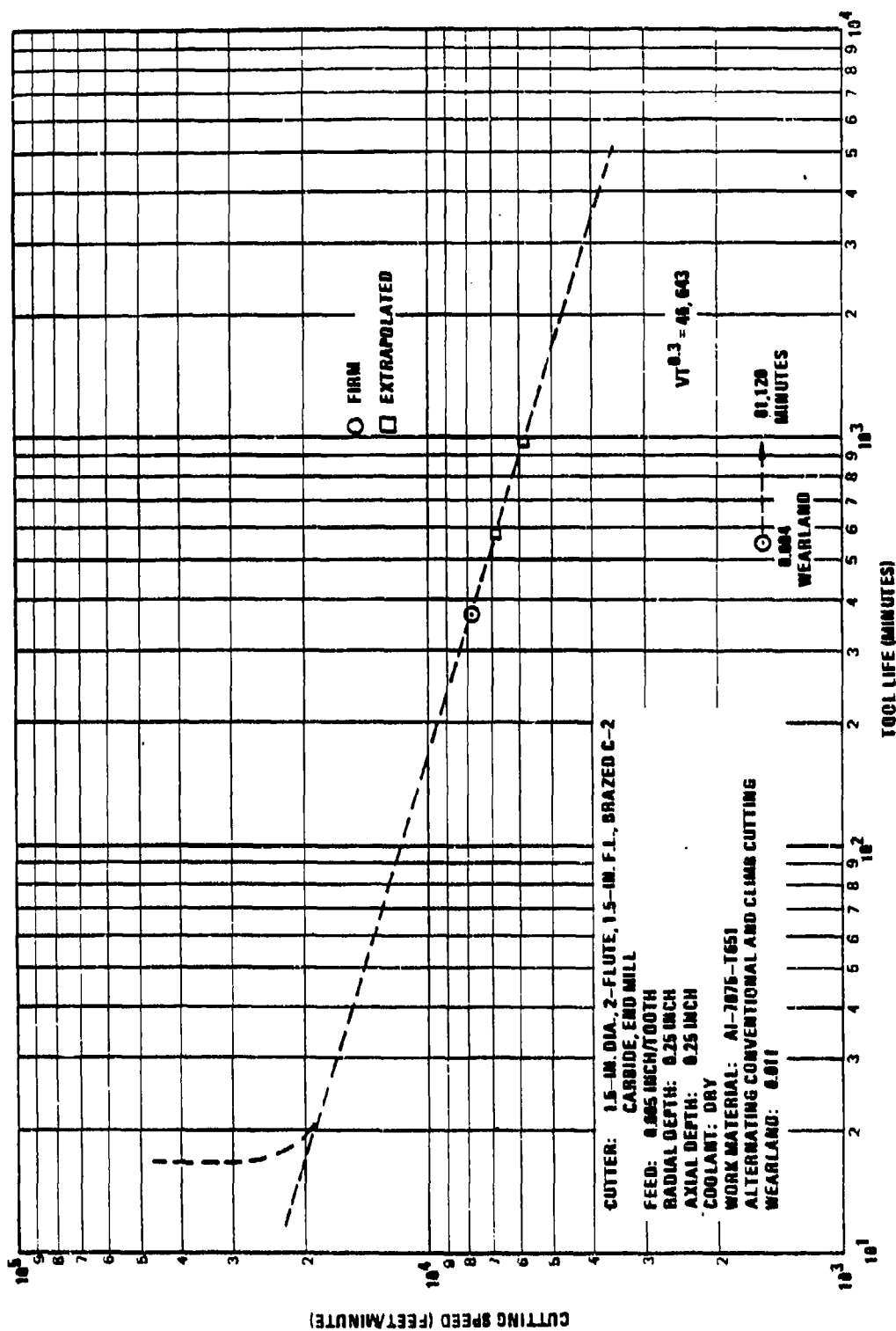


Figure 95. Theoretical Effect of Cutting Speed on Carbide Cutter Life

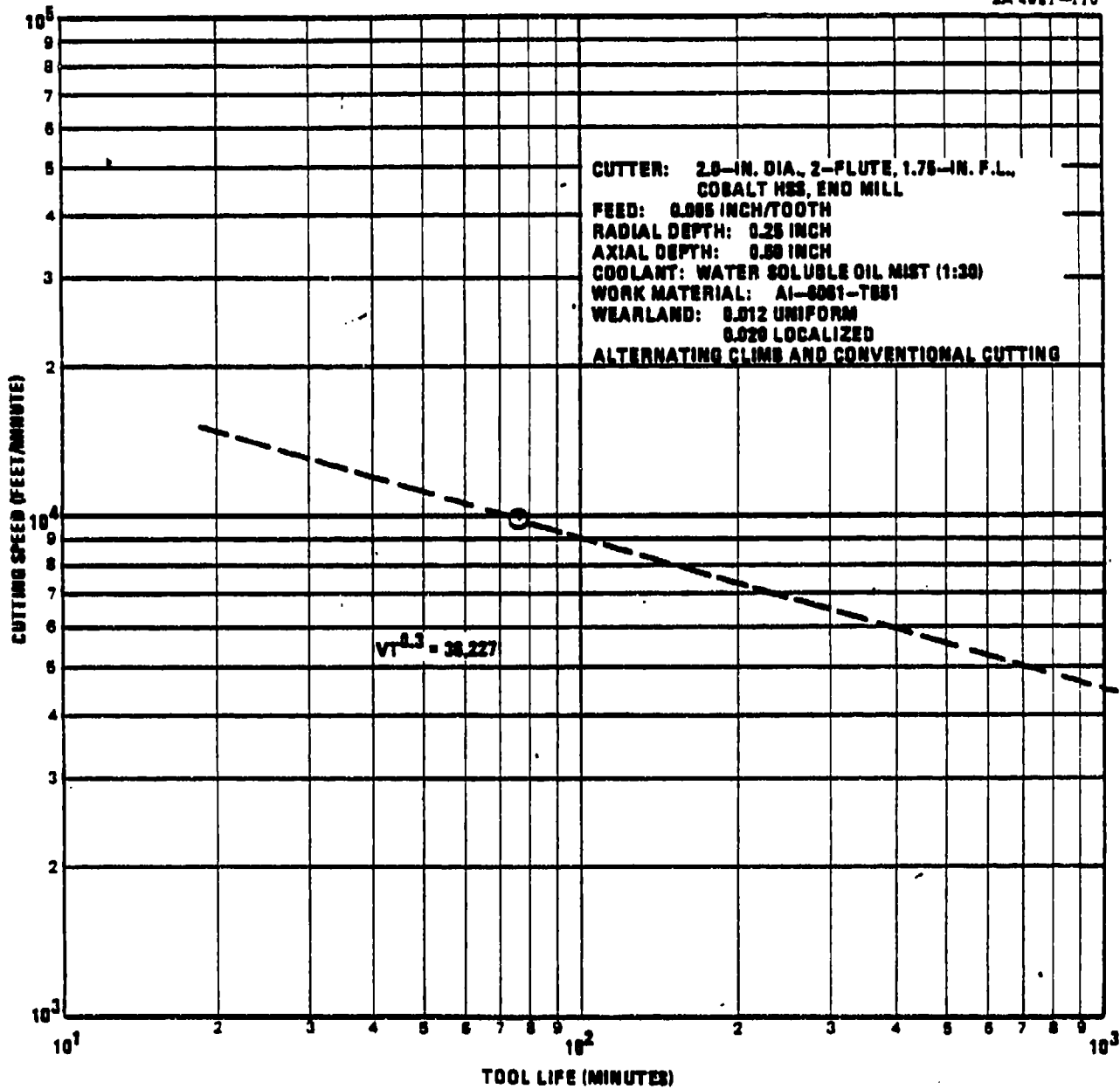
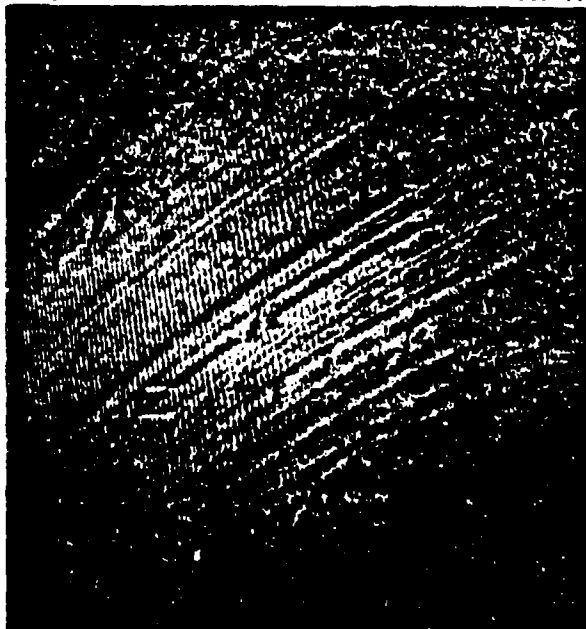


Figure 98. Theoretical Effect of Cutting Speed on HSS Cutter Life

P-4081-111.1

SA 4081-111

1,570 FEET/MINUTE  
(130X)



P-4081-111.2

7,900 FEET/MINUTE  
(160X)

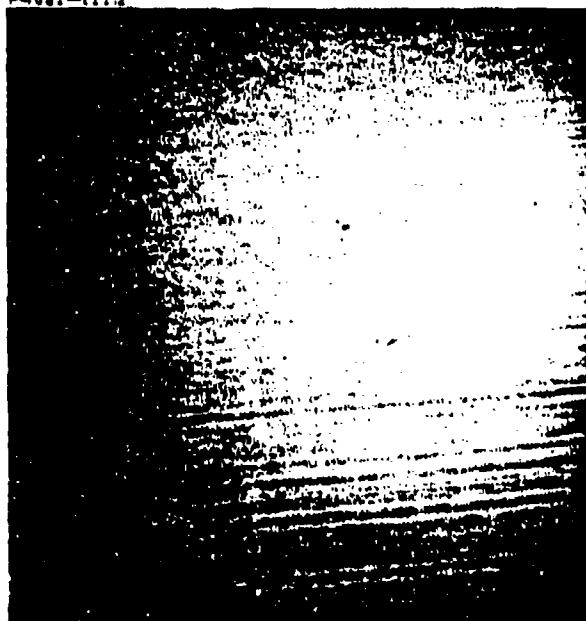


Figure 97. Typical Effect of Cutting Speed on Chip Surface for Al-7075-T651

$$T_c = \left[ \frac{1}{n} - 1 \right] \left[ \frac{t}{MLO} + TCT \right]$$

where:

- $T_c$  = tool life in cut for minimum part cost (minutes)
- $n$  = slope of Taylor tool life curve
- $t$  = total cost of cutting edge including cost to change the tool and to regrind the cutting edge and depreciation of the tool (\$).
- $MLO$  = machine, labor and overhead rate (\$/minute)
- $TCT$  = tool changing time (minutes).

In addition, the tool life which will yield a maximum production rate can be similarly found from the following equation:

$$T_p = \left[ \frac{1}{n} - 1 \right] TCT$$

where:

- $T_p$  = tool life in cut for maximum production (minutes).

By using typical aerospace rates for MLO, and actual figures for the variables TCT and  $t$ , the above equations yielded most economical and maximum production rates of 225 minutes and 23 minutes, respectively. The corresponding cutting speeds were found by substituting these data into the Taylor tool life equation superimposed on Figure 95. When this was done, it was found that the most economical and maximum production cutting speeds for aluminum were on the order of 9,190 feet/minute and 18,210 feet/minute, respectively, for this case.

The above cutting speeds can be translated into spindle speeds for different sized cutters with the aid of the following equation:

$$N = \frac{3.82 V}{d}$$

where:

M = spindle speed (revolutions/minute)  
V = cutting speed (feet/minute)  
d = diameter of cutter (inches).

When this was done for the case of 1.5-inch diameter carbide cutters, it was found that the spindle speeds required to achieve maximum economy and production were on the order of 23,400 and 46,400 revolutions/minute, respectively. For 1.0-inch diameter cutters, these spindle speeds would increase to approximately 40,730 and 69,570 revolutions/minute, respectively. All of these values exceed the 20,000 revolutions/minute spindle speed that is currently maximum for 20-horsepower spindles; however, these are indicative of future spindle speed design needs.

It should be re-emphasized that most of the calculated values above were based on very meager test data. As a consequence, these were only rough estimates and should be considered as being merely indicative of the magnitude of optimum cutting speed requirements for aluminum.

At this point in the investigation, it appeared that if any defensible cutting speed technology were going to be developed for aluminum, it would have to be done with shorter-lived high speed steel cutters. Consequently, testing was resumed with 2- and 4-flute high speed steel (HSS) end mills. Initially, tests were conducted on 7075-T651 aluminum; but when it became evident that there was not enough work material left to complete the tests, the 6061-T651 aluminum test material was used instead. Additionally, 1.0-inch diameter cutters yielded excessive tool lives for the task at hand on Al-7075-T651 as shown in Figure 98; therefore, when the work material was switched to Al-6061-T651, cutter diameters were switched to 2.0 inches and axial depths of cut were increased to 0.5 inch. The higher cutting speed obtainable with the 2.0-inch diameter cutter reduced tool life to a more realistic level for test purposes (see Figure 98). With this setup, only one good data point was obtained; and that is presented in Figure 96. Shortly after that test was conducted, the shaft of the high speed spindle was accidentally bent and had to be repaired. As a result of the long delay in repairing the spindle and other program commitments, the cutting speed tests were never fully resumed and, thus, no defensible cutting speed technology was completely developed.

To establish some order of magnitude for the optimum cutting speeds that can be obtained with high speed steel cutters, the curve shown in Figure 96 was prepared. As before, that curve was constructed by drawing a line having a 0.3 slope through a known data point on log-log paper. The equation for the resulting curve was superimposed on Figure 96 for reference. Like the curve in Figure 95, this curve is useful for discussion purposes but merely represents a best estimate and should not be treated as being anything more.

**CUTTER:****MATERIAL:** COBALT HSS**DIAMETER:** ○ 1.0 INCH

□ 1.5 INCH

**OVERALL LENGTH:** 4.25/4.5 INCHES**FLUTE LENGTH:** 1.75/2.0 INCHES**FLUTES:** ○ 4

□ 2

**HELIX:** ~30°**RADIAL RAKE:** 10°**CORNER ANGLE:** 9°**NOSE RADIUS:** 0.020 INCH**CLEARANCE:** 12°/22°**CUTTING SPEED:** AS SHOWN**FEED:** 0.0025 INCH/TOOTH**DEPTH:****RADIAL:** 0.25 INCH**AXIAL:** 0.50 INCH**CUTTING FLUID:** CODAL 8741 MIST (1:30)**WORK MATERIAL:** ○ 7075-T651 ALUMINUM

□ 6061-T651 ALUMINUM

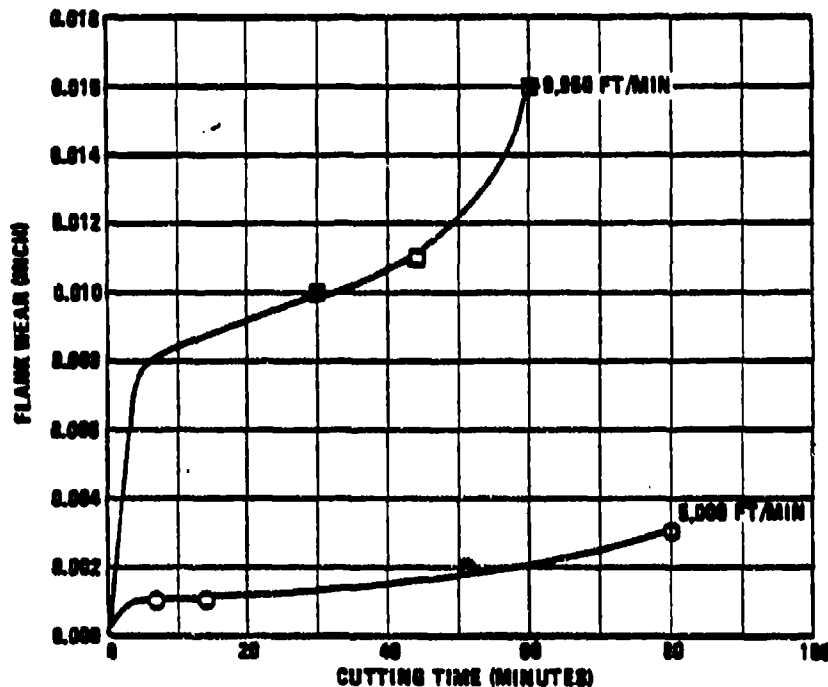
**ALTERNATING CLIMB AND CONVENTIONAL MILLING**

Figure 98. Approximate Effect of Cutting Speed on Cutter Wear

The theoretical curve in Figure 96 indicates that a cutting speed of 36,227 feet/minute would yield a one-minute tool life for the referenced HSS cutter. If cutting temperatures stabilize at a cutting speed of 19,600 feet/minute as suggested in subsection 3.5, a cutter life of at least seven minutes might be obtainable at any cutting speed with the referenced HSS cutter. Other calculations indicate that the tool life yielding maximum economy and production rates for 1.5-inch diameter, HSS, end mills would be on the order of 133 minutes and 23 minutes, respectively. The cutting speeds corresponding to these tool lives were calculated to be on the order of 8,350 feet/minute and 14,140 feet/minute, respectively. Similarly, the spindle speeds were computed to be 21,280 and 36,000 revolutions/minute, respectively.

For comparative purposes, the theoretical tool lives, cutting speeds and spindle speeds calculated for 1.0- and 1.5-inch diameter end mills were tabularized in Table V.

TABLE V - THEORETICAL MOST ECONOMICAL CUTTING SPEEDS  
FOR SELECTED CUTTERS AS DEVELOPED FROM  
FIGURES 95 AND 96

	End Mill Diameter			
	1.0 Inch		1.5 Inch	
	HSS	Carbide	HSS	Carbide
Most economical tool life (minutes)	94	137	133	225
Most economical cutting speed (SFPN)	9,270	10,660	8,350	9,190
Most economical spindle speed (RPM)	35,410	40,730	21,280	23,400
Maximum production tool life (minutes)	23	23	23	23
Maximum production cutting speed (SFPN)	14,140	18,210	14,140	18,210
Maximum production spindle speed (RPM)	54,000	69,570	36,000	46,380
Work material	Al-6061	Al-7075	Al-6061	Al-7075
Axial depth of cut (inch)	0.500	0.250	0.500	0.250

In Table V, it can be observed that there were more variables than just tool material and size involved in the data presented. Such an occurrence generally makes any direct comparisons difficult if not impossible to achieve. However, the effect of variations in cut depth and work material on the above data were thought to be offsetting. For example, any advantage gained by a carbide cutter in machining at a shallower depth of cut would be partially offset, at least, in this instance, by its having to machine a more difficult material. The opposite would be true for a HSS cutter. It was thus concluded that the test conditions for each cutter material offered an advantage and disadvantage over the other that were largely compensatory. If that hypothesis, along with theoretical based data, can be accepted, then several interesting deductions can be made from the above table.

As may have been suspected, the data in Table V indicated that carbide cutters can be expected to cut longer and faster than high speed steel (HSS) cutters. These data also point out that, barring premature

failures, the superiority of carbide cutters increase as cutter diameters decrease. Further, these data point out that, all other things being equal, cutting speeds and, therefore, metal removal rates increase as cutter diameters decrease. It was interesting to note from the data that recommended spindle speeds for all the cutters 1.5 inches in diameter and under exceeded the speed capacities of both the Bryant (20,000 rpm) and Ekstrom, Carlson (14,400 rpm) 20 horsepower spindles used in this program. This result signified that HSS cutters can be readily used with this equipment and that both spindles should generally be operated at maximum speed when using either carbide or HSS cutters. These recommended or optimum spindle speeds also provide needed criteria or goals for future, large horsepower, spindle designs. Finally, these data give some idea of what the magnitude of optimum cutting speeds for milling aluminum would be. For instance, as shown in Table V, optimum cutting speeds for the heat-treatable aluminum alloys would be on the order of 10,000 feet/minute. For the lower strength or softer aluminum alloys, it could be logically expected that optimum milling speeds would have a somewhat higher magnitude. However, a notable exception to such a hypothesis is presented at the bottom of Table IV for the case of A356-T6 aluminum. There, it can be deduced that the optimum milling speed for that very abrasive, high silicon content, cast aluminum alloy will be significantly less than 3,700 feet/minute. Thus, it can only be concluded that the optimum cutting speed for milling aluminum alloys will usually be on the order of 10,000 feet/minute.

### 8.3

#### Drilling

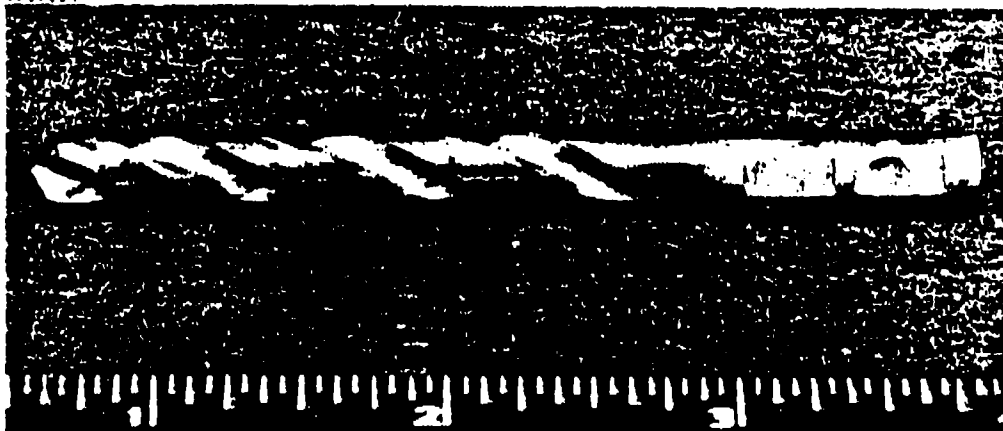
Drilling tests were performed with the 20,000 revolutions/minute spindle on the Omnimil as described in subsection 6.2. The test set-up that was used is shown in Figure 77. Both carbide and cobalt high speed steel (HSS) drills were obtained for testing; however, due to the impressive results obtained with the HSS drills, it was felt at the time that it would not be beneficial to evaluate carbide drills. Drill sizes were limited to 1/4-inch diameter; because special milling machine type toolholders (cf. Figure 77) would have been required for each different drill size, and 1/4-inch drills were of a practical size.

Progress for this event went about as far as it could with a 20,000 revolutions/minute spindle. Thousands of holes were drilled through 1/2-inch thick Al-7075-T651 plates with 1/4-inch diameter, cobalt HSS drills at a speed of 20,000 revolutions/minute (1,300 feet/minute) and a feed of 100 inches/minute (0.0025 inch/tooth). Based on end mill test results, it may be possible to increase both these parameters eight-fold; however, faster equipment will have to be made available to verify such a supposition.

A typical drill used in this study is shown in Figure 99. That particular tool had just drilled 3,547 holes through 1/2-inch thick Al-7075-T651 at a feed rate of 100 inches/minute and a cutting speed of 20,000 revolutions/minute when it was photographed. As can be observed, its corners have not broken down; and it is not badly worn. That drill

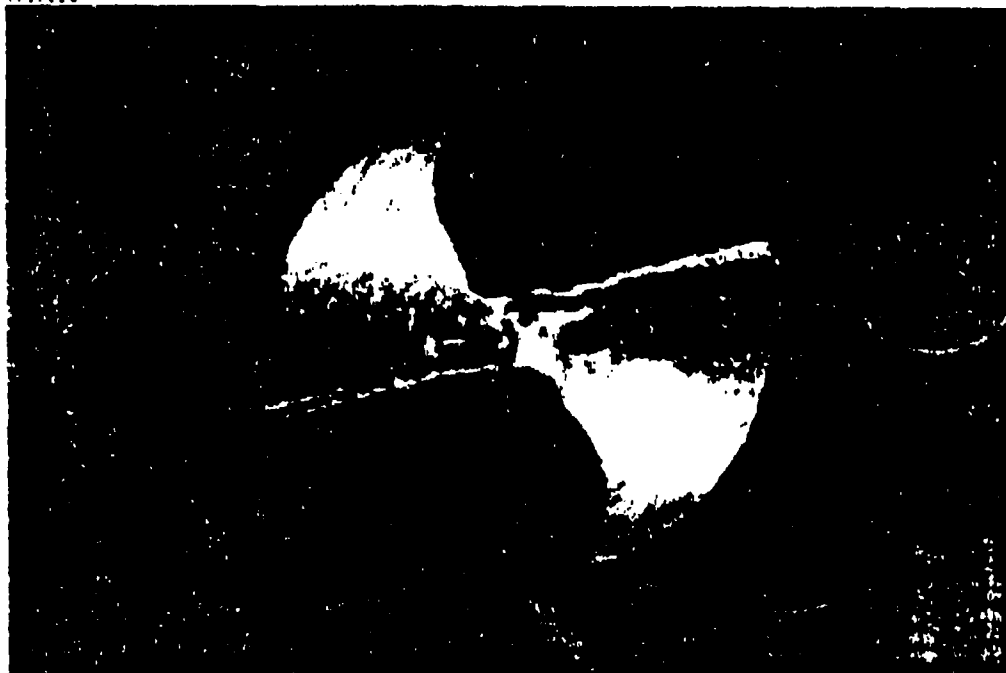
N-17114

SA 4081-113



SIDE VIEW

N-17113



END VIEW

Figure 99. Typical Test Drill After Producing 5,547 Holes

which was made from cobalt high speed steel was a general purpose drill made by Straight Line and having the following modified geometry:

Overall length:	3-1/4 inches
Flute length:	1-3/4 inches
Point angle:	121 degrees
Chisel edge angle:	131 degrees
Lip relief angle:	16 degrees
Point:	Notched
Web thickness:	0.035 inch
Flute flats:	12 degrees positive

Feed rates were varied between 100 and 200 inches/minute in the tests by overriding the N/C program, while maintaining a cutting speed of 20,000 revolutions/minute. A feed rate of 200 inches/minute may have been satisfactory for drilling Al-A356-T6, but such a feed rate produced too much noise and chatter when drilling Al-7075-T651. That unwanted result could possibly be overcome by injecting sufficient cutting fluid into the holes in time to do some good. As it was, the drills were in and out of the holes so fast that conventionally applied cutting fluid never had a chance to get to the cutting zone. Even at a feed rate of 100 inches/minute, the drilling operation gave all the appearance of being a punching operation. Indeed, if it were not for the chips produced (see Figure 100), one might be justified in believing that the high speed drilling operation being witnessed was, in fact, a punching operation. A typical specimen produced by high speed drilling is shown in Figure 101. The drill that was used to produce the 2,408 holes in that test piece was indexed at 200 inches/minute and fed at 100 inches/minute by an N/C program. The resulting sight was very impressive and indicative of high speed machining's potential.

#### 8.4

##### Turning

Turning tests were performed on a Bullard vertical turret lathe equipped with an Ekstrom, Carlson Company (ECCO) high speed spindle as shown in Figure 70, using end mills as cutting tools. That electric D.C. spindle which was capable of producing 20 horsepower at 14,400 revolutions/minute was mounted on the Bullard's side turret, perpendicular to the Bullard spindle's centerline of rotation. Cuts were taken with the high speed spindle traversing downward while the Bullard's spindle was slowly rotated. Cutting speed was altered by varying the speed of the high speed spindle or the cutter diameter. Chip load was altered by varying the speed of either spindle or the number of flutes on the cutter (cf. Figure 79). Principally, chip load was altered by varying the speed of the Bullard spindle. Workpieces (see Figure 102) were of a cylindrical form and approximately 24 inches outside diameter by 18 inches inside diameter by 18 inches long. The Al-7075-T6 and Al-6061-T6 workpieces were forgings, and the Al-A356-T6 workpieces were castings. Machining parameter tests for turning were conducted on all three alloys, and the results obtained are presented in the subsections to follow.



Figure 100. Typical Chips Produced When Drilling Al-7075-T851 At 100 Inches/Minute Feed Rate

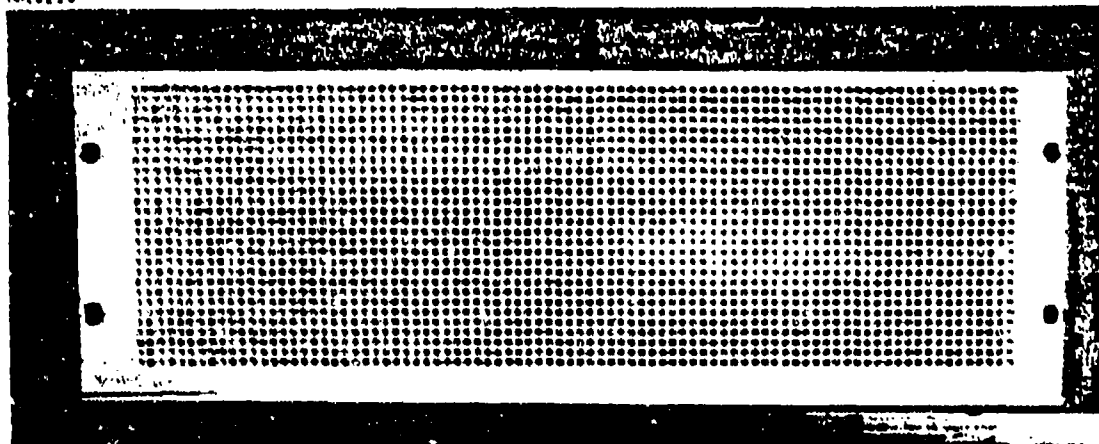


Figure 101. Typical Al-7075-T851 High-Speed Drilling Test Specimen



Figure 182. Typical Workpieces for Turning Tests

#### 8.4.1 Feed Rate Optimization

As mentioned in subsection 8.2.1 for peripheral and milling, chip load tests could not be fully accomplished on the Omnimil due to the limited speed at which its table could be moved. Since this was no problem for the Bullard, chip loads for both operations were established with the Bullard.

For all tests, standard one-inch diameter, 2-flute, end mills were used. That small diameter, coupled with the maximum 14,400 revolutions/minute spindle speed available, limited cutting speeds to 3,770 feet/minute. High speed steel end mills were used for the Al-7075 and Al-6061 tests, but carbide end mills had to be used for tests on the very abrasive A356 aluminum alloy. Axial depths of cut were maintained at 0.250 inch, and radial depths of cut were maintained as close to 0.550 inch as practical. Cutter geometries were modified to provide

12° primary and 24° secondary clearance on cutter peripheries and 10° primary and 20° secondary clearance on end cutting edges. Additionally, when the centerlines of rotation for both the cutter and workpiece were perpendicular to each other, as was the case on the Bullard, end cutting edge angles were ground to 0° to provide an acceptable surface finish. On the Omnimil, it was not found necessary to grind end cutting edge angles to 0°; as excellent finishes were produced by moving the cutter's axis of rotation off the workpiece centerline as indicated in Figure 103. However, since the tests were conducted on the Bullard, cutters were centered on workpiece centerlines, and the respective end cutting edge angles were ground to 0°.

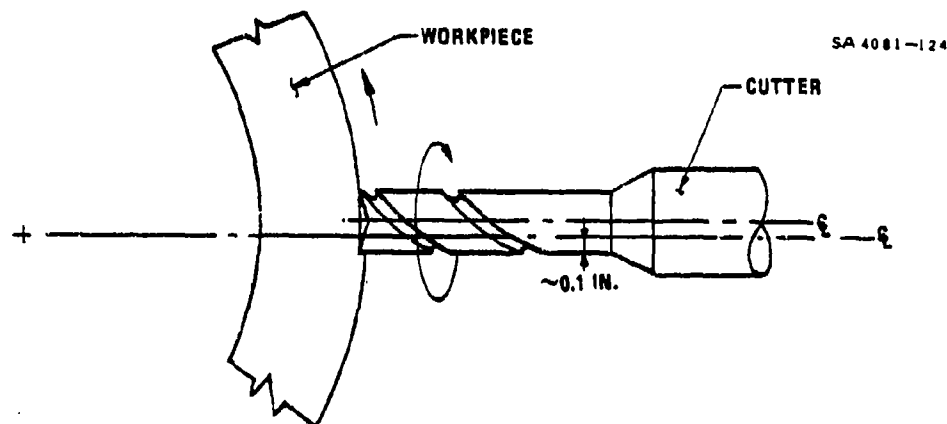


Figure 103. Recommended Cutter-Workpiece Orientation for End Mill Turning

The mode of cutter wear varied with all three aluminum alloys. As illustrated in Figure 104, cutters wore mostly on the nose when milling Al-7075-T6 (cf. Figure 86). In contrast, cutters wore very uniformly when milling Al-A356-T6 and mostly at the depth-of-cut line when milling Al-6061-T6. Bearing these results in mind, feed rate optimization test results are presented for each alloy in Figures 105 through 107.

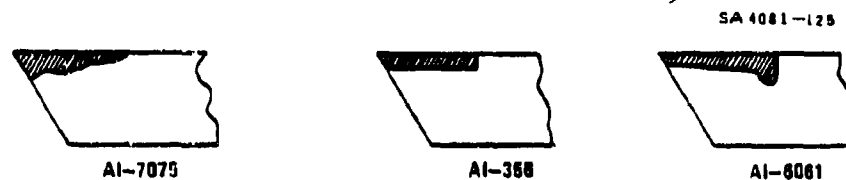


Figure 104. Typical Wearlands Produced on End Mills by Aluminum Alloys

The optimum feed rate found for Al-6061-T6 was 0.010 inch/tooth as shown in Figure 105. At that feed rate, cutter life reached a maximum. Cutter life was considered to be ended when the flanks of cutters had worn 0.015-inch uniformly or 0.020-inch localized. Where

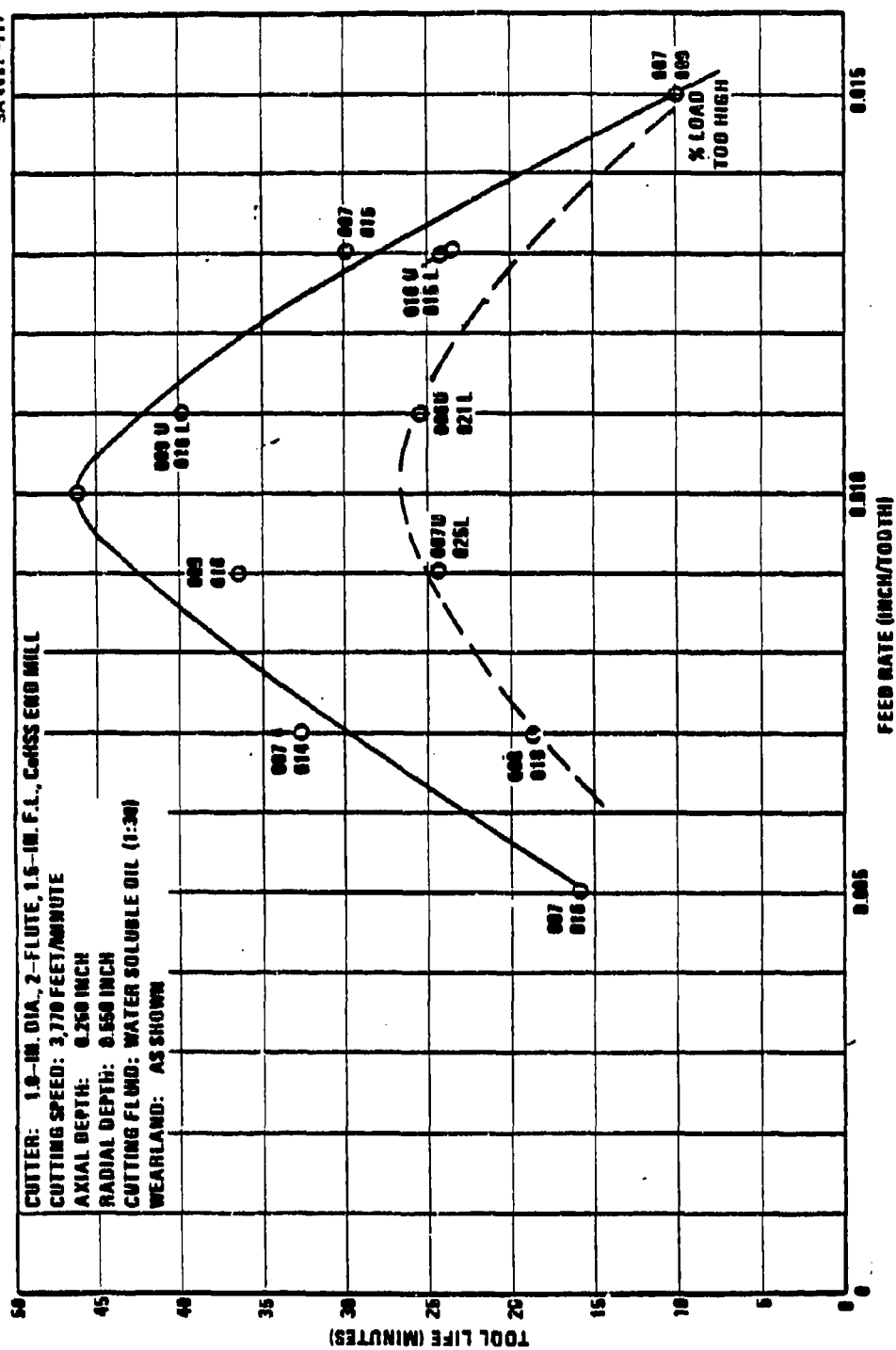


Figure 106. Effect of Feed Rate on Tool Life for Al-8061-T6

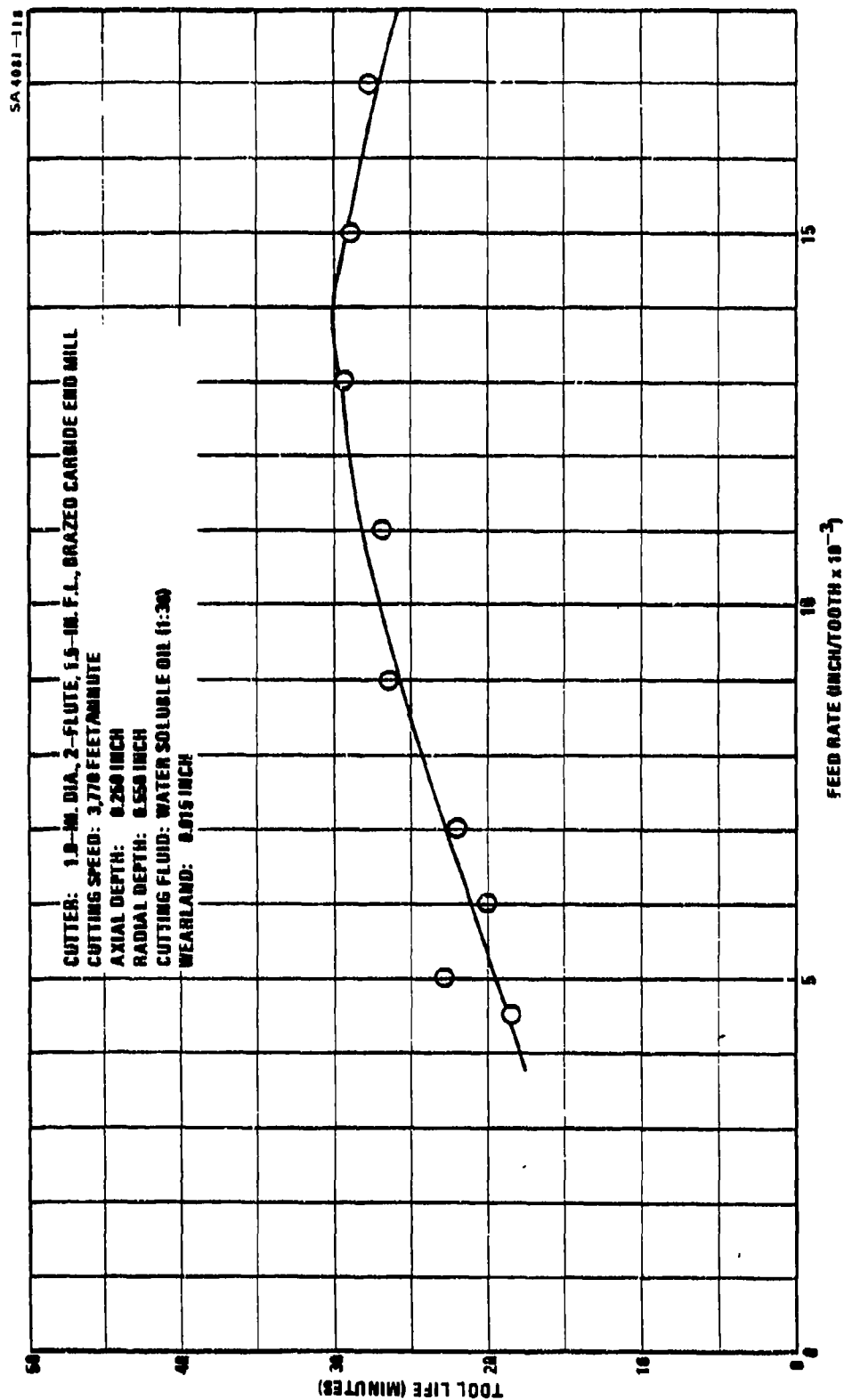
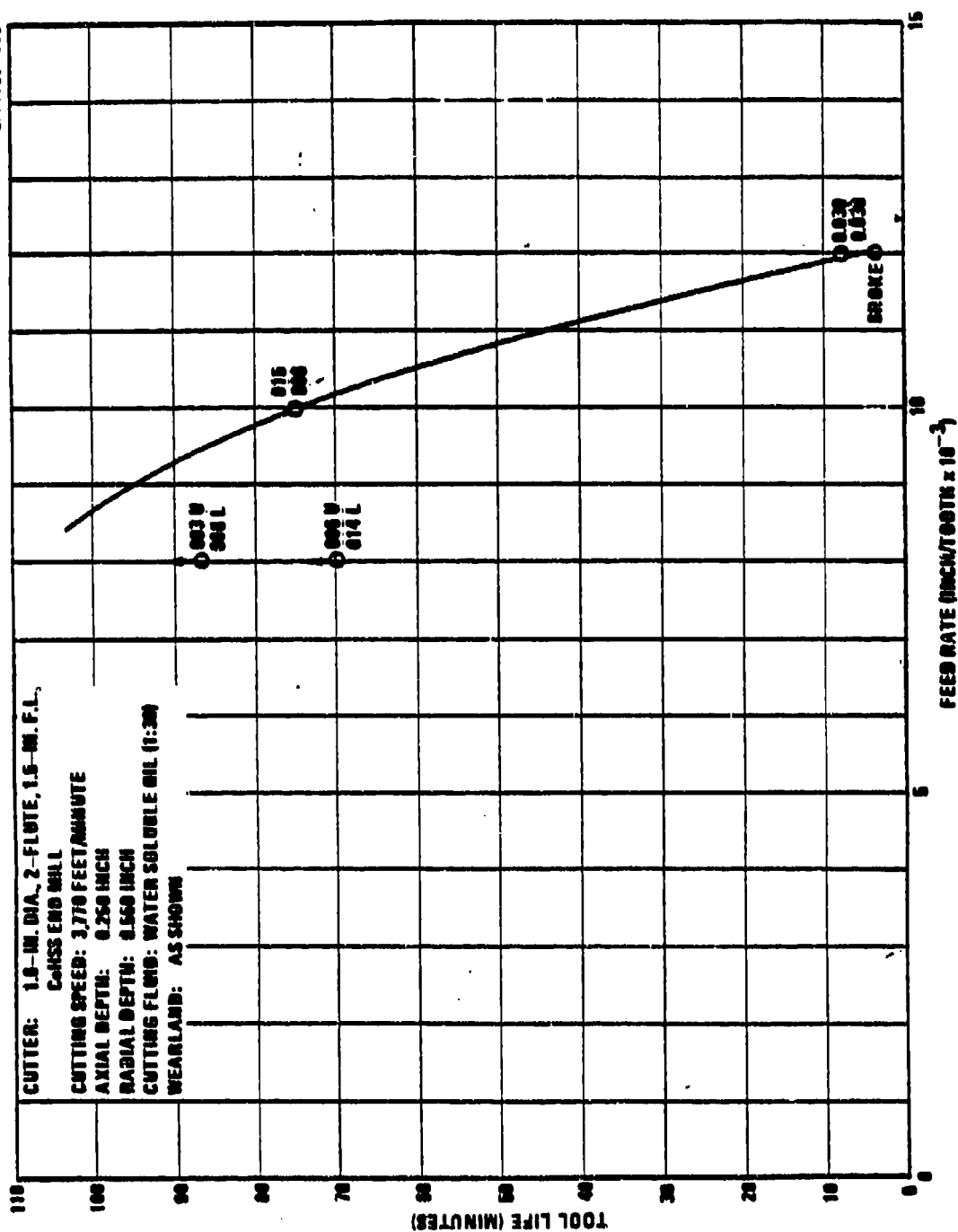


Figure 106. Effect of Feed Rate on Tool Life for Al-A356-T6



two numbers are given opposite a data point, these either signify the uniform and localized wear at that point or the wear for each tooth. Some wide scatter can be noted in Figure 105 for tool life. That can be attributed to an early breakdown of the cutter at the depth-of-cut line. If such a breakdown is allowed to progress to a point where the cutter becomes notched, a strange event may occur. For instance, as implied in Figure 108, the cutter, though still turning at 14,400 revolutions/minute, had ceased to function as an end mill and was producing a continuous chip. This event was not observed with the other aluminum alloys, so it was concluded that it was attributable to cutter notching. In summation, the optimum feed rate for Al-6061-T6 was shown to be 0.010 inch/tooth for either condition.

N-17106

SA 4081-120

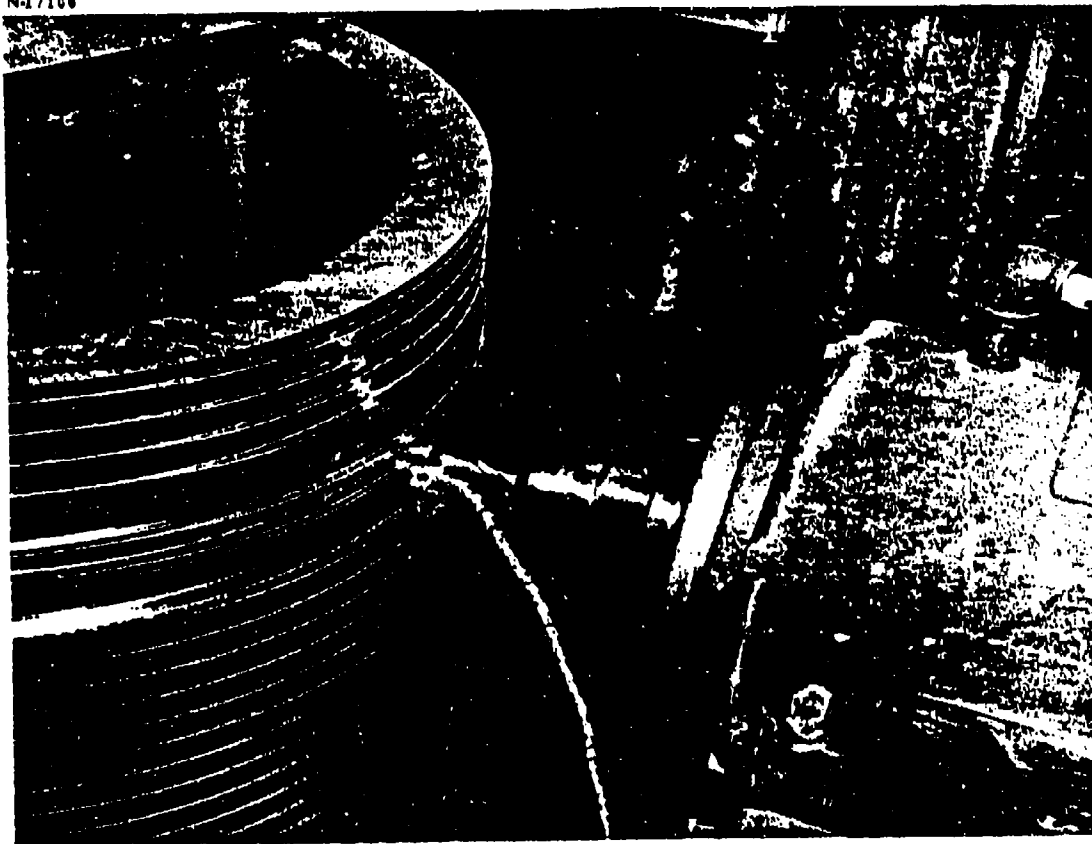


Figure 108. Continuous Chip Produced by End Mill Turning At 14,400 RPM

Feed rate did not appear to have a large effect on cutter life when milling the relatively soft, but abrasive, A356-T6 aluminum alloy. As shown in Figure 106, the resultant curve was relatively flat; and it is likely that cutting force will be more of an optimum feed rate criterion than cutter life in this case. An item of interest also occurred for this event. That is, when chip loads of 0.017 inch/tooth were investigated, feed rates of 500 inches/minute were readily achieved. At that feed rate, metal removal rates of nearly 70 cubic inches per minute were realized. Though not as remarkable, the optimum chip load for Al-A356-T6 was found to be a very good 0.014 inch/tooth.

Feed rates for Al-7075-T6 were not completely defined in these studies. As shown in Figure 107, only one leg of the curve was established. From that figure, however, it is evident that chip loads will not run as high for Al-7075-T6 as they did for Al-6061-T6 and Al-A356-T6. That result would be understandable because Al-7075-T6 is a harder, stronger alloy. However, it was surprising to note that cutter life was so much longer for Al-7075-T6 than the other alloys at comparable chip loads. For now, the optimum chip load for Al-7075-T6 has been established as lying between 0.005 and 0.008 inch/tooth; and it is estimated to be 0.008 inch/tooth.

When cutting many alloys, it is found that cutter life increases as feed rates are decreased. As discussed above, this was not found to be the case for the aluminum alloys. For these alloys, it was found that cutter lives reached a maximum at some unique feed rate value. As a consequence, it will be found that cutter life on aluminum alloys increases up to a point as feed rates are increased. That this can be true is shown rather emphatically in Figure 109. In that figure, it can be observed that chip welding and, therefore, cutter breakage was eliminated by increasing the feed rate.

Before concluding this subsection, the question of tooth density limitation on cutters should be addressed. Normally, aluminum cutting end mills are provided with only two flutes so that adequate chip clearance can be provided to minimize chip packing in the flutes. At ultra-high cutting speeds; e.g., 20,000 revolutions/minute, however, it was found that 4-flute cutters presented no chip-packing problems when making peripheral cuts (cf. Figure 75) or shallow pocketing cuts (cf. upper slot in Figure 109). At those speeds, centrifugal forces hurl aluminum chips away from cutters with a sand blasting effect that virtually precludes any chip packing. Such an occurrence could permit the use of even higher tooth densities and table feed rates. For example, if a 0.010 inch/tooth feed rate could be maintained with a 6-flute end mill revolving at 20,000 revolutions/minute, then the table feed rate could be increased to 1,200 inches/minute. On the other hand, if chips cannot escape the cutting zone; e.g., in a slotting cut deeper than the cutter diameter, chip packing (cf. lower slot in Figure 109) would be apt to occur. If such a problem could

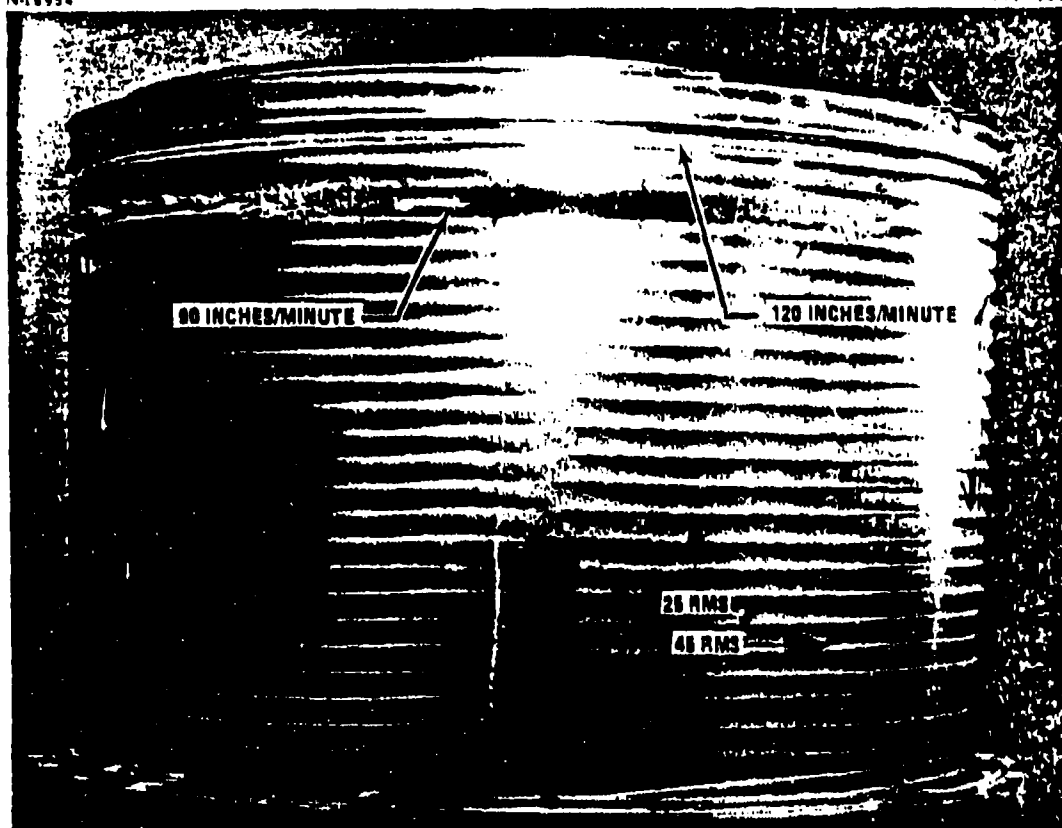


Figure 108. Effect of Feed Rate on Chip Welding

not be corrected by increasing the chip load, then it might be necessary to use a single flute cutter such as the one shown in Figure 110. That type of cutter was prepared by partially grinding one flute off a 2-flute end mill, leaving a heavy body section for strength. Such cutters were successfully used for three high speed machining applications on the Guidance and Control shell (cf. Figure 63).



Figure 110. Router Bit Made From 2-Flute End Mill

#### 8.4.2 Depths of Cut

For all practical purposes, optimum radial and axial depth of cut combinations were established on the better instrumented Omnimil. Therefore, the results presented in Figures 91 through 93 are recommended for any applications involving the Bullard vertical turret lathes.

#### 8.4.3 Cutting Speed Optimization

The Ekstrom, Carlson high speed spindle had three fixed speeds. These were 3,600, 7,200 and 14,400 revolutions/minute. Of these, only the 14,400 revolutions/minute speed was really applicable to high speed machining studies. This shortcoming plus the trial-and-error methods that had to be used to set table speeds (feed rates) and coordinate down-feeds, drastically reduced the versatility of the Bullard V.T.L. as a test machine. However, an effort was made to develop a Taylor tool life curve for Al-A356-T6, and the results obtained are shown in Figure 111. There, it can be observed that the data developed was not sufficient to establish a defensible curve. At least three data points would have been required for that purpose. However, the data were used to approximate the most economical cutting speed for the very abrasive, cast aluminum alloy, A356-T6. Using the same analytical methods that were used in subsection 8.2.3, it was calculated that the most economical tool life and cutting speed for end milling Al-A356-T6 under the conditions specified in Figure 111 were on the order of 72 minutes and 2,290 feet/minute, respectively.

The most economical cutting speed estimated above for Al-A356-T6 is much less than the 10,000 feet/minute cutting speed that was roughly estimated for Al-7075-T651 and Al-6061-T651 in Table V. At this time, it is believed that most aluminum alloys can be economically milled at that estimated cutting speed of, roughly, 10,000 feet/minute. It is only for the few aluminum alloys which have high silicon contents; e.g., Al-A356, or other detrimental alloying that cutting speed reductions for optimization would be anticipated.

#### 8.5 General Observations

It has been pointed out in this section that current spindle speeds on 20 horsepower machines are not fast enough to produce "most economical" cutting speeds for many aluminum alloys. In the same vein, it has been suggested that future spindle designs should correct that situation. However, it would do little good to increase spindle speeds without first increasing table speeds or feed rates. For instance, if the optimum feed rate of 0.010 inch/tooth were used to peripheral mill Al-6061-T651 with a 1.25-inch diameter, 4-flute, end mill turning at 20,000 revolutions/minute, a table speed of 800 inches/minute would be required. Since a 20 horsepower machine with that capability did not knowingly exist at the time, it was concluded that existing

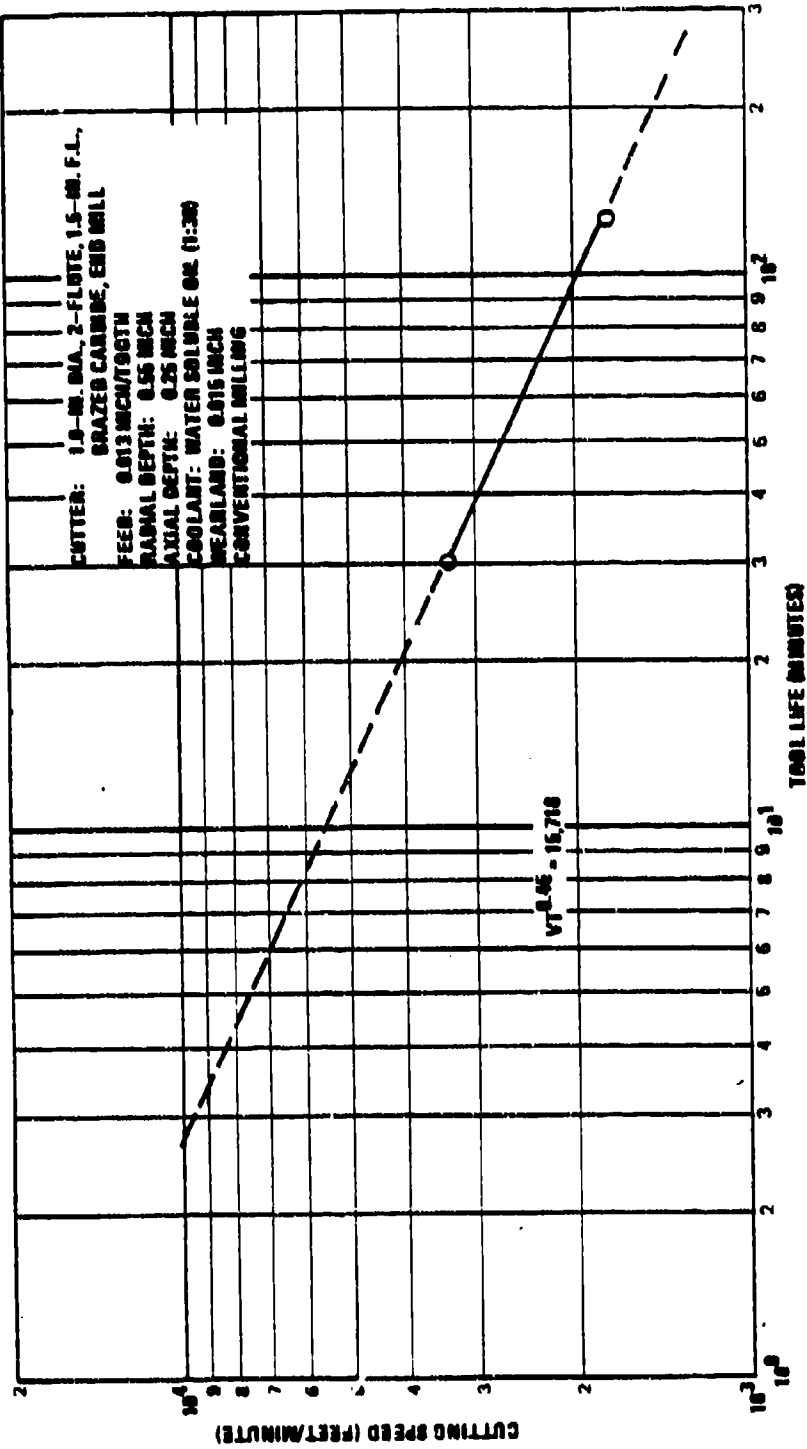


Figure 111. Theoretical Effect of Cutting Speed on Cutter Life for Al-A355-T5

table speeds were already too slow for the high speed spindles then available. Thus, it was further concluded that faster spindle speeds will not be needed until faster table speeds are provided to close the gap between the two.

## 9.0 TEST RESULTS - CUTTING FORCE, HORSEPOWER, CUTTER DEFLECTION AND PULL-OUT

### 9.1 Cutting Forces

A knowledge of cutting forces is needed by N/C programmers, production planners and others to help control dimensional tolerances, machine more economically, minimize component distortion, and prevent cutter breakage. Force knowledge is also useful to tool designers in preparing holding fixtures; and it is particularly needed for those machine tools equipped with adaptive control.

In this section, results showing the effect of feed rates, cutting speeds and depths of cut on cutting, feed, and thrust forces for Al-6061-T651 are presented.

#### 9.1.1 Test Procedure

The setup used to perform these tests is shown in Figure 72 and discussed in subsection 6.1. The workpiece blocks shown in that figure measured approximately 2.25 inches thick by 12 inches square. The blocks were drilled, counterbored and bolted to the face of the 3-axis milling dynamometer which had been mounted in a vertical position on the Omnimil. Previously, the dynamometer had been calibrated in the laboratory by systematically setting known weights on the three axes of the dynamometer and adjusting the pen deflection produced by the measuring and recording devices (cf. Figures 73 and 74). For this case, the pens were adjusted to deflect one centimeter for each 20 pounds of load or force. Some cross talk was noted among the three axes when each was individually loaded; but this was minimal, varying between 1 and 2 percent. After the dynamometer had been calibrated and made a part of the Omnimil setup, the calibration was rechecked then and from time to time. This was accomplished by electronically placing a simulated load across the force measuring system and noting the deflection of the oscillograph or plotter pens. If necessary, the recording pens were readjusted to give the proper calibration; i.e., deflect the proper number of centimeters for the simulated loads.

Having established the means for measuring cutting forces, selected machining parameters were established next. For this purpose, a test matrix was prepared as illustrated in Figure 112. As shown in that figure, axial depths of cut were varied systematically from 2.0 inches down to 0.125 inch. For each axial depth of cut, radial depths of cut were selected from Figure 92 to give machine loads of approximately 25, 50, 75, and 100 percent. Feed rates and cutting speeds were held constant at 200 inches/minute and 20,000 revolutions/minute for those depth of cut tests. For the feed rate tests, axial and radial depths of cut were held constant at 0.750 and 0.200 inch, respectively. Those values were chosen because they were expected to use 45 percent of the machine load. Cutting speeds were held constant at 11,000

AXIAL DEPTH (IN.)	RADIAL DEPTH (IN.)	RPM	FEED (IPM)	CUBIC INCH PER MINUTE	MAXIMUM DEFLECTION	% LOAD	VOLTS	FORCE F <sub>t</sub> F <sub>r</sub> F <sub>a</sub>			HP F <sub>t</sub> /WATTS	SPINDLE EFF. (%)
-------------------------	--------------------------	-----	---------------	--------------------------	-----------------------	-----------	-------	---	--	--	-----------------------------	------------------------

## 1.25-IN. DIA., 4-FLUTE, 2.50-IN. F.L., CoHSS

2.000	0.040	20,000	200	10	0.002	28	281	28	21	10	4.21/7.54	66
2.000	0.060	20,000	200	32	0.002	56	281	43	52	20	10.42/14.88	70
2.000	0.120	20,000	200	48	0.004	79	281	70	77	30	16.42/21.20	77
2.000	0.181	20,000	200	84	—	100	281	—	—	—	—	—
1.500	0.060	20,000	200	16	0.0036	25	281	28	11	12	2.2/6.73	33
1.500	0.100	20,000	200	30	0.0048	47.5	281	38	40	24	8.81/12.79	63
1.500	0.150	20,000	200	46	0.006	68	281	58	61	40	12.82/18.3	69
1.500	0.210	20,000	200	63	—	100	—	—	—	—	—	—
1.000	0.070	20,000	200	14	0.002	28	281	17	14	14	2.9/7	40
1.000	0.100	20,000	200	32	0.004	48.5	281	41	43	30	8.81/13.08	66
1.000	0.200	20,000	200	80	0.0068	73	281	60	74	30	14.82/19.68	76
1.000	0.334	20,000	200	80	—	100	—	—	—	—	—	—
0.750	0.080	20,000	200	12.5	0.002	28	281	16	10	16	2.48/6.73	36
0.750	0.220	20,000	200	33	0.0036	68	281	30	46	22	10.82/13.48	74
0.750	0.340	20,000	200	81	0.002	73	281	40	86	28	17.23/19.68	80
0.750	0.480	20,000	200	70	—	100	—	—	—	—	—	—
0.500	0.140	20,000	200	14	0.003	23	281	18	16	16	3.2/6.19	62
0.500	0.300	20,000	200	35	0.004	40	281	30	67	20	11.82/13.10	67
0.500	0.500	20,000	200	55	—	72	281	46	74	14	14.82/19.4	76
0.500	0.700	20,000	200	70	—	100	—	—	—	—	—	—
0.250	0.350	20,000	200	17.5	0.0025	27.5	281	18	28	18	6.81/7.4	78
0.250	0.776	20,000	200	30	—	81	281	10	67	8	11.42/13.73	83
0.250	1.200	20,000	200	80	—	70	281	—	72	24	14.82/21.20	70
0.250	1.830	20,000	200	81.5	—	100	281	—	—	—	—	—
0.750	0.200	10,000	100	—	0.0036	42	223	24	—	—	7.14/10.94	—
0.750	0.200	10,000	100	—	0.003	46	100	30	61	12	9.88/9.86	101
0.750	0.200	14,400	140	—	0.002	42	177	32	64	12	8.8/7.97	87
0.750	0.200	12,000	120	—	—	44.5	147	34	42	12	6.08/7.82	71
0.750	0.200	10,800	110	—	—	46	122	35	46	12	4.82/6.81	76
0.750	0.200	20,000	200	—	0.004	43	281	38	37	29	7.41/11.67	84

## 1.875 IN. DIA., 2-FLUTE, 2.50-IN. F.L., CoHSS

0.125	0.660	20,000	200	18	—	23	281	10	13	8	2.6/6.19	42
0.125	1.400	20,000	200	38	—	46	281	—	30	15	5.41/7.238	44
0.125	(1.800)	20,000	200	64	—	58	281	—	34	20	8.4/18.81	41
0.125	(2.825)	20,000	200	73	—	100	281	—	—	—	—	—

## 1.25-IN. DIA., 2-FLUTE, 2.50-IN. F.L., CoHSS

0.750	0.200	11,000	20	—	0.002	16	134.5	—	17	4	1.98/2.31	80
0.750	0.200	11,000	40	—	0.001	24.5	134.5	16	21	8	2.29/3.83	86
0.750	0.200	11,000	80	—	—	31	134.5	18	23	11	2.81/4.47	86
0.750	0.200	11,000	80	—	0.006	38.5	134.5	28	32	14	3.48/5.26	88
0.750	0.200	11,000	100	—	0.005	42.5	134.5	32	30	19	4.16/6.13	88
0.750	0.200	11,000	120	—	0.006	50	134.5	38	44	20	4.98/7.21	87
0.750	0.200	11,000	140	—	0.0068	56	134.5	—	46	—	6.24/8.88	86
0.750	0.200	11,000	160	—	0.008	62.5	134.5	—	—	—	—/8.01	—
0.750	0.200	11,000	180	—	0.0088	67	134.5	—	—	—	—/8.86	—
0.750	0.200	11,000	200	—	0.010	73	134.5	—	66	—	7.91/10.53	87

MATERIAL: 6061-T681

Figure 112. Matrix for Cutting Force Tests — Cutting Force and Power Data

revolutions/minute for the feed rate tests to permit a more practical range of feeds; while feed rate itself was varied from 20 to 200 inches/minute or from 0.001 to 0.009 inch/tooth. Finally, cutting speeds were varied from a lowest possible 10,800 to a highest possible 20,000 revolutions/minute, and feed rates were varied from 110 to 200 inches/minute to maintain a constant chip load, in determining the effect of cutting speed on cutting force. Axial and radial depths of cut were again held constant at 0.750 and 0.200 inch, respectively. While force tests were performed with other parameters, the ones listed in Figure 112 served as a nucleus for the cutting force tests.

As shown in Figure 112, most of the cuts were made with 1.25-inch diameter, 4-flute, 4-percent cobalt high speed steel end mills. The only exceptions were made for the feed rate tests and for those radial depth of cut tests that exceeded 1.200 inches. For the feed rate tests, 1.25-inch diameter, 2-flute, 4-percent cobalt high speed steel, end mills were used; while 2.0-inch diameter cutters were used for the deeper radial depth of cut tests. Cutters of 1.25-inch diameter were selected for testing purposes because balancing was generally not a problem for cutters this size and under. Additionally, these cutters were of a practical size, offering good strength, fair chip clearance, and moderately high cutting velocities. The 2-flute cutters were used to obtain higher chip loads, and the 4-flute end mills were selected for their greater section modulus and breaking strength. Additionally, all cuts were made in the climb milling mode.

After setting selected axial and radial depths of cut, feeds and speeds on the Omnimil which had also been previously calibrated, both the milling machine and oscillograph were activated and force recordings were made from the beginning to the end of the cut. The force recordings were inked on graph paper by the X-Y plotters shown in Figure 74 because the printer on the galvanometer-type oscillograph shown in Figure 73 proved to be too noisy. Readings from the recordings were made after the force traces had stabilized. This procedure was repeated for each combination of cut depth, speed and feed listed in Figure 112 plus a few supplementary combinations.

#### 9.1.2 Force Measurements

Along with the depth of cut tests reported in subsection 8.2.2, cutting force tests were conducted on Al-6061-T651 in particular, using the test procedures described above. The forces measured are exemplified in Figure 113. These are the cutting force ( $F_c$ ), which in this case is directed parallel with the Z-axis of the Omnimil, the feed force ( $F_f$ ), the thrust force ( $F_t$ ), and the resultant force ( $R$ ). For simplicity, the force diagram was constructed at the aft end of the cutter instead of the cutting end. In compliance with the type of cuts made in these tests, the diagram shown in Figure 113 is representative of peripheral milling in the climb mode.

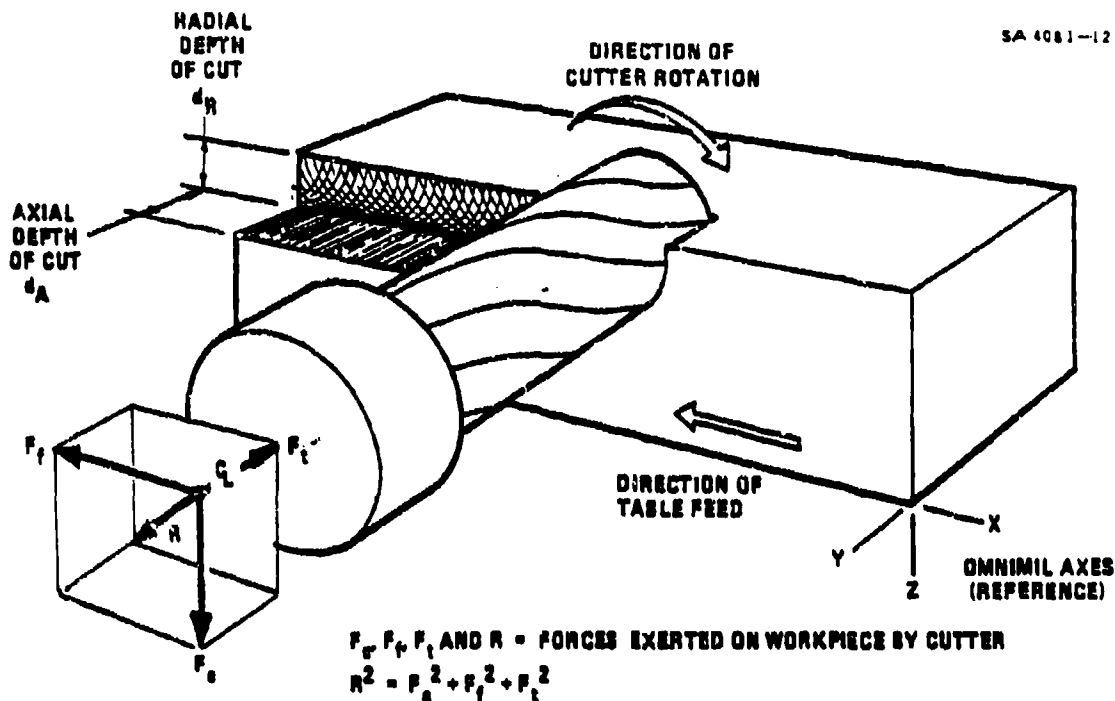


Figure 113. Cutting Force Diagram for Climb Milling

The force results obtained on Al-6061-T651 with relatively sharp cutters are presented in Figures 114 through 119. Except for the results shown in Figure 115, most of the plots were orderly and empirical equations were developed by linear regression for most from the data. The plot in Figure 115 was corrected by working backwards from the spindle horsepower recorded for the speeds shown. Those for which extrapolations were made were in obvious error, because the corresponding cutting forces indicated higher cutting horsepower than spindle horsepower, an impossibility. Force results for the other two axes (cf. Figure 118) support that corrective procedure. In summation, the effect of feed rates on cutter forces are given in Figures 114 and 117; the effect of cutting speeds on cutter forces are given in Figures 115 and 118; and the effects of cut depths on cutter forces are given in Figures 116 and 119.

### 9.1.3 General Observations on Cutter Forces

Based on data presented in Figures 115 and 118, cutter forces do not appear to be influenced by cutting speeds varying between 3,500 feet/minute and 7,000 feet/minute.

Feed rates and cut depths have a significant effect on cutter forces. However, the effect of radial depths on cutter forces decrease as axial depths decrease.

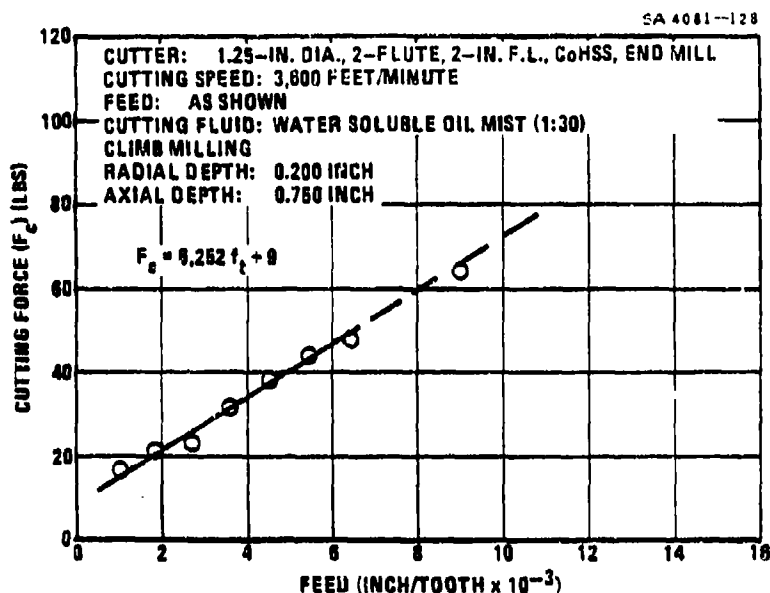


Figure 114. Effect of Feed Rate on Cutting Force for Al-8061-T851 Aluminum

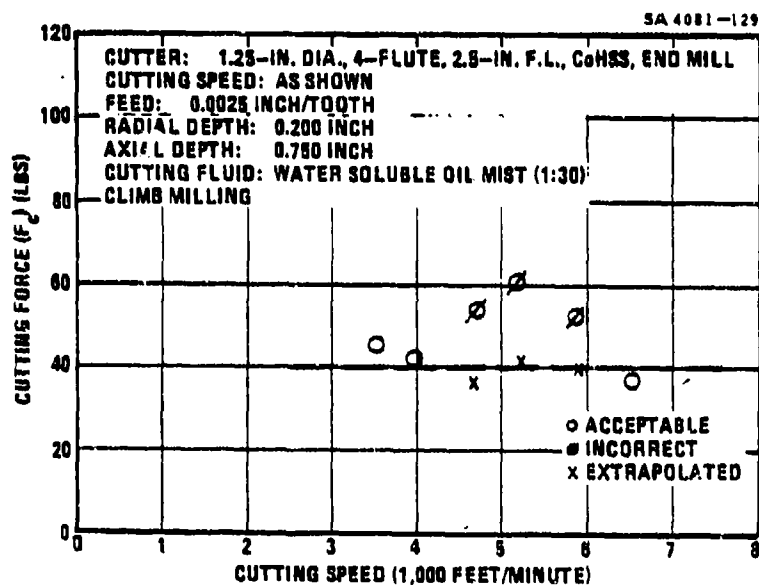


Figure 115. Effect of Cutting Speed on Cutting Force for Al-8061-T851 Aluminum

CUTTER 1/2 IN DIA. 6-FLUTE, 0.5-IN F.C. CORNER, END MILL  
 CUTTING FLUID: COOLANT  
 FEED: 0.005 IN/REV  
 SPIN: 1000 RPM  
 SECTION: FEMO. WATERS VALVE 0.5 IN DIA. (1.25 IN)  
 CLAMP: 0.001 IN

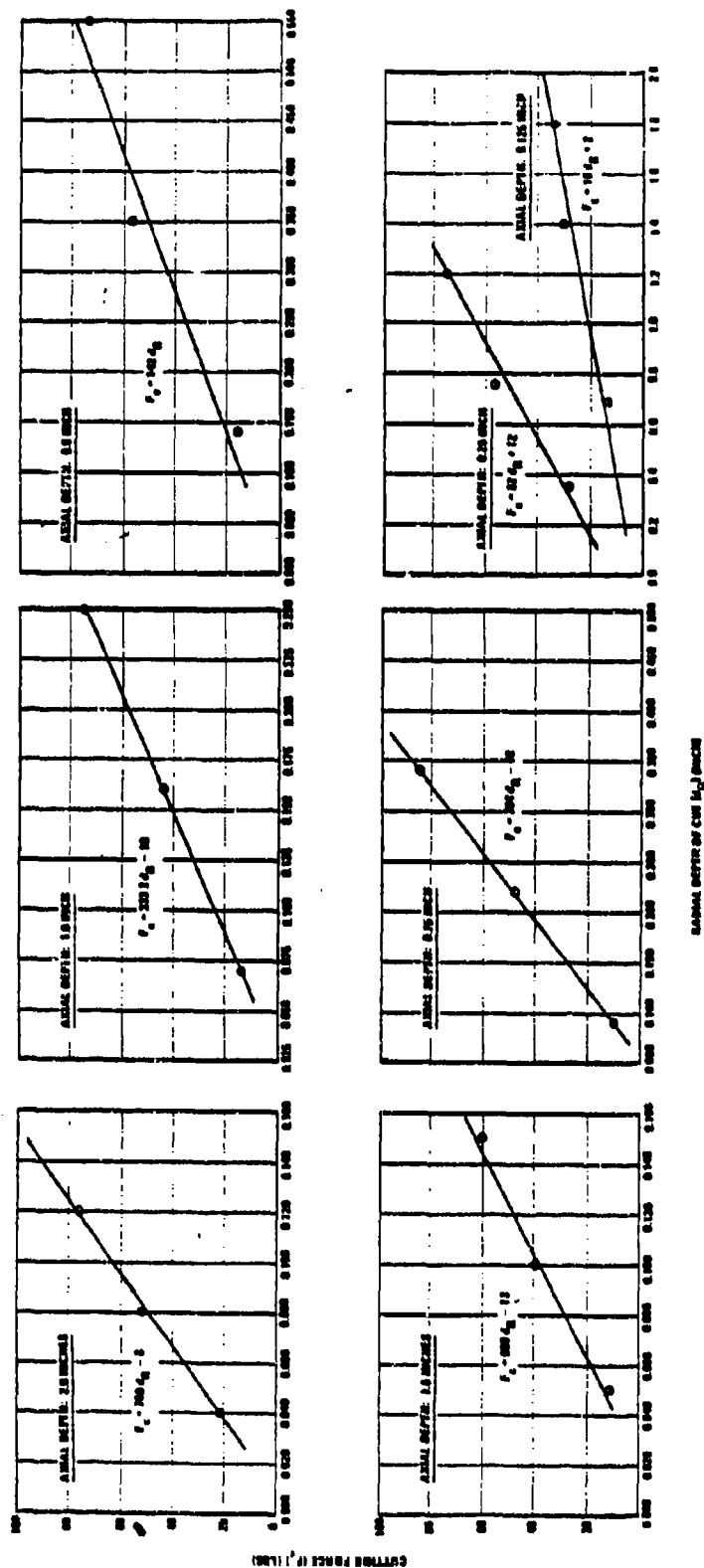


Figure 118. Effect of Radial Depth of Cut on Cutting Force for Al-6061-T651 Aluminum

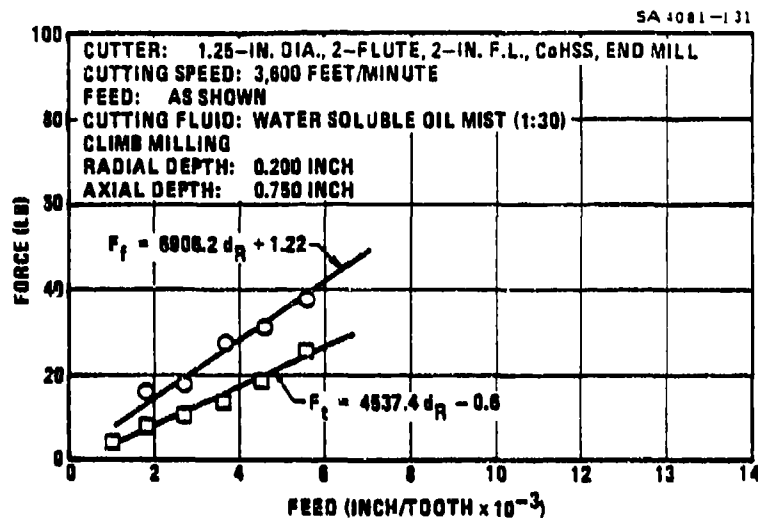


Figure 117. Effect of Feed Rate on Feed and Thrust Force for 6061-T651 Aluminum

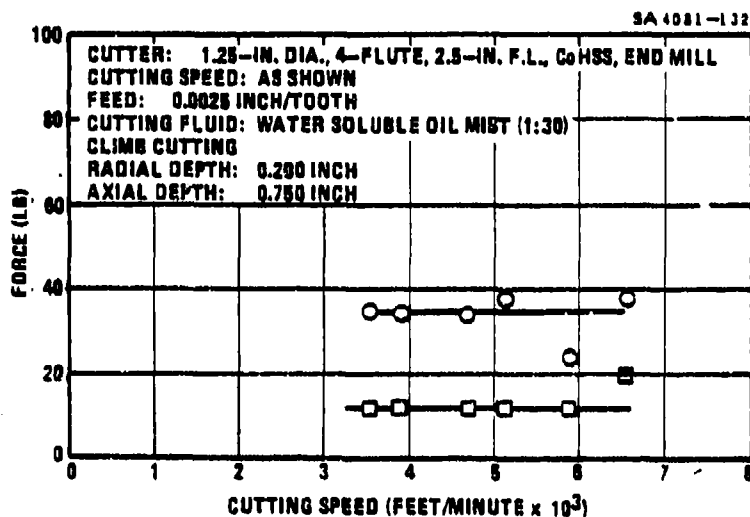


Figure 118. Effect of Cutting Speed on Feed and Thrust Force for 6061-T651 Aluminum

CUTTER: 1.5 IN DIA. 5 FLUTE, 24-DEG FL. CROWN, 6000 RPM  
 CUTTING SPEED: 100 FT/MIN  
 FEED: 0.010 IN/REV  
 WORK: 1140S, 6061-T6 ALUMINUM  
 TOOL: 1.5 IN DIA. 5 FLUTE, 24-DEG FL. CROWN, 6000 RPM

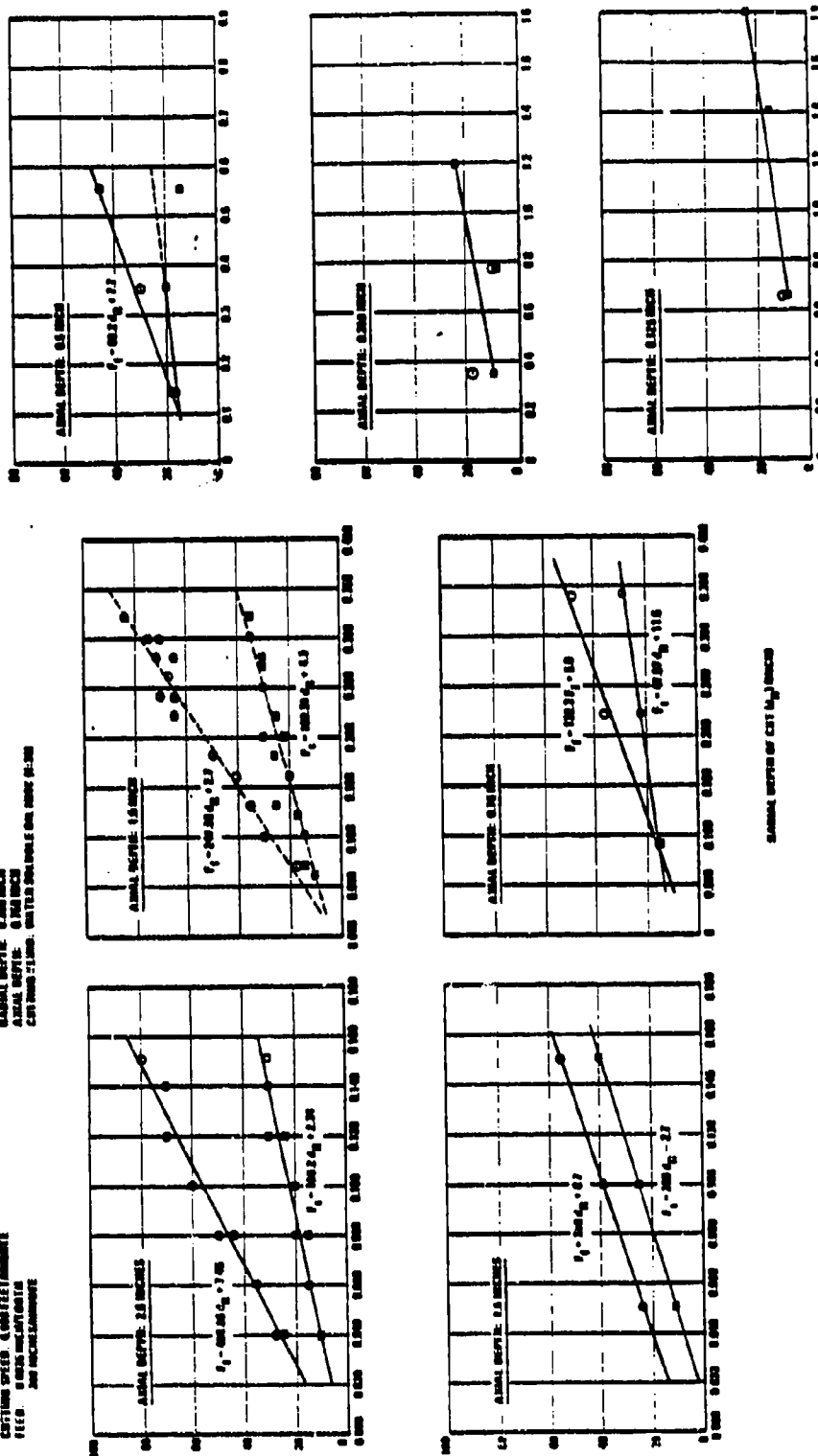


Figure 118. Effect of Radial Depth of Cut on Feed and Thrust Force for 6061-T6 Aluminum

Generally, the cutting force component ( $F_c$ ) was less than the feed force component ( $F_f$ ) for machine loads under 25%. However, at some machine load value between 25 and 50 percent, this trend reversed; and the cutting force component became dominant. As machine loads were further increased, so did the domination of the cutting force component.

Most of the plots in Figures 116 and 119 are based on three data points. These data points are representative of machine loads of approximately 25, 50, and 75 percent. From these data, it was deduced that the Bryant high speed spindle should not be used for applications requiring more than approximately 80 pounds of cutting force; i.e., a 75-percent machine load. While it is not expected that a 100-pound force would break a cutter or damage a part or machine tool, it is likely that such a force would trigger protective interlocks and shut down the machine.

## 9.2

### Horsepower

Since a part should never be put on a machine tool that does not have the power to produce it, a knowledge of horsepower requirements is needed by machine loading groups in particular. Horsepower requirements can be controlled since these are functions of cutting speeds, feeds, depths of cut, cutter geometry, cutting fluids and other machining parameters. Thus, a knowledge of the effect that each of these has on horsepower is needed by N/C programmers and production planners to help design a machining operation so that it can stay within machine power limitations. High speed machining introduces another need for horsepower knowledge. That is, all things being equal, horsepower will increase linearly with cutting speed; and a high horsepower spindle may be required for high speed machining. Thus, a knowledge of horsepower demands is also needed by spindle designers to help build adequately powered, high speed spindles.

Horsepower is usually expressed in terms of spindle (input) horsepower or cutter (output) horsepower. Spindle horsepower is generally determined with a wattmeter, and cutter horsepower is usually determined with a dynamometer. Of the two, cutter horsepower is more difficult to measure. Additionally, cutter horsepower will always be less than its corresponding spindle horsepower because of the transmission, frictional and thermal losses sustained in just driving the spindle. The ratio between the two is a measure of a spindle's efficiency.

In this section, results showing the effect of depths of cut on spindle horsepower requirements for Al-7075-T651, Al-6061-T651, and Al-A356-T6 are presented. Additionally, results showing the effect of feed rates and cutting speeds on spindle horsepower requirements for Al-7075-T651 and Al-6061-T651 are given. Finally, results showing the effect of feed rates, cutting speeds, and depths of cut on cutter horsepower requirements are presented for Al-6061-T651.

### 9.2.1 Test Procedure

Spindle horsepowers were determined by measuring machine loads and cutting speeds for all of the tests indicated in Figures 91, 92, 93, and 112 plus those from a few supplementary tests. These data were then converted to horsepowers with the aid of formulae described in subsection 6.1 or the nomograph shown in Figure 71.

Cutter horsepowers were calculated from the cutting force ( $F_C$ ) and cutting speed data contained in Figures 112, 114 through 119. The formula used for that purpose was also presented in subsection 6.1.

Unit power requirements were determined for both spindle and cutter horsepower. This was accomplished by dividing each horsepower value by its corresponding metal removal rate value in cubic inches/minute.

Spindle efficiencies were determined by dividing each cutter horsepower value by its corresponding spindle horsepower value.

### 9.2.2 Horsepower Measurements

Using the procedures described above, spindle horsepower was determined for all three aluminum alloys and cutter horsepower was determined for Al-6061-T651. The results obtained are shown in Figures 120 through 126. While most of the plots were orderly, some inconsistency was noted among the spindle efficiency plots contained in Figures 120 through 122 and Figure 125.

The effect of feed rates on horsepower are given in Figures 120 and 123 for Al-6061-T651 and Al-7075-T651, respectively. The effect of cutting speeds on horsepower requirements for the same materials are shown in Figures 121 and 124. For convenience, empirical equations were developed from and superimposed on these plots. The abbreviations used in the equations are defined as follows:

$HP_s$	=	spindle horsepower
$HP_C$	=	cutter horsepower
$f_t$	=	feed (inch/tooth)
$V$	=	cutting speed (feet/minute)

The effect of depths of cut on horsepower requirements are presented in Figure 122 for Al-6061-T651, Figure 125 for Al-7075-T651, and Figure 126 for Al-A356-T6. Finally, the effect of aluminum alloys on horsepower requirements are shown in Figure 127; and the effect of carbide cutters on horsepower requirements are presented in Figure 128 for Al-7075-T651.

A summary of horsepower and metal removal rate data obtained for Al-6061-T651 at different machine load percentages is presented in Table VI. Also included in this table are the unit horsepower and spindle efficiency results.

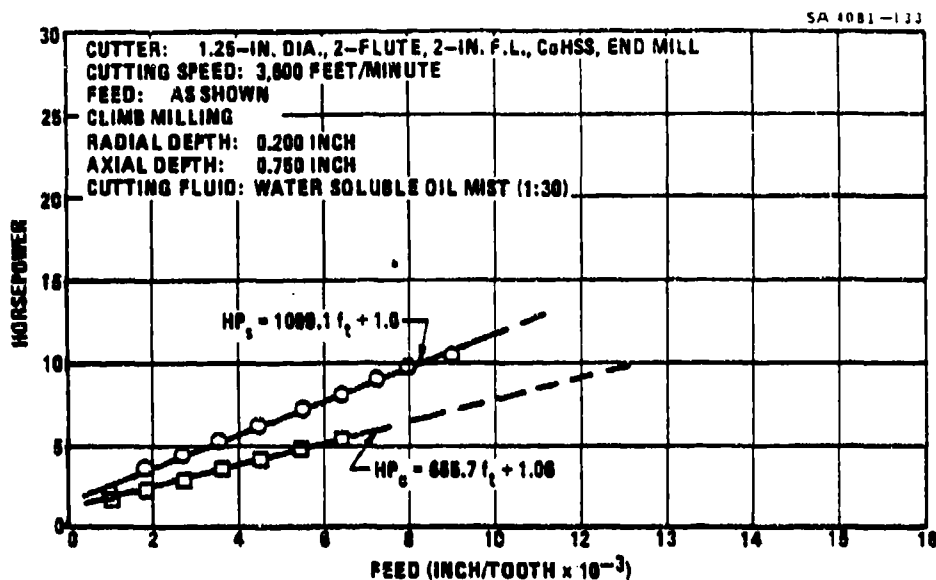


Figure 120. Effect of Feed Rate on Spindle and Cutter Horsepower for Al-6061-T651 Aluminum

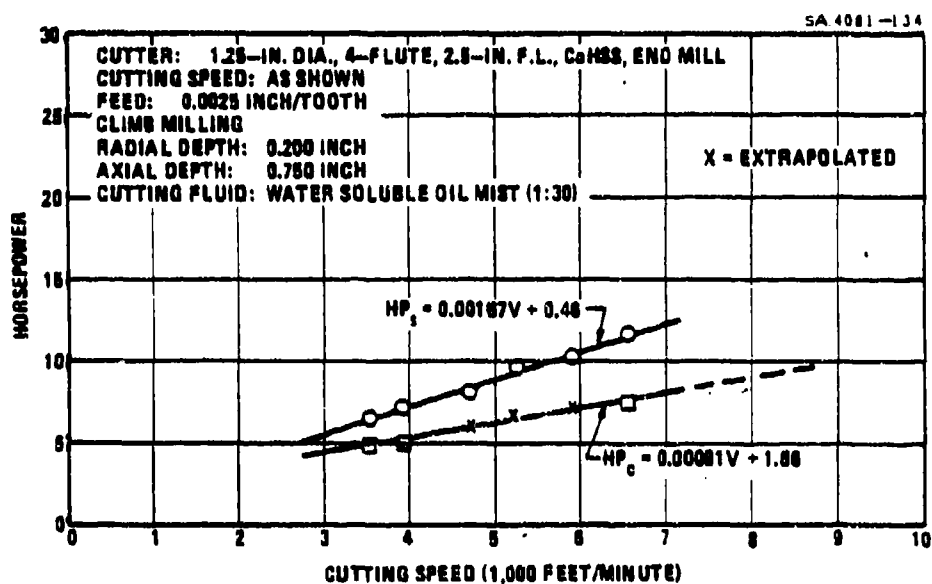


Figure 121. Effect of Cutting Speed on Spindle and Cutter Horsepower for Al-6061-T651 Aluminum

CUTTING: 1.25 IN DIA. C-FLUTE, 2.5 IN F.L. CAMS, 600 BALL  
 CUTTING DEPTH: 0.000 FEET/REV  
 FIELD: 0.000 INCHES/REV  
 300 INCHES/REV

CLAMP MILLING  
 BALL MILLING  
 BALL MILLING  
 BALL MILLING

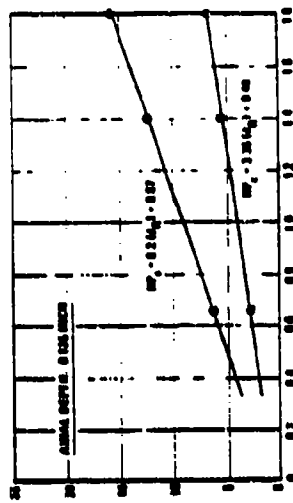
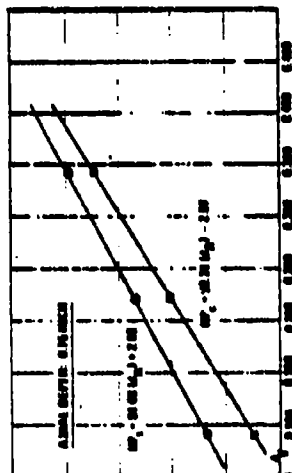
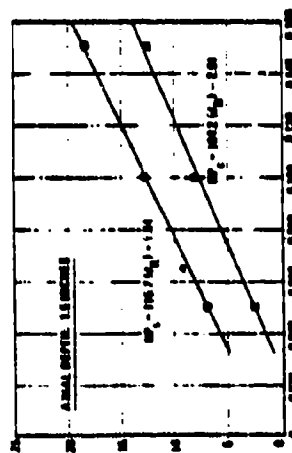
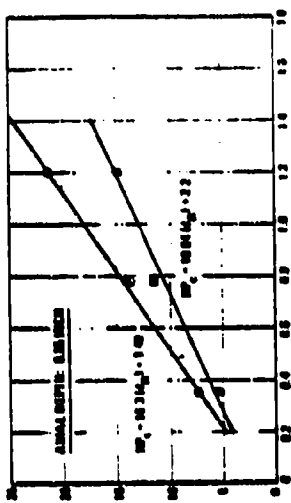
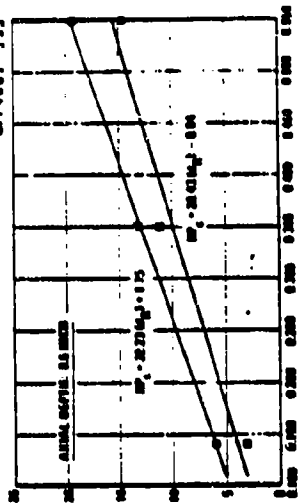
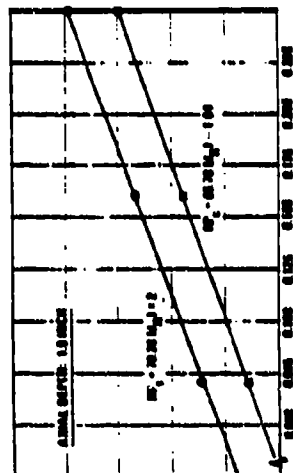
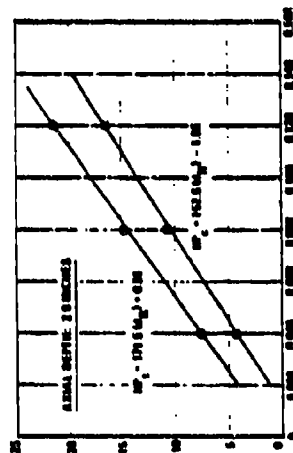


Figure 122. Effect of Depth of Cut on Spindle and Cutter Horsepower for AI-0001-T651 Aluminum

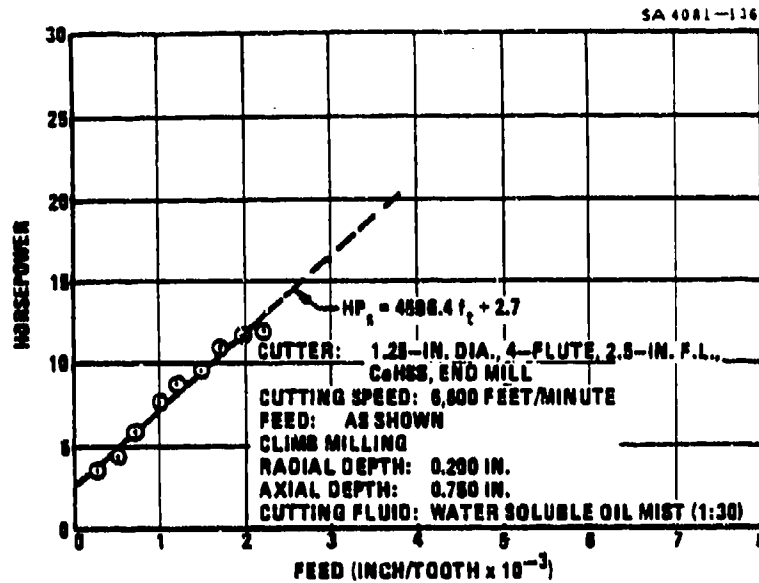


Figure 123. Effect of Feed Rate on Spindle Horsepower for Al-7075-T651 Aluminum

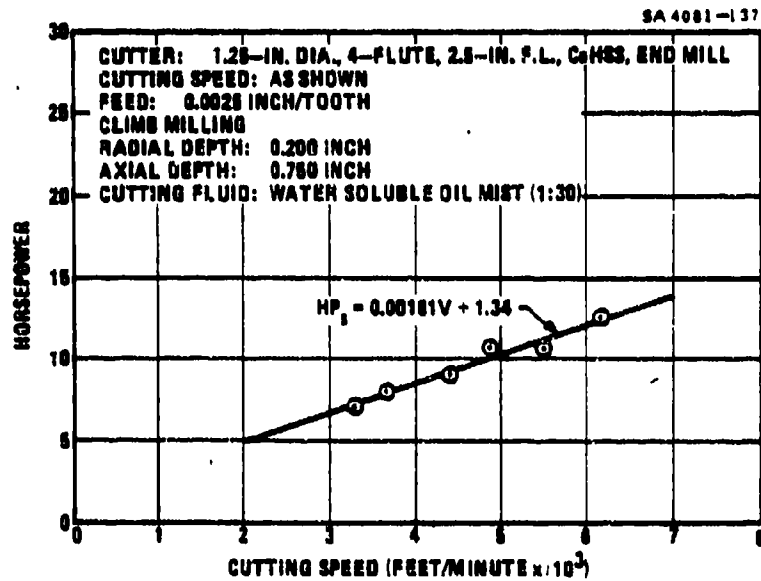
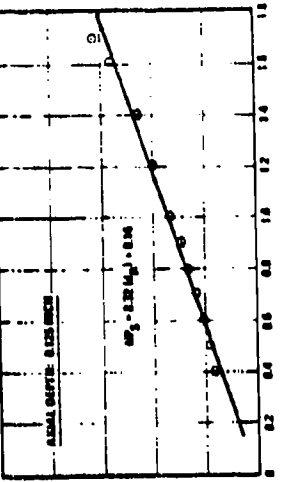
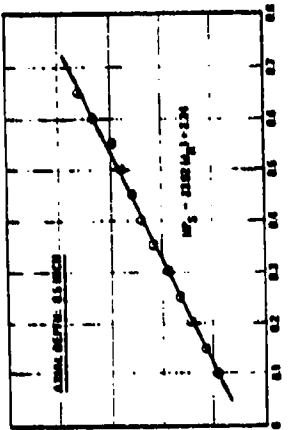
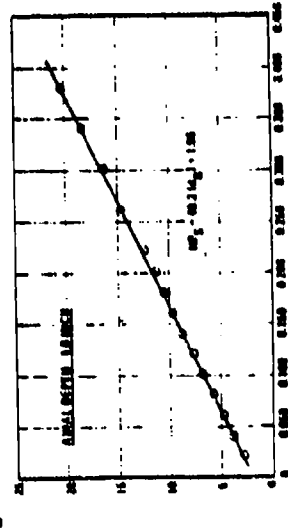
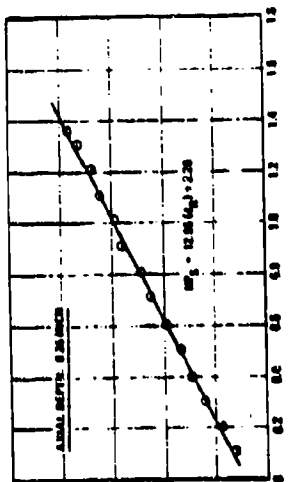
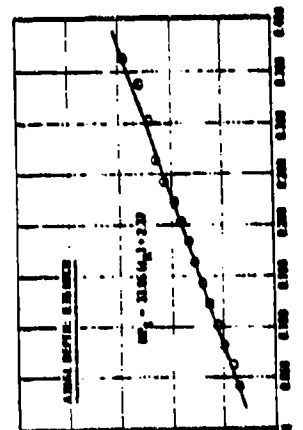
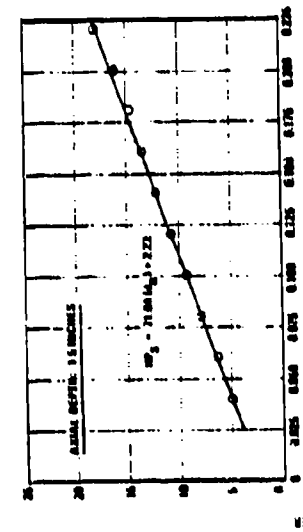


Figure 124. Effect of Cutting Speed on Spindle Horsepower for Al-7075-T651 Aluminum

COILS: 1.25-10.00, 4-11.00, 2.5-10.0, 1.25-10.0, 0.50-10.0  
 CAPSULES: 1.25-10.0, 4-11.00, 2.5-10.0, 1.25-10.0, 0.50-10.0  
 PLEO: 0.50, 1.00, 2.00, 4.00, 8.00, 16.00, 32.00, 64.00, 128.00, 256.00, 512.00, 1024.00, 2048.00, 4096.00, 8192.00, 16384.00, 32768.00, 65536.00, 131072.00, 262144.00, 524288.00, 1048576.00, 2097152.00, 4194304.00, 8388608.00, 16777216.00, 33554432.00, 67108864.00, 134217728.00, 268435456.00, 536870912.00, 1073741824.00, 2147483648.00, 4294967296.00, 8589934592.00, 17179869184.00, 34359738368.00, 68719476736.00, 137438953472.00, 274877906944.00, 549755813888.00, 1099511627776.00, 2199023255552.00, 4398046511104.00, 8796093022208.00, 17592186044416.00, 35184372088832.00, 70368744177664.00, 140737488355328.00, 281474976710656.00, 562949953421312.00, 1125899906842624.00, 2251799813685248.00, 4503599627370496.00, 9007199254740992.00, 18014398509481984.00, 36028797018963968.00, 72057594037927936.00, 144115188075855872.00, 288230376151711744.00, 576460752303423488.00, 1152921504606846976.00, 2305843009213693952.00, 4611686018427387904.00, 9223372036854775808.00, 18446744073709551616.00, 36893488147419103232.00, 73786976294838206464.00, 147573952589676412928.00, 295147905179352825856.00, 590295810358705651712.00, 1180591620717411303424.00, 2361183241434822606848.00, 4722366482869645213696.00, 9444732965739290427392.00, 18889465931478580854784.00, 37778931862957161709568.00, 75557863725914323419136.00, 151115727451828646838272.00, 302231454903657293676544.00, 604462909807314587353088.00, 1208925819614629174706176.00, 2417851639229258349412352.00, 4835703278458516698824704.00, 9671406556917033397649408.00, 19342813113834066795298816.00, 38685626227668133590597632.00, 77371252455336267181195264.00, 154742504910672534362390528.00, 309485009821345068724781056.00, 618970019642690137449562112.00, 1237940039285380274899124224.00, 2475880078570760549798248448.00, 4951760157141521099596496896.00, 9903520314283042199192993792.00, 19807040628566084398385987584.00, 39614081257132168796771975168.00, 79228162514264337593543950336.00, 158456325028528675187087900672.00, 316912650057057350374175801344.00, 633825300114114700748351602688.00, 1267650600228229401496703205376.00, 2535301200456458802993406410752.00, 5070602400912917605986812821504.00, 10141204801825835211973625643008.00, 20282409603651670423947251286016.00, 40564819207303340847894502572032.00, 81129638414606681695789005144064.00, 162259276829213363391578010288128.00, 324518553658426726783156020576256.00, 649037107316853453566312041152512.00, 1298074214633706907132624082305024.00, 2596148429267413814265248164610048.00, 5192296858534827628530496329220096.00, 10384593717069655257060992658440192.00, 20769187434139310514121985316880384.00, 41538374868278621028243970633760768.00, 83076749736557242056487941267521536.00, 166153499473114484112975882535043072.00, 332306998946228968225951765070086144.00, 664613997892457936451903530140172288.00, 1329227995784915872903807060280344576.00, 2658455991569831745807614120560689152.00, 5316911983139663491615228241121378304.00, 10633823966279326983230456482242756608.00, 21267647932558653966460912964485513216.00, 42535295865117307932921825928971026432.00, 85070591730234615865843651857942052864.00, 170141183460469231731687303715884105728.00, 340282366920938463463374607431768211456.00, 680564733841876926926749214863536422912.00, 1361129467683753853853498429727072845824.00, 2722258935367507707706996859454145691648.00, 5444517870735015415413993718908291383296.00, 10889035741470030830827987437816582766592.00, 21778071482940061661655974875633165533184.00, 43556142965880123323311949751266331066368.00, 87112285931760246646623899502532662132736.00, 174224571863520493293247799005065324265472.00, 348449143727040986586495598010130648530944.00, 696898287454081973172991196020261297061888.00, 1393796574908163946345982392040522594123776.00, 2787593149816327892691964784081045188247552.00, 5575186299632655785383929568162090376495104.00, 11150372599265311570767859136324180752990208.00, 22300745198530623141535718272648361505980416.00, 44601490397061246283071436545296723011960832.00, 89202980794122492566142873090593446023921664.00, 178405961588244985132285746181186892047843328.00, 356811923176489970264571492362373784095686656.00, 713623846352979940529142984724747568191373312.00, 1427247692705959881058285969449495136382746624.00, 2854495385411919762116571938898990272765493248.00, 5708990770823839524233143877797980545530986496.00, 11417981541647679048466287755595961091061972992.00, 22835963083295358096932575511191922182123945984.00, 45671926166590716193865151022383844364247891968.00, 91343852333181432387730302044767688728495783936.00, 182687704666362864775460604089535377456991567872.00, 365375409332725729550921208179070754913983135744.00, 730750818665451459101842416358141509827966271488.00, 1461501637330902918203684832716283019655932542976.00, 2923003274661805836407369665432566039311865085952.00, 5846006549323611672814739330865132078623730171904.00, 11692013098647223345629478661730264157247460343808.00, 23384026197294446691258957323460528314494920687616.00, 46768052394588893382517914646921056628989841375232.00, 93536104789177786765035829293842113257979682750464.00, 187072209578355573530071658587684226515959365500928.00, 374144419156711147060143317175368453031918731001856.00, 748288838313422294120286634350736906063837462003712.00, 1496577676626844588240573268701473812127674924007424.00, 2993155353253689176481146537402947624255349848014848.00, 5986310706507378352962293074805895248510699696029696.00, 11972621413014756705924586149611790497021399392059392.00, 23945242826029513411849172299223580994042798784118784.00, 47890485652059026823698344598447161988085597568237568.00, 95780971304118053647396689196894323976171195136475136.00, 191561942608236107294793378393788647952342390272950272.00, 383123885216472214589586756787577295904684780545900544.00, 766247770432944429179173513575154591809369561091801088.00, 1532495540865888858358347027150309183618739122183602176.00, 3064991081731777716716694054300618367237478244367204352.00, 6129982163463555433433388108601236734474956488734408704.00, 12259964326927110866866776217202473468949912977468817408.00, 24519928653854221733733552434404946937899825954937634816.00, 49039857307708443467467104868809893875799651909875269632.00, 98079714615416886934934209737619787751599303819750539264.00, 196159429230833773869868419475239575503198607639501078528.00, 392318858461667547739736838950479151006397215279002157056.00, 784637716923335095479473677900958302012794430558004314112.00, 1569275433846670190958947355801916604025588861116008628224.00, 3138550867693340381917894711603833208051177722232017256448.00, 6277101735386680763835789423207666416102355444464034512896.00, 12554203470773361527671578846415332832204710888928069025792.00, 25108406941546723055343157692830665664409421777856138051584.00, 50216813883093446110686315385661331328818843555712276103168.00, 100433627766186892221372630771322662657637687111424552206336.00, 200867255532373784442745261542645325315275374222849104412672.00, 401734511064747568885490523085290650630550748445698208825344.00, 803469022129495137770981046170581301261101496891396417650688.00, 1606938044258990275541962092341162602522202993782792835301376.00, 3213876088517980551083924184682325205044405987565585670602752.00, 6427752177035961102167848369364650410088811975131171341205504.00, 12855504354071922204335696738729300820177623950262342682411008.00, 25711008708143844408671393477458601640355247900524685364822016.00, 51422017416287688817342786954917203280710495801049370729644032.00, 102844034832575377634685573909834406561420991602098741459288064.00, 205688069665150755269371147819668813122841983204197482918576128.00, 411376139330301510538742295639337626245683966408394965837152256.00, 822752278660603021077484591278675252491367932816789931674304512.00, 1645504557321206042154969182557350504982735865633579863348609024.00, 3291009114642412084309938365114701009965471731267159726697218048.00, 6582018229284824168619876730229402019930943462534319453394436096.00, 13164036458569648337239753460458804039861886925068638906788872192.00, 26328072917139296674479506920917608079723773850137277813577744384.00, 52656145834278593348959013841835216159447547700274555627155488768.00, 105312291668557186697918027683670432318895095400549111254310977536.00, 210624583337114373395836055367340864637790190801098222508621955072.00, 421249166674228746791672110734681729275580381602196445017243910144.00, 842498333348457493583344221469363458551160763204392890034487820288.00, 1684996666696914987166688442938726917102321526408785780068975640576.00, 3369993333393829974333376885877453834204643052817571560137951281152.00, 6739986666787659948666753771754907668409286105635143120275902562304.00, 13479973333575319897333507543509815336818572211270286240551805124608.00, 26959946667150639794667015087019630673637144422540572481103610249216.00, 53919893334301279589334030174039261347274288845081144962207220498432.00, 107839786668602559178668060348078522694548577690162289924414440996864.00, 215679573337205118357336120696157045389097155380324579848828881993728.00, 431359146674410236714672241392314090778194310760649159697657763987456.00, 862718293348820473429344482784628181556388621521298319395315527974912.00, 1725436586697640946858688965569256363112777243042596638790631055949824.00, 3450873173395281893717377931138512726225554486085193277581262111899648.00, 6901746346790563787434755862277025452451108972170386555162524223799296.00, 13803492693581127574869511724554050904902217944340773110325048447598592.00, 27606985387162255149739023449108101809804435888681546220650096895197184.00, 55213970774324510299478046898216203619608871777363092441300193790394368.00, 110427941548649020598956093796432407239217743554726184882600387580788736.00, 220855883097298041197912187592864814478435487109452369765200775161577472.00, 441711766194596082395824375185729628956870974218904739530401550323154944.00, 883423532389192164791648750371459257913741948437809479060803100646309888.00, 1766847064778384329583297500742918515827483896875618958121606201292619776.00, 3533694129556768659166595001485837031654967793751237916243212402585239552.00, 7067388259113537318333190002971674063309935587502475832486424805170479104.00, 14134776518227074636666380005943348126619871175004951664972849610340958208.00, 28269553036454149273332760011886696253239742350009903329945699220681916416.00, 56539106072908298546665520023773392506479484700019806659891398441363832832.00, 113078212145816597093331040047546785012958969400039613319782796882727665664.00, 226156424291633194186662080095093570025917938800079226639565593765455331328.00, 452312848583266388373324160190187140051835877600158453279131187530910662656.00, 904625697166532776746648320380374280103671755200316906558262375061821325312.00, 1809251394333065553493296640760748560207343510400633813116524750123642650624.00, 3618502788666131106986593281521497120414687020801267626233049500247285301248.00, 7237005577332262213973186563042994240829374041602535252466099000494570602496.00, 14474011154664524427946373126085988481658748083205070504932198000989141204992.00, 28948022309329048855892746252171976963317496166410141009864396001978282409984.00, 57896044618658097711785492504343953926634992332820282019728792003956564819968.00, 115792089237316195423570985008687907853269984665640564039457584007913129639936.00, 231584178474632390847141970017375815706539969331281128078915168015826259279872.00, 463168356949264781694283940034751631413079938662562256157830336031652518559744.00, 926336713898529563388567880069503262826159877325124512315660672063305037119488.00, 1852673427797059126777135760139006525652319754650249024631321344126610074238976.00, 3705346855594118253554271520278013051304639509300498049262642688253220148477952.00, 7410693711188236507108543040556026102609279018600996098525285376506440296955904.00, 14821387422376473014217086081112052205218558037201992197050570753012880593911808.00, 29642774844752946028434172162224104410437116074403984394101141506025761187823616.00, 59285549689505892056868344324448208820874232148807968788202283012051522375647232.00, 118571099379011784113736688648896417641748464297615937576404566024103044751294464.00, 237142198758023568227

CUTTING: 1.25-IN. DIA. 3-FLUTE, 20-DEG. S.A., C-2 CARBIDE, 600 RPM, 1.0  
 FEED, 24"  
 WORKPIECE: 6061-T6 ALUMINUM  
 CUTTING SPEED: 0.250 FEET/MINUTE  
 FEED: 0.002 INCHES/REV  
 AND RECORDING

CUTTING: 1.25-IN. DIA. 3-FLUTE, 20-DEG. S.A., C-2 CARBIDE, 600 RPM, 1.0  
 FEED, 24"  
 WORKPIECE: 6061-T6 ALUMINUM  
 CUTTING SPEED: 0.250 FEET/MINUTE  
 FEED: 0.002 INCHES/REV  
 AND RECORDING



AXIAL DEPTH OF CUT (inches)

Figure 126. Effect of Depths of Cut on Spindle Horsepower for Al-A356-T6 Aluminum

CUTTER:  $\phi$  0.125 IN. DIA., 4-FLUTE, 2.5-IN. F.L., C-HSS, END MILL  
 FEED: 200 INCHES/MINUTE  
 $\phi$  0.0025 INCH/TOOTH  
 $\phi$  0.0033 INCH/TOOTH  
 CUTTING SPEED:  $\phi$  8000 FEET/MINUTE  
 $\phi$  0.270 FEET/MINUTE  
 CUTTING FLUID: WATER SOLUBLE OIL MIST (1:30)  
 CLAMP MILLING

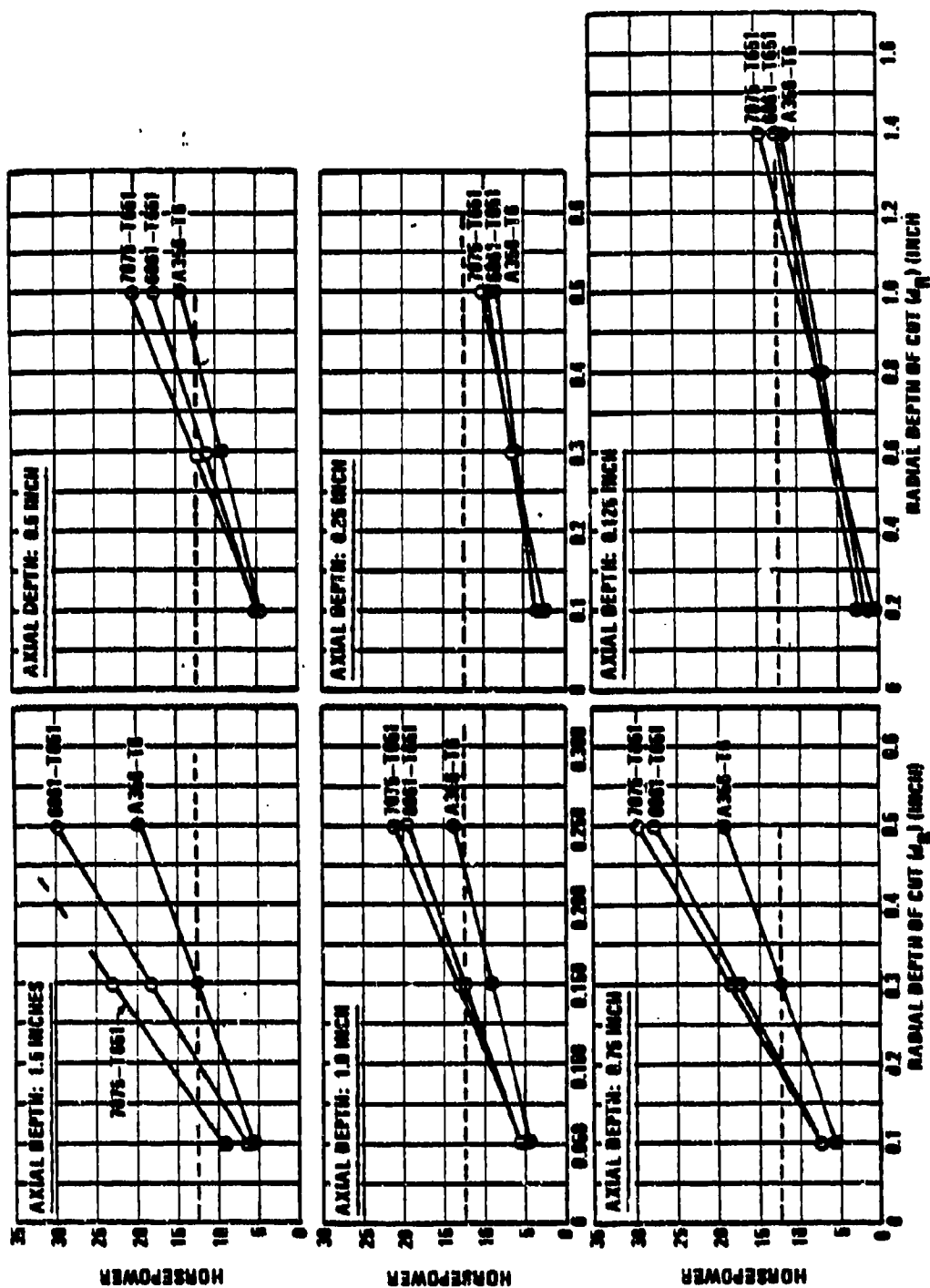


Figure 127. Effect of Aluminum Alloy on Spindle Horsepower

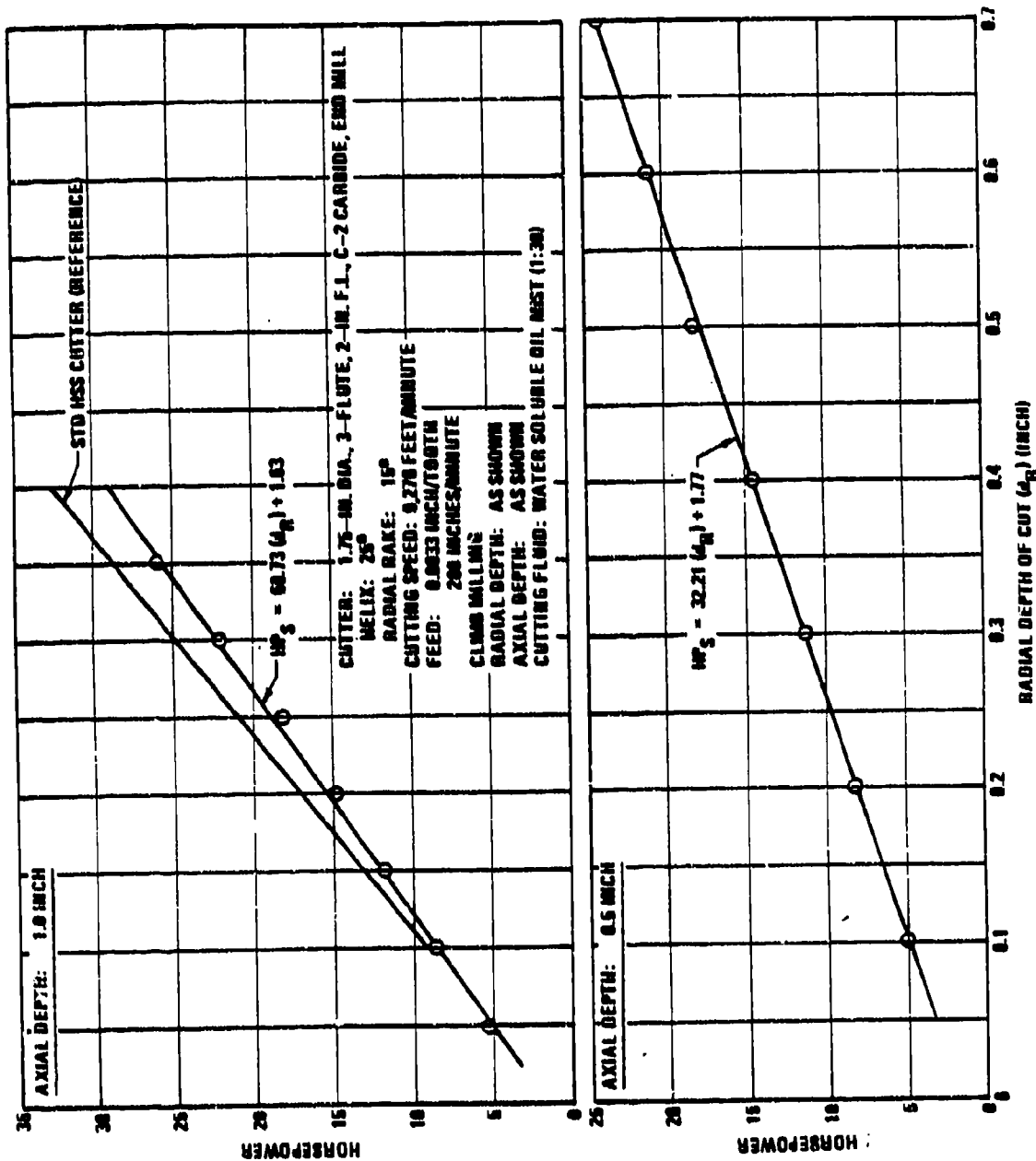


Figure 128. Effect of Depths of Cut and Carbide Cutters on Spindle Horsepower for 7075-T651 Aluminum

TABLE VI - SUMMARY OF HORSEPOWER AND METAL REMOVAL RATE  
DATA DEVELOPED FROM END MILLING TESTS ON  
6061-T651 ALUMINUM

Cutter	Axial Depth (inch)	Radial Depth (inch)	RPM	Feed (IPM)	Metal Removal Rate (in. <sup>3</sup> /min.)	Horsepower		Cu. In./ Min./HP		Spindle Eff. (%)
						Spindle	Cutter	Spindle	Cutter	
25% Load										
*	2.00	0.040	20,200	200	16	7.5	4.2	2.12	3.80	56
*	1.50	0.050			15	6.7	2.2	2.23	6.82	33
*	1.00	0.070			14	7.0	2.8	2.00	5.00	40
*	0.75	0.090			14	6.7	2.4	2.01	5.60	39
*	0.50	0.140			14	6.2	3.2	2.26	4.38	52
*	0.25	0.350			17	7.4	5.6	2.36	3.13	76
**	0.125	0.650			16	6.2	2.6	2.58	6.15	42
50% Load										
*	2.00	0.080			37	14.8	10.4	2.16	3.07	70
*	1.50	0.100			3	12.8	8.0	2.35	3.75	63
*	1.00	0.160			32	13.1	8.6	2.44	3.72	66
*	0.75	0.220			33	13.5	10.0	2.44	3.30	74
*	0.50	0.350			35	13.2	11.4	2.65	3.07	86
*	0.25	0.775			39	13.7	11.4	2.85	3.42	83
**	0.125	1.400			35	12.4	5.4	2.82	6.48	44
75% Load										
*	2.00	0.120			48	21.3	16.4	2.26	2.92	77
*	1.50	0.150			45	18.3	12.6	2.46	3.57	69
*	1.00	0.250			50	19.7	14.8	2.54	3.38	75
*	0.75	0.340			51	19.7	17.2	2.59	2.97	87
*	0.50	0.550			55	19.4	14.8	2.84	3.72	76
*	0.25	1.200			60	21.3	14.8	2.82	4.05	69
**	0.125	2.165			54	---	---	---	---	---
**	0.125	1.800	20,200	200	45	15.6	6.4	3.46	8.44	41
Overall Average								2.49	4.32	63

\*1.25-inch diameter, 4-flute, 2.5-inch flute length, cobalt HSS, end mill

\*\*1.9-inch diameter, 2-flute, 2-inch flute length, cobalt HSS, end mill

### 9.2.3 General Observations on Horsepower Measurements

Based on results shown in Table VI, the maximum metal removal rate that can be obtained on a continuous duty cycle basis with the Bryant 20 horsepower, high speed spindle is approximately 33 cubic inches/minute.

In Figures 121 and 124, it can be observed that horsepower requirements increase with cutting speeds. Since horsepower is the product of cutting force and cutting velocity and cutting forces were not effected by cutting speeds, that is a logical result.

According to the spindle horsepower equation given in Figure 121, a 170-horsepower spindle motor would be required to make the same cut at 100,000 feet/minute.

The spindle horsepower equation given in Figure 122 for 1.0-inch axial depths infers that a 37 horsepower spindle motor would be required to make a 1.0-inch deep slotting cut with a 1.0-inch diameter cutter. If it were desired to make this cut at a 50-percent duty cycle, a 75 horsepower spindle motor would be required.

A comparison of Figures 120 and 123 shows that Al-7075-T651 is much more feed rate sensitive than Al-6061-T651.

Results shown in Table VI indicate that approximately 2.5 cubic inches of Al-6061-T651 can be milled per minute for each unit of spindle horsepower that is available.

### 9.3

#### Cutter Deflection

Cutter deflection data are needed by N/C programmers to help maintain dimensional tolerances. Generally, one or more floating cuts are included in an N/C program to correct for cutter deflection induced tolerance errors. When the number of floating cuts provided are insufficient, a new program generally has to be made; and that is costly. On the otherhand, if the number of floating cuts provided is excessive, the N/C machine will loaf a part of the time; and that, too, is costly. Thus, cutter deflection data are needed to help reduce machining costs as well as maintain dimensional tolerances.

In this section, results showing the effect of feed rates, cutting speeds, and depths of cut on cutter deflection are given for Al-6061-T651. Additionally, results showing the effect of depths of cut on cutter deflection for Al-7075-T651 and Al-A356-T6 are presented.

#### 9.3.1 Test Procedure

The experimental setup used in performing these tests is shown in Figure 72 and discussed in subsection 6.1. Since these tests were conducted in conjunction with the optimum depth of cut (cf. subsection 8.2.2) and cutting force (cf. subsection 9.1) tests, the same end mills and test blocks used in those investigations were also used in this study. However, to show the effect that flute length has on cutter deflection, some additional tests were performed with 4-inch flute length, 1.25-inch diameter cutters.

After a pass had been made across one of the 12-inch test blocks (see Figure 72) in the above referenced tests, the cutter was brought back to the end of the test block and allowed to dwell in the cut until it reached an undeflected position. The end mill was then worked back and forth a fraction of an inch to produce a small, undeflected flat on the machined surface. Cutter deflection was then determined by measuring the height of the resulting step with a depth gage micrometer. The deflection measurements were made at the bottom of the axial depth of cut and were, therefore, representative of maximum cutter deflections.

As before, these tests were performed with relatively sharp cutters, using peripheral milling in the climb mode.

### 9.3.2 Cutter Deflection Measurements

The cutter deflection measurements obtained with the above described procedure are presented in Figures 129 through 133. The curve fit in these plots, while not as good as before, was adequate for the most part. A notable exception to that observation is shown in Figure 130 for the case of cutting speed versus cutter deflection. In that plot, no definite trend was established. However, when an extrapolated value was obtained for a cutting speed of 3,600 feet/minute and a 0.0025 inch/tooth feed rate with the formula in Figure 129, the curve in Figure 130 took on a zero slope-lock, as shown. If that procedure can be accepted, then it can be concluded that cutting speed has little effect on cutter deflection over the range tested. It is believed that much of the scatter shown in Figure 130 can be attributed to vibrations induced at resonant frequencies.

As mentioned, the effect of feed rates on cutter deflection are given in Figure 129 for Al-6061-T651, and the effect of cutting speeds on cutter deflection are indicated in Figure 130 for the same material. The effect of depths of cut on cutter deflection are presented in Figure 131 for Al-6061-T651, Figure 132 for Al-7075-T691, and Figure 133 for Al-A356-T6. The formulas developed from and superimposed on those plots were established statistically with linear regression.

### 9.3.3 General Observations on Cutter Deflections

While no direct comparison can be made, it does not appear from these data that high cutting speeds have any detrimental effect on cutter deflection. Cutter deflections of 0.006 inch and 0.008 inch are common at conventional cutting speeds.

Cutter deflection increases significantly as flute lengths are increased. Increasing the flute length of a 1.25-inch diameter end mill from 2.0 inches to 4.0 inches can increase cutter deflections as much as fourfold.

Cutter deflection was observed to be quite sensitive to feed rate changes. As shown in Figure 129, cutter deflection increased or decreased almost identically with feed rate.

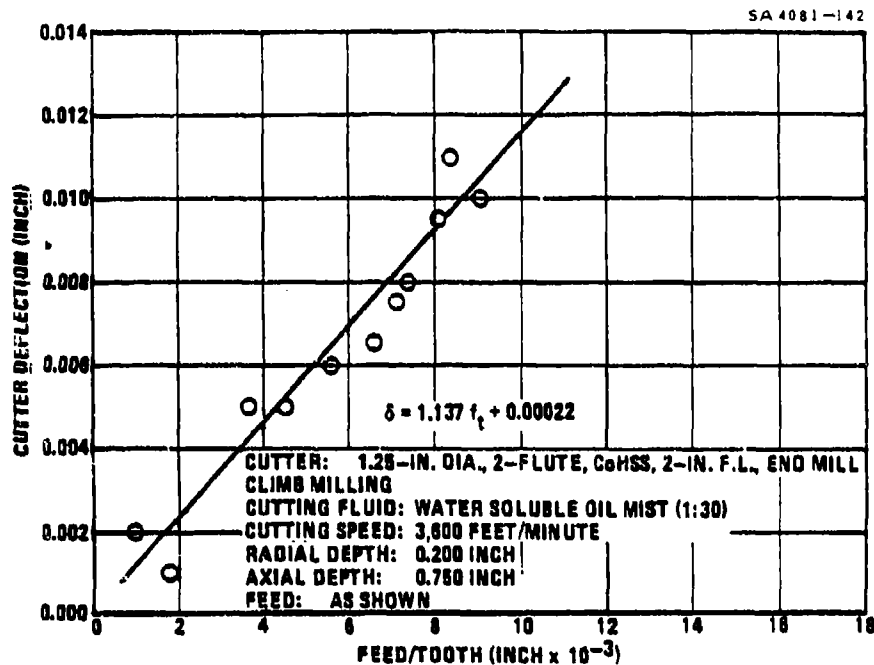


Figure 129. Effect of Feed Rate on Cutter Deflection for 6061-T651 Aluminum

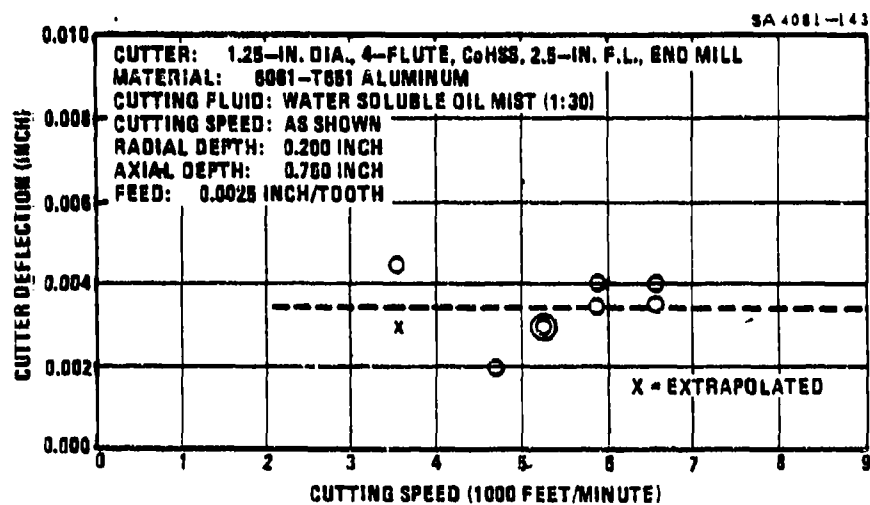


Figure 130. Effect of Cutting Speed on Cutter Deflection for 6061-T651 Aluminum

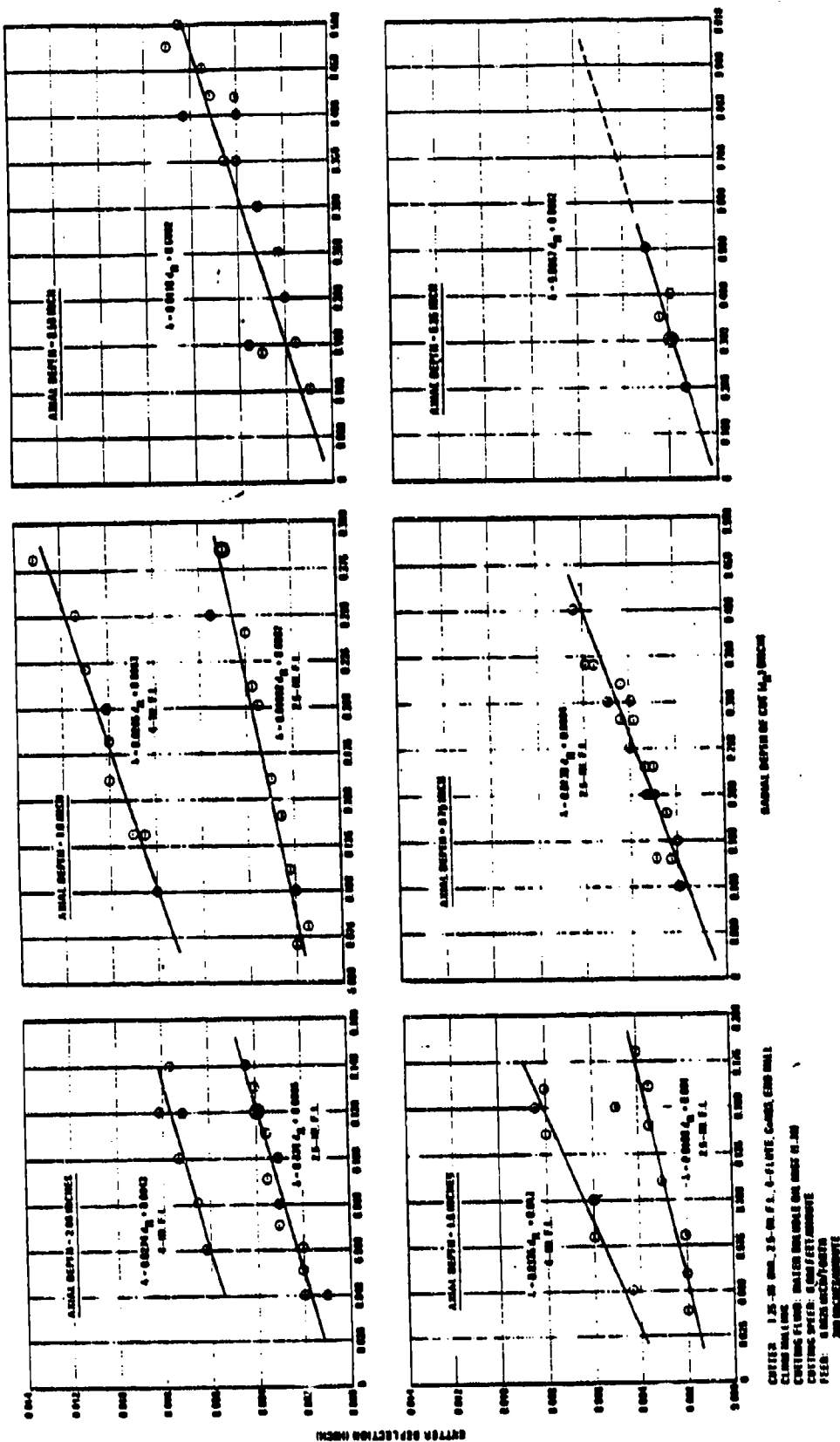


Figure 131. Effect of Depth of Cut on Cutter Deflection for 6061-T651 Aluminum

CUTTER: 1.25-IN DIA. 6-FLUTE 24-DEG. CLANK, END MILL  
 CUTTING SPEED: 1500 FEET PER MINUTE  
 FEED: 0.008 FEET PER MINUTE  
 CLANK AND LANE

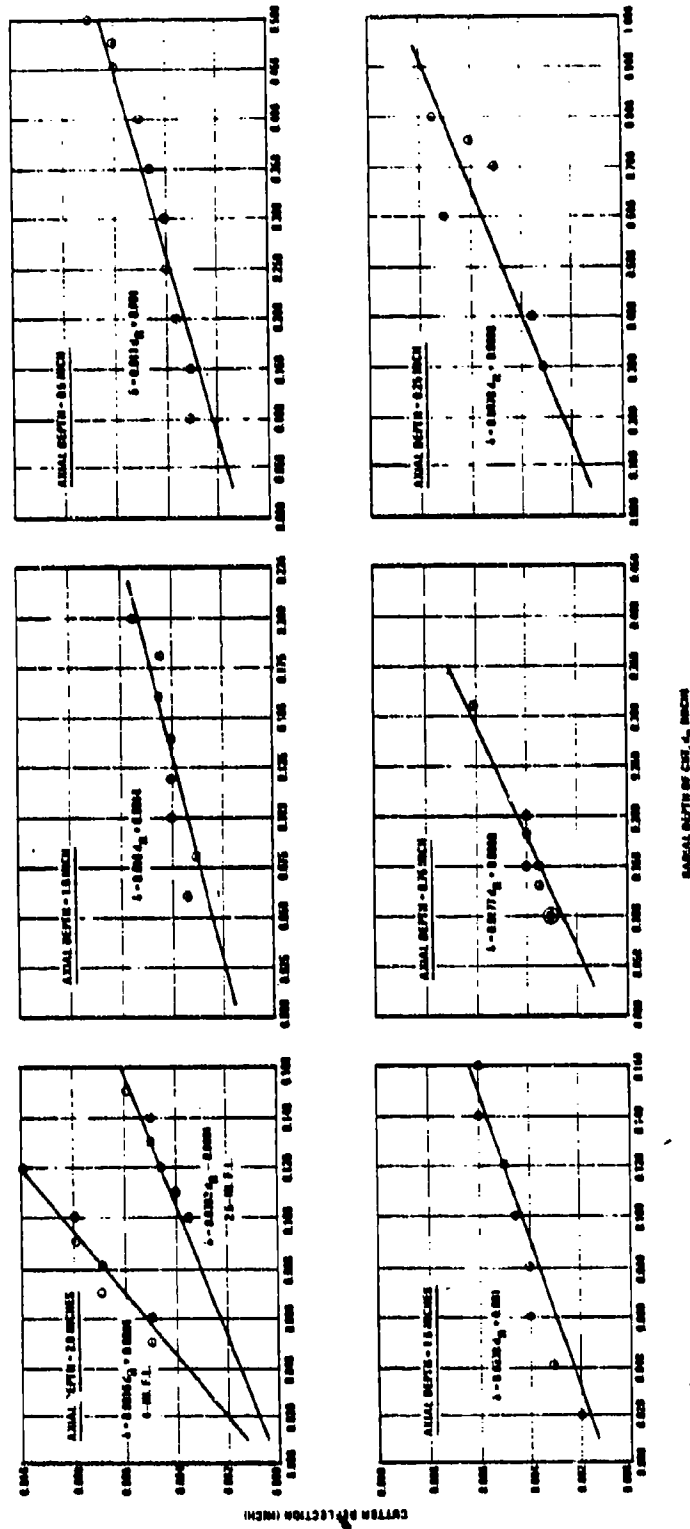


Figure 132. Effect of Depths of Cut on Cutter Deflection for Al-7075-T651 Aluminum

CUTTER: 1.75-IN. DIA., 3-FLUTE, 2-IN. F.L., CARBIDE, END MILL  
 CUTTING FLUID: WATER SOLUBLE OIL MIST (1:30)  
 CUTTING SPEED: 9,270 FEET/MINUTE  
 FEED: 0.0033 INCH/TOOTH  
 200 INCH/MINUTE  
 CLIMB MILLING

SA 4081-1-46

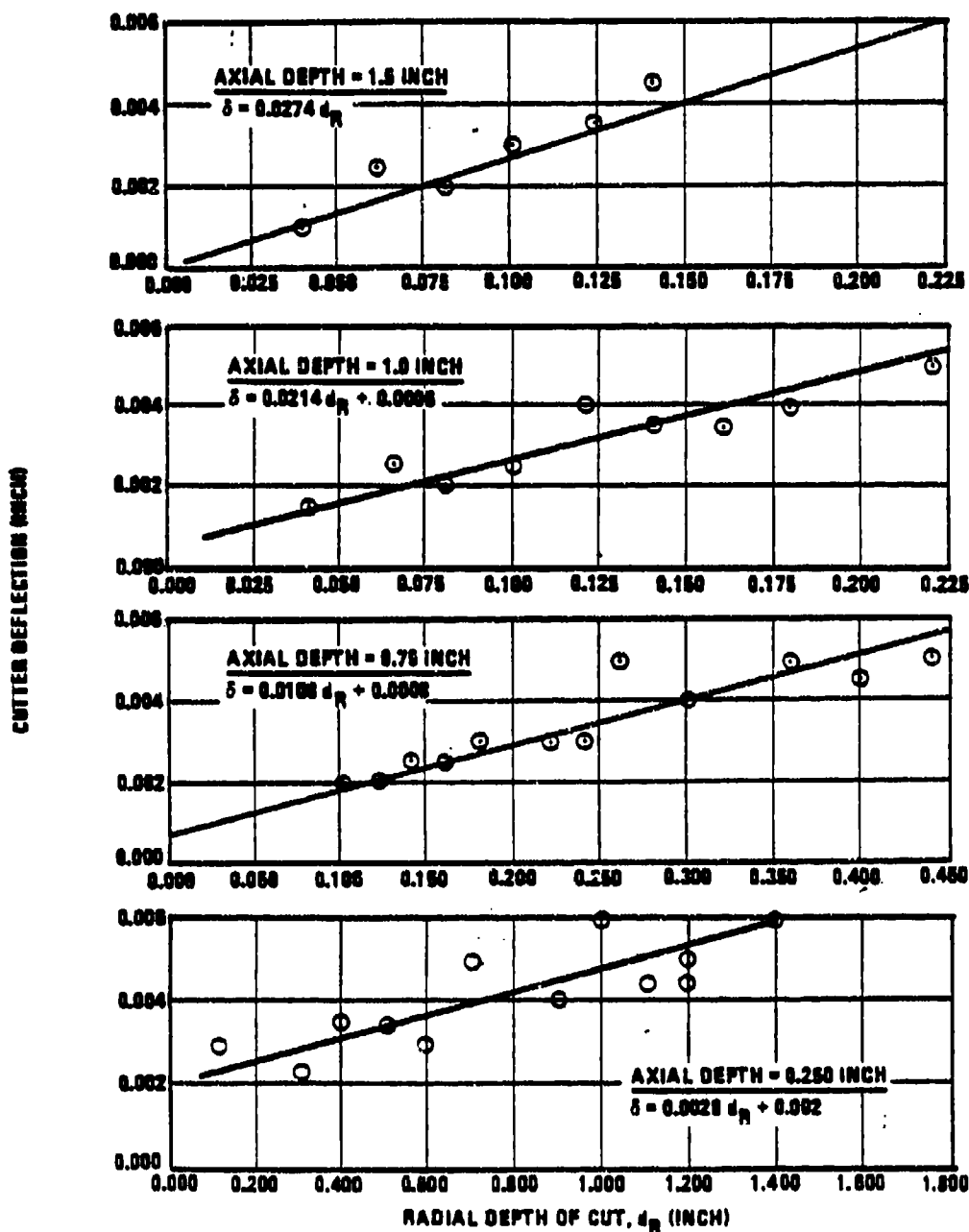


Figure 133. Effect of Depths of Cut on Cutter Deflection for Al-A388-T6 Aluminum

#### 9.4 Cutter Pullout

In an end milling operation, a cutter, by design, will try to pull out of its toolholder. If unable to do that, the cutter will try to pull the toolholder out of the spindle. If unable to do that, the cutter will try to pull the spindle out of its housing. The magnitude of the pull appears to increase specifically with feed rates, cut depths, cutter helix angles and, to some extent, cutting speed or, in general, with machine loads. If the load becomes high enough, something has to give. Generally, it will be nothing more than the axial depth of cut increasing, rendering the part out of tolerance. In extreme cases, a part may be sucked into the cutter and ruined; or the spindle shaft or bearings may become damaged. While such results occur for conventional milling as well as high speed milling, these are more critical for the latter. For instance, if a spindle is turning at 20,000 revolutions/minute and a heavy pull is induced on its shaft, there will be a tendency to pull the bearings apart. Even if the bearings are only stretched rather than pulled apart, excessive heat may be generated at that speed which, if not the applied load, may warp the shaft, bearing races, et cetera, rendering the spindle out-of-balance and, essentially, inoperable. Such a result occurred twice during this program. Any future reoccurrences of this result could, probably, best be alleviated by redesigning the spindle; e.g., adding thrust or hydraulic preload bearings at the forward journal. However, to help alleviate reoccurrences of the above result for now and to help maintain dimensional tolerances, this test program was initiated to establish the effect of cut geometry on cutter pullout.

In this section, results showing the effect of feed rate and radial depths on axial depth growth (cutter pullout) are presented for Al-6061-T651.

##### 9.4.1 Test Procedure

The experimental setup used in performing these tests is shown in Figure 72. These tests were performed simultaneously with the cutting force tests (cf. subsection 9.1) and cutter deflection tests (cf. subsection 9.3). Consequently, the same end mills, test blocks and parameters used in those tests were also used in this investigation. Likewise, relatively sharp cutters were used to make peripheral end milling cuts in the climb mode.

After a pass was made across one of the 12-inch test blocks shown in Figure 72, the true axial depth of cut was determined by measurement with a depth gage micrometer. The difference between that measurement and the original setting was the measure of cutter pullout.

Cutter Pullout Measurements

The cutter pullout measurements obtained with the above described procedure are plotted in Figure 134. The curve fit for the two plots was considered to be satisfactory.

As shown in Figure 134(a), cutter pullout appeared to peak at a machine load of approximately 75% when cut depths were varied. In contrast, the feed rate curve in Figure 134(b) did not exhibit any peaking tendency; and its slope indicated that feed rate has a more pronounced effect on cutter pullout than radial depth of cut.

The results of Figure 134(b) also imply that optimum feed rates (cf. Figure 105) would overload the existing Omnimil high speed spindle (cf. Figure 62) and would tend to pull its bearings apart. Based on those observations, it was concluded that more powerful and rugged spindle motors were needed for high speed machining.

As mentioned in subsection 8.5, faster spindle speeds will not be needed until faster table speeds are provided. However, faster table speeds may not be usable until more powerful and rugged spindle motors are provided. For these reasons, it was further concluded that future developmental efforts for high speed machining equipment should be accomplished in the following order of priority:

- a. More powerful and rugged spindle motors
- b. Faster table speeds
- c. Faster spindle speeds.

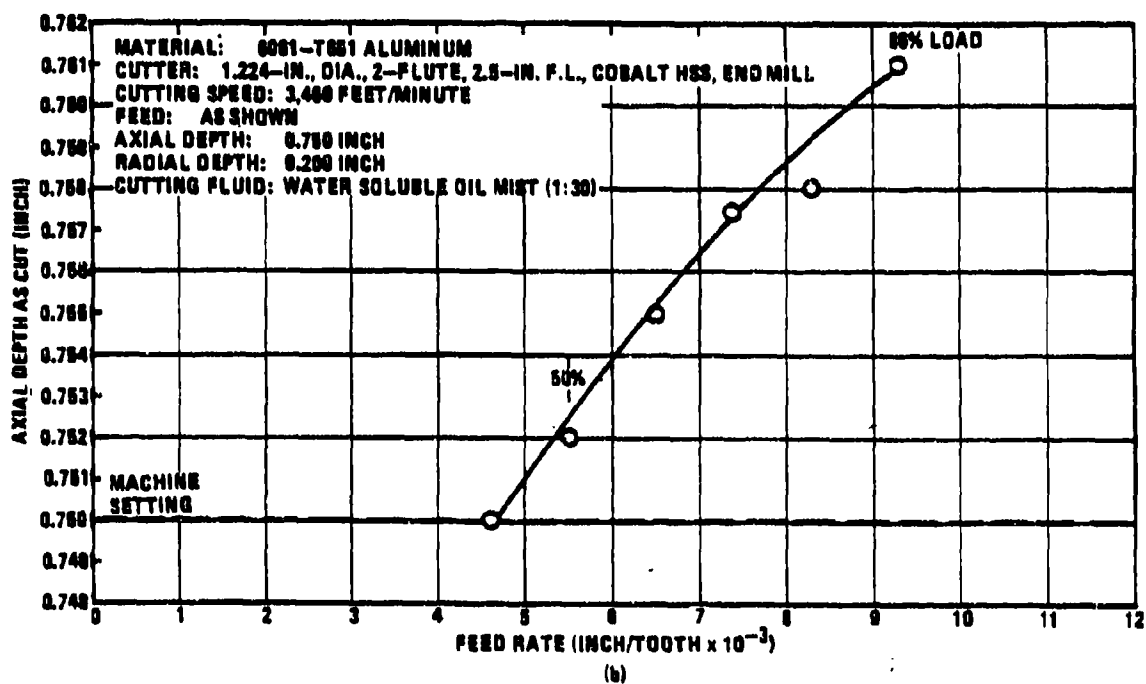
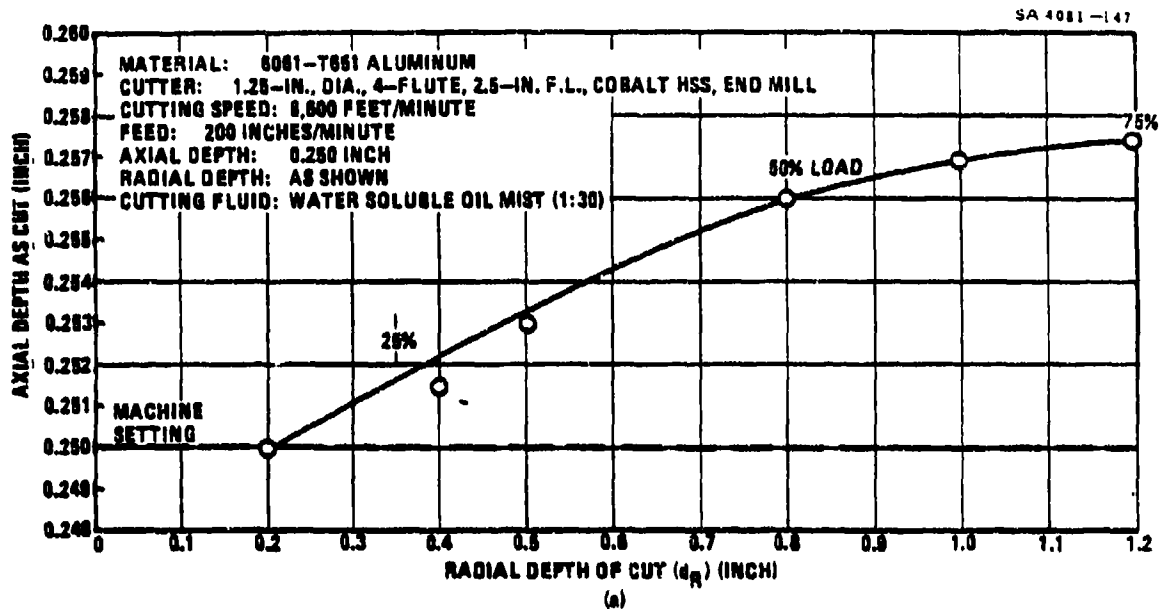


Figure 134. Typical Examples Showing the Effect of Cut Geometry on Cutter or Spindle Pull-out and Resulting Axial Depth of Cut Errors

## 10.0 TEST RESULTS - SURFACE FINISH AND RESIDUAL STRESS

### 10.1 Introduction

Before using any new manufacturing process, it is usually necessary to determine what effect, if any, it has on part quality. In the preceding section, it was shown that cutter deflection on aluminum was no worse at high cutting speeds than it was at conventional cutting speeds. From that result and subsequent machining studies on Guidance and Control shells (cf. Figure 63), it was concluded that high speed machining was not detrimental to machining tolerances. That observation, coupled with ones which showed that aluminum parts stayed cooler and were subjected to lower cutter forces during high speed machining operations than conventional machining operations, signified that part accuracy may be enhanced by high speed machining. In this section, the effect that high speed machining has on surface finish and residual stress generation was investigated to further evaluate the process' effect on part quality.

### 10.2 Surface Finish

Practically every machined part is given a maximum permissible surface finish or roughness value. This is done to improve the wear, performance or appearance of the part. Along with dimensional tolerance, this important property determines what the machining parameters will be for finishing cuts. Generally, surface finishes will improve with cutting speed increases or feed rate reductions. For that reason, it was expected that high speed machining would be especially beneficial for surface finishes, and tests were performed to substantiate that conclusion.

In this section, results showing the effect of cutting speed and feed rate on surface finish are presented for Al-7075-T651, Al-6061-T651, and Al-A356-T6.

#### 10.2.1 Test Procedure

The equipment used to perform these tests is shown in Figure 72. That setup was modified for the surface finish tests in that the dynamometer and test block were replaced with the vise shown on top of the angle block. The angle block was then rotated 90 degrees so that the vise would be parallel (facing the reader) to the cutter axis. After clamping a 2.0- by 2.0- by 2.0-inch test block in the vise and squaring it, a conventional milling cut was made, using a prescribed cutting speed and feed rate, a 0.050-inch radial depth and a 2.0-inch axial depth of cut. After a series of peripheral milling operations had been performed in that manner, the blocks (see Figure 135) were taken to inspection, where, surface finish measurements were made with a Taylor-Hobson, Surtronic 2, profilometer.

SA 4881-149

N-16697

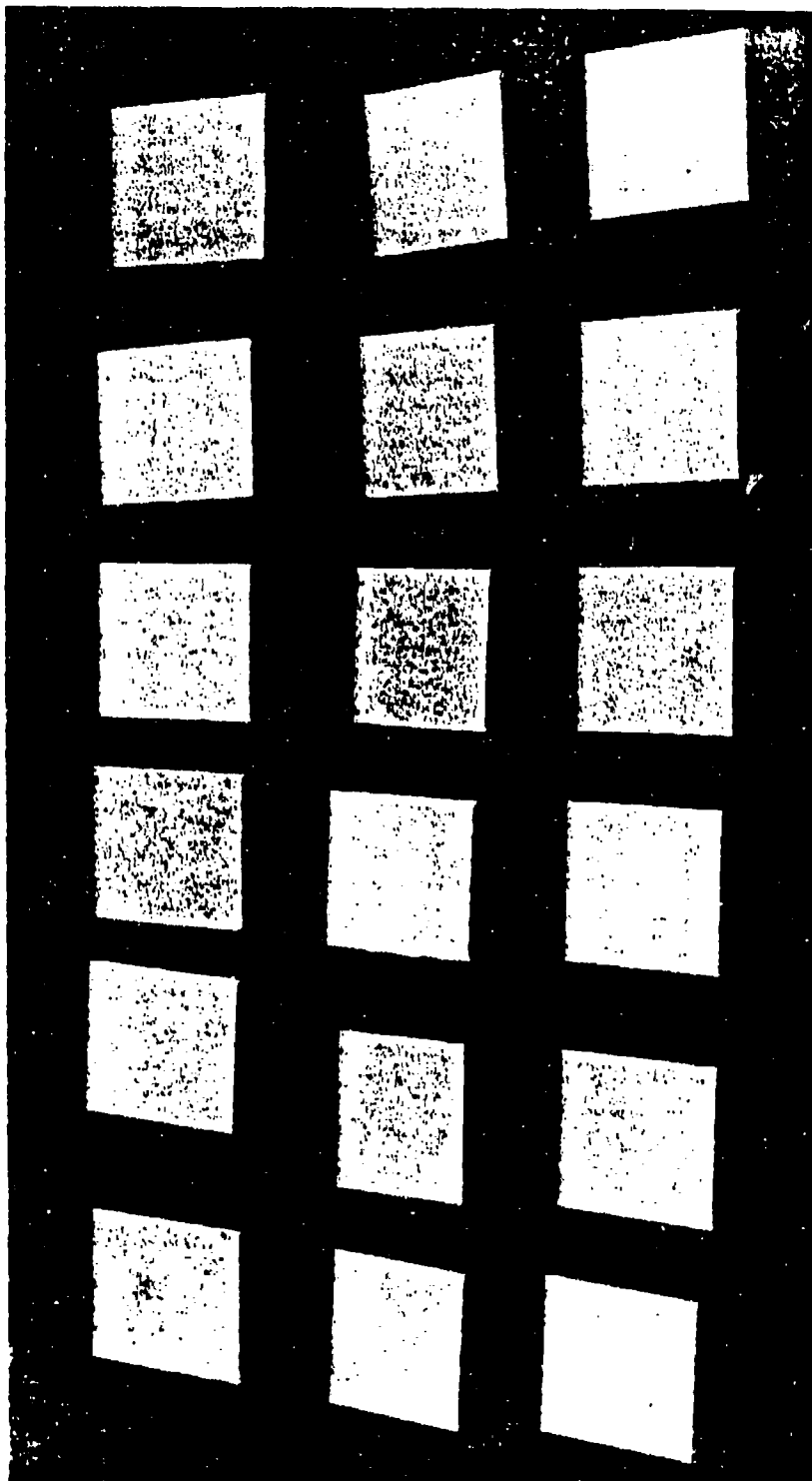


Figure 135. Surface Finish Test Blocks

The cutter used in these tests was a 2.0-inch diameter, 2-flute, 2.5-inch flute length, 4-percent cobalt, high speed steel end mill. That size cutter was used so that cutting speeds to 10,000 feet/minute could be obtained.

To obtain the range of cutting speeds desired, tests had to be run on two Omnimils. A standard Omnimil was used to obtain cutting speeds under 2,000 feet/minute, and the modified Omnimil (cf. Figure 62) was used to obtain cutting speeds over 5,000 feet/minute. The cutting speed gap between 2,000 and 5,600 feet/minute could not be filled with comparable equipment.

Feed rate selections were limited to a maximum of 0.005 inch/tooth on the Omnimil. Additional tests were run at a feed rate of 0.0025 inch/tooth for comparative purposes.

#### 10.2.2 Surface Finish Measurements

Using the above described procedures, surface finishes for all three alloys were measured over a wide range of cutting speeds for two different feed rates. Measurements were made both perpendicular and parallel to the direction of lay (see Figure 136). The results obtained are presented in Figures 137 through 139. The numerals opposite some of the data points in those figures indicate the number of times that test result was obtained. The curve fit was not very good in the plots; therefore, scatter bands were drawn instead of curves for most of the cases.

SA 4081-150  
Courtesy of METCUT

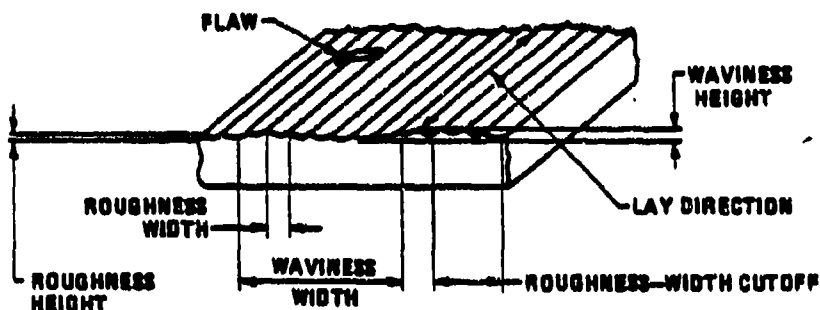


Figure 138. Surface Finish Nomenclature

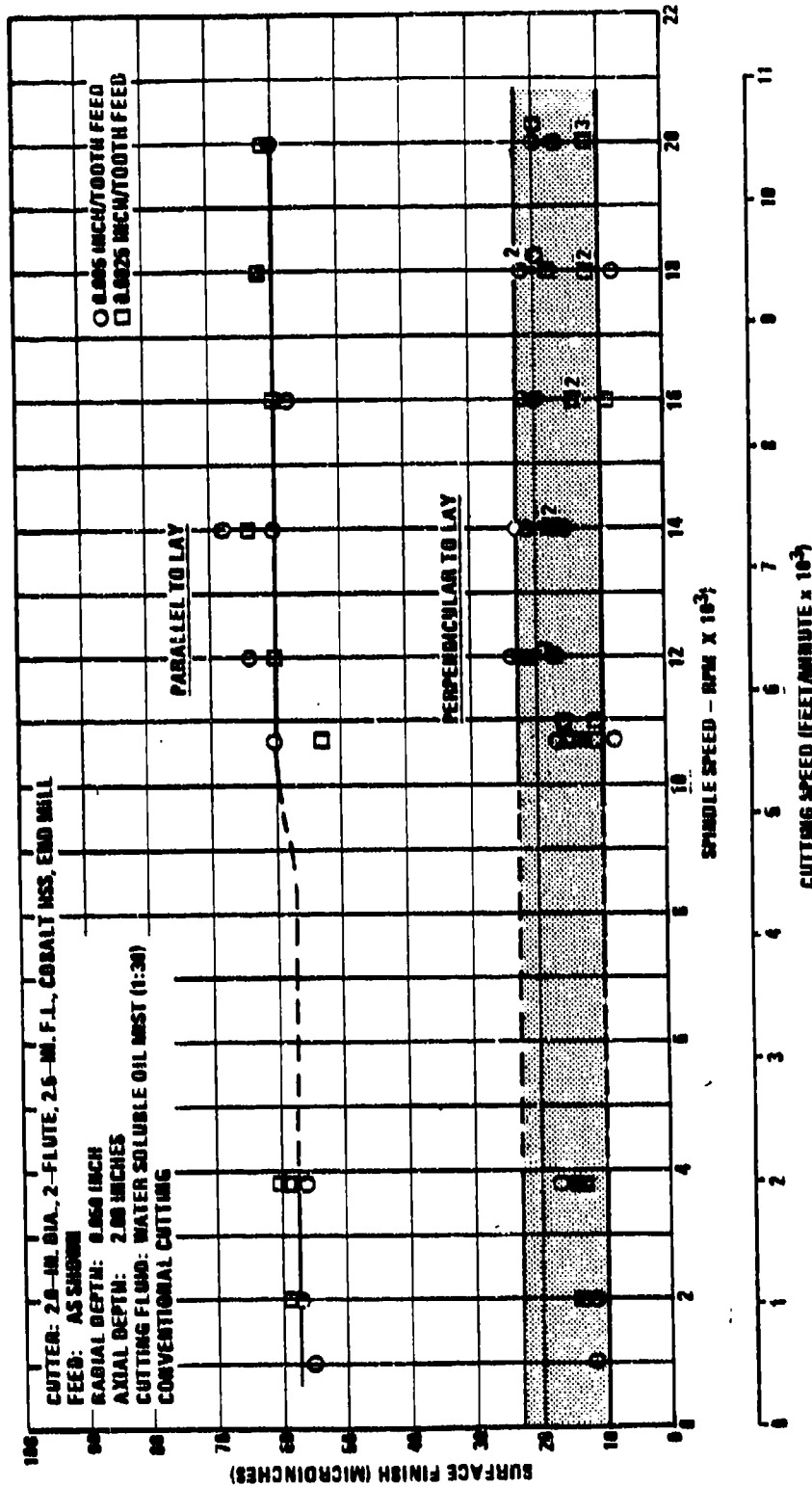


Figure 137. Effect of Cutting Velocity on Surface Finish for 7075-T651 Aluminum

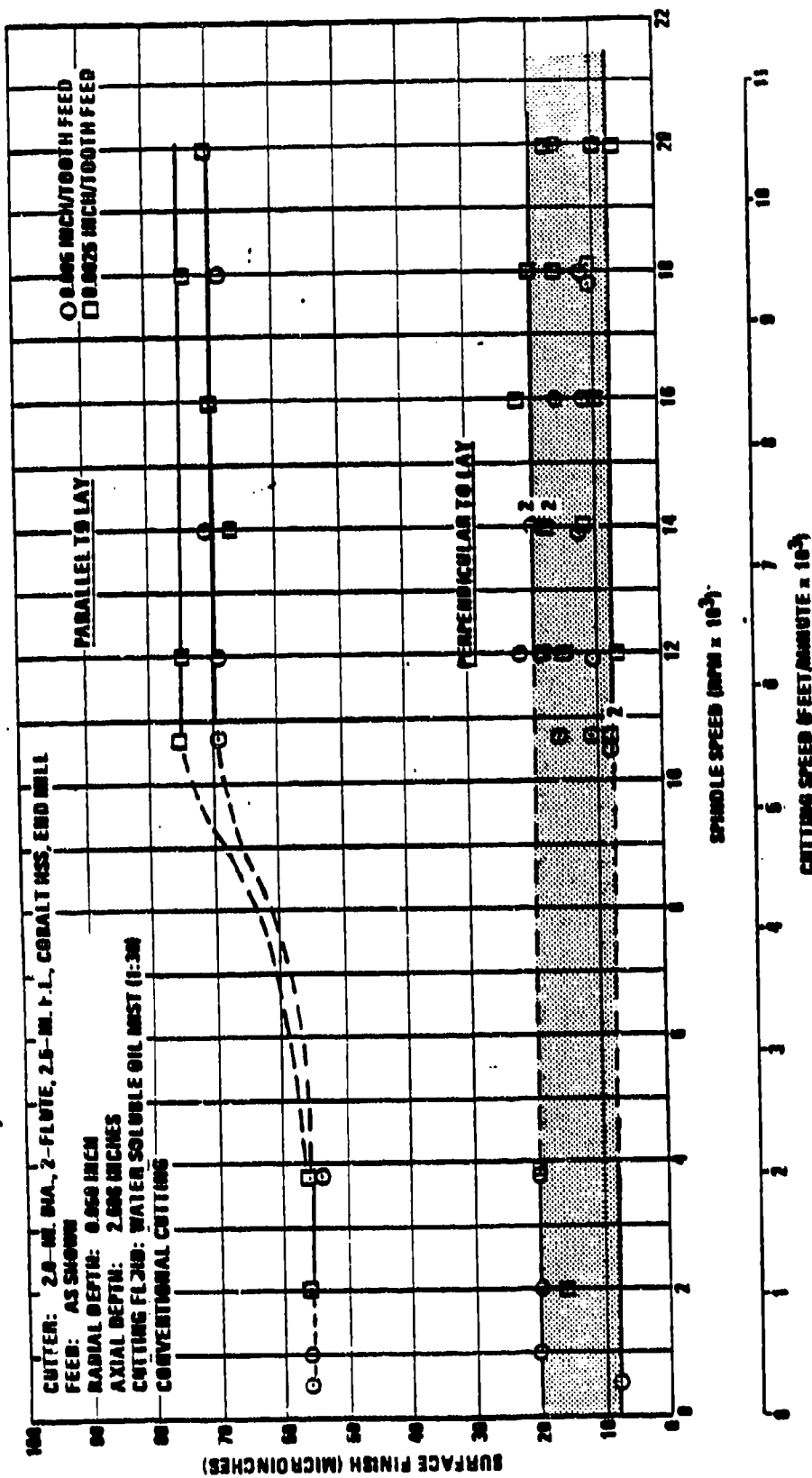


Figure 130. Effect of Cutting Velocity on Surface Finish for 0001-T001 Aluminum

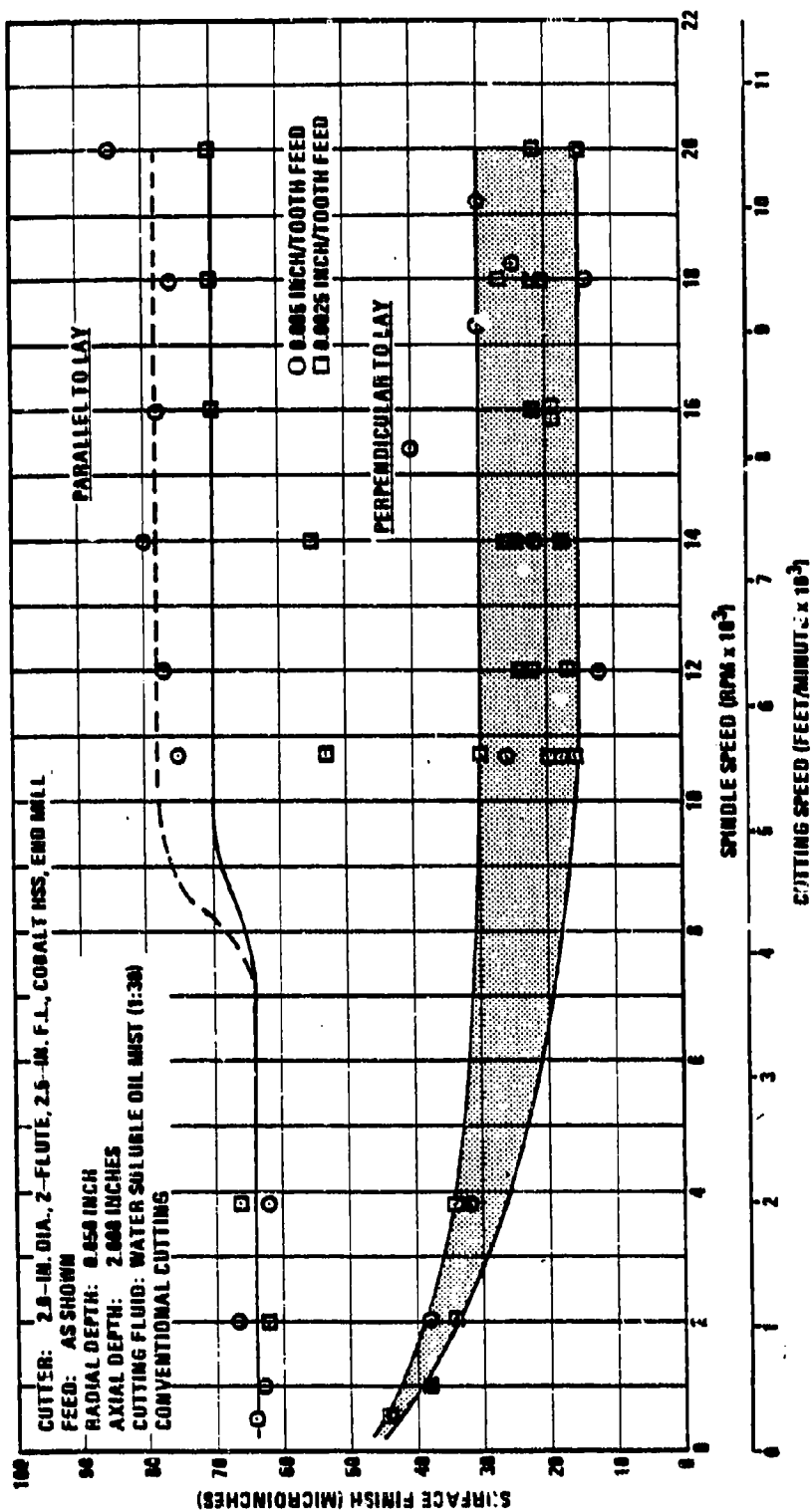


Figure 139. Effect of Cutting Velocity on Surface Finish for A356-T6 Aluminum

### 10.2.3 General Observations on Surface Finish Measurements

All of the surface finish values shown in Figures 137 through 139 are good; and some were much better than expected. In particular, the surface finishes obtained at low cutting speeds in the perpendicular-to-lay direction far exceeded expectations. Only those shown in Figure 139 came near to following an expected trend. All of the other surface finishes produced at conventional speeds were as good as those produced at high speeds. No good explanation can be offered for such an uncharacteristic result at this time.

Another unusual result concerns itself with the direction of measurement. For instance, it appears from Figure 136 that a rougher surface reading would be obtained in a direction perpendicular to the lay than parallel to it. However, the opposite result was found for all cases in this investigation. Again, no good explanation can be offered for such an unexpected result at this time.

Overall, a feed rate of 0.0025 inch/tooth produced better surface finishes than a 0.005 inch/tooth feed rate. However, the margin of superiority was hardly discernible and unworthy of any production sacrifices. For now, a feed rate of 0.005 inch/tooth can be recommended for finishing cuts on aluminum. That figure will probably be raised when faster table speeds with which to investigate it become available.

This investigation did not do what was expected of it. That is, it did not prove conclusively that high speed machining would improve surface finishes. However, it did prove that high speed machining was not detrimental to and could produce outstanding surface finishes.

### 10.3 Residual Stress

Whenever a machining cut is made, a surface layer is produced on the workpiece that is different from the parent metal. This surface layer may be shallow or deep, depending upon the severity or abusiveness of the machining operation. Such a surface layer can be seen if a photomicrograph is made of it. In the photomicrograph, the surface layer appears to consist of several compressed rows of the metal's grains or crystals, indicating that plastic deformation has occurred in the layer. As a result of the plastic deformation, the layer is more highly stressed than the parent metal; and since the stresses were left by the machining operation, these are called residual stresses.

Residual stresses can be beneficial or detrimental. A small amount of compressive stress can increase the fatigue strength of a component, and parts are frequently shot peened or cold worked for that purpose. If overdone, however, residual stresses can warp or distort a workpiece and detrimentally affect its stress corrosion, fatigue strength and other mechanical or physical properties.

Abusive machining operations are generally the type which produce the most plastic deformation and heat and, thus, the greatest change in the surface layer. Consequently, abusive machining is the type which is most likely to generate excessive residual stresses and the type to be avoided. This can best be done by using more gentle machining practices.

It is evident from the above discussion that the machining method or parameters selected to produce a component can have an important effect on its quality. High speed machining could easily have been considered abusive; therefore, this study was initiated to determine its effect on residual stress generation.

In this section, results showing the effect of cutting speed on residual stress are presented for Al-7075-T651, Al-6061-T651, and Al-A356-T6.

#### 10.3.1 Test Procedure

The same setup used for the surface finish tests (see subsection 10.2.1) was used to machine specimens for the residual stress tests. Even the same 2.0-inch diameter, 2-flute, 2.5-inch flute length, 4-percent cobalt, high speed steel end mill was used.

The test blocks for this study measured 1.0-inch thick by 2.0 inches square. In all, 24 test blocks from three different aluminum alloys were machined at four different cutting speeds. From these, two residual stress test specimens were produced for each alloy and cutting speed combination. For clarity, the combinations and number of test specimens fabricated for each are given as follows:

<u>Cutting Speed</u> <u>(ft/min)</u>	<u>Number of Test Specimens</u>		
	<u>Al-7075-T651</u>	<u>Al-6061-T651</u>	<u>Al-A356-T6</u>
1,000	2	2	2
4,000	2	2	2
7,000	2	2	2
10,000	2	2	2

A test specimen was prepared by first clamping it in the vise and squaring it, as before. Three conventional milling cuts were then made across the 2.0-inch square face of the specimen at a radial depth of 0.050 inch, an axial depth of 2.0 inches, a feed rate of 0.005 inch/tooth, and at one of the prescribed cutting speeds. Upon completing the milling cuts, the specimen was carefully removed from the vise so as not to scratch the milled surface. The specimen was then cleansed and protectively covered with masking tape.

All 24 of the residual stress test specimens were prepared in the above manner. These were subsequently packaged and delivered to Metcut Research Associates, Incorporated. Metcut had been subcontracted to measure the residual stresses in the test specimens with techniques it had perfected.

The method used by Metcut to measure residual stresses utilized an x-ray diffraction technique recommended by the Society of Automotive Engineers (SAE). The specific technique employed differed from the more common SAE technique in two respects. First, the diffraction peak used for stress measurement was located using a five-point parabolic regression procedure rather than the three-point algebraic procedure more commonly used. Second, the intensities measured at each of the five points were corrected for the background intensity. These modifications improved the repeatability of stress measurements. Except for these modifications, the technique used was identical to that described in the SAE publication, "Residual Stress Measurement by X-ray Diffraction", SAE J784a. Details of the technique and diffractometer fixturing are outlined below:

Diffraction peak: (331)  
Radiation: Cr  $K_\alpha$   
Incident beam divergence: 3.0 degrees  
Detection slit: 0.5 and 0.7 degrees  
Counts per point: 40,000, 100,000 and 200,000  
Beam size: 0.25 x 0.4 inch  
 $E/(1+\nu)$ :  $8.83 \times 10^6$  psi

The value of the elastic property  $E/(1+\nu)$  in the direction normal to the (331) planes was determined previously by calibration for 7075 aluminum alloy. The determination of the elastic properties for the A356 and 6061 alloys was beyond the scope of this project.

Residual stress measurements were made at the surface and at four levels below the surface on one of each kind of sample. The exact depths below the surface at which measurements were made are given with the stress data in Table VII. Material was removed for the subsurface measurements by electropolishing the measurement area in a nitric acid ethanol solution to minimize the effects of material removal upon the existing subsurface stresses. The determinations were made at a point near the center of the milled face of the block in a direction parallel to the milling lay.

#### 10.3.2 Residual Stress Measurements

Using the above described procedures, residual stress measurements were made for all three alloys at four different cutting speeds. The results are given in Table VII; where each sample was coded with a sample number specifying the sample's alloy and the milling speed used to finish the sample. Compressive stresses are reported as negative values. All data were corrected for the effect of the penetration of the radiation into the subsurface stress gradient and for stress relaxation caused by layer removal, using a digital computer.

TABLE VII - RESIDUAL STRESS MEASUREMENTS

Sample No.	Depth (in.)	Residual Stress (ksi)	Sample No.	Depth (in.)	Residual Stress ( $\times 10^3$ psi)
A-356-1K	Surface	23.2	A-356-4K	Surface	26.3
	0.0008	-17.0		0.0008	3.4
	0.0015	0.9		0.0015	1.0
	0.0050	11.7		0.0031	16.7
	0.0064	5.3		0.0070	6.5
A-356-7K	Surface	7.6	A-356-10K	Surface	17.3
	0.0008	-1.9		0.0008	9.1
	0.0015	-3.4		0.0017	-3.5
	0.0032	-5.4		0.0035	-3.9
	0.0075	0.4		0.0062	1.0
6061-1K	Surface	10.4	6061-4K	Surface	15.4
	0.0009	10.4		0.0009	-0.5
	0.0018	1.0		0.0019	8.6
	0.0030	-1.9		0.0032	7.2
	0.0065	4.7		0.0060	-7.2
6061-7K	Surface	58.4	6061-10K	Surface	25.3
	0.0013	-18.8		0.0008	20.5
	0.0015	-19.6		0.0014	7.1
	0.0033	-8.3		0.0031	7.7
	0.0072	11.7		0.0068	-0.6
7075-1K	Surface	20.4	7075-4K	Surface	38.0
	0.0008	30.1		0.0009	-16.6
	0.0015	19.7		0.0015	0.4
	0.0030	-4.4		0.0035	5.6
	0.0076	-1.5		0.0064	-1.9
7075-7K	Surface	49.3	7075-10K	Surface	18.7
	0.0009	-5.6		0.0008	-3.1
	0.0015	-10.7		0.0015	5.0
	0.0037	+1.1		0.0031	-4.0
	0.0070	-2.6		0.0063	-3.0

The data in Table VII was plotted in graphical form to portray the effect of subsurface depth on residual stresses. The results obtained for Al-7075-T651, Al-6061-T651, and Al-A356-T6 are presented in Figures 140 through 142, respectively.

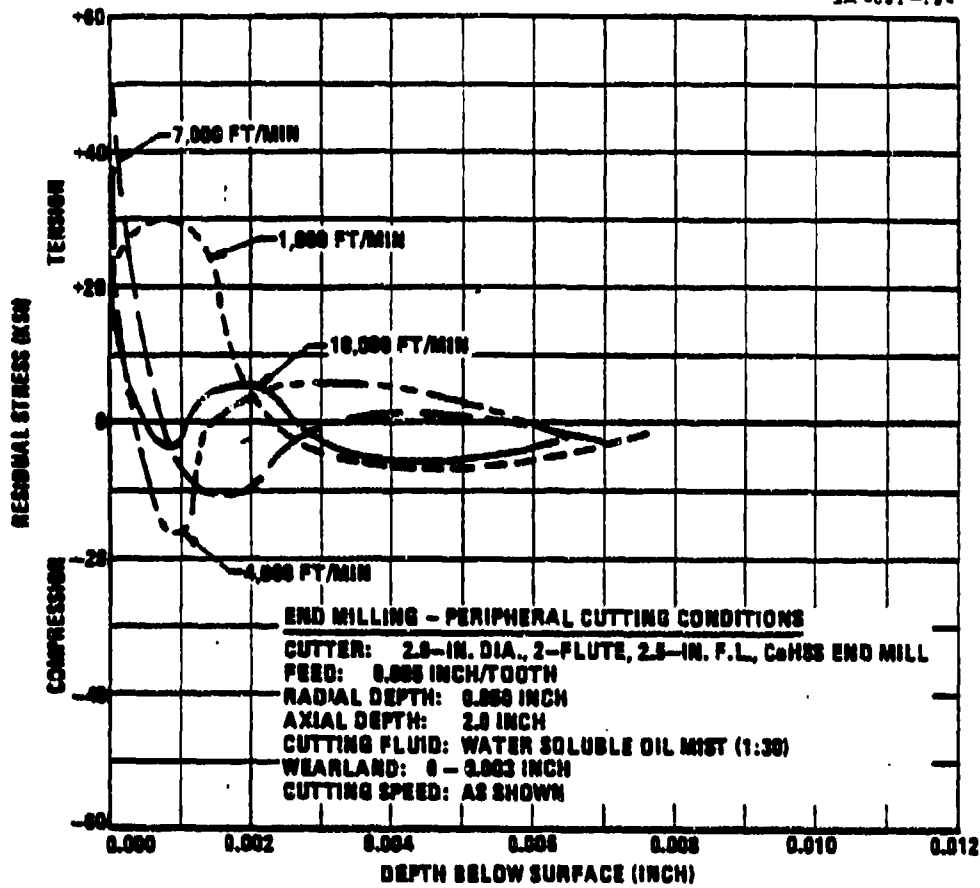


Figure 140. Residual Surface Stress Profiles in Al-7075-T651 Produced by End Milling

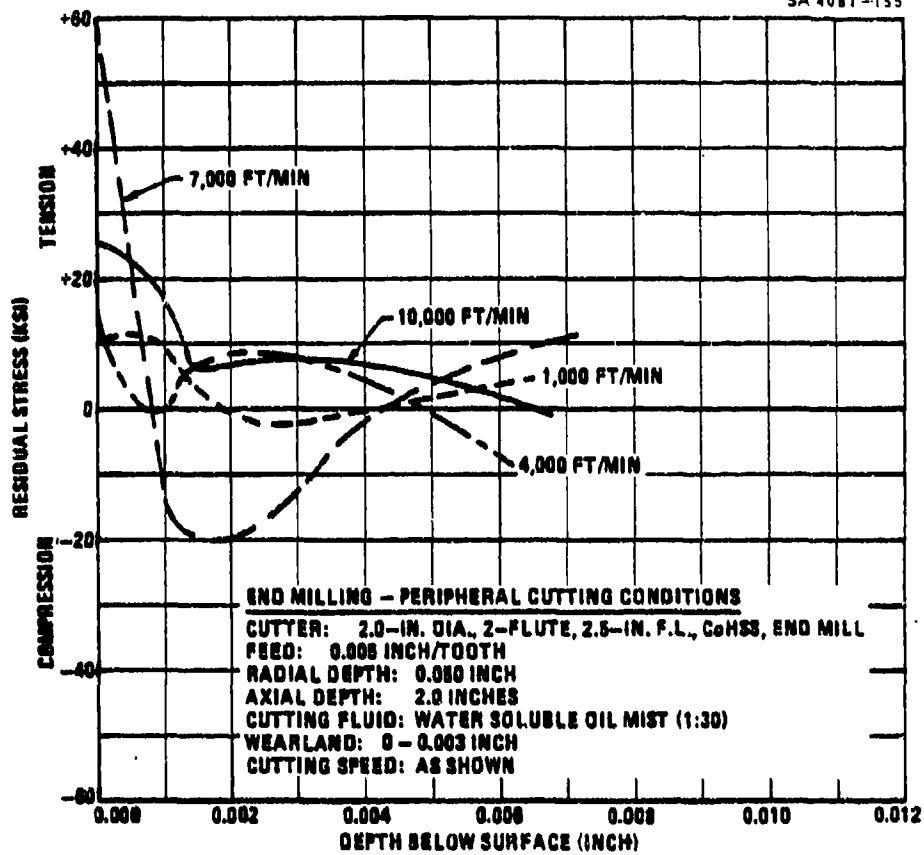


Figure 141. Residual Surface Stress Profiles in Al-6061-T681 Produced by End Milling

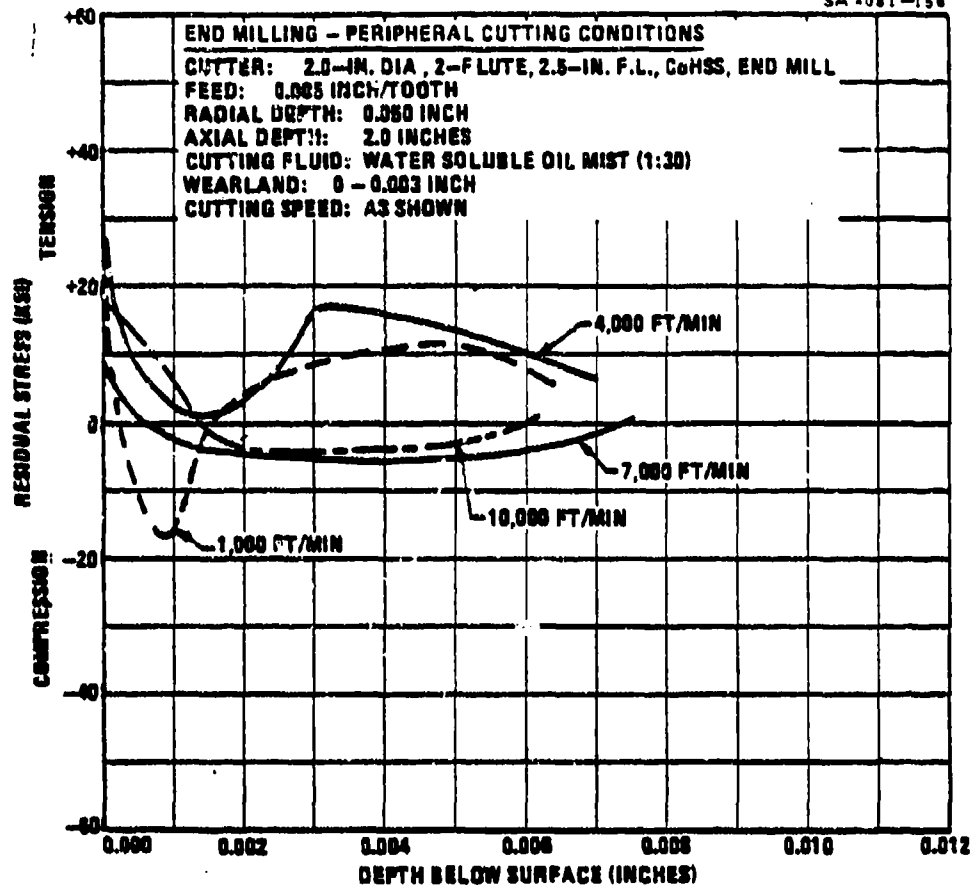


Figure 142. Residual Surface Stress Profiles in Al-A356-T6 Produced by End Milling

### 10.3.3 General Observations on Residual Stress Measurements

Ideally, the residual stress at the surface of a component should be slightly compressive so as to enhance its fatigue strength. Tensile stresses on a surface are thought to lower stress corrosion resistance and are, therefore, undesirable, especially if such stresses are high. An examination of Figures 140 through 142 revealed that undesirable condition occurred for every alloy and cutting speed combination. Metcut remeasured sample number 6061-7K (see Figure 141) to investigate the possibility that location dependant variations in surface residual stresses may have contributed to the observed lack of correlation between the previously measured residual stresses and milling speed. Of five measurements made, three were consistent and two were inconsistent. Metcut concluded that the consistency of the overall results was an indication that the original results were accurate and were representative of the residual stresses induced by the milling procedure.

No trend was established in the test results. For example, a cutting speed of 7,000 feet/minute produced the best results for Al-A356-T6 and the worst results for Al-6061-T6 and Al-7075-T651. In contrast, a cutting speed of either 1,000 or 10,000 feet/minute yielded the best surface layer conditions on Al-7075-T651. From these and other comparisons, it was concluded that the absence of any consistency in the test results indicated that cutting speeds have little effect on residual stress generation.

## 11.0 COST AND PRODUCTION TIME ANALYSIS

### 11.1 Introduction

When making any changes in a process, it is important to make an analysis of cost and production time changes caused by the process change. The objective of this section was to perform a preliminary cost and production rate comparison between conventional machining and high speed machining. To assure that this comparison was performed in an unbiased manner, Matcut Research Associates, Incorporated was contracted to do the study.

### 11.2 Cost and Production Time Calculations

When dealing with a machining operation, there are three main contributors to cost and production time. These are the constant costs and times, feed cost and times, and tool costs and times. The *constant costs and times* are load-unload setup, cutter index and rapid traverse. By constant, it is meant that these terms are not cutting rate controlled. The *feeding costs and times* are those accrued while chips are being made. For this term, the cost and time is decreased by increasing the cutting rate. The *tool times and costs* are the penalties for wearing out a tool. The downtime for replacement of a dull tool and the tool purchase and resharpening costs are included in this term. The equations for *production time and cost* are shown in Table VIII.

### 11.3 Application

To compare high speed machining with conventional machining, Operations 50 and 60 on the Shell Guidance Set, part number 10162178-500EN (see Figure 63), were selected for analysis. Operation 50 is now a conventional turning operation that is performed on a Bullard, N/C, vertical turret lathe. In this operation, the top and bottom surface are faced, the top flange is bored, and the outside diameter is turned. Operation 60 is now a conventional milling, drilling and tapping operation that is performed on a Sundstrand, 5-axis, N/C, OM-3 Omimil. The production times and costs for these existing operations were compared to the production times and costs that would be realized by *replacing these two operations with one high speed milling operation.*

It should be noted, however, that a machine tool does not now exist which could handle this part on a production basis at ultra high cutting speeds. Although high speed spindles are available as an add-on for existing machine tools, the installation of one of these spindles renders the automatic tool changer inoperable. Extra shielding was required to contain the chips which came off the part at very high speeds. This extra shielding restricted the use of the existing pallet system for quick workpiece loading and unloading.

TABLE VIII - COST AND PRODUCTION TIME EQUATIONS

Constant time: $(t_1) = R/r + t_L + t_o/N_L + t_i$	Feeding time: $(t_2) = L/f_m$
*Tool time: $(t_3) = t_d/T_p$	Production time = $t_1 + t_2 + t_3$
Constant cost: $(C_1) = t_1 M$	Feeding cost: $(C_2) = t_2 M$
Tool cost: $(C_3) = t_3 M + C_s/T_p$	Total cost = $C_1 + C_2 + C_3$
Where:	
<p> <math>R</math> = Total rapid traverse distance for one tool on one part (in.).  <math>r</math> = Rapid traverse rate (in./min.).  <math>t_L</math> = Time to load and unload workpiece (min.).  <math>t_o</math> = Time to set up machine tool for operation (min.).  <math>N_L</math> = Number of workpieces in lot.  <math>t_i</math> = Time to index from one cutter type to another between operations (min.).  <math>L</math> = Length of travel of cutter at feed rate (in.).  <math>f_m</math> = Feed rate (in./min.).  <math>t_d</math> = Machine tool downtime to replace a dull tool (min.).  <math>T_p</math> = Tool life (number of parts).  <math>M</math> = Labor plus overhead (\$/min.).  <math>C_s</math> = Cost per sharp tool (\$).                 </p>	
<p>The value <math>C_s</math> is calculated using the appropriate terms from the following equation, depending on the type of tool:</p>	
$C_s = \frac{C_p}{(K_1 + 1)} + G t_s + \frac{G t_b}{K_2} + \frac{Z C_o}{K_3} + C_w + G t_p$	
Where:	
<p> <math>C_p</math> = Purchase cost of tool or cutter (\$/cutter).  <math>K_1</math> = Number of times cutter is resharpened before being discarded.  <math>G</math> = Labor and overhead in tool reconditioning department (\$/min.).  <math>t_b</math> = Time to rebraze cutter teeth or reset blades (min.).  <math>K_2</math> = Number of times milling cutter is resharpened before inserts or blades are rebrazed or reset.  <math>Z</math> = Number of teeth in milling cutter.  <math>C_o</math> = Cost of each insert or inserted blade (\$/blade).  <math>K_3</math> = Number of times blades (or inserts) are resharpened (or indexed) before blades (or inserts) are discarded.  <math>C_w</math> = Cost of grinding wheel for resharpening tool or cutter (\$/cutter).  <math>t_p</math> = Time to preset tools away from machine (in tool room) (min.).  <math>t_s</math> = Time to resharpen a tool.                 </p>	

\*This factor is zero if a tool does not require changing for an entire lot.

Using the equations in Table VIII, lists of individual operation times and costs were developed. A breakdown of data for the conventional method of producing one part in Operation 50 is presented in Table IX. For comparison, a breakdown of data for the high speed milling method of producing one part in Operation 50 is shown in Table X.

The analysis of the conventional production method for Operation 50 revealed that a standard setup time of 2.5 hours is prorated over a typical lot size of 100 parts. Since the lathe cannot be running while one part is being unloaded and another loaded, a load-unload time of ten minutes appears as a constant time. When replacing this turning operation with the high speed milling operation, no extra setup is required since one setup on the mill will suffice for both Operations 50 and 60. The elimination of the turning setup is reflected in the zero constant time term in Table X. Also, since the mill uses a pallet system, there is no machine tool downtime for load-unload. Since rapid traverse is faster on the milling machine than the production lathe, that factor was not entered into this preliminary comparison. Therefore, constant times and costs due to rapid traverse have been eliminated from the turning comparison. When turning on the lathe, the tools used for facing and boring are good for an entire lot; therefore, no downtime for dull tool replacement was assumed. When the turning operations are replaced by a high speed production milling operation, an automatic tool changer would be used and dull tools could be replaced while a different cutter was being used.

The total average cycle time for the turning operation was calculated as 57.80 minutes. Doing this operation on the mill at high speeds would take only 18.8 minutes, saving 67 percent in cycle time. Cost savings would not be as high since the milling cutter is much more expensive than the inserts used for turning. Cost per part on the lathe is \$26.49 as compared to \$17.04 on the mill. This is a savings of 36 percent.

The most detailed and time consuming part of the analysis was made for Operation 60, the milling operation. A complete breakdown of Operation 60 data for conventional milling can be found in Table XI. These data were gathered from 3,000 lines of APT output in order to calculate rapid traverse and cutting times. Since it was not possible from the APT output to tell when the cutters were actually making contact with the workpiece, any feed rate over 50 inches/minute was considered as a rapid traverse and, therefore, constant time or cost. Anything under 50 inches/minute was considered as feed or cutting time. Units for tool life values were number of parts per tool; so it was not necessary to tell when the cutter was contacting the work. Rapid traverse and cut times were calculated by dividing the cutter travel distance by the feed rate. Costs were calculated by multiplying these times by the overhead rate at Vought Corporation. Tool costs per sharp edge and tool life in number of parts were supplied by Vought Corporation from their existing production data.

TABLE IX - PRODUCTION TIMES AND COSTS FOR MACHINING  
ONE PART BY CONVENTIONAL OPERATION 50

Operation	Tool	Constant Time (min.)	Feeding Time (min.)	Tool Time (min.)	Total Time (min.)	Constant Cost (\$)	Feeding Cost (\$)	Tool Cost (\$)	Total Cost (\$)
Setup	--	1.5	--	--	1.5	0.68	--	--	0.68
Load-unload	--	10.0	--	--	10.0	4.51	--	--	4.51
Face top	TPG532	--	1.25	0.	0.	--	0.56	0.02	3.51
Finish face top	TPG532	--	5.00			--	2.25		
Face bottom	TPG532	--	0.50			--	0.23		
Finish face bottom	TPG532	--	1.00			--	0.45		
Turn outside diameter at bottom	DPEA532W	--	0.71	0.08	0.08	--	0.32	0.41	17.01
Turn outside diameter at top	DPEA532W	--	5.00			--	2.25		
Turn outside diameter at top	DPEA532W	--	1.43			--	0.64		
Turn outside diameter at angle	DPEA532W	--	0.33			--	0.15		
Turn outside diameter at bottom	DPEA532W	--	0.50			--	0.23		
Turn outside diameter at top	DPEA532W	--	10.00			--	4.51		
Finish outside diameter at top	DPEA532W	--	10.00			--	4.51		
Turn outside diameter at top	DPEA532W	--	2.50			--	1.13		
Finish outside diameter at top	DPEA532W	--	3.33			--	1.50		
Turn outside diameter at angle	DPEA532W	--	0.50			--	0.23		
Finish outside diameter at angle	DPEA532W	--	1.00			--	0.45		
Turn outside diameter at bottom	DPEA532W	--	0.50			--	0.23		
Finish outside diameter at bottom	DPEA532W	--	1.00			--	0.45		
Bore inside diameter	TPG531	--	0.67	0.	0.	--	0.30	0.03	0.78
Bore inside diameter	TPG531	--	1.00			--	0.45		
Total Operation 50		11.50	46.22	0.08	57.80	5.19	20.84	0.46	26.49

TABLE X - PRODUCTION TIMES AND COSTS FOR MACHINING  
ONE PART BY HIGH SPEED MILLING OPERATION 50

Operation	Tool	Constant Time (min.)	Feeding Time (min.)	Tool Time (min.)	Total Time (min.)	Constant Cost (\$)	Feeding Cost (\$)	Tool Cost (\$)	Total Cost (\$)
Setup		No extra setup	--	--	--	--	--	--	--
Load-unload		--	None (pallets)	--	--	--	--	--	--
Face top rough	2-in. dia. end mill	--	0.56	--	0.56	--	0.25	7.56	15.56
Bore inside diameter rough		--	0.50	--	0.50	--	0.23		
Turn outside diameter rough		--	7.82	--	7.82	--	3.52		
Face top finish		--	0.56	--	0.56	--	0.25		
Bore inside diameter finish		--	0.50	--	0.50	--	0.23		
Turn outside diameter finish	2-in. dia. end mill	--	7.82	--	7.82	--	3.52		
Face bottom rough	1-in. dia. end mill	--	0.52	--	0.52	--	0.23	1.02	1.48
Face bottom finish	1-in. dia. end mill	--	0.52	--	0.52	--	0.23		
Total turning on mill		0.	18.8	0.	18.8	0.	8.46	8.58	17.04

TABLE XI - PRODUCTION TIMES AND COSTS FOR MACHINING ONE PART BY CONVENTIONAL OPERATION 60  
(Sheet 1 of 2)

Operation	Tool	Constant Time (min.)	Feeding Time (min.)	Total* Time (min.)	Constant Cost (\$)	Feeding Cost (\$)	Tool* Cost (\$)	Total* Cost (\$)
Setup machine tool, 6 hours	--	3.00	--	3.00	1.35	--	--	1.35
Load-unload	--	None (pallets)	--	--	--	--	--	--
Machine launch slot	88915MC	0.43	11.85	12.28	0.19	5.34	0.30	5.83
Finish mill umbilical flat	115-062-1098	0.45	1.85	2.30	0.20	0.83	0.21	1.24
90° rectangular port	115-062-1098	0.37	0.97	1.34	0.17	0.44	4.44	
Top pocket at 340°	115-062-1098	0.08	1.56	1.63	0.03	0.70		
30° angle at 340°	115-062-1098	0.23	0.29	0.52	0.10	0.13		
Rough flat at 340°	115-062-1098	0.05	0.14	0.19	0.02	0.06		
Face of webs in 340° pocket	115-062-1098	0.04	1.34	1.38	0.02	0.60		
*D° holes at 20° and 340°	115-062-1098	0.51	0.66	1.17	0.23	0.30	0.30	8.16
Mount slots at 45° (4)	115-062-1098	0.37	1.03	2.05	0.44	0.48		
6.012 true pocket at 90°	88570-2-MC	0.24	4.96	5.20	0.11	2.24	0.30	5.50
True pocket at 325°	88570-2-MC	0.59	5.73	6.32	0.27	2.58		
Rough top corners in 340° pocket	115-000-1267	0.25	0.68	0.93	0.11	0.31	1.27	9.47
Machine inside of webs at 20° and 340°	115-000-1267	0.30	8.82	9.12	0.14	3.97		
Inside periphery of 325° pocket	115-000-1267	0.40	7.75	8.15	0.18	3.49		
Spot face both *D° holes	88311-1-MC (No. 1)	0.80	1.77	2.57	0.36	0.80	2.03	3.19
Bottom of 45° mount slots 4 places	88311-1-MC (No. 2)	1.04	1.79	2.83	0.47	0.81	2.03	5.84
Step under top flange at 90°	88311-1-MC (No. 2)	0.57	5.05	5.62	0.26	2.27		
(4) Lock slots in 325° pocket	88333MC	0.64	1.70	2.34	0.29	0.77	2.39	3.45
Small pocket in top of 325° pocket	115-006-1039	0.37	1.11	1.48	0.17	0.50	0.13	0.80
Top corners in 340° pocket	115-055-0263-SI	0.48	0.94	1.32	0.22	0.38	0.17	0.77
30° angle on lock slot	81728MC	0.45	10.01	10.49	0.20	4.53	1.02	5.75
Total for milling		9.26	69.97	79.23	4.18	31.53	14.29	50.00
Center drill two holes	112-019-0620	0.46	0.13	0.59	0.21	0.06	0.01	0.28
0.375 diameter spade drill	112-048-0005	0.65	0.33	0.98	0.29	0.15	0.07	0.51
0.750 diameter spade drill	112-048-0062	1.22	1.16	2.38	0.55	0.52	0.08	--
Center drill 4 holes in top flange	112-048-0362	1.05	0.15	1.20	0.47	0.07		
								1.69

\*Assuming no downtime to change drill tool.

TABLE XI - PRODUCTION TIMES AND COSTS FOR MACHINING ONE PART BY CONVENTIONAL OPERATION 60  
(Sheet 2 of 2)

Operation	Tool	Constant Time (min.)	Feeding Time (min.)	Total Time (min.)	Constant Cost (\$)	Feeding Cost (\$)	Tool Cost (\$)	Total Cost (\$)
Drill 0.126 diameter at 0.18 deep pocket	112-001-1303	0.60	0.30	0.90	0.27	0.17	0.01	0.45
Drill 2 0.5 diameter holes in 0.18 pocket	112-027-0505	0.55	0.27	0.82	0.25	0.12	0.01	0.38
Drill 2 holes in small pocket at 325°	112-000-4915	0.57	0.24	0.81	0.26	0.11	0.01	0.38
Drill 3 holes for tap in top pocket	112-001-1094	0.61	0.35	0.96	0.28	0.16	0.01	0.45
Drill 2 holes in top pocket	112-001-1093	0.60	0.23	0.83	0.27	0.11	0.01	0.39
Drill 2 holes in top pocket	112-003-0150-RI	0.59	0.23	0.82	0.27	0.11	0.01	0.39
Drill 0.193 hole around periphery of shell	112-001-1933	0.54	0.43	0.97	0.34	0.26	0.01	0.61
Drill 4 holes in outside diameter and 2 holes in top of shell	112-003-0280	0.83	0.75	1.57	0.37	0.34	0.01	0.72
Drill 4 holes in top flange for 1/2-13 tap	112-027-0456	0.74	0.60	1.34	0.33	0.27	0.02	0.62
Drill launch slot	112-005-2721	0.69	0.57	1.26	0.31	0.25	0.01	0.57
TOTAL FOR DRILLING		9.09	5.82	15.01	4.37	2.65	0.27	7.29
Tap launch slot	114-005-0424	0.65	0.64	1.29	0.29	0.29	0.04	0.62
Tap top pocket	114-004-2330	0.61	0.46	1.06	0.27	0.22	0.04	0.53
Tap 4 holes top flange	114-005-1020	0.92	0.83	1.75	0.41	0.37	0.01	0.79
Tap to G-32-UNC-2B	114-010-2614	0.23	0.25	0.48	0.15	0.16	0.16	0.47
TOTAL FOR TAPPING		2.51	2.20	4.81	1.12	1.04	0.25	2.41
Operation 60 total		24.46	70.09	102.55	11.02	35.22	14.81	61.05

Tool No.	Key No.	Tool Life (Number of Pieces)	Tool No.	Key No.	Tool Life (Number of Pieces)
MC 80015	00015	21	112-001-1303	10242	300
115-002-1000	10200	120	112-027-0505	11246	300
115-055-6313	10275	6	112-000-4915	12046	300
MC 80076	10173	120	112-001-1094	12021	300
115-000-1267	10003	10	112-001-1093	12018	300
MC 80311 (No. 1)	00311	94	112-003-0150-RI	12021	300
MC 80311 (No. 2)	00312	94	112-001-1533	12243	120
MC 80333	00333	66	112-003-0280	12244	120
115-000-1000	03125	48	112-027-0456	12249	120
115-055-206351	10042	40	112-004-2721	12245	120
MC 81726	01726	84	114-005-0424	12378	60
MC 80313	00312	28	114-004-2330	20432	40
115-010-0025	12376	260	114-005-1020	12250	60
115-040-0005	12375	120	114-010-2614	20120	20
112-040-0002	12377	120			

The total average production time for the conventional machining of Operation 60 was 102.55 minutes per part. Of this time, 24 percent was attributable to prorated setup and rapid traverse movements. The remaining 76 percent of the time was at cut feed rate. Time to replace dull tools was not considered since dull tools could be replaced in the tool holder while other tools were being used. The total average production cost for the conventional machining of Operation 60 was \$61.05 per part. Prorated setup and rapid traverse time accounted for 18 percent of this cost. Feeding cost was 58 percent of the total, with replacement of expendable tooling accounting for the remaining 24 percent of the cost. Breaking the total time down by operation, 3 percent of the time goes to setup, 77 percent for milling, 15 percent for drilling, and 5 percent for tapping. For cost, this comes to 2 percent for setup, 82 percent for milling, 12 percent for drilling and 4 percent for tapping.

To the extent possible, Operations 50 and 60 were performed on two Guidance and Control (G&C) shells with one high speed milling operation. These are shown in Figure 143. A stop watch was used to measure the in-cut times of comparable milling and drilling operations. Tapping operations were not considered in the comparison due to the inability of the high speed spindle to reverse quickly, a requirement for tapping spindles. The total cut time for these operations at high speed was 31 minutes. Therefore, by using high speed milling and drilling operations (not changing tapping rate) with no change in tool life, a reduction in average cycle time for Operation 60 from 102.55 minutes per part to 57.76 minutes per part could be realized. This is a 44 percent savings in production time. The cost would decrease 33 percent from \$61.05 per part to \$40.84 per part.

#### 11.4

##### Potential Realization

The high metal removal rates possible with high speed machining can cause drastic reductions in the feeding times and costs. Also, there is no drastic reduction in tool life when going to these high speeds. One thing that must be kept in mind though is that it takes time for the machine tool to accelerate and decelerate from these rapid feeding rates. This limits the application of high speed machining when many cutter direction changes are necessary. The cutter paths necessary for machining the test parts, in many cases, did not allow taking full advantage of high speed machining technology. Although the existing machine tool loses use of the automatic tool changer with the high speed spindle installed, each separate operation was run at high speeds. With a machine tool design for high speed machining, rapid traverse, as well as contouring and direction change rates, would increase. By doubling the rapid traverse rates along with the cutting rate increase, total reductions of 54 percent in production time and 41 percent in costs could be realized.

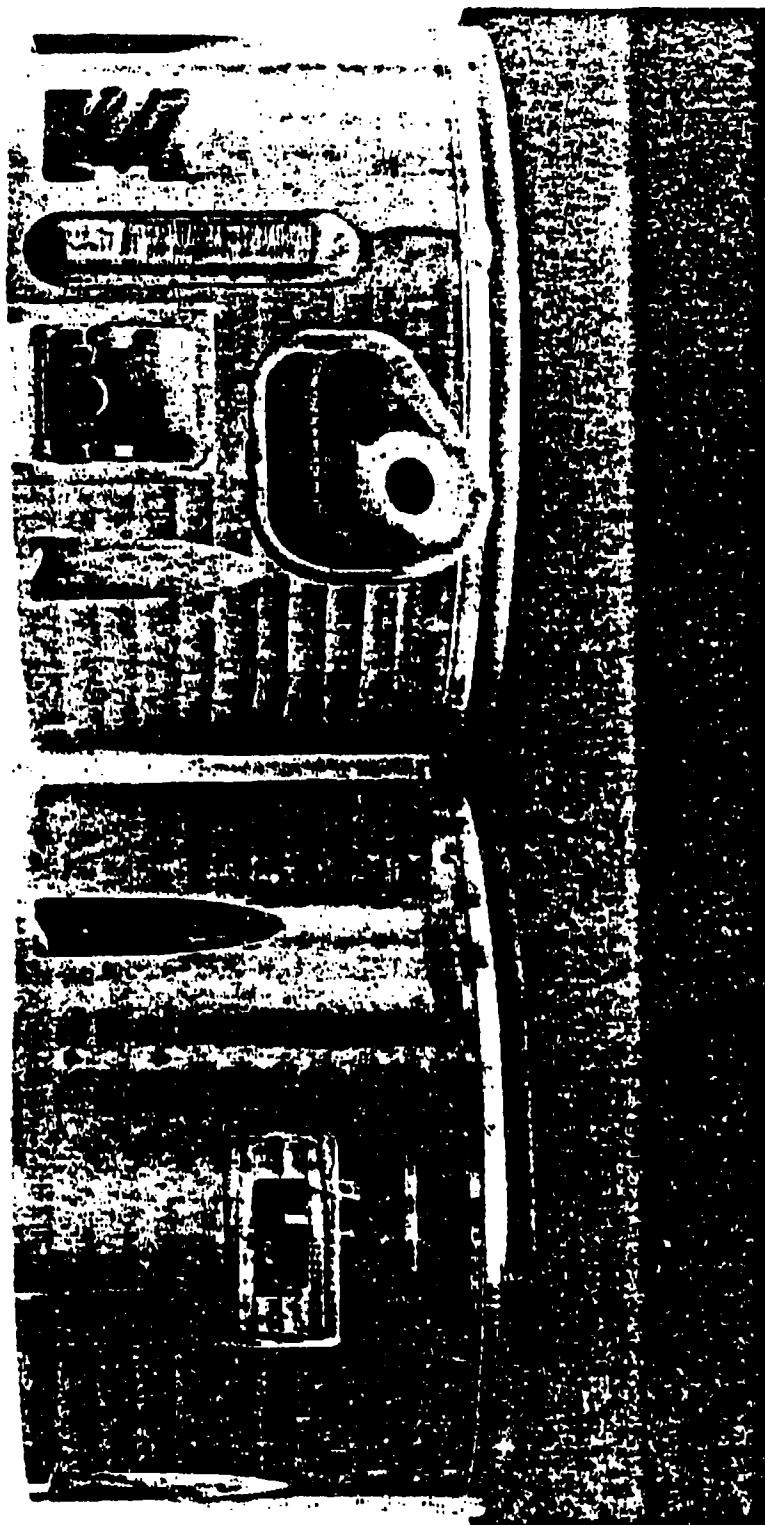


Figure 141. High Speed Mechanical Test Cell

Although testing does not show any large effect on tool life by going to high speed machining, the conservative approach should be used to find what effect tool life could have on cost. If the tool life is halved when going to high speed milling and drilling, assuming the doubled rapid traverse rates, the production time would still decrease by 54 percent, but the cost would be decreased by only 17 percent as opposed to 41 percent when no reduction in tool life is assumed.

11.5

#### Conclusion

Calculations show that given a machine tool capable of high speed machining with all the requirements of a production machine tool; e.g., automatic tool changer and pallets for quick part load-unload, large cost and production time savings can be realized for the G&C shell part analyzed. A total of 59 percent savings in production time and a 23-39 percent savings in cost can be achieved.

## 12.0 CONCLUSIONS AND RECOMMENDATIONS

Major improvements in productivity and cost effectiveness were demonstrated for high speed machining processes in this program. High speed machining is not exactly a new process. Aside from routing operations, high speed machining has been proven many times in production shops to be a worthwhile operation for special cases. For example, spar mills have routinely spun 8.0-inch diameter cutters at 3,000 revolutions/minute to produce aluminum spars at a cutting speed of 6,280 feet/minute. The reader could probably cite some examples of his own, but this example and the ones in the report can serve to illustrate that the high speed machining processes are for real and can work.

The factor which allows high speed machining to work so well on aluminum is that material's low melting point. The melting point of aluminum varies between 950°F and 1180°F; and it follows that the cutting temperature will never exceed approximately 1200°F and, more than likely, will usually be less. At those temperatures, cutter life did not prove to be much of a problem except for the very abrasive aluminum alloy, A356. Therefore, it was generally concluded that, thermally speaking, there does not appear to be any limit to the cutting speed at which aluminum can be machined.

Cutting speeds were found to have an effect on cutter life; however, and it was estimated that spindle speeds on the order of 40,000 revolutions/minute would be required to produce a most-economical cutting speed for 1.0-inch diameter end mills. Smaller cutters would require an even faster spindle speed to reach the most economical cutting speed, estimated to be on the order of 10,000 feet/minute. Consequently, it was concluded that the existing spindle with its 20,000 revolutions/minute maximum speed was too slow to achieve maximum machining economies in aluminum with cutters less than about 1.5 inches in diameter.

Tool life increased with feed rates up to about 0.008 inch/tooth on Al-7075-T651, 0.010 inch/tooth on Al-6061-T651, and 0.014 inch/tooth on Al-A356-T6. To achieve those feed rates with 2-flute end mills rotating at 20,000 revolutions/minute, milling table speeds of 320,400 and 560 inches/minute, respectively, would have to be provided. For 4-flute end mills, those table speeds would have to be doubled. Since the fastest milling table speed known was 400 inches/minute, it was concluded that it would do little good to increase spindle speeds further unless table speeds were increased, accordingly.

In the same vein, it was found that rotary tables on machining centers were also generally too slow for a 20,000 revolutions/minute spindle. To provide a feed rate of 0.010/tooth for a 2-flute end mill cutting at 20,000 revolutions/minute on a 22-inch diameter workpiece, a table speed of 6 revolutions/minute would be required. Consequently, it is

recommended that table speeds of that magnitude be provided on future machining cutters.

While faster spindle speeds can be delayed until faster table speeds are provided, more powerful spindles are needed now. Both the Ekstrom, Carlson and Bryant spindles were found to be lacking in torque and useful horsepower output. This limits the size of cut that can be made with either and can be attributed to the physics of the process. That is, for a given size cut, horsepower requirements increase as speed increases. Using formulae developed in this program, 20 horsepower was calculated to be the requirement for producing a 1.0-axial depth, 0.25-inch radial depth, and milling out at a speed of 6,600 feet/minute and a feed rate of 200 inches/minute. Those parameters would permit a metal removal rate of 50 cubic inches/minute. To machine at that rate on a continuous duty cycle basis, the spindle could only be operated at approximately 50-percent capacity. Consequently, a 40 horsepower spindle would be needed for the task. The size of cut under discussion is not large by production standards; therefore, it is recommended that one of the primary goals for spindle manufacturers be the development of at least a 40 horsepower, 20,000 revolutions/minute spindle.

Two other design changes are needed for the high speed spindles. First, a more positive spindle stop; e.g., a forward thrust bearing or a hydraulic preloaded bearing, is needed to prevent a loaded spindle shaft from trying to pullout of its housing by taking up excessive slacks in the assembly. Under extreme conditions, such pullout can overstress a forward bearing that is turning at an ultra high speed, causing overheating and possible damage to the bearing or its shaft. Second, a low spindle speed is needed on machining centers for tapping operations. Without such a capability, much of the economic advantage of a high speed machining center might be lost. Since other low speed applications can be visualized for machining centers, it is recommended that spindle manufacturers look into the possibilities of using electronic switching to provide both a high and low speed range.

Except for the abrasive aluminum alloys like A356 which must be machined with carbide, either carbide or high speed steel cutters can be used to machine the remaining aluminum alloys at ultra high speeds. Generally, end mills of either material cannot be rotated fast enough to reach a most economical cutting speed; so there is little danger of cutting too fast with either material. The best end mill geometry observed in this program for cutting aluminum with carbide consisted of a 25-degree helix angle, 5-degree radial rake angle and about 10-degree primary clearance. For cutters over 1.0-inch diameter in particular, cutter balance was found to be critical to tool life and surface finish. Consequently, it will probably be necessary for users of the high speed machining processes to have dynamic balancing equipment available.

Cutting fluids are not always required but are generally recommended for the high speed machining of aluminum. The fluids are not needed to cool workpieces and cutters, because these do not get hot. The fluids are beneficial, however, in alleviating built-up-edges on cutter flanks, particularly on high speed steel cutters. The built-up-edges are formed from small chip particles which have been pressure-welded to cutter flanks; and these, in effect, replace the cutter material that was ground away to provide cutter clearance. With no clearance, such cutters rub workpieces, increasing heat and horsepower consumption and decreasing cutter life. Centrifugal force will alleviate flute packing, but cutting fluids are needed to minimize built-up-flanks.

High speed steel drills are adequate for the high speed drilling of aluminum. Over five thousand holes were drilled through one-half inch thick 7075-T651 aluminum with one (1) one-fourth-inch diameter drill operated at 20,000 revolutions/minute and a feed of 100 inches/minute. At those rates, drilling operations were spectacular, resembling a punching operation. If desired, those rates could probably be doubled with higher spindle speed, drilling equipment that is now available.

While some equipment changes which could make high speed milling a better process were pointed out, nothing detrimental to high speed milling was observed in this program. With the equipment at hand, a very good metal removal rate of 33 cubic inches/minute was established as a standard for 50-percent spindle loads. Additionally, metal removal rates of 69 cubic inches/minute and feed rates of 504 inches/minute were sustained with a 1.0-inch diameter, 2-flute, brazed-carbide end mill in another instance. In short, productivity was significantly improved by the process. While high speed machining can be more profitably used to make "hogging" cuts, an economic analysis showed that with the proper machine tool, a 23 to 39 percent cost savings could be achieved by using high speed machining to help finish machine as-cast Guidance and Control shells. Part stability may also be improved by high speed milling, because cutting forces were observed to vary between only 40 and 50 pounds at 50-percent machine loads and 10 to 20 pounds at 25-percent machine loads. Additionally, high speed machined workpieces remained cool to minimize any thermally induced distortions, and cutting speed was not found to have any effect on residual stress generation. Good dimensional tolerances and finishes were also maintained with high speed milling. For examples, maximum cutter deflection was about 0.003 inch at 50-percent spindle loads and 0.002 inch at 25-percent spindle loads. Additionally, the two guidance and control shells were high speed machined within tolerances, and excellent surface finishes were obtained at all speeds. High speed machining was found to be a relatively safe process. While several cutters were smashed, only two were broken and those, not unexpectedly. In summation, these highlights from the program exemplify that high speed machining is a sound, viable process.

Machine tools can be beneficially retrofitted with high speed spindles to perform the same operation or family of operations repeatedly. However, the type of high speed machine tool needed by the missile and other general type machine shops has not been built as yet. Basically, the type of machine tool envisioned would be a machining center with rapid, automatic tool and part changers. It would have a protective cover and a lightweight machining table with infinitely variable feed rates to 800 inches/minute. Its corresponding rotary table would have a minimum speed of 5 revolutions/minute. The spindle on that machine would have both a low and a high range; or two spindles would be provided, as on the OM-3 Omnimil. The high speed range would vary infinitely between 10,000 and 25,000 revolutions/minute, and the low speed range would vary infinitely between 0 and 1,000 revolutions/minute and be reversible. Minimum power outputs would be 40 horsepower at 20,000 revolutions/minute at the high speed spindle and 1.5 horsepower at 1,000 revolutions/minute at the low speed spindle. The system would be well protected and instrumented and computer (DNC) controlled. Such a machine would provide the versatility needed for job-shop type operations and move a good process beyond its threshold.

Appendix  
BIBLIOGRAPHY

1. "Machining Experts Fall Out -- Is There Really a 'Valley of Death'", American Machinist, pp 148-150, October 20, 1958.
2. H.J. Siekmann, "High Speed Cutting With Ceramic Tools", The Tool Engineer, pp 85-88, April 1958.
3. R.L. Vaughn, "Ultra High Speed Machining", AMC Technical Report 60-7-635(I), June 1960.
4. R.I. King and J.C. McDonald, "Product Design Implications of New High-Speed Milling Techniques", ASME Paper No. 76-DE-22, January 7, 1976.
5. "Speeds and Feeds for Better Turning Results", Monarch Machine Tool Co., pp 37-38, 1957.
6. F.W. Taylor, "On the Art of Cutting Metals", Trans. ASME, Vol. 28, p 31, 1907.
7. M.C. Shaw, "Principles of Metal Cutting", Harvard Cooperative Press, 1954.
8. E.J. Krabacher and M.E. Marchant, "Basic Factors in Hot-Machining of Metals", Trans. ASME, Vol. 73, pp 761-769, 1951.
9. D.R. Olberts, "A Study of the Effects of Tool Flank Wear on Tool-Chip Interface Temperatures", Trans. ASME, Vol. 81, pp 152-158, May 1959.
10. K.J. Trigger, R.K. Campbell, and B.T. Chao, "A Tool-Work-Thermocouple Compensating Circuit", Trans. ASME, Vol. 80, p 302, 1958.
11. J. Datsko, "Material Properties and Manufacturing Processes", John Wiley and Sons, Inc., p 451, 1966.
12. F.J. McGee, P. Albrecht, H.N. McCalla, "Development of Cutter Geometry Based on Material Properties", Technical Report No. AFML-TR-68-350, Air Force Systems Command, December 1968.
13. "Some Effects of Flute Helix and Rake Angles on Milling Cutter Performance", National Twist Drill and Tool Co., Metal Cuttings, Vol. II, No. 3, July 1963.
14. W.W. Gilbert, "Economics of Machining", Machining-Theory and Practice, American Society of Metals, pp 465-485, 1950.